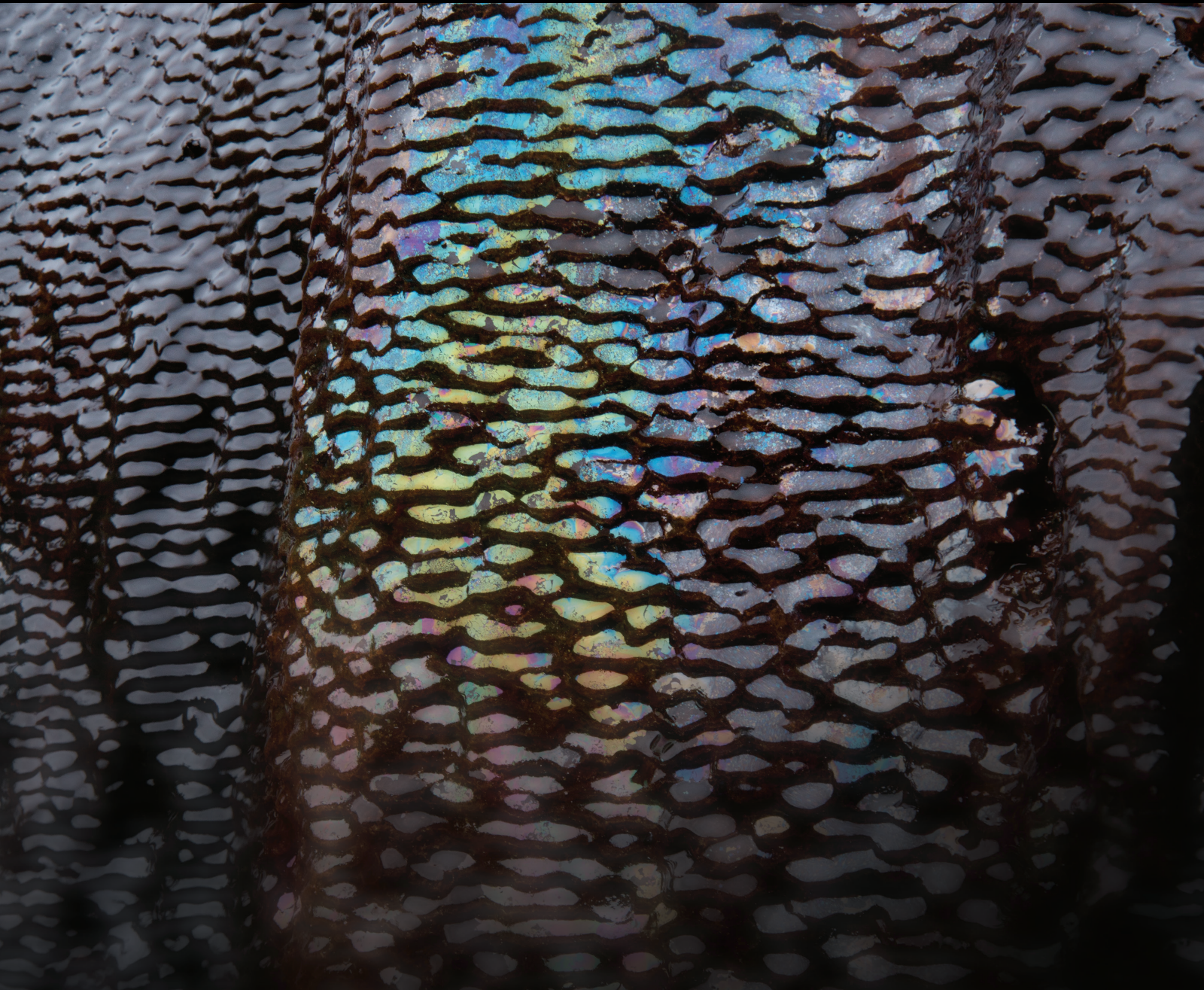# Groundwater Quality in the Mediterranean Region

Lead Guest Editor: Giovanni Mongelli
Guest Editors: Ariadne Argyraki, Mari L. García-Lorenzo, Maisa'a W. Shammout, Michele Paternoster, and Vincenzo Simeone

Groundwater Quality in the Mediterranean Region

Groundwater Quality in the Mediterranean Region

Lead Guest Editor: Giovanni Mongelli
Guest Editors: Ariadne Argyraki, Mari L. García-Lorenzo,
Maisa'a W. Shammout, Michele Paternoster, and Vincenzo Simeone

Editorial Board

Contents

Editorial

Groundwater Quality in the Mediterranean Region

Giovanni Mongelli [1,2] **Ariadne Argyraki,**[3] **Mari Luz García Lorenzo,**[4]
Maisa'a Wasif Shammout,[5] **Michele Paternoster** [1,6] **and Vincenzo Simeone**[7]

[1]*Department of Sciences, University of Basilicata, 85100 Potenza, Italy*
[2]*National Research Council of Italy, Institute of Methodologies for Environmental Analysis (CNR-IMAA), 85050 Tito Scalo, Italy*
[3]*Department of Geology and Geoenvironment, Section of Economic Geology and Geochemistry, National and Kapodistrian
University of Athens, 15784 Athens, Greece*
[4]*Department of Mineralogy and Petrology, Faculty of Geology, University Complutense of Madrid, 28040 Madrid, Spain*
[5]*Water, Energy and Environment Center, The University of Jordan, Amman 11942, Jordan*
[6]*Section of Palermo, National Institute of Geophysics and Volcanology, 90146 Palermo, Italy*
[7]*DICATECh, Polytechnic University of Bari, 70125 Bari, Italy*

Correspondence should be addressed to Giovanni Mongelli; giovanni.mongelli@unibas.it

In recent decades, the percentage increase in water use on a global scale has exceeded twice that of population growth. This has led to more, and larger, regions in the world being subject to water stress where the current restricted rates of water use and consumption, let alone the desired rates, are unsustainable [1, 2]. In the Mediterranean area, water availability is a main economic and social target for most countries since most of them share several features including, for instance, similar water and land resources, agricultural development, demographic pressure coupled with tourism increase and, last but not least, a climate change evolving toward semiarid to arid conditions [3–5]. This precious resource, widely exploited, is not distributed, at a regional level and within each country, in a homogeneous fashion. The increase in groundwater exploitation poses a severe risk for the availability of water resources, and the resulting resource scarcity is a major concern in most countries of the Mediterranean region. Groundwater paucity often occurs in combination with poor groundwater quality, not only in areas heavily conditioned by human activities [6] or in the often highly saline coastal aquifers [7–9] but also in zones characterized by geogenic contamination sources. In such areas, although human pressure is absent, water-rock interaction processes, as those promoting, for instance, geogenic

Cr(VI) water contamination [10], may cause pollution with critical effects on the public health.

More in detail, overuse of fertilizers and pesticides in agriculture, overexploitation of groundwater causing sea water intrusion, increases in the discharge of untreated or poorly treated domestic and industrial water, injection of brine and hydrocarbon by-products from oil production, and refinery operation into aquifers, and naturally occurring contaminants are among the principal causes of groundwater pollution. Thus, in the last two decades, many Mediterranean countries planned policies devoted to the assessment of the groundwater quality and trends [11, 12]. This special issue is aimed at delivering contributions presenting a wide range of aspects related to groundwater quality in the Mediterranean countries such as contaminants' input and origin, salinization effects, and protection and remediation approaches. Within this frame, we encouraged submissions of paper dealing with a wide range of groundwater-related topics including the following:

(i) Elemental and isotope hydrogeochemistry

(ii) Hydrology and hydrogeology

(iii) Groundwater geophysics

(iv) Groundwater modeling

(v) Groundwater contamination and toxicology

(vi) Groundwater protection and remediation

(vii) Water resources management

From March 2018 to November 2018, a total of 14 papers have been submitted to be considered for publication in the special issue. After rigorous editorial check and peer-review processes which involved external and independent experts, 4 manuscripts were rejected, 2 have been withdrawn, and 8 papers have been accepted, with an acceptance rate of 57%. Twenty-four authors from Mediterranean European countries and northern Africa contributed to the special issue. In the following paragraphs, a short presentation of each is given.

In the article titled "Inferred Industrial and Agricultural Activities Impact on Groundwater Quality of Skhira Coastal Phreatic Aquifer in Southeast of Tunisia (Mediterranean Region)," S. Melki et al., using a geochemical approach coupled with statistical procedures through principal component analysis, assessed the processes affecting water quality and showed that the industrial activities, especially those related to phosphate treatment in an area close to a phosphogypsum storage site, may seriously influence a part of the aquifer where the water is acidic and very charged in SO_4^{2-}, $H_2PO_4^-$, F^-, and Zn^{2+}. As for nitrates, their distribution is controlled, in addition to the excessive use of fertilizers, by physical and chemical factors. Overall, most analysed samples do not meet the World Health Organization Norms and therefore are not suitable as drinking waters, and the study sheds light on the increasing deterioration risk of the aquifer suggesting the need for urgent solutions by decision makers.

In the article titled "A Modelling Approach for Assessing the Hydrogeological Equilibrium of the Karst, Coastal Aquifer of the Salento Peninsula (Southeastern Italy): Evaluating the Effects of a MAR Facility for Wastewater Reuse," G. De Filippis et al. focused on the characterization of the deep aquifer of the Adriatic portion of the Salento peninsula from a quantitative point of view by means of modelling tools for the simulation of groundwater dynamics. The implementation of a density-dependent flow model, the lateral extent of such phenomenon, and the vertical depth of the transition zone between freshwater and saltwater were inferred, highlighting also the role of major faults which characterize the hydraulic behaviour of the karst system. The model was also applied to design a Managed Aquifer Recharge (MAR) facility for the management and protection of the hydrogeological equilibrium of the deep aquifer. Model results allowed also identifying areas where the lack of data prevents a proper comprehension of the hydrogeological processes investigated, thus representing supporting tools for planning further monitoring campaigns.

In the article titled "Hydrogeology and Hydrogeochemistry of the Lauria Mountains Northern Sector Groundwater Resources (Basilicata, Italy)," F. Canora et al. presented the hydrogeological characterization of a carbonate hydrostructure in the southern Apennines, in an area including springs having high annual mean discharges. The results elucidate that the main hydrogeochemical processes controlling the chemical content of the groundwater composition are strongly affected by the lithology, especially limestones and dolomitic limestones. The analysis, in all studied groundwater samples, shows that facies groundwater type is Ca–HCO_3; bicarbonate is the dominant anion, and calcium is the dominant cation with appreciable magnesium contents. Further, $\delta^{18}O$ and δD signatures for the groundwater of the major springs allow identifying the recharge area of these occurrences at elevations ranging from 900 m to 1000 m (a.s.l.), pointing out the presence of deeper flow regime feeding of these springs. The groundwater isotopic feature record suggests that most of the groundwater recharged directly by infiltration in high permeable media.

In the article titled "Geochemical Modeling of Water-Rock Interaction in the Granulite Rocks of Lower Crust in the Serre Massif (Southern Calabria, Italy)," C. Apollaro highlighted the irreversible water–rock mass exchanges occurring in a shallow hydrogeological metamorphic complex through a reaction path modelling in a kinetic mode. The secondary solid phases that were allowed to precipitate are kaolinite, vermiculite solid mixture, and hydroxide solid mixture. The reaction path modelling shows that the release of major dissolved constituents is mainly controlled by plagioclase weathering. Computed contents of key dissolved components are comparable with analytical data, although not all the details are reproduced, probably due to insertion in the model of average composition of primary minerals, in spite of their nonnegligible chemical variations and to the fact that some elements, such as Na and K, are controlled by varying contributions of atmospheric marine salts. Due to the worldwide occurrence of granulite rocks, the results can be transferred to other sites where the lithology occurs.

In the article titled "Groundwater Quality Assessment in a Karst Coastal Region of the West Aurunci Mountains (Central Italy)," G. Sappa et al. presented the groundwater quality assessment in the karst coastal region of the West Aurunci Mountains (central Italy). A large chemical dataset of springs and well water, collected from 2016 to 2018, is discussed in order to unroof the processes controlling the groundwater hydrogeochemical evolution. The groundwater is mostly characterized by a Ca-HCO_3 facies, indicating its evolution is mainly controlled by the carbonate mineral dissolution/precipitation. Well water samples show, over the time, an increasing mineralization compared to spring water, and their Ca^{2+}, Na^+, and Cl^- enrichment is mainly due to the dissolution of calcite, dolomite, and halite and subordinately to a probable ion exchange related to seawater intrusion. Results suggest that carbonate weathering, ion exchange, and seawater intrusion in this karst coastal region are the major factors controlling groundwater geochemistry.

In the article titled "Boron Isotopes in the Mount Vulture Groundwaters (Southern Italy): Constraints for the Assessment of Natural and Anthropogenic Contaminant Sources," M. Paternoster discussed the application of boron contents and isotopes (^{11}B) as tools for assessing water quality in one

of the most significant aquifer systems of Southern Italy. In the area, two different hydrofacies are observed. The first one (BAW) has bicarbonate alkaline and alkaline-earth composition whereas the second one (HSW) has bicarbonate-sulphate alkaline composition. The HSW is enriched in boron and has low $\delta^{11}B$ values similar to those measured in the local magmas suggesting B contents in these waters are affected by the interaction with volcanic rocks. As to BAW, a wide variability in B concentrations and B isotope composition is observed, likely due to anthropogenic input. Water samples with high B concentrations and negative $\delta^{11}B$ values are probably influenced by agricultural activities; for water samples characterized by positive $\delta^{11}B$ values and low B contents, a slight contamination by sewage effluents cannot be excluded. This study highlights the relevance of B isotopes coupled with the B/Cl ratio as a tool for the assessment of natural and anthropogenic contaminant sources.

In the article titled "Deep Electrical Resistivity Tomography for the Hydrogeological Setting of Muro Lucano Mounts Aquifer (Basilicata, Southern Italy)," E. Rizzo et al. presented the application of a deep geoelectrical survey to a carbonate aquifer in order to define the best location for exploitation well drilling for increasing water supply. The work summarizes the hydrogeological knowledge at west of the Basilicata Region (Southern Italy). The investigated area is characterized by the presence of a karst aquifer which is made up by a carbonate ridge that tectonically dips southward. The assessment of the complex hydrogeological framework of the area was detailed by the use of a new multichannel deep geoelectrical technique (DERT). The proposed technique was able to successfully locate a less-resistive zone connected to more fractured limestone resulting suitable for the localization of a groundwater exploitation well.

In the article titled "Groundwater Quality on the Adriatic Karst Island of Mljet (Croatia) and Its Implications on Water Supply," S. Borović et al. focused on the peculiar source of water supply in the Island of Mljet, Croatia: desalination of water from brackish lakes is fed by groundwater and connected to the sea by karst conduits. All waters sampled from the lakes are of Na-Cl type. Daily monitoring of total dissolved solids in the feed water was recently introduced: maximum concentrations were observed during September and interpreted to be caused by a combination of natural and anthropogenic pressures during the summer tourist season. According to the presented data on groundwater quality, climate change predictions, the connection of water supply system to the mainland, and problems with the effluent treatment, the main future issue will be the creation of an island-wide sustainable water management plan followed by continuous monitoring and research, in a global scenario where water supply of the islands is a relevant challenge.

Conflicts of Interest

The guest editors declare that they have no conflicts of interest or private agreements with companies.

References

[1] W. J. Cosgrove and D. P. Loucks, "Water management: current and future challenges and research directions," *Water Resources Research*, vol. 51, no. 6, pp. 4823–4839, 2015.

[2] C. J. Vörösmarty, P. Green, J. Salisbury, and R. B. Lammers, "Global water resources: vulnerability from climate change and population growth," *Science*, vol. 289, no. 5477, pp. 284–288, 2000.

[3] Mediterranean Groundwater Working Group (MED-EUWI WG on groundwater), "Mediterranean groundwater report," Technical Report on Groundwater Management in the Mediterranean and the Water Framework Directive, 2007.

[4] J. M. García-Ruiz, J. I. López-Moreno, S. M. Vicente-Serrano, T. Lasanta–Martínez, and S. Beguería, "Mediterranean water resources in a global change scenario," *Earth-Science Reviews*, vol. 105, no. 3-4, pp. 121–139, 2011.

[5] C. Leduc, A. Pulido-Bosch, and B. Remini, "Anthropization of groundwater resources in the Mediterranean region: processes and challenges," *Hydrogeology Journal*, vol. 25, no. 6, pp. 1529–1547, 2017.

[6] S. Parisi, M. Paternoster, F. Perri, and G. Mongelli, "Source and mobility of minor and trace elements in a volcanic aquifer system: Mt. Vulture (southern Italy)," *Journal of Geochemical Exploration*, vol. 110, no. 3, pp. 233–244, 2011.

[7] M. Antonellini, P. Mollema, B. Giambastiani et al., "Salt water intrusion in the coastal aquifer of the Southern Po Plain, Italy," *Hydrogeology Journal*, vol. 16, no. 8, pp. 1541–1556, 2008.

[8] G. Mongelli, S. Monni, G. Oggiano, M. Paternoster, and R. Sinisi, "Tracing groundwater salinization processes in coastal aquifers: a hydrogeochemical and isotopic approach in the Na-Cl brackish waters of northwestern Sardinia, Italy," *Hydrology and Earth System Sciences*, vol. 17, no. 7, pp. 2917–2928, 2013.

[9] M. Argamasilla, J. A. Barbera, and B. Andreo, "Factors controlling groundwater salinization and hydrogeochemical processes in coastal aquifers from southern Spain," *Science of The Total Environment*, vol. 580, pp. 50–68, 2017.

[10] S. Margiotta, G. Mongelli, V. Summa, M. Paternoster, and S. Fiore, "Trace element distribution and Cr(VI) speciation in Ca-HCO$_3$ and Mg-HCO$_3$ spring waters from the northern sector of the Pollino massif, southern Italy," *Journal of Geochemical Exploration*, vol. 115, pp. 1–12, 2012.

[11] M. A. Massoud, M. D. Scrimshaw, and J. N. Lester, "Qualitative assessment of the effectiveness of the Mediterranean action plan: wastewater management in the Mediterranean

region," *Ocean & Coastal Management*, vol. 46, no. 9-10, pp. 875–899, 2003.

[12] J. Terzic, Z. Peh, and T. Markovic, "Hydrochemical properties of transition zone between fresh groundwater and seawater in karst environment of the Adriatic islands, Croatia," *Environmental Earth Sciences*, vol. 59, no. 8, pp. 1629–1642, 2010.

Research Article

A Modelling Approach for Assessing the Hydrogeological Equilibrium of the Karst, Coastal Aquifer of the Salento Peninsula (Southeastern Italy): Evaluating the Effects of a MAR Facility for Wastewater Reuse

Giovanna De Filippis [iD],[1] **Stefano Margiotta,**[2] **Claudia Branca,**[2] and **Sergio Luigi Negri**[2]

[1]Institute of Life Sciences, Scuola Superiore Sant'Anna, Pisa, Italy
[2]DiSTeBA, Università del Salento, Lecce, Italy

Correspondence should be addressed to Giovanna De Filippis; g.defilippis@santannapisa.it

The Salento Peninsula is characterized by poor surface water resources, due to the karstic nature of its territory. On the other hand, important groundwater resources are located in the deep, karst, coastal aquifer, which is of strategic importance for the economic and social development of the area. The increasing water demand, however, if not properly managed may pose serious problems to the hydrogeological equilibrium of this aquifer, which is highly susceptible to natural and anthropogenic changes and to saltwater intrusion. Taking steps from the previous works, the present paper focuses on the characterization of the deep aquifer of the Adriatic portion of the Salento Peninsula from a quantitative point of view by means of modelling tools for the simulation of groundwater dynamics. Conclusions about the extent of the saltwater intrusion phenomenon are consequently inferred. As a result of the implementation of a density-dependent flow model, the lateral extent of such phenomenon and the vertical depth of the transition zone between freshwater and saltwater were inferred, highlighting also the role of major faults which characterize the hydraulic behaviour of the karst system under exam. The model was also applied to design a Managed Aquifer Recharge facility for management and protection of the hydrogeological equilibrium of the deep aquifer. Its positive effects on the advancement of the saline front were highlighted. Model results also allowed identifying areas where the lack of data prevents a proper comprehension of the hydrogeological processes investigated, thus representing a supporting tool for planning further monitoring campaigns.

1. Introduction

Coastal aquifers are major sources of freshwater in arid and semiarid areas of the Mediterranean basin, which face large precipitation variability, frequent drought episodes, high evapotranspiration rates, and increasing population growth [1–3]. Also, karst landforms are pretty widespread in Mediterranean areas [4]. As karst regions often are characterized by scarce surface water supply, costal, karst aquifers contribute to a large part of the water supply in many European countries because of their high storage capacity and permeability [5]. Due to anthropogenic increasing exploitation of groundwater resources and as a direct impact of climate change, coastal areas in the Mediterranean region are facing alarming water level decline and severe water quality degradation due to saltwater intrusion. This in turn affects human health, socioeconomic development, and ecosystem service sustainability [6–8].

The effects of climate change and human stresses on groundwater salinization and quantity in coastal, karst areas of the Mediterranean region are major concerns and are widely being faced by scientists, water decision-makers, and politicians [4, 9]. In view of achieving a sustainable use of groundwater resources, different approaches have been

adopted to characterize coastal aquifer behaviour and their spatiotemporal evolution in response to different hydrologic and anthropogenic stresses [3, 7]. Among these approaches, geochemical methods based on measures of electrical conductivity, chloride concentration, and other cation and anion concentrations have been used to detect seawater contamination [10, 11]. Eissa et al. [12] pointed out the use of groundwater chemistry and stable isotopes to evaluate seawater intrusion in a coastal Egyptian area. Hammami Abidi et al. [13] deal with the combination of hydrogeochemical, isotopic, statistical, and GIS approaches to infer controlling factors on groundwater composition in northeastern Tunisia. Also, a great attention is being focused on remote sensing [14] and geophysical methods for subsurface exploration, which can contribute to coastal environment characterization [12, 15–17]. The scientific literature is also rich in examples of numerical models, which are evaluated as efficient tools to test a wide range of assumptions and to predict groundwater body evolution under different scenarios of hydrologic and anthropogenic stresses [18]. Also, the European and national regulations on coastal aquifer management foster the use of modelling tools to assess the quantitative status of these natural systems and to predict the evolution of the saltwater intrusion phenomenon and their hydrogeological equilibrium as a result of overexploitation and climate change. All the studies mentioned above emphasize the importance of monitoring groundwater salinization and quantity to assure a sustainable and safe use of this resource.

Monitoring groundwater salinization and quantity and the abovementioned approaches may support policy makers to design management strategies. Among these, Managed Aquifer Recharge (MAR) schemes are being taken into consideration to protect stressed groundwater systems, by enhancing the underground water storage capacity, and to improve groundwater quality [19]. In coastal aquifers, improvement of water volumes by means of MAR techniques results in reduction and prevention of seawater intrusion [20]. Examples of MAR application to manage coastal aquifers may be found in Bonilla Valverde et al. [21], Kazakis et al. [22, 23], and Tzoraki et al. [24].

Due to its karstic nature, the Salento Peninsula is characterized by scarce availability of surface water resources. On the other hand, important volumes of groundwater are hosted in the deep, karst aquifer, which represents a strategic resource for the socioeconomic aspects of this Mediterranean region [25]. Such aquifer, indeed, is the main source of freshwater in the region able to satisfy the increasingly widespread demand related to productive activities [26]. Regione Puglia & Autorità di Bacino della Puglia [27] estimate that an average volume of about 358 Mm^3 of freshwater is pumped yearly from the deep aquifer of the Salento Peninsula. 69% of this volume is intended to agriculture activities, while 25% meets drinking water needs, and the remaining 6% is addressed to the industrial sector.

Anyway, the karstic nature of the deep aquifer of the Salento Peninsula poses serious management problems, as it is highly susceptible to overexploitation and it is characterized by low recharge rates, due to scarce precipitation rates,

high evapotranspiration rates, and lack of surface water bodies [28]. Anthropogenic stresses are further exacerbated by tourism activities during the summer season. In this framework, an alarming imbalance between freshwater demand and groundwater availability and a high vulnerability to saltwater intrusion have been detected in the last decades either by monitoring [29, 30] and modelling [28, 31–36]. This represents a major concern in this coastal ecosystem, as salinization may cause negative impacts on irrigated crops, soil fertility [37], and the socioeconomic development of the region.

Climate change and the non-sustainable use of groundwater resources in this area contribute to the deterioration of the quantitative status of the deep, karst aquifer and exacerbate the saltwater intrusion phenomenon. As such, defining sustainable management strategies is of paramount importance to counteract the negative trend of these issues. To this aim, adopting numerical modelling techniques may represent a valuable methodology to assess the occurrence of saltwater intrusion and to propose solutions to cope with the advancement of this phenomenon.

The deep aquifer of the Salento Peninsula has been the object of some previous modelling studies. The first steady-state numerical model was developed for the deep aquifer over the whole Salento Peninsula by Giudici et al. [28]. The aim of that analysis was to evaluate how the complex hydrostratigraphic architecture and the hydrogeological conditions of the region affect the hydrodynamics of such aquifer and its balance. In that paper, the areas potentially affected by saltwater intrusion were inferred adopting a sharp-interface approach. The conceptual model reported in Giudici et al. [28] was then enhanced by De Filippis et al. [32], focusing on an in-depth investigation of the hydrostratigraphic setup in areas where the deep aquifer was found to be saturated with saltwater. Furthermore, a sensitivity analysis was performed to identify the most sensitive parameters in the numerical model. Two scenarios were consequently developed to quantify the piezometric head changes in case of rainfall decrease and abstraction increase. In both cases, the model predicted a lowering of the piezometric head in the central part of the peninsula. Areas affected by saltwater intrusion were calculated accordingly, using the same approach adopted by Giudici et al. [28].

In the following, Romanazzi et al. [36] developed a 3D density-dependent flow model of the southern part of the Salento Peninsula (Lecce province) under transient conditions. In that paper, the authors developed three scenarios: scenario P1 was referred to the period 1930-1979 and was calibrated using piezometric data dating back to 1930s at 11 wells. Results of scenario P1 were used to initialize the piezometric head for scenario P2, referred to the period 1980-1989, and results of scenario P2 were consequently used to initialize the piezometric head for scenario P3, referred to the period 1990-1999. Both scenarios P2 and P3 were validated with piezometric data at 10 wells in the study area. As a result of scenarios P1, P2, and P3, a decrease of the piezometric head up to 2.5 m was identified from 30s to 90s. They further simulated an increase of salinity values, up to more than 1000 mg/l between 50 and 100 m below the mean

sea level and up to 6 km inland. The same result was also detected about 10 years before by Margiotta and Negri [38]. The same modelling approach was also adopted to simulate future scenarios, F1 from 2001 to 2020, F2 from 2021 to 2040, and F3 from 2041 to 2060, in order to include predictions of changes in rainfall, temperature, sea level, and seawater salinity. The results show a piezometric decrease of more than 2.5 m up to 2060 with respect to the steady-state conditions. On the other hand, salinity would increase up to more than 5000 mg/l in 2060, especially along the western Ionian coast.

Generally speaking, a full comparison between results obtained by Giudici et al. [28] and De Filippis et al. [32] and those obtained by Romanazzi et al. [36] cannot be performed. As an example, the piezometric trend simulated by Romanazzi et al. [36] is smoother, with a watershed which can be clearly identified in the center of the peninsula. On the other hand, the former results by Giudici et al. [28] and De Filippis et al. [32] identified a critical area near Otranto, where high piezometric levels were detected. This was also reported in the previous studies [39, 40], while it is not mentioned at all by Romanazzi et al. [36].

In this paper, a modelling approach taking steps from the analysis reported in De Filippis et al. [32] is presented. It is aimed at characterizing the deep aquifer of the Adriatic portion of the Salento Peninsula by means of modelling tools for the simulation of groundwater dynamics and the saltwater intrusion phenomenon. This was carried out by applying the following finite difference codes: MODFLOW-2005 [41] for the simulation of groundwater flow and SEAWAT [42] for the simulation of density-dependent flow. Both codes were applied through the QGIS-integrated FREEWAT interface [43–45], which allows taking advantage of GIS spatial analysis tools for model implementation and benefiting from several numerical codes (such as MODFLOW, SEAWAT, and other MODFLOW-related codes) for the simulation of a number of hydrological processes.

A major advancement with respect to the previous works consists in modelling the karst aquifer under exam with an equivalent porous medium approach (as already done in the abovementioned papers), but taking also into account the occurrence of structural features typical of karst environments (e.g., main fractures identified at the regional scale).

A management strategy to counteract the advancement of the saline wedge has been proposed as well. This consists in a MAR technique involving a set of injection wells, which use treated wastewater coming from a near wastewater treatment plant.

The methodology presented in this paper allowed identifying still existing gaps in the understanding of the hydrogeological equilibrium of the deep, karst aquifer of the Salento Peninsula and sets the stage for further investigations in this regard.

2. Geographical and Hydrogeological Setting of the Study Area

The study area (Figure 1) extends for about 1850 km². It is bounded by the Adriatic coast on the eastern and southern sides, while the western boundary is represented by a straight line which roughly connects the municipalities of S. Pancrazio S.no and Tiggiano, and the northern one is nearly located along the boundary between Lecce and Brindisi provinces.

The northern boundary identifies a no-flow boundary according to De Filippis et al. [32].

From a geological point of view, the underground of the whole Salento Peninsula is characterized by a complex stratigraphic setup related to geotectonic events and eustatic variations which characterized the geomorphology of the region. The base of such structure is represented by a basement of Cretaceous limestones overlayed by clayey-sandy sediments of Neogene and Pleistocene. As stated in Margiotta and Negri [29], seven lithostratigraphic units can be identified in the Salento Peninsula and in the study area. From the bottom to the top, these units are the following:

(i) The Altamura limestone, made of fractured, karst sediments dating back to Cretaceous and deposited after periodic emergences of the Apulian platform

(ii) The Galatone unit, made of thin layers of compact limestone dating back to Oligocene, overlies Cretaceous limestones with interbedded residual deposits

(iii) The Miocene unit, which includes different lithologies made of calcarenites and marly limestones

(iv) The Pliocene unit, which includes different lithologies made of breccias and calcareous conglomerates. The Miocene and Pliocene units were deposited during a period when the region was submerged by seawater

(v) The Gravina calcarenites, dating back to Lower Pleistocene

(vi) The Subappennine clays, dating back to Middle Pleistocene. These last two units were deposited during a further period of submersion which affected a portion of the peninsula

(vii) The Terrace deposits, made of sands and silty sands deposited after repeated lifting and lowering of the mean sea level

The underground of the Salento Peninsula is characterized by a rather complex hydrodynamics, from the hydrogeological perspective, as the abovementioned units set the framework for a multilayered system, where the main groundwater body is represented by the deep, karst aquifer hosted in the Altamura limestone sediments [28, 36, 46, 47]. Such aquifer, indeed, is the widest one and the most exploited for human activities. Over the whole peninsula, this aquifer takes the shape of a lens floating above saltwater, with a maximum thickness in the center of the peninsula. Since this aquifer is characterized by a high degree of permeability, mostly related to the karstic nature of its sediments, the piezometric head stands at heights which range between the mean sea level (at the coastline) and about 4 m above the mean sea level (msl). Furthermore, the deep
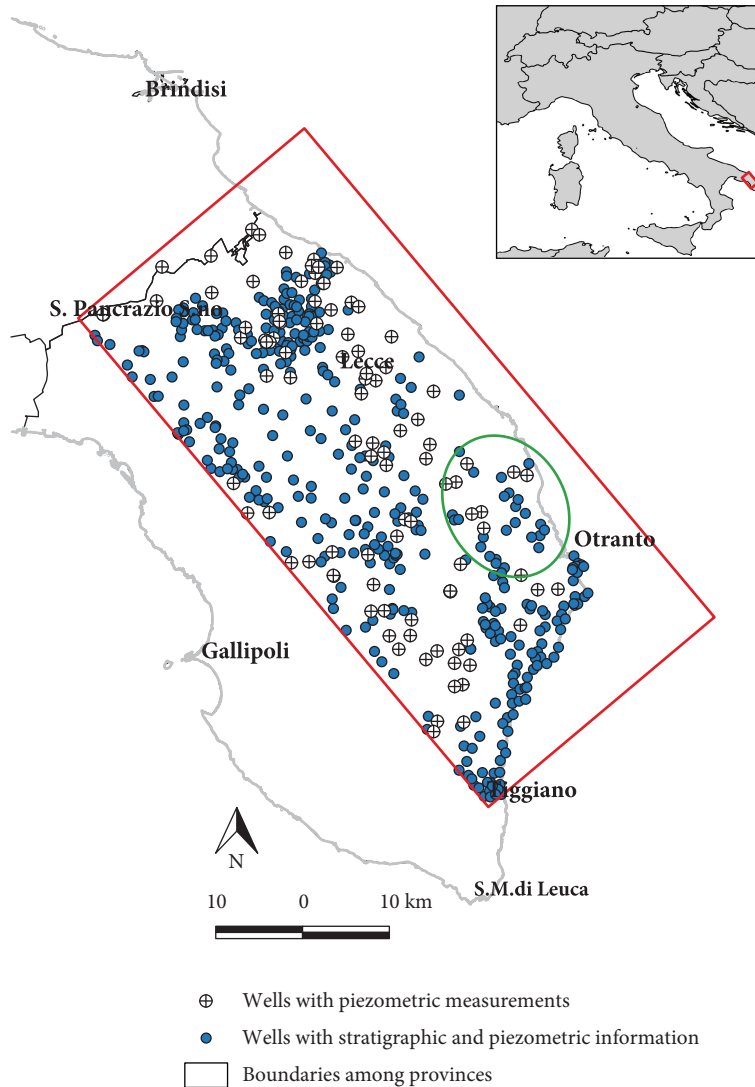
FIGURE 1: Location and extent of the study area and location of the wells where lithostratigraphic and piezometric information was available. The green circle indicates an area where the reconstruction of the stratigraphic setup needed specific data processing.

aquifer is mostly phreatic in the central-western part of the region, while the top of the Altamura limestone stands at hundreds of meters below msl in the eastern portion, where the aquifer is mainly confined.

Some local aquifers can be found in the Plio-Pleistocene sediments, mostly located at topographically depressed locations. However, these can be hardly identified, due to the heterogeneous permeability characteristics of the lithotypes which make up these sediments. For this reason, the analysis presented in this paper refers to the deep aquifer only, while the contribution of the overlying units to the vertical component of the hydraulic flow was taken into account while evaluating the rainfall recharge term.

The Galatone unit, residual deposits, and the Subappennine clays are made of poorly permeable sediments. As such, from a hydrogeological point of view, they mainly act as aquitards.

Figure 2 reports a lithological map of the southern part of the Salento Peninsula (Lecce province) and four schematic cross sections of the complex hydrostratigrahic setup. Table 1 reports a list of the lithostratigraphic units identified, along with their lithological and hydrogeological features.

3. Materials and Methods

This section reports a thorough discussion about the reconstruction of the stratigraphic setup, the hydrogeological conceptual model, and the setting up of the density-dependent flow model in the study area.

Model results will be discussed in detail in the following section, where a management strategy proposal based on a MAR scheme and insights about the major criticalities identified will be presented as well.

3.1. Reconstruction of the Stratigraphic Setup. The geometry of the underground in the study area was inferred from interpolation of an integrated dataset, consisting of point lithostratigraphic data reported in Margiotta and Negri [29]

(a)

(b)
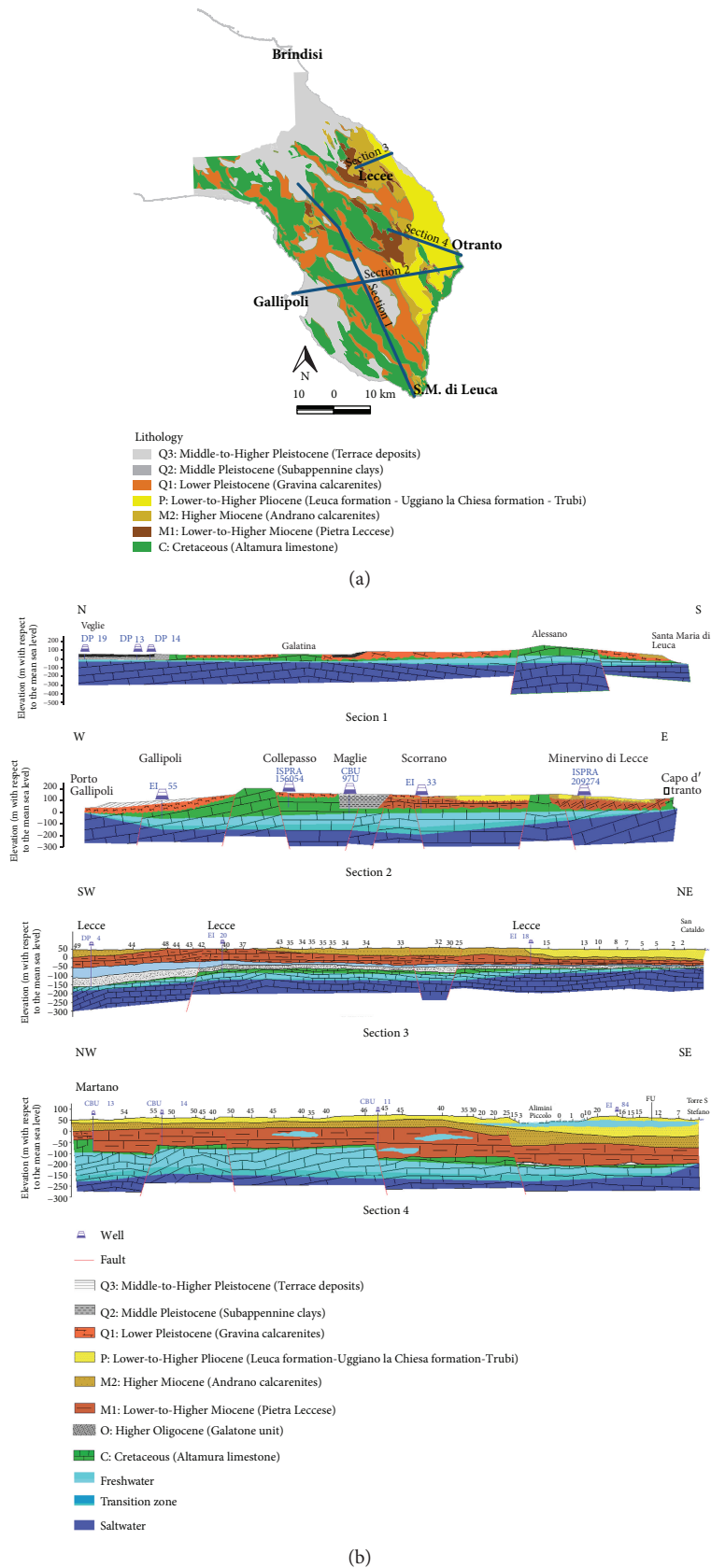
FIGURE 2: (a) Lithological map of the southern part of the Salento Peninsula. (b) Hydrostratigraphic cross sections along profiles drawn in subfigure (a). Fill colors and legend items are the same in both subfigures.

TABLE 1: List of the lithostratigraphic units identified and their hydrogeological characteristics (modified after De Filippis et al. [33]).

Lithostratigraphic unit	Lithological features	Geological age	Hydrogeological characteristics
Altamura limestone	Limestones and dolomitic limestones	Cretaceous	Fractured and karst main aquifer
Galatone unit	Compact limestones, marls, and sandy clay	Oligocene	Generally impermeable deposits
Miocene unit	Calcarenites and marly limestones	Miocene	Porous aquifers
Pliocene unit	Breccias and calcareous conglomerates	Pliocene	Porous aquifers
Gravina calcarenites	Biodetritic calcarenite	Lower Pleistocene	Porous aquifers
Subappennine clays	Clays	Lower to Middle Pleistocene	Aquitard
Terrace deposits	Sands and silty sands	Upper Pleistocene	Porous shallow aquifers

and cross sections produced at the Laboratory of Hydrogeo-physics and Stratigraphy for Natural Hazards of the University of Salento. The whole dataset is made of 504 points reported in Figure 1. At each point, values of the top elevation of the Altamura limestone and values of the thicknesses of the overlying lithostratigraphic units are available. Such values were processed by interpolation with the kriging method over a grid of square cells 20 m × 20 m wide.

A critical area (circled area in Figure 1) was highlighted. At this location, indeed, the interpolation of the top elevation of the Altamura limestone resulted in a surface intersecting the thickness of the overlying Galatone unit. To overcome this inconsistency, the top elevation of the Altamura limestone at those points was inferred by subtracting the thicknesses of the overlying units from the elevation of the ground surface.

Figure 3(a) reports the resulting top elevation of the deep aquifer, while Figure 3(b) shows the ratio among the thicknesses of the lithostratigraphic units identified in the study area, along a SW-NE profile. As stated in the section above, two portions can be identified in the study area: (i) the one along the coastline, where the top elevation of the deep aquifer is far below the msl and the aquifer is confined, and (ii) the western portion, where the Altamura limestone locally outcrops and the aquifer is unconfined.

The color map reported in Figure 3(a) allows identifying three important graben structures at least: the one located near Lecce, the one between Cavallino and the area south of Vernole, and the one in the Otranto area. A rather clear horst, NW-SE oriented, intersects the line which roughly connects Lecce and San Cataldo. The major faults drawn in red are mainly NW-SE oriented, even if some NE-SW oriented faults can be identified too. These findings are in accordance with results found in Grassi et al. [39] and Margiotta and Negri [38].

3.2. Hydrogeological Conceptual Model. In order to define the hydrogeological conceptual model in the study area, the hydrodynamics of the deep aquifer inferred from piezometric head measurements at some of the abovementioned points (96 cross-shaped points in Figure 1) was analysed. The available head values refer to the static level measured when the wells were drilled, between 1952 and 1987, and belong to a database managed at the Laboratory of Hydrogeophysics and Stratigraphy for Natural Hazards of the University of Salento. Piezometric measurements collected after 1987, mostly belonging to databases managed by the regional authority and other organizations, are not readily available. As such, it was not possible to perform an in-depth evaluation of the evolution of the deep hydrodynamics in time. Consequently, all results reported in the following intend to describe an average hydrogeological state for the deep aquifer on the regional scale.

Figure 4 reports the contour lines obtained by interpolation of the available head values through the kriging method over a grid of square cells 20 m × 20 m wide.

From contour lines in Figure 4, the following can be inferred about the hydrodynamics of the deep aquifer in the study area. The piezometric head values generally range between about 3 m above msl in the central part of the area, and 0 m with respect to msl at the southern portion of the coastline. A local maximum (head values up to 4 m above msl) can be detected near Otranto. This could be related to the occurrence of possible superficial aquifers hosted in the overlaying sediments of the Mio-Pliocene units or to the presence of a watershed beyond the coastline or also to the complex geometry of the deep aquifer in that zone, as highlighted in the previous section. As stated above, this was also reported in the previous studies [39, 40], but the reason for this phenomenon has not yet been investigated. By the way, in the absence of detailed lithostratigraphic information and updated piezometric data in this area, no conclusions can be drawn about this occurrence and a deeper insight in this issue on the local scale is necessary.

Arrows in Figure 4 indicate inflow and outflow components across the boundary of the study area, due to sink and source terms. These allow conceptualizing the hydrodynamic behaviour of the deep aquifer and identifying inflows and outflows to the system through the boundaries. These are related to (i) infiltration from the northwestern corner of the active domain, (ii) infiltration through the central-eastern part of the Adriatic coast, (iii) outflow through the remaining part of the coastline, with the exception of the abovementioned coastal area near Otranto, and (iv) outflow through the western boundary. Furthermore, the groundwater budget is also affected by (v) effective infiltration of precipitation (I_p), (vi) the recharge action due to karst depressions locally known as "vore" (v), (vii) evapotranspiration (EVT), and (viii) abstractions for drinking and irrigation purposes (Q).

(a)

(b)
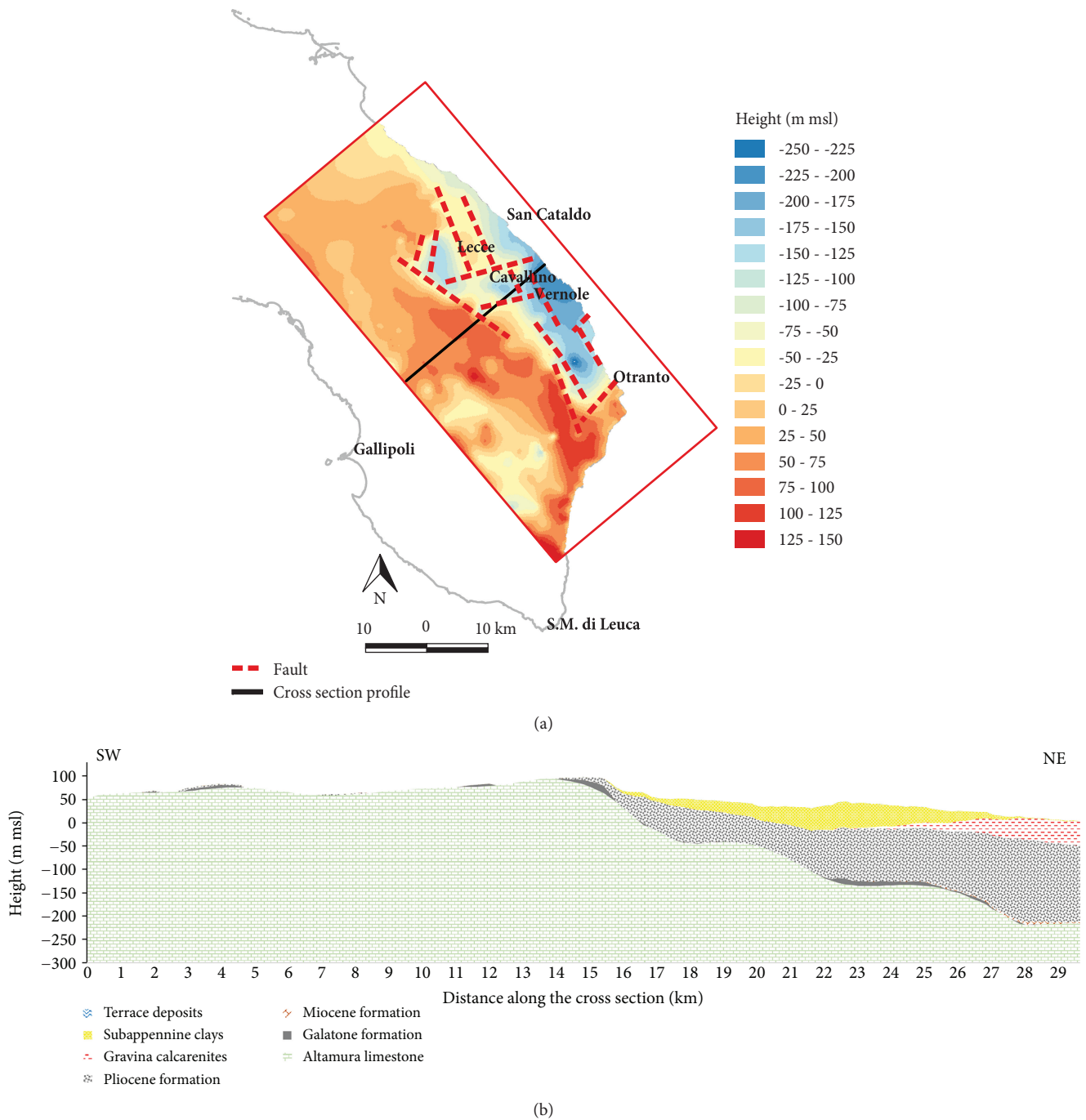
FIGURE 3: (a) Top elevation of the deep aquifer. (b) Stratigraphic cross section along the SW-NE profile drawn in subfigure (a).

An important mechanism of recharge for the aquifer is related to the effective infiltration of meteoric waters (I_p term in Figure 4) through the sediments of the overlying units. To estimate such contribution, evapotranspiration (EVT term in Figure 4) was also taken into account in the way specified below.

First of all, we estimated the average annual precipitation, P, by interpolating the average annual rainfall measured between 1952 and 1987 at 12 meteorological stations within the study area [48]. In the period considered, P values range

between 600 mm/year and 800 mm/year and increase from north-west to south-east.

To estimate EVT, we first determined potential evapotranspiration, based on the average air temperature and solar radiation at the study area, as expressed by the Thornthwaite method [49]. As a result, potential evapotranspiration in the period considered was worth on average 730 mm/year. We furthermore analysed the land use in the study area [32], which shows that the most widespread crop is olive. As a consequence, potential evapotranspiration

Hydrostratigraphic unit	w_i coefficients used to calculate C_{irf}
Altamura limestone	0.7
Galatone unit	0.2
Miocene units	0.4
Pliocene units	0.5
Gravina calcarenites	0.7
Subappennine clays	0.2
Terrace deposits	0.6
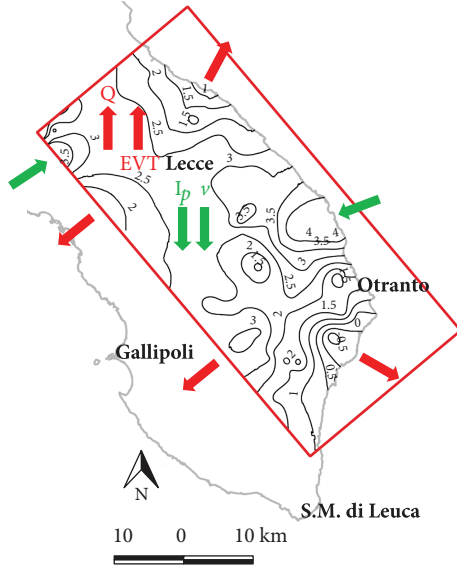
FIGURE 4: Hydrodynamics of the deep aquifer. Contour lines were obtained by interpolation of the available head data (values in m above msl; contour line interval: 0.5 m). Arrows indicate inflow (green arrows) and outflow (red arrows) to the aquifer across the boundary of the study area and due to sink and source terms.

was multiplied by 0.7, an average value for the olive K_c coefficient [50], resulting in efficient evapotranspiration (EVT) of 510 mm/year on average.

EVT was so subtracted to P and the hydraulic effect of the identified hydrostratigraphic units was further taken into account in the second step. This was done by multiplying the calculated quantity (P − EVT) by an infiltration coeffi-

cient, C_{irf}, which takes into account the thicknesses and the hydraulic behaviour of the Altamura limestone and of the units above it, as well as the morphological characteristics of the region.

Specifically, C_{irf} was calculated as the weighted average of the hydraulic behaviour of the identified hydrostratigraphic units and the thicknesses of such units were adopted as weights. The hydraulic behaviour of the Altamura limestone and of the units above was estimated through coefficients (Table 2) which account also for the morphological characteristics of the region. As an example, the value 0.7 adopted for the Altamura limestone takes into account either the good permeability of the sediments and the presence of hilly areas, mostly located in the southern part of the study area, where the Altamura limestone outcrops and runoff rates are higher than infiltration rates.

As such, I_p was calculated according to the following equation:

$$I_p = \begin{cases} 0.7(P - EVT), & \text{where the Altamura limestone outcrops,} \\ P, & \text{where major faults (Figure 3(a)) and "vore" (Figure 5) are located,} \\ (P - EVT) * C_{irf} = (P - EVT) * \dfrac{\sum_{i=1}^{6} t_i w_i}{\sum_{i=1}^{6} t_i}, & \text{elsewhere,} \end{cases} \tag{1}$$

where t_i is the thickness of one of the six units above the Altamura limestone and w_i is the associated coefficient (Table 2).

As widely reported in the geomorphological maps of the Salento Peninsula (consult, e.g., the regional geoportal SIT Puglia; http://www.sit.puglia.it/), the occurrence of karst sinkholes is widespread in the region. These are locally known as "vore" and contribute to the recharge component of the deep aquifer (v term in Figure 4). 71 "vore" may be located within the study area (Figure 5), and we assumed that the local recharge contributed by these sinkholes was equal to the rainfall rate at the location of each of them.

Abstraction terms (Q term in Figure 4) were also taken into account. These are mostly intended to meet the water demand for irrigation and drinking purposes. Since several

illegal wells can be found in the region and since no monitoring on abstraction rates is performed for the legal ones, these terms were evaluated based on estimations available in Regione Puglia & Autorità di Bacino della Puglia [27]. According to such estimates, the water needs for irrigation purposes in the Adriatic portion of the Salento Peninsula is about 84.5 Mm³/year. Such rate has been equally distributed among 15 fictitious wells located into the irrigated districts within the study area. Similarly, in the abovementioned report, the total abstraction rate for drinking purposes in the Adriatic part of the Salento Peninsula is estimated to be about 63.8 Mm³/year. This was equally distributed among the 62 legal drinking wells scattered in the study area. Figure 5 shows the location of abstraction wells in the study area.
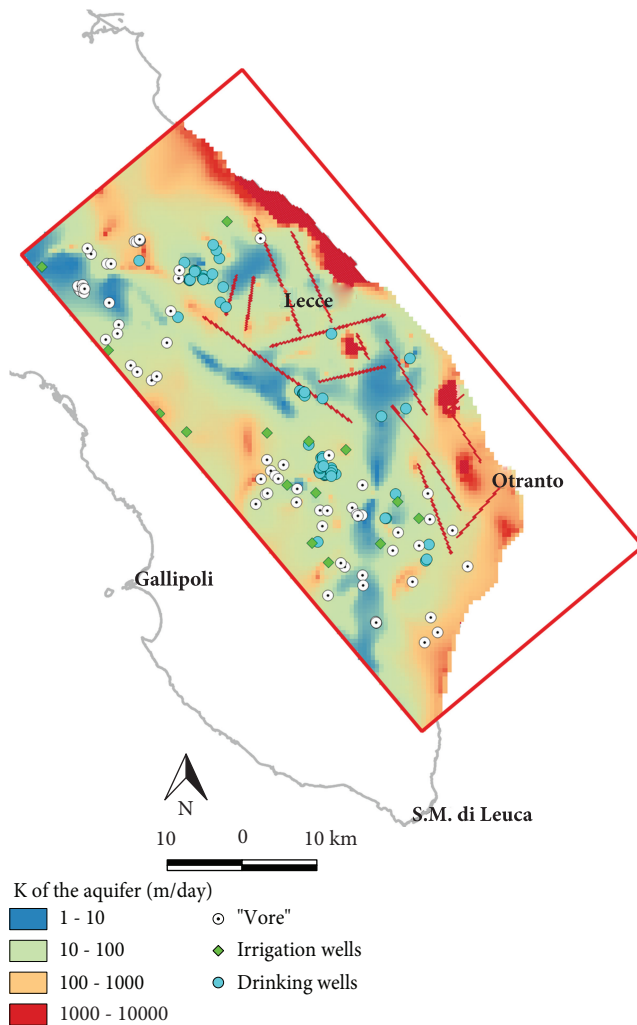
FIGURE 5: Location of irrigation and drinking pumping wells and "vore." The color map refers to the horizontal hydraulic conductivity distribution used for the deep aquifer in the modelling approach.

3.3. The Modelling Approach

3.3.1. Objectives and Assumptions. The objective of the present work is to characterize the deep aquifer of the Adriatic portion of the Salento Peninsula from a quantitative point of view, as well as with regard to groundwater salinization, by means of modelling tools for the simulation of groundwater dynamics with MODFLOW-2005 [41] and the saltwater intrusion phenomenon with SEAWAT [42]. The motivations behind such analysis are related to several environmental issues which affect the hydrogeological equilibrium of an aquifer which represents the major source of freshwater in a karstic region characterized by poor surface water potential. The model developed is thus intended to represent a starting point for further enhancements, in view of providing a tool for groundwater management in the area.

Specifically, this analysis is aimed at:

(i) identifying the main processes which affect the groundwater flow dynamics

(ii) detecting the areas potentially affected by saltwater intrusion

(iii) identifying the areas where the lack of data prevents a proper comprehension of the hydrogeological processes investigated

(iv) highlighting criticalities which prevent a deep comprehension of the hydrogeological system under exam and set the stage for further investigations

For the aims listed above, the model was developed on a regional scale.

The following assumptions hold true in this paper.

The available head data did not allow investigating the evolution of the aquifer system in time, i.e., to evaluate the change in time of the amount of water stored in the domain. As such, a simplified investigation of the groundwater flow dynamics was carried out, by adopting a steady-state flow approach. With this assumption, we were able to describe an average hydrogeological state for the deep aquifer, i.e., to provide a "picture" of the groundwater flow dynamics, which could represent a starting point for further investigations of transient flow conditions. By the way, even if the flow component was run in steady-state conditions, there is no option in the SEAWAT code to run the transport component as steady state [51]. This is because the transport component in the SEAWAT engine has either stability constraints and/or accuracy requirements that are more restrictive than those for the flow component. As such, each flow time step is further divided into smaller transport steps, during which heads are constant. As a consequence, in the application of the SEAWAT code for the simulation of density-dependent flow, the transport model was run in transient conditions. The same approach was already adopted for another portion of the Salento Peninsula by De Filippis et al. [34].

Another important assumption is the adoption of the "equivalent porous medium" approach, which allows modelling the karst, fractured, deep aquifer of the study area as a continuous, porous medium, instead of a dual-porosity medium. The equivalent porous medium approach involves the replacement of the fractured medium by a representative continuum in which spatially defined values of its hydraulic properties can be assigned [52, 53]. This approach is valid as long as the fracture spacing is sufficiently dense that the fractured medium acts in a hydraulically similar fashion to granular porous media. Besides the density of fractures and the degree of interconnection among them, the spatial scale of the analysis is fundamental for this choice. As stated in Scesi and Gattinoni [54], treating a karst, fractured medium like an equivalent porous medium can be justified in case of a large scale analysis. In such case, the equivalent porous medium approach can provide reliable results if the scope of the analysis is to infer the groundwater flow dynamics and flow-related processes on a large scale.

The equivalent porous medium approach is being widely adopted to simulate groundwater flow in karst systems all over the world [46, 55] and in the region under exam [28, 31–36].

In this contribution, we made a step forward with respect to the previous modelling studies referred to the deep aquifer of the Salento Peninsula. As stated in Scesi and Gattinoni [54], indeed, the optimal solution to model the behaviour of karst aquifers is to use the equivalent porous medium approach accounting also for the occurrence of structural features (e.g., fractures), which have an important role on the hydrodynamics of such systems. To accomplish this task, we modelled the main fractures recognized on the regional scale (red dotted lines in Figure 3(a)) as zones which contribute higher infiltration rates to the aquifer system.

3.3.2. Groundwater Flow Model Setup. The groundwater flow model was developed by applying the finite-difference approach adopted in MODFLOW-2005 [41] for porous aquifers. To this aim, at the scale of the present analysis, we assumed that the sediments of the Altamura limestone are characterized by a high fracture density and that fractures have small openings. With this assumption, it is possible to treat the deep, karst aquifer under exam as an equivalent porous medium. In addition, the role of major fractures was modelled by introducing zones where higher infiltration rates occur. Further details will be provided below.

The MODFLOW model was set up and run using FREE-WAT [43–45] as a graphical user interface integrated in QGIS [56]. The FREEWAT platform allows simulating several water-related processes (e.g., hydrodynamics, solute transport, and conjunctive use of ground- and surface-water) for integrated water management, by coupling the power of GIS tools for spatial data analysis and that of free and open source numerical codes (e.g., MODFLOW and MODFLOW-related programs).

The study area was discretized using a rotated, regular grid made of square cells 200 m × 200 m wide. For the aims of the groundwater flow model, the deep aquifer was represented using a single model layer extending from the top surface reported in Figure 3(a) to 500 m below msl. As explained in the next section dedicated to saltwater intrusion, such layer was then discretized through 7 sublayers, in order to properly simulate the hydrodynamic dispersion mechanism, which occurs on a finer scale with respect to the advection process.

For the horizontal hydraulic conductivity of the model layer, the distribution obtained by inverse calibration by De Filippis et al. [32] was used. Such distribution was obtained through the application of the Comparison Model Method (CMM) [57–60], which is based on the solution of a forward problem for a "comparison model," namely, with a hypothetical (often uniform) conductivity field. The fluxes computed for the "comparison model" are assumed to be a good approximation of the "real" ones, estimated as the product of the "real" transmissivities and the hydraulic gradients inferred from interpolation of field data. Then, the "real" hydraulic conductivity field can be obtained from this comparison. Figure 5 shows values ranging 10-10^2 m/day inland, while values of the order of 10^3-10^4 m/day were estimated along the coastline. As stated above, a step forward was made to account for major faults in the study area (red dotted lines in Figure 3(a)). In this regard, the highest K values (of the

order of 10^4 m/day) were also set along the profiles of such faults, in order to model zones where higher infiltration rates occur.

We further assumed that the aquifer presented vertical anisotropy only, by assuming for the vertical hydraulic conductivity values equal to 1/10 of the horizontal one.

In order to define boundary conditions, the contour lines reported in Figure 4 were analysed. Specifically, the inflow/outflow components through the western boundary were represented as head-dependent boundary conditions through the application of the General Head Boundary (GHB) MODFLOW package [41]. The same package was also applied to reproduce the hydraulic contact with the Adriatic Sea along the coastline. To this aim, different pieces of the coast were distinguished, and the contact between the deep aquifer and the sea at each piece was supposed to occur between 0 m and 200 m far from the coastline. Furthermore, the northern boundary of the study area was treated as a no-flow boundary. The same was assumed at the base of the model, meaning that no vertical water exchange occurs at the bottom of the deep aquifer.

Source and sink terms related to effective infiltration, local "vore," and abstractions for irrigation and drinking purposes, respectively, were estimated as explained in the previous subsection (Figure 5). The Recharge MODFLOW package was applied for effective infiltration, as specified in the above section. The Well MODFLOW package was used for "vore" (positive flow rates) and abstraction wells (negative flow rates).

The model was run over a steady-state stress period 365 days long.

A sensitivity analysis was performed using UCODE_2014 [61] integrated in the FREEWAT platform as well. Specifically, the Composite Scaled Sensitivity (CSS) index [62] was evaluated to assess the information content of the whole head dataset (cross-shaped points in Figure 1) for the estimation of the most sensitive parameters. Figure 6 reports results of the sensitivity analysis, which included the following parameters:

   (i) The recharge flux related to effective infiltration (rch in Figure 6)

  (ii) The abstraction rates for irrigation and drinking purposes (wells in Figure 6)

 (iii) The horizontal and vertical components of the hydraulic conductivity of the deep aquifer (kxx and kzz in Figure 6)

 (iv) The inflow/outflow terms related to the GHB boundary condition (ghb_cond in Figure 6)

As highlighted in Figure 6, the model fit is insensitive to variations of the vertical hydraulic conductivity, meaning that the available head data does not contain enough information for the estimation of the kzz parameter. On the contrary, the most sensitive parameters are the recharge flux (rch) and the horizontal component of the hydraulic conductivity (kxx), while the sensitivities of
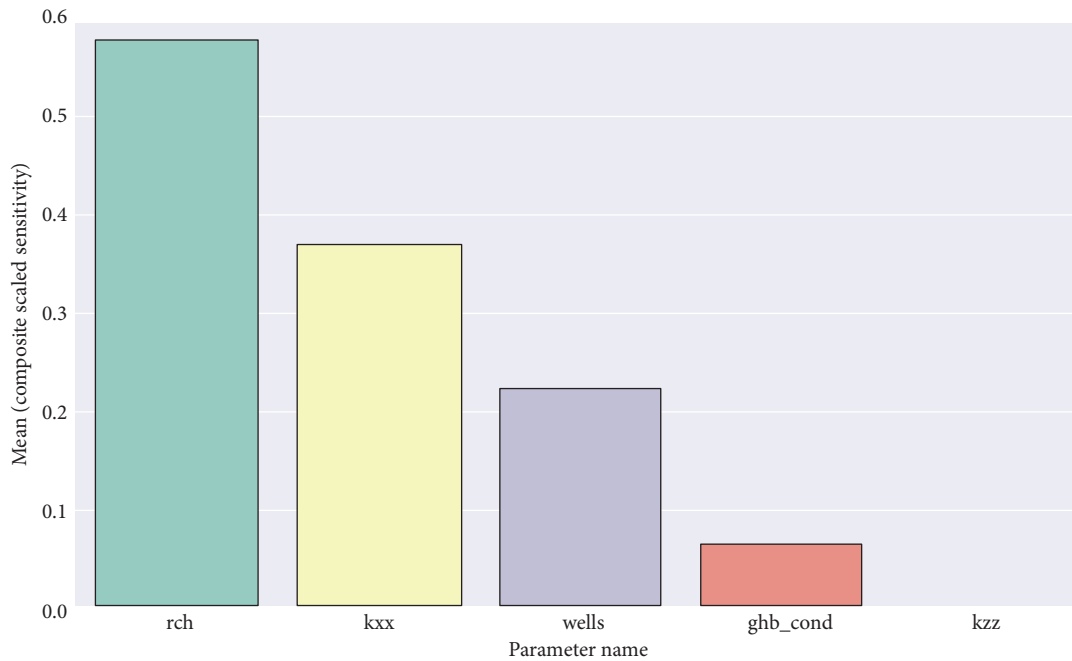
Figure 6: Values of the Composite Scaled Sensitivity for the model parameters considered as the most sensitive ones.

parameter wells are worth about 1/3 of the maximum CSS and the sensitivity of ghb_cond is worth about 1/9 of the maximum CSS. As such, the parameter kzz was not included in the trial-and-error calibration of the remaining parameters, whose results are reported in the following section.

3.3.3. Density-Dependent Flow Model Setup. In order to get an insight on groundwater salinization, the groundwater flow model was applied to simulate the saltwater intrusion phenomenon. This was accomplished by developing a density-dependent flow model to assess the extent of lateral intrusion and vertical upconing of saltwater, applying the SEAWAT code [42], which is integrated within the FREEWAT platform as well.

To this aim, the deep aquifer was further discretized through 7 sublayers with equal thickness, in order to properly simulate the hydrodynamic dispersion mechanism, which occurs at a finer scale with respect to the advection process [51].

The following parameters were set for the deep aquifer to solve the solute transport component:

(i) Effective porosity: 0.1

(ii) Coefficient of molecular diffusion: 10^{-5} m^2/day

(iii) Longitudinal dispersivity: 200 m

(iv) Transverse dispersivity: 20 m

(v) Vertical dispersivity: 20 m

A concentration of 38 g/l was assigned at cells along the coastline, where the GHB MODFLOW package was applied.

Concentration values were left free to vary at the remaining grid cells.

The model was run over 10 years. At this stage, it was not possible to calibrate the model, due to the lack of good-quality concentration data.

4. Results and Discussion

4.1. Results of the Groundwater Flow Model. As mentioned in the previous section, the groundwater flow model was calibrated adopting a trial-and-error approach over the most sensitive parameters. All parameters reported in Figure 6, except for kzz, were included in the calibration procedure, aimed at improving the model fit with respect to the observed piezometric head values measured at the cross-shaped points in Figure 1. The scatter plot of observed vs. simulated head values is reported in Figure 7 along with statistics on residuals (i.e., the difference between observed and simulated values).

We can infer from Figure 7 that all points are within the 90% confidence interval. Furthermore, the model fit differs for about 0.04 m on average from the observations, with a standard deviation of 0.35 m. Also, the absolute residual mean is about 0.29 m, with a standard error of the estimate of about 0.04 m.

Figure 8(a) reports the simulated piezometric head distribution. With respect to contour lines reported in Figure 4, we can infer that the general trend (i.e., inflow and outflow components) was reproduced by the model. Of course, since abstractions in the model were derived from assumptions and estimates, the local minima displayed in Figure 4 could not be reproduced. Despite this, taking into account the statistics reported in Figure 7, model results can be considered satisfactory in reproducing the involved processes.

(a)

Residual statistics	Value
Residual count	96
Mean	0.04
SD	0.35
Min	-0.66
Max	0.81
Absolute residual mean	0.29
Standard error of the estimate	0.04
Residual RMS	0.04
Normalized RMS	0.04
Pearson correlation coefficient	0.01

(b)
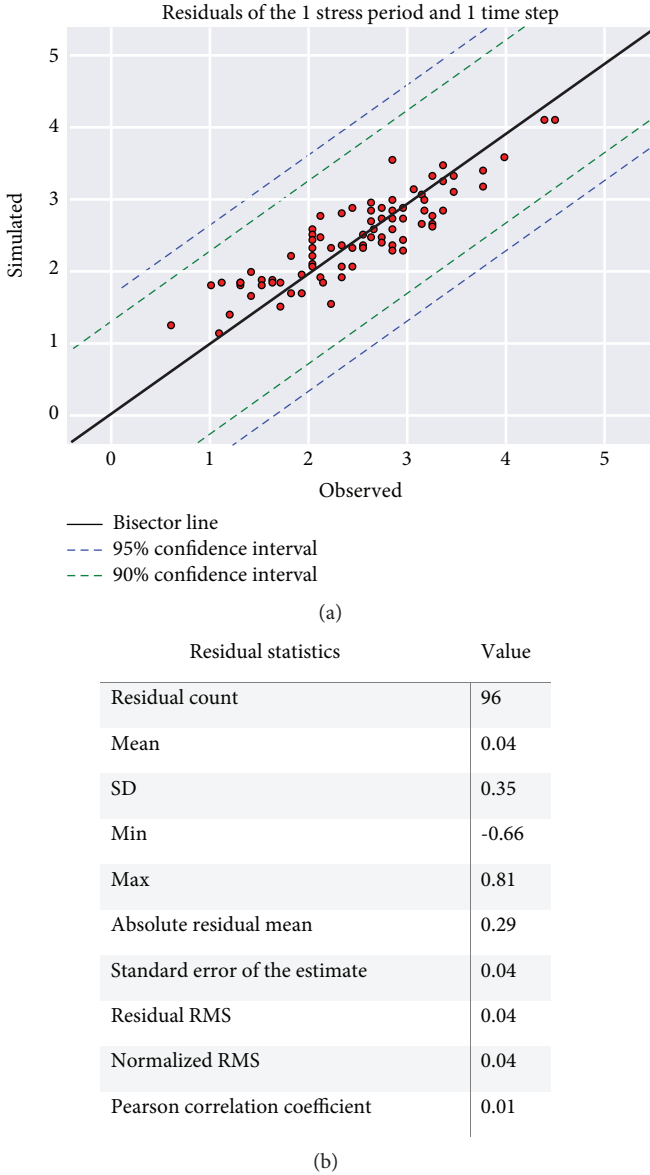
Figure 7: Comparison between observed and simulated head values and statistics on residuals.

Through interpreting the map in Figure 8(a) with the support of the model budget reported in Table 3, the following can be stated:

(i) Inflow and outflow terms can be identified through the GHB boundaries of the active domain. Altogether, inflow terms are worth about 8.24 Mm³/day, including the inflow occurring across the coast near Otranto; outflow terms are worth about 10.22 Mm³/day

(ii) The source term related to effective infiltration contributes to the overall budget with about 2.48 Mm³/day

(iii) The pumped groundwater is about 0.52 Mm³/day

Regarding the high head values recorded north of Otranto (up to 4.2 m above msl), we must notice that these have been repeatedly highlighted in the past, e.g., by Zorzi and Reina [40], Grassi et al. [39], Giudici et al. [28], and De Filippis et al. [32]. By the way, possible reasons for this phenomenon have never been explored. Cotecchia et al. [31] highlight three areas characterized by high head values along the NE-SW oriented line which roughly connects Otranto and a zone south of Gallipoli. A similar finding has been reported recently by Fidelibus and Pulido-Bosch [63]. This line corresponds to a major discontinuity feature, and the high head values detected would therefore have a structural cause and would generate drainage both towards the north and the south, determining a hydrogeological watershed. In any case, the presence of this watershed, with particular reference to the one located north of Otranto, puts in crisis the models [64] according to which the Salento Peninsula is almost entirely crossed by a hydrogeological watershed NW-SE oriented in its central part.

In any further study dedicated to this topic, a very important aspect that must be taken into account is linked to the eustatic oscillations that have affected the Salento Peninsula in the past 20000 years [65]. In fact, it cannot be excluded that the high head values detected north of Otranto are linked to the presence of freshwater trapped in tectonic grabens, due to the rising of the sea level [66–69] and for the presence of impermeable Miocene and Pliocene clayey deposits.

Taking steps from the previous theories [70], a recent study [71] analysed the occurrence of offshore fresh groundwater at 27 coastal areas worldwide, using an analytical model for estimating the extent of such occurrence. Two main drivers of such phenomenon are identified: (1) the presence of entrapped paleofreshwater during periods characterized by lower sea levels and (2) freshwater discharge from onshore aquifers to subsea aquifers under current sea level conditions. In both cases, the onshore-offshore coastal aquifer is conceptualized with an aquitard extending from the coastline offshore, which prevents vertical exchange between freshwater and saltwater, and a potentiometric surface which declines to the sea level offshore, far from the coastline. Based on the review of the 27 case studies, seven conceptual models were developed to show in both cases (options (1) and (2) above) the effects of groundwater pumping, which may result in pumping freshwater or saltwater according to the equilibrium of the interface in the offshore part of the aquifer.

The groundwater flow model was validated using a dataset of piezometric head values collected at 6 points in 2018 (Figure 8(b)). According to residuals statistics, the model fit differs for about 0.07 m on average from the observations, with a standard deviation of about 0.22 m. Also, the absolute residual mean is about 0.20 m, with a standard error of the estimate of about 0.10 m. This confirms that the model developed represents a valuable tool and a good starting point for further enhancements, as it is able to reproduce the physical processes for which the available observations contain information.

(a)

Residuals of the 1 stress period and 1 time step

— Bisector line
-- 95% confidence interval
-- 90% confidence interval
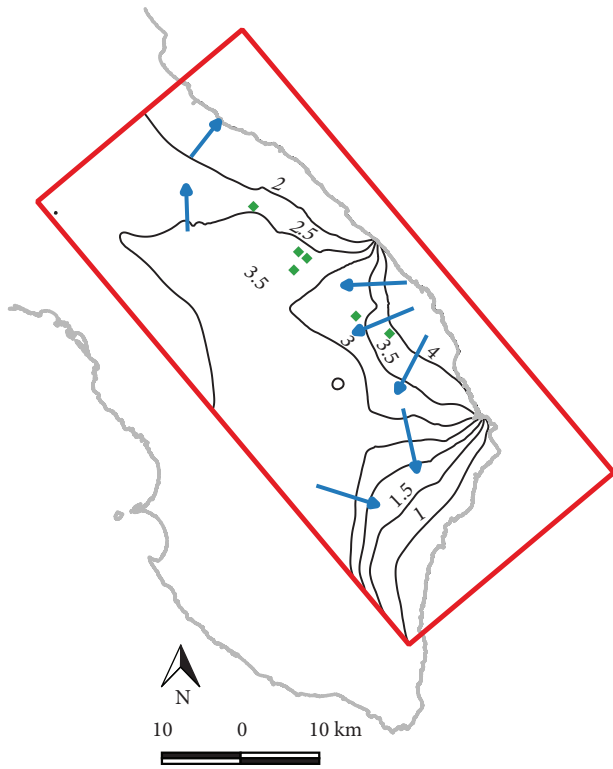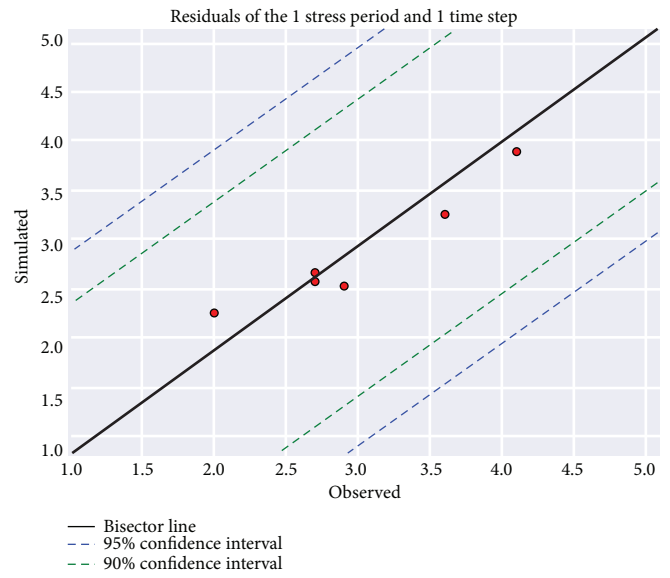
Residual statistics	Value
Residual count	6
Mean	-0.07
SD	0.22
Min	-0.29
Max	0.35
Absolute residual mean	0.20
Standard error of the estimate	0.10
Residual RMS	0.07
Normalized RMS	0.07
Pearson correlation coefficient	0.03

(b)

(c)

FIGURE 8: (a) Simulated piezometric head (values of contour lines are expressed in m above msl; contour line interval: 0.5 m; arrows reproduce the flow lines). Green dots indicate the location of wells used for model validation. (b) Results of model validation and statistics on residuals. (c) Effects of the application of a MAR scheme.

TABLE 3: Simulated water budget.

Inflow terms	Simulated flow rate (Mm³/day)	% over the total inflow	Outflow terms	Simulated flow rate (Mm³/day)	% over the total outflow
Recharge due to "vore"	$2.73 * 10^{-3}$	Negligible			
Effective infiltration	2.48	23			
Inflow through model boundaries	8.24	77	Outflow through model boundaries	10.22	95
			Abstractions	0.52	5
Total	**10.74**		Total	**10.74**	

The groundwater flow model was applied to simulate the effects of a MAR facility on the quantitative status of the deep aquifer in the study area, as well as with regard to groundwater salinization. Specifically, an increase of the piezometric head in the deep aquifer was assessed, by setting up five injection wells located about 3 km far from a wastewater treatment plant in Lecce and about 4 km far from the coastline. Each of these wells was assigned a recharge rate of 40 l/s, resulting in a total infiltration rate of 200 l/s (about 6.31 Mm³/year). Based on estimates made by the local land reclamation authority, this corresponds to the yearly volume of water treated in the wastewater treatment plant and discharged towards the sea.

According to this scenario with the infiltration wells in operation, an increase in the simulated piezometric head was simulated. Such increase is worth about 0.12 m at the location of the recharge wells. Furthermore, an increase of at least 0.03 m would be recorded over an area of about 2.3 km² (Figure 8(c)).

4.2. Results of the Density-Dependent Flow Model. The extent of the saltwater intrusion phenomenon is presented in Figure 9 in terms of concentration distribution obtained at each sublayer in the density-dependent flow model. Such distribution is reported at different depths, and it is shown either in the horizontal or vertical directions, in order to assess the lateral extent and the vertical upconing of saltwater. Moreover, to make Figure 9(a) more readable, a concentration threshold was set to 0.5 g/l, as suggested in Cotecchia et al. [31].

We can infer from Figure 9(a) that saltwater gradually intrudes from the coast towards inland, driven by the hydrodynamic dispersion process. Also, the width of the strip where concentration values higher than 0.5 g/l were simulated is about 5 km in sublayer 1, while the intrusion front advances up to more than 6 km from the coast inland in sublayer 7. As a consequence of comments and results presented above, we can notice that the inflow component simulated in the Otranto area makes saltwater intrusion to affect that area to a higher extent with respect to the rest of the coastline. Furthermore, the effects of the regional faults taken into account within the model are clearly highlighted.

Figure 9(b) reports concentration values simulated for the deep aquifer up to 500 m below msl along a SW-NE profile near Lecce, crossing one of the regional faults. This cross section confirms the above results and clearly shows the effects of faults, which would cause upconing of seawater from below the bottom of the model.

Cross sections reported in Figure 10 are drawn along a profile which crosses one of the injection wells set in the model for MAR purposes. In particular, Figures 10(a) and 10(b) report concentration values simulated for the deep aquifer up to 500 m below msl before and after the application of the injection MAR wells, respectively. The location of an injection well is reported as well in Figure 10(b). At that location, the cone of injected freshwater results from the specific boundary condition set in the density-dependent flow model. With respect to the scenario reported in Figure 10(a), we can infer that setting in operation such a MAR scheme would result in containing the lateral saltwater intrusion phenomenon. In such case, the intrusion front would retreat by about 1 km.

5. Conclusions

This paper focuses on the Adriatic portion of the Salento Peninsula, where a major freshwater resource is represented by the deep, karst, coastal aquifer hosted in limestone sediments. Such aquifer is particularly sensitive to human impacts, climate change, and saltwater intrusion. Taking steps from the previous works [28, 32], the deep aquifer in the study area was characterized by means of modelling tools for the simulation of groundwater dynamics and the saltwater intrusion phenomenon.

The interpolation of the available piezometric data over the study area allowed conceptualizing the hydrodynamic behaviour of the deep aquifer and identifying inflows and outflows to the system through the boundaries and source/sink terms, which were then implemented in a groundwater flow model by applying specific MODFLOW packages.

The groundwater flow model was developed adopting two main limitations: (a) the model was run under steady-state conditions, due to the lack of piezometric data regularly recorded in time, and (b) the karst medium was modelled with an equivalent porous medium approach. A remarkable advancement with respect to the previous models included the representation of major structural features of the karst environment (i.e., faults), which affect the groundwater flow dynamics on the regional scale. These were modelled introducing zones where high infiltration rates occur.

As a result of the groundwater flow model, the budget terms mentioned above were quantified and the piezometric head distribution describing the hydrodynamics of the deep aquifer during an average hydrogeological year was obtained.

Particular attention deserves the high head values recorded north of Otranto which are responsible for the

(a)

(b)
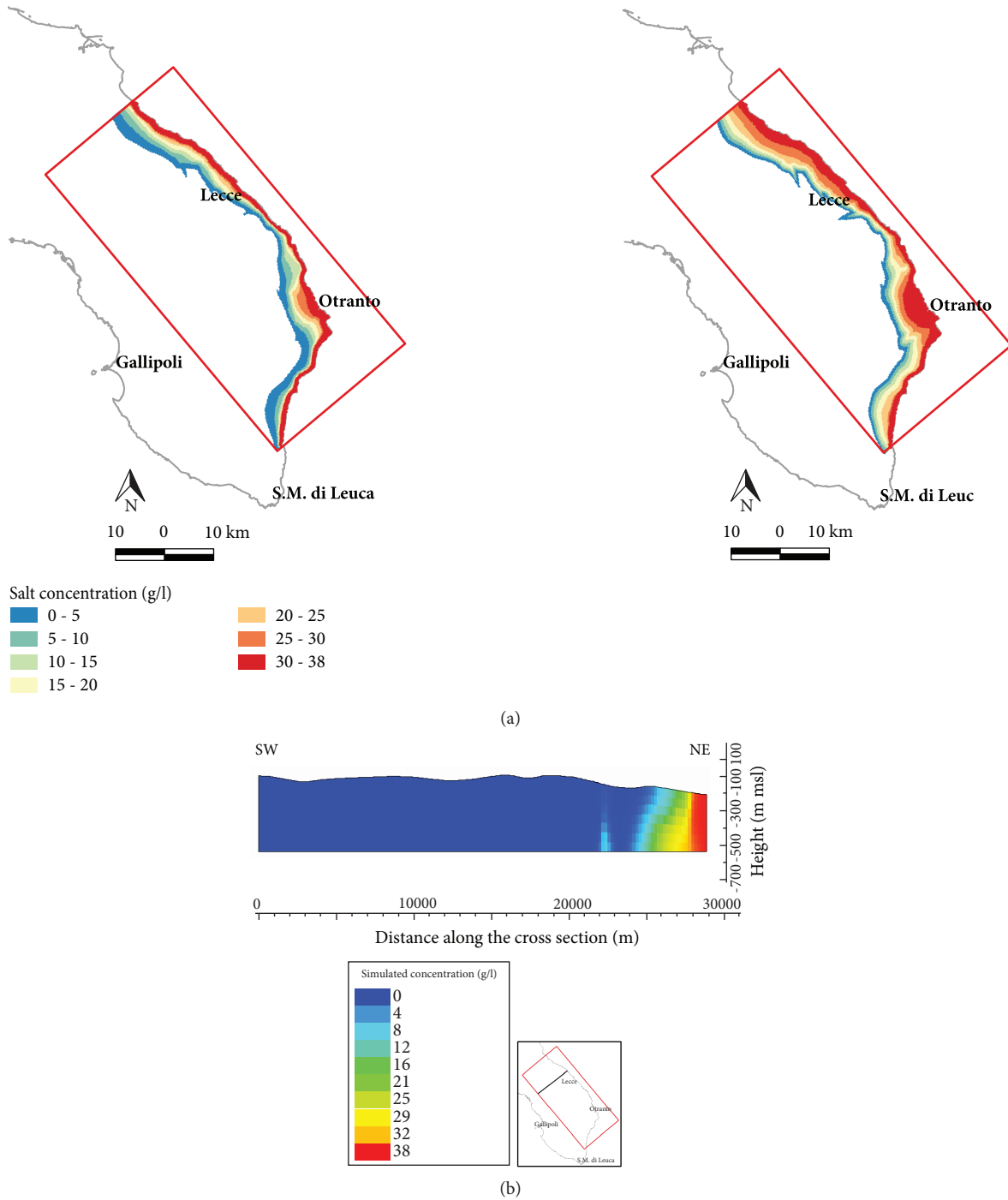
FIGURE 9: (a) Lateral saltwater intrusion simulated for sublayer 1 (left side) and for sublayer 7 (right side). (b) Vertical cross section along a SW-NE profile near Lecce.

infiltration term through the central-eastern part of the Adriatic coast. Such phenomenon has been widely highlighted in the past, but the causes still remain pretty uncertain. A discussion has been reported in this regard, about the role of structural features and of eustatic variations in the region. By the way, confirming the presence of such critical area puts in crisis all models according to which a hydrogeological watershed is clearly identified at the center of the Salento Peninsula. Of course, a thorough explanation

for this phenomenon has still to be found, but this discussion is a starting point for further research. Few lithostratigraphic and piezometric data, indeed, are available, but the results obtained deserve attention and set the stage for further investigations involving the drilling of new piezometers, whose measured values would help the understanding of the deep groundwater dynamics.

The groundwater flow model was applied to develop a density-dependent flow model for the assessment of the

(a)

(b)
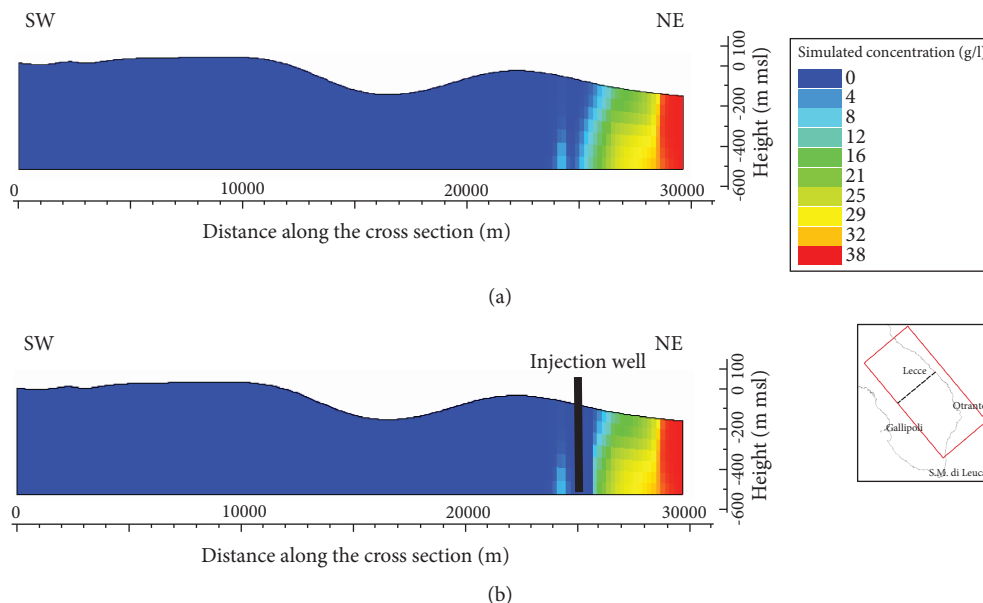
Figure 10: Vertical cross section along the SW-NE profile across one of the injection wells. (a) With injection wells inactivated. (b) With injection wells in operation.

saltwater intrusion phenomenon. With respect to the previous works, where a sharp-interface approach was adopted, the SEAWAT code was applied instead to assess the extent of lateral intrusion and vertical upconing of saltwater, resulting in worsening of irrigation and drinking water quality. The model was run over 10 years and allowed assessing that salt concentration values higher than 0.5 g/l would be detected up to 6 km from the coast inland. Results of the SEAWAT model allowed highlighting the role of regional faults in the upconing of saltwater and inferring that the critical zone near Otranto deeps particular attention as it would be affected by saltwater to a higher extent with respect to the remaining areas along the coastline.

A further application of these models consisted in simulating the effects induced by a MAR facility consisting in injecting treated wastewater produced by the treatment plant located in Lecce. This allowed evaluating the resulting piezometric head increase (up to 12 cm at the location of the injection wells) and the changes induced in the advancement of the saltwater intrusion front (this would retreat by about 1 km at the location of the injection wells). Such results make the methodology adopted a valuable tool, which can be replicated to propose further insights along the coast, testing the effectiveness of using rainwater and improving infiltration through the local "vore."

The methodology presented in this paper has a valuable importance from the environmental point of view, as it allowed assessing the quantitative status of the major freshwater resource available in the study area and in the whole Salento Peninsula and drawing conclusions about groundwater salinization. Such methodology allowed testing management and protection strategies based on efficient and up-to-date techniques, such as MAR solutions. Model results also allowed identifying areas where the lack of data prevents a proper comprehension of the hydrogeological processes

investigated, thus representing supporting tools for planning further monitoring campaigns. In this view, the research activities presented in this paper represent an advancement with respect to the previous works and lay the basis for further scientific investigations on this topic, aimed at characterizing the hydrogeological equilibrium of the deep aquifer in transient conditions and at undertaking further analysis on local scale.

Data Availability

The SpatiaLite database of the numerical model developed using the FREEWAT interface is available upon request.

Disclosure

This paper exploits results of the research activity carried on at the Laboratory of Hydrogeophysics and Stratigraphy for Natural Hazards of the Department of Biological and Environmental Sciences and Technologies of the University of Salento (Lecce, Italy), managed by prof. Sergio Luigi Negri. Such paper takes steps from the MSc thesis of Claudia Branca "Implementazione di un Modello di Flusso per la Gestione della Falda Profonda Carbonatica del Salento Adriatico mediante Applicazione della Piattaforma FREEWAT Integrata in GIS" ("Implementation of a Flow Model for Managing the Deep, Karst Aquifer of the Adriatic Part of the Salento Peninsula by Means of the Application of the GIS-Integrated FREEWAT Platform") (available in Italian language upon request).

Conflicts of Interest

The authors declare that there is no conflict of interest regarding the publication of this paper.

Acknowledgments

References

[1] W. Cramer, J. Guiot, M. Fader et al., "Climate change and interconnected risks to sustainable development in the Mediterranean," *Nature Climate Change*, vol. 8, no. 11, pp. 972–980, 2018.

[2] J. M. García-Ruiz, J. I. López-Moreno, S. M. Vicente-Serrano, T. Lasanta–Martínez, and S. Beguería, "Mediterranean water resources in a global change scenario," *Earth-Science Reviews*, vol. 105, no. 3-4, pp. 121–139, 2011.

[3] J. Lorenzo-Lacruz, C. Garcia, and E. Morán-Tejeda, "Groundwater level responses to precipitation variability in Mediterranean insular aquifers," *Journal of Hydrology*, vol. 552, pp. 516–531, 2017.

[4] M. Bakalowicz, "Karst and karst groundwater resources in the Mediterranean," *Environmental Earth Sciences*, vol. 74, no. 1, pp. 5–14, 2015.

[5] A. Hartmann, T. Gleeson, R. Rosolem, F. Pianosi, Y. Wada, and T. Wagener, "A large-scale simulation model to assess karstic groundwater recharge over Europe and the Mediterranean," *Geoscientific Model Development*, vol. 8, no. 6, pp. 1729–1746, 2015.

[6] N. Alfarrah and K. Walraevens, "Groundwater overexploitation and seawater intrusion in coastal areas of arid and semi-arid regions," *Water*, vol. 10, no. 2, p. 143, 2018.

[7] B. Tlili-Zrelli, M. Gueddari, and R. Bouhlila, "Spatial and temporal variations of water quality of Mateur aquifer (northeastern Tunisia): suitability for irrigation and drinking purposes," *Journal of Chemistry*, vol. 2018, Article ID 2408632, 15 pages, 2018.

[8] P. Venetsanou, K. Voudouris, N. Kazakis, and C. Mattas, "Impacts of urbanization, agriculture and touristic development on groundwater resources in the eastern part of Thermaikos Gulf (North Greece): an application of DPSIR model for sustainable development," *Eur Water*, vol. 51, pp. 3–13, 2015.

[9] L. Tadić, T. Dadić, and M. Leko-Kos, "Variability of hydrological parameters and water balance components in small catchment in Croatia," *Advances in Meteorology*, vol. 2016, Article ID 1393241, 9 pages, 2016.

[10] C. Petalas and N. Lambrakis, "Simulation of intense salinization phenomena in coastal aquifers—the case of the coastal aquifers of Thrace," *Journal of Hydrology*, vol. 324, no. 1-4, pp. 51–64, 2006.

[11] M. A. Somay and Ü. Gemici, "Assessment of the salinization process at the coastal area with hydrogeochemical tools and geographical information systems (GIS): Selçuk plain, Izmir, Turkey," *Water, Air, and Soil Pollution*, vol. 201, no. 1-4, pp. 55–74, 2009.

[12] M. A. Eissa, H. H. Mahmoud, O. Shouakar-Stash, A. El-Shiekh, and B. Parker, "Geophysical and geochemical studies to delineate seawater intrusion in Bagoush area, Northwestern coast, Egypt," *Journal of African Earth Sciences*, vol. 121, pp. 365–381, 2016.

[13] J. Hammami Abidi, B. Farhat, A. Ben Mammou, and N. Oueslati, "Characterization of recharge mechanisms and sources of groundwater salinization in Ras Jbel coastal aquifer (northeast Tunisia) using hydrogeochemical tools, environmental isotopes, GIS, and statistics," *Journal of Chemistry*, vol. 2017, Article ID 8610894, 20 pages, 2017.

[14] L. Jarlan, S. Khabba, S. Er-Raki et al., "Remote sensing of water resources in semi-arid Mediterranean areas: the joint international laboratory TREMA," *International Journal of Remote Sensing*, vol. 36, no. 19-20, pp. 4879–4917, 2015.

[15] D. Boubaya, "Combining resistivity and aeromagnetic geophysical surveys for groundwater exploration in the Maghnia plain of Algeria," *Journal of Geological Research*, vol. 2017, Article ID 1309053, 14 pages, 2017.

[16] T. McCormack, Y. O'Connell, E. Daly, L. W. Gill, T. Henry, and M. Perriquet, "Characterisation of karst hydrogeology in Western Ireland using geophysical and hydraulic modelling techniques," *Journal of Hydrology: Regional Studies*, vol. 10, pp. 1–17, 2017.

[17] A. Satriani, A. Loperte, V. Imbrenda, and V. Lapenna, "Geoelectrical surveys for characterization of the coastal salt-water intrusion in Metapontum forest reserve (southern Italy)," *International Journal of Geophysics*, vol. 2012, Article ID 238478, 8 pages, 2012.

[18] C. Leduc, A. Pulido-Bosch, and B. Remini, "Anthropization of groundwater resources in the Mediterranean region: processes and challenges," *Hydrogeology Journal*, vol. 25, no. 6, pp. 1529–1547, 2017.

[19] P. Dillon, P. Stuyfzand, T. Grischek et al., "Sixty years of global progress in managed aquifer recharge," *Hydrogeology Journal*, vol. 27, no. 1, pp. 1–30, 2019.

[20] C. Masciopinto, M. Vurro, V. N. Palmisano, and I. S. Liso, "A suitable tool for sustainable groundwater management," *Water Resources Management*, vol. 31, no. 13, pp. 4133–4147, 2017.

[21] J. P. Bonilla Valverde, C. Blank, M. Roidt, L. Schneider, and C. Stefan, "Application of a GIS multi-criteria decision analysis for the identification of intrinsic suitable sites in Costa Rica for the application of managed aquifer recharge (MAR) through spreading methods," *Water*, vol. 8, no. 9, 2016.

[22] N. Kazakis, "Delineation of suitable zones for the application of managed aquifer recharge (MAR) in coastal aquifers using quantitative parameters and the analytical hierarchy process," *Water*, vol. 10, no. 6, 2018.

[23] N. Kazakis, M. Spiliotis, K. Voudouris, F. K. Pliakas, and B. Papadopoulos, "A fuzzy multicriteria categorization of the GALDIT method to assess seawater intrusion vulnerability of coastal aquifers," *Science of the Total Environment*, vol. 621, pp. 524–534, 2018.

[24] O. Tzoraki, Z. Dokou, G. Christodoulou, P. Gaganis, and G. Karatzas, "Assessing the efficiency of a coastal Managed Aquifer Recharge (MAR) system in Cyprus," *Science of the Total Environment*, vol. 626, pp. 875–886, 2018.

[25] G. De Filippis, S. Margiotta, S. Negri, and M. Giudici, "The geothermal potential of the underground of the Salento peninsula (southern Italy)," *Environmental Earth Sciences*, vol. 73, no. 11, pp. 6733–6746, 2015.

[26] M. Polemio, P. P. Limoni, D. Mitolo, and R. Virga, "Il degrado qualitativo delle acque sotterranee pugliesi," *Giornale di Geologia Applicata*, vol. 3, pp. 25–31, 2006.

[27] Regione Puglia and Autorità di Bacino della Puglia, *Aggiornamento del Bilancio Idrogeologico dei Corpi Idrici Sotterranei della Regione Puglia. All. 4.10 alla Relazione Finale*, 2011, in Italian.

[28] M. Giudici, S. Margiotta, F. Mazzone, S. Negri, and C. Vassena, "Modelling hydrostratigraphy and groundwater flow of a fractured and karst aquifer in a Mediterranean basin (Salento peninsula, southeastern Italy)," *Environmental Earth Sciences*, vol. 67, no. 7, pp. 1891–1907, 2012.

[29] S. Margiotta and S. Negri, *Alla Ricerca dell'Acqua Perduta*, Congedo Editore, in Italian, 2004.

[30] M. Polemio, "Monitoring and management of karstic coastal groundwater in a changing environment (Southern Italy): a review of a regional experience," *Water*, vol. 8, no. 4, p. 148, 2016.

[31] V. Cotecchia, D. Grassi, and M. Polemio, "Carbonate aquifers in Apulia and seawater intrusion," *Giornale di Geologia Applicata*, vol. 1, pp. 219–231, 2005.

[32] G. De Filippis, M. Giudici, S. Margiotta, F. Mazzone, S. Negri, and C. Vassena, "Numerical modeling of the groundwater flow in the fractured and karst aquifer of the Salento peninsula (Southern Italy)," *Acque Sotterranee-Italian Journal of Groundwater*, vol. 2, no. 1, 2013.

[33] G. De Filippis, M. Giudici, S. Margiotta, and S. Negri, "Conceptualization and characterization of a coastal multi-layered aquifer system in the Taranto Gulf (southern Italy)," *Environmental Earth Sciences*, vol. 75, no. 8, 2016.

[34] G. De Filippis, L. Foglia, M. Giudici, S. Mehl, S. Margiotta, and S. L. Negri, "Seawater intrusion in karstic, coastal aquifers: current challenges and future scenarios in the Taranto area (southern Italy)," *Science of the Total Environment*, vol. 573, pp. 1340–1351, 2016.

[35] G. De Filippis, L. Foglia, M. Giudici, S. Mehl, S. Margiotta, and S. L. Negri, "Effects of different boundary conditions on the simulation of groundwater flow in a multi-layered coastal aquifer system (Taranto Gulf, southern Italy)," *Hydrogeology Journal*, vol. 25, no. 7, pp. 2123–2138, 2017.

[36] A. Romanazzi, F. Gentile, and M. Polemio, "Modelling and management of a Mediterranean karstic coastal aquifer under the effects of seawater intrusion and climate change," *Environmental Earth Sciences*, vol. 74, no. 1, pp. 115–128, 2015.

[37] T. Darwish, T. Atallah, M. El Moujabber, and N. Khatib, "Salinity evolution and crop response to secondary soil salinity in two agro-climatic zones in Lebanon," *Agricultural Water Management*, vol. 78, no. 1-2, pp. 152–164, 2005.

[38] S. Margiotta and S. Negri, "Geophysical and stratigraphical research into deep groundwater and intruding seawater in the Mediterranean area (the Salento Peninsula, Italy)," *Natural Hazards and Earth System Science*, vol. 5, no. 1, pp. 127–136, 2005.

[39] D. Grassi, T. Tadolini, and L. Tulipano, *Influenza delle Caratteristiche Morfologiche – Strutturali e Paleogeografiche sull'Idrogeologia della Zona Situata a Nord di Otranto (Penisola Salentina)*, III Conv. Int. sulle Acque Sott., Palermo, 1975.

[40] L. Zorzi and C. Reina, "Le acque sotterranee in terra d'Otranto," in *Cassa per il Mezzogiorno*, pp. 1–94, Arti Grafiche "G. Menaglia", Roma, 1955.

[41] A. W. Harbaugh, *MODFLOW-2005, The U.S. Geological Survey Modular Ground-Water Model - The Ground-Water Flow Process*, U.S. Geological Survey, Techniques and Methods 6-A16, 2005.

[42] C. D. Langevin, D. T. J. Thorne, A. M. Dausman, M. C. Sukop, and W. Guo, *SEAWAT Version 4: A Computer Program for Simulation of Multi-Species Solute and Heat Transport*, U.S. Geological Survey Techniques and Methods 6-A22, 2007.

[43] G. De Filippis, I. Borsi, L. Foglia et al., "Software tools for sustainable water resources management: the GIS-integrated FREEWAT platform," *Rendiconti Online della Società Geologica Italiana*, vol. 42, pp. 59–61, 2017.

[44] R. Rossetto, I. Borsi, and L. Foglia, "FREEWAT: FREE and open source software tools for WATer resource management," *Rendiconti Online della Società Geologica Italiana*, vol. 35, pp. 252–255, 2015.

[45] R. Rossetto, G. De Filippis, I. Borsi et al., "Integrating free and open source tools and distributed modelling codes in GIS environment for data-based groundwater management," *Environmental Modelling & Software*, vol. 107, pp. 210–230, 2018.

[46] M. Abusaada and M. Sauter, "Studying the flow dynamics of a karst aquifer system with an equivalent porous medium model," *Groundwater*, vol. 51, no. 4, pp. 641–650, 2013.

[47] Regione Puglia & Autorità di Bacino della Puglia, *Aggiornamento del Bilancio Idrogeologico dei Corpi Idrici Sotterranei della Regione Puglia; All.4.5: Caratteristiche della Circolazione Idrica negli Acquiferi Carbonatici Pugliesi: Deflussi a Mare e Scambi Idrici tra Idrostrutture Confinanti*, 2010, in Italian.

[48] PROTEZIONE CIVILE PUGLIA, 2018, October 2018, http://www.protezionecivile.puglia.it.

[49] C. W. Thornthwaite, "An approach toward a rational classification of climate," *Geographical Review*, vol. 38, no. 1, pp. 55–94, 1948.

[50] R. G. Allen, L. S. Pereira, D. Raes, and M. Smith, *FAO Irrigation and Drainage Paper No. 56*, Food and Agriculture Organization of the United Nations 56, no. 97, Rome, 1998.

[51] W. Guo and C. D. Langevin, *User's Guide to SEAWAT: A Computer Program for Simulation of Three-Dimensional Variable-Density Ground-Water Flow*, U.S. Geological Survey, Tallahassee, FL, USA, 2002.

[52] R. A. Freeze and J. A. Cherry, *Groundwater*, Prentice Hall, Englewood Cliffs, NJ, USA, 1979.

[53] F. W. Schwartz and P. A. Domenico, *Physical and Chemical Hydrogeology*, John Wiley, 1990.

[54] L. Scesi and P. Gattinoni, *La Circolazione Idrica negli Ammassi Rocciosi*, CEA, 2007.

[55] B. R. Scanlon, R. E. Mace, M. E. Barrett, and B. Smith, "Can we simulate regional groundwater flow in a karst system using equivalent porous media models? Case study, Barton Springs Edwards aquifer, USA," *Journal of Hydrology*, vol. 276, no. 1-4, pp. 137–158, 2003.

[56] QGIS Development Team, *QGIS Geographic Information System. Open Source Geospatial Foundation Project*, 2009, http://qgis.osgeo.org.

[57] G. Ponzini and A. Lozej, "Identification of aquifer transmissivities: the comparison model method," *Water Resources Research*, vol. 18, no. 3, pp. 597–622, 1982.

[58] G. Ponzini and G. Crosta, "The comparison model method: a new arithmetic approach to the discrete inverse problem of groundwater hydrology, 1, one-dimensional flow," *Transport in Porous Media*, vol. 3, no. 4, pp. 415–436, 1988.

[59] G. Ponzini, G. Crosta, and M. Giudici, "Identification of thermal conductivities by temperature gradient profiles: one-dimensional steady flow," *Geophysics*, vol. 54, no. 5, pp. 643–653, 1989.

[60] S. Scarascia and G. Ponzini, "An approximate solution for the inverse problem in hydraulics," *L'Energia Elettrica*, vol. 49, pp. 518–658, 1972.

[61] E. P. Poeter, M. C. Hill, D. Lu, C. R. Tiedeman, and S. Mehl, *UCODE_2014, with New Capabilities to Define Parameters Unique to Predictions, Calculate Weights Using Simulated Values, Estimate Parameters with SVD, Evaluate Uncertainty with MCMC, and More*, Integrated Groundwater Modeling Center Report Number GWMI 2014-02, 2014.

[62] M. C. Hill and C. R. Tiedeman, *Effective Groundwater Model Calibration with Analysis of Data, Sensitivities, Predictions, and Uncertainty*, Wiley & Sons, New York, NY, USA, 2007.

[63] M. Fidelibus and A. Pulido-Bosch, "Groundwater temperature as an indicator of the vulnerability of karst coastal aquifers," *Geosciences*, vol. 9, no. 1, p. 23, 2019.

[64] Regione Puglia & SOGESID SpA, *Piano di Tutela delle Acque*, 2009, in Italian.

[65] G. C. Calò, R. Tinelli, D. Lucrezio, and M. Stani, "Riscontri delle oscillazioni eustatiche Flandriane nelle acque profonde degli acquiferi salentini (Puglia)," *Giornale di Geologia Applicata*, vol. 2, pp. 341–347, 2005.

[66] G. Aiello and F. Budillon, "Lowstand prograding wedges as fourth-order glacio-eustatic cycles in the Pleistocene continental shelf of Apulia (southern Italy)," in *Cyclostratigraphy: Approaches and Case Histories SEPM (Society for Sedimentary Geology), No. 81 ISBN 1-56576-108-1*, pp. 215–230, 2004.

[67] S. Margiotta and P. Sansò, "The geological heritage of Otranto–Leuca Coast (Salento, Italy)," *Geoheritage*, vol. 6, no. 4, pp. 305–316, 2014.

[68] G. Mastronuzzi and P. Sansò, "Coastal towers and historical sea level change along the Salento coast (southern Apulia, Italy)," *Quaternary International*, vol. 332, pp. 61–72, 2014.

[69] M. Primavera, O. Simone, G. Fiorentino, and M. Caldara, "The palaeoenvironmental study of the Alimini Piccolo lake enables a reconstruction of Holocene sea-level changes in southeast Italy," *The Holocene*, vol. 21, no. 4, pp. 553–563, 2011.

[70] M. Bakker, "Analytic solutions for interface flow in combined confined and semi-confined, coastal aquifers," *Advances in Water Resources*, vol. 29, no. 3, pp. 417–425, 2006.

[71] A. C. Knight, A. D. Werner, and L. K. Morgan, "The onshore influence of offshore fresh groundwater," *Journal of Hydrology*, vol. 561, pp. 724–736, 2018.

Research Article

Hydrogeology and Hydrogeochemistry of the Lauria Mountains Northern Sector Groundwater Resources (Basilicata, Italy)

Filomena Canora [iD],[1] **Giovanna Rizzo,**[2] **Simona Panariello,**[3] **and Francesco Sdao**[1]

[1]*School of Engineering, University of Basilicata, 85100 Potenza, Italy*
[2]*Department of Science, University of Basilicata, 85100 Potenza, Italy*
[3]*Lucanian Aqueduct SpA, Chemistry Division, 85100 Potenza, Italy*

Correspondence should be addressed to Filomena Canora; filomena.canora@unibas.it

In this study, the hydrogeological characterization of the northern sector of the Lauria Mounts carbonate hydrostructure (southern Apennines, Basilicata region) has been carried out and the hydrochemical properties of different collected groundwater samples have been characterized. Several normal springs drain the hydrostructure, some of them characterized by high annual mean discharges. Groundwater samples were collected from different springs; many parameters such as pH, electrical conductivity, and total dissolved solids have been measured, and major (cations and anions) elements and stable isotopes have been analysed following standard test procedures. Other chemical characteristics were derived from the analysed quality parameters. The results elucidate that the main hydrogeochemical processes control the chemical content and assess the quality of the groundwater within the hydrostructure. The analyses highlight that the chemical compositions of groundwater are strongly influenced by the lithology, especially limestones and dolomitic limestones; they explain and confirm the hydrogeological setting of the system. The groundwater system displays light different geochemical signatures. The processes contributing to the concentrations of major ions depend primarily on carbonate dissolution. The analysis, in all studied groundwater samples, shows that the facies groundwater type is Ca–HCO$_3$, bicarbonate is the dominant anion, and calcium is the dominant cation with appreciable magnesium concentrations. To identify the aquifer's recharge areas, the environmental stable isotopes oxygen and hydrogen, deuterium, and ^{18}O were analysed. The unaltered δ^{18}O and δD signatures for the groundwater of the major springs allows identifying the recharge area of these emergencies at elevations ranging from 900 m to 1000 m (a.s.l.), pointing out the presence of deeper flow regime feeding of these springs. The groundwater sample isotopic characteristics of D and ^{18}O suggest that most of the groundwater is recharged directly by infiltration in a high-permeability medium.

1. Introduction

In Mediterranean countries, water availability is a key factor for social and economic development. Recent changes in demography and lifestyle, agricultural land use and irrigation, tourism development, and climate change projections point to an increase in water scarcity and environmental problems with negative implications towards current and future sustainability [1–3]. The balance between water demand and water availability has reached critical levels in many regions; for this reason, a sustainable approach to water resource management is required. This is able to

consider the interactions among climate change impacts and water scarcity, surface water and groundwater pollution, and water engineering and human systems including societal resilience and adaptations [4, 5]. Groundwater represents important freshwater resources, used as drinking water supply for agricultural and industrial purposes. Climate variability and human change affect groundwater systems contributing to the decrease in water availability, both directly through modifications in aquifer recharge and indirectly through changes in groundwater quality and use [6]. According to the European and Italian Laws [7–9] on the protection of groundwater against deterioration and

pollution, it is necessary to apply the most appropriate actions and procedures at the hydrogeological basin scale. These actions, finalized to define strategic sustainable management processes, must be able to prevent or contain the potential depletion and pollution of groundwater resources, also taking into account mitigation strategies for climate change impacts [10, 11].

These precious resources, widely exploited, are not distributed at regional level and within each country, in a homogeneous way. The increase in groundwater exploitation poses a severe risk to the availability of the water resources, and the resulting resource scarcity is a major concern in most countries of the Mediterranean region.

Thus, in the last decades, many researches and studies have been planned, devoted to the assessment of the groundwater quantity, quality, and trends. The hydrogeological and groundwater hydrogeochemical assessments have a primary importance to define the hydrogeological conditions of the systems for implementing a sustainable integrated management of groundwater.

Hydrochemical characteristics and stable isotope compositions of groundwater provide important data regarding the water–rock interaction along flow paths, groundwater mixing due to different aquifers and hydrological processes, and area and timing of groundwater recharge for the comprehensive understanding of the hydrodynamic and hydrogeological setting [12–15]. In particular, stable isotopes of oxygen and hydrogen ($\delta 18O$ and δD) are useful as space tracers of hydrological processes in aquifers, to determine the elevation and conditions of the recharge areas [16–18].

In the Basilicata region (southern Italy), extensive karst and fractured carbonate hydrostructures due to their peculiar geostructural features and hydrogeological conditions are characterized by the presence of a considerable number of springs of good quality.

In order to contribute to an improved understanding of the hydrogeological setting and the groundwater hydrogeochemical characterization of the still poorly understood carbonate hydrostructure of the Lauria Mountains northern sector (southern Apennines), a comprehensive methodological approach was applied. Investigations included geological and hydrogeological field studies to understand the specific characteristics of the hydrogeological system, groundwater sampling at the springs, and chemical analysis of the major elements and stable isotopes ($\delta 18O$ and δD) to define the hydrogeochemical processes and the recharge area of the major springs.

This will help to provide insight and support in defining groundwater appropriate development actions and strategies, into comprehensive, sustainable, and efficient water resource assessment and management to overcome the future and increase freshwater demands, during the drought periods and in a changing climate scenario.

2. Study Area

The morphostructure of the northern sector of the Lauria Mounts, geographically located along the Calabrian-Lucanian regional border, in the southern-western part of the Basilicata region, is oriented in the W-E direction from Lauria to Castelluccio villages. It is bordered by the watershed of the Sinni River to the N, by the Torrente Peschiera to the NE, and by the urban areas of Castelluccio Superiore and Castelluccio Inferiore to the E. The Mercure River basin bounds the carbonate massif in the SE sector, the Valico Prestieri and Fosso Mancosa in the southern sector, Serra La Nocara to the SW by the Lauria urban area, and the lower part of the Torrente Caffaro tributary of the Noce River to the W. The morphostructure includes the reliefs of La Spina (1652 m) and Zaccana (1580 m) Mounts, Castello Starsia (1387 m), Serra Rotonda (1285 m), and Serra Tornesiello (1185 m) (Figure 1).

The geographic location of the study area, immediately inside the imposing Apennine Chain, which rises along the Tyrrhenian coast, has a strong impact on climate factors. The nearness to the sea confers its beneficial effect to the climate which results to be substantially mild, despite the elevations of the territory, with a very high average annual precipitation of about 1550 mm. The annual typical Mediterranean rainfall regime involves very rainy winters and dry summers. The maximum monthly precipitation value is recorded in December, the minimum in July. The regime of temperature is essentially characterized by the mean maximum value of about 23°C in summer that always occurs in the months of July-August and the mean minimum value of about 6.5°C in winter. The average annual temperature is instead about 14°C. The hydrographic network is mainly present on the carbonate rocks that form the central structure and on the alluvial deposits characterized by good permeability and low slope gradients. The development of minor streams is controlled by the state of fracturing of the carbonate and is distributed around several directions.

The straight segments of streams (e.g., Torrente Caffaro, Fosso Mancosa) are strongly related to the main fault systems that evidently have conditioned the hydrographic network development. In the SE edge of Serra Rotonda, a small lake, Lago La Rotonda, with a seasonal regime is located in a small endorheic basin; it has a water-extended surface in rainy months and dry in the summer. The lake is generated in correspondence of a karst polje, in which, at the bottom, detrital and palustrine deposits are present. The morphostructure hosts an important carbonate hydrostructure, drained by many springs some of which are characterized by huge groundwater discharges.

3. Geological Setting of the Lauria Mounts

The Lauria Mountains consist of a series of ridges, coincident with morphostructures with a N120° SE pattern, located to the west of the Mercure Basin, which separates them from the neighbouring mountains of the Pollino Chain and represents the link between the Campanian-Lucanian Apennine and the domains belonging to the crystalline-metamorphic sedimentary rocks of the Calabrian-Peloritan Arc.

The Lauria Mountains, characterized by a significant geological and structural complexity, represent a high structure consisting of the Meso-Cenozoic calcareous-dolomitic succession, referable to the Alburno-Cervati-Pollino Unit
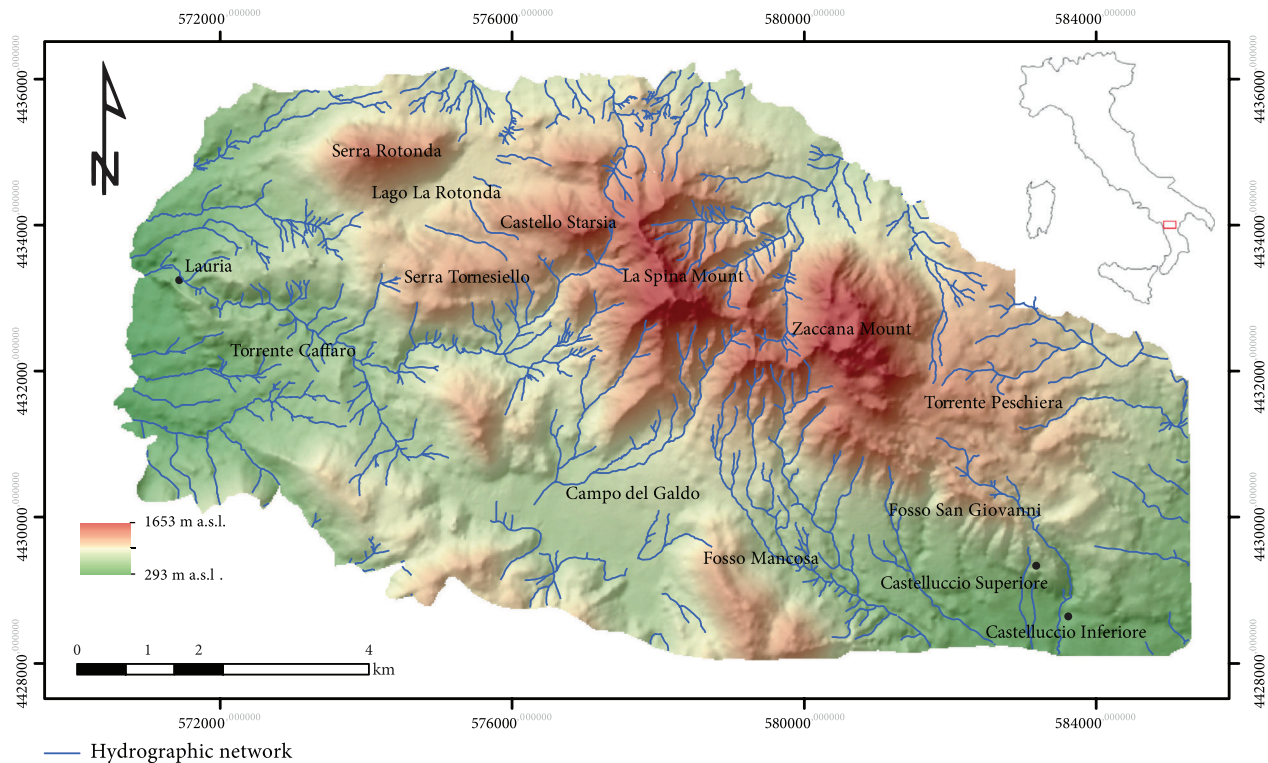
Figure 1: Geographic location, digital elevation, and hydrographic network of the study area.

[19], constituting the monoclines of the Calabrian-Lucanian border, confined by the Miocene argillite-marly flysch.

In particular, in the Lauria Mountains it is possible to distinguish the Lauria-Castelluccio northern ridge, consisting of the main reliefs of Castello Starsia, Serra Rotonda, La Spina, and Zaccana, where carbonates, from Triassic to Cretaceous, such as dolomites, dolomitic limestones, and limestones constitute the central structure, while terrigenous sediments are present along the lower part of the northern slopes. Quaternary sediments organized in different continental depositional environments fill the southern sector. This morphostructure is separated from the southern Trecchina-Laino ridge by a tectonic line with a transcurrent trend oriented N110°-120° that has cut the existing plicative structures. Cretaceous limestones of the Serra San Filippo and Serra La Nocara reliefs and Jurassic-Cretaceous limestones of the Rossino and Fossino Mounts constitute the southern morphostructure.

The morphodynamic evolution of the Pollino Chain and Lauria Mountains has been highly controlled by the transcurrent and distensive Plio-Quaternary fragile tectonics [20–22].

The transcurrent deformation, active from the Upper Pliocene, whose faults are subsequently reactivated in the extensional system [22, 23], produces a complex structural pattern [24]. Several geological and structural studies of the entire area [21, 23, 25] made it possible to place a time constraint to the transcurrent activity, which is still present during the Sicilian, while the extensional tectonic, still active, develops starting from the passage between the Lower and Middle Pleistocene.

The tectonic structures oriented approximately N120° are extremely important, as responsible for the genesis and evolution of many quaternary basins, including those present in the Calabrian-Lucanian border [22].

The morphostructure of the northern sector of the Lauria Mountains, oriented in the WNW-SSE direction, is located to the north-west sector of the Mercure Basin, which separates the carbonate structure from the neighbouring mountains of the Pollino Chain [26].

The study area highlights different fault systems, with predominantly Apennine faults orientation N120 ± 10° and distributed fault systems oriented N-S and N30°-50°, generally in association with thrusts and folds [26] (Figure 2).

The carbonate morphostructure is bordered by high-angle transcurrent and extensional faults that generated a series of depressions filled by Quaternary continental deposits and by Miocene terrigenous deposits [25]. Carbonate successions are bounded to the north by an important thrust front with N-NE vergence, produced by the translational tectonics that led Liguridi and Sicilidi-Affinity Units to overlap on Carbonate Units of the Apennine Platform and on Lagonegresi Units [27].

The presence of the fault with NNW-SSE direction, which plunges to WSW with a fault throw of about 400 m, divides the limestone-dolomitic area in two zones, the first one to the west and the second to the east of the mentioned fault.

This fault starts from Lago La Rotonda and, passing between Castello Starsia and the right side of Serra Tornesiello, reaches Campo del Galdo, in correspondence
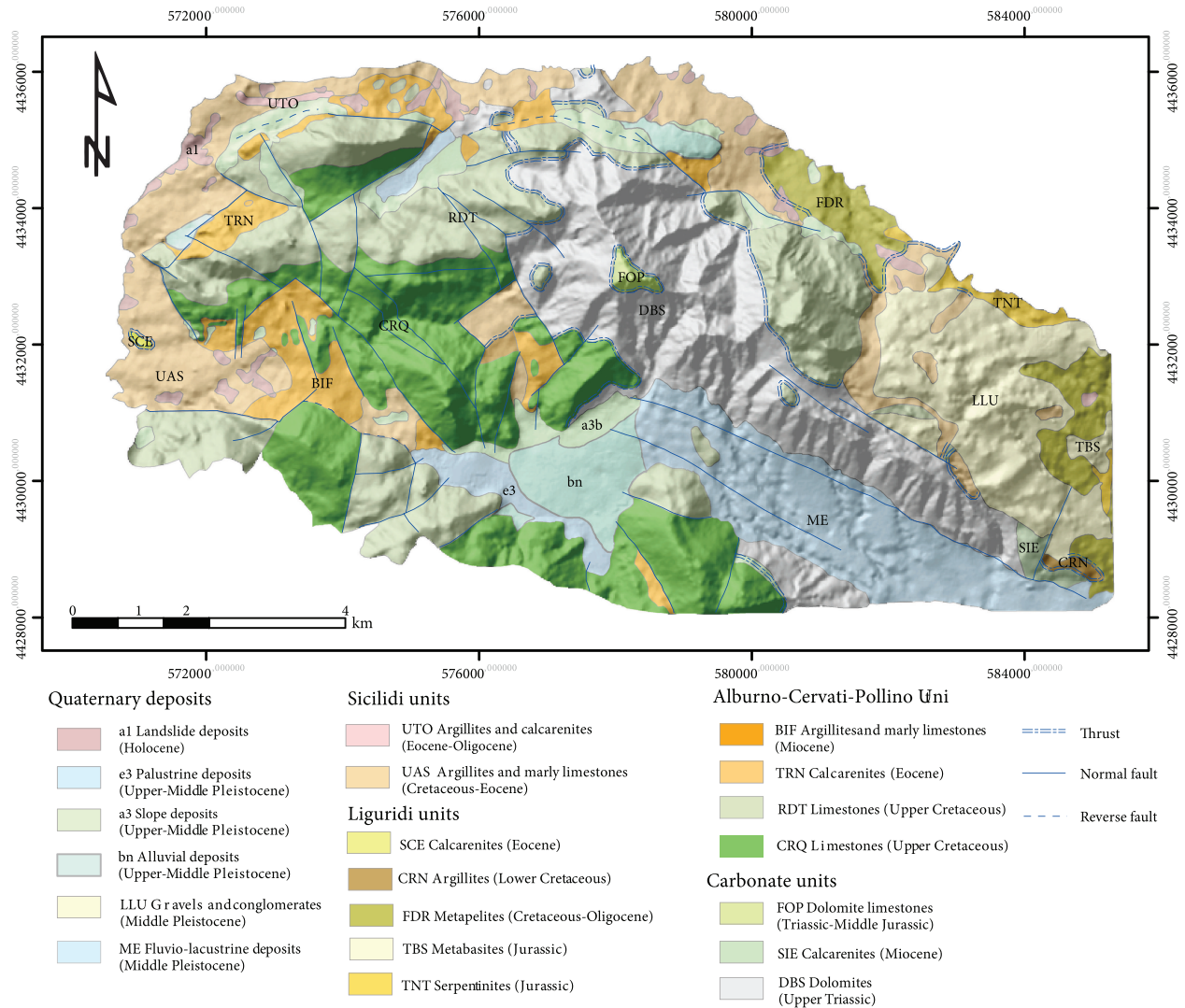
FIGURE 2: Geological map of the Lauria Mountains northern sector (adapted from ISPRA, 2016 [31]).

to the base of the western slope of the La Spina Mount. A network of normal faults characterized by three main systems with NNW-SSE, SW–NE, and E-W directions, globally affects and lowers the western area of this fault.

In the study area are different distinguishable stratigraphic-tectonic units that constitute the structure of the Lucanian Apennines [19] (Figure 2).

Lagonegresi Units, outcropping only limited along the northern external borders of the morphostructure, represent the sedimentary succession of the Lagonegrese Basin [28] constituted, from the bottom to the top, by the Monte Facito Formation (Lower-Middle Triassic), the Cherty Limestone Formation (Upper Triassic), the Siliceous Schist Formation (Cretaceous-Jurassic), and the Galestri Formation (Jurassic Superior) [27, 29–31].

Carbonate Units of the Campanian-Lucanian Platform, represented by the calcareous and calcareous-dolomitic Mesozoic succession [32], overlay the Lagonegro Units. Carbonate Units constitute the entire structure of the Lauria Mountains. Carbonate successions belong to the tectonic units of the Maddalena Mounts and Foraporta Mount and to the Alburno-Cervati-Pollino Unit and comprehend, from the bottom to the top, red shales and cherty limestone of the Middle Triassic, followed by a powerful succession of dolomites (Upper Triassic) and limestones, with subordinate marls [32].

Liguridi Units, present in the area surrounding the northern morphostructure of the Lauria Mountains and extensively to the north-east sector of Castelluccio Superiore, include the turbidite succession of the Liguride Complex (Cretaceous-Oligocene) [33–35].

It represents the remaining part of an accretionary wedge, subsequently divided into two tectonic units: the metamorphic Frido Unit and the unmetamorphosed Cilento Unit [19, 29, 36, 37], which include the Crete Nere, Saraceno (north-Calabrian Units), and Albidona Formations (intra-Chain Basin Deposits) [38]. At these formations are tectonically overlapping deposits ascribed to the "Sicilide Affinity Units," made up of marly, calcarenite-clayey, and arenaceous-pelitic deposits (Upper Cretaceous-Oligocene);

the Torbido River Unit, consisting of marly and calcilutite limestone with nodules of chert, calcarenites, sandstones, and red argillites (Middle-Oligocene Eocene), stands above tectonically to these deposits [39].

The aforementioned deposits appear to be those geometrically higher than the south-Apennine Chain and mainly outcrop along the western border of the morphostructure, at N and NE of Serra Rotonda.

Quaternary deposits include different clastic deposits such as gravelly-sandy and subordinately sandy-loamed deposits, as well as clayey and marly continental sediments of the Noce and Mercure fluviolacustrine basins. These deposits are present mostly in the SE part of the study area attributable to different accumulation phases and intercalations of paleosols formed by brown silty clays with skeletons of different sizes, which testify to repeated periods of stasis in alluvial sedimentation. Sandy-gravelly deposits, colluvial deposits, and detrital cones of the Upper Pleistocene-Holocene outcropping almost everywhere along the southern slopes of the hydrostructure form a series of alluvial fan deposits that are interdigitated to the middle-Pleistocene lacustrine deposits of the Mercure Basin [22].

4. Hydrogeological Characterization of the Carbonate Hydrostructure

4.1. Geomorphological and Structural Factors' Role on the Aquifer System. The geostructural and geomorphological peculiarities of the morphostructure strongly affect the complex hydrogeological setting of the hydrostructure, the groundwater flow directions, and the presence of the springs.

The carried-out hydrogeological and hydrogeochemical surveys highlight that the geometrical configuration of the carbonate hydrostructure of the Lauria Mounts northern sector is structured according to different carbonate aquifers. Major faults and karst or fracturing conditions define the hydrogeological watersheds, to places with underground water interchanges, with different hydrogeological and hydrodynamic characteristics, and organize in the carbonate rocks' distinct groundwater flow patterns.

Based on the distinct geolithological, structural features and relative permeability of the stratigraphic-tectonic units, different hydrogeological complexes have been distinguished in the study area [40], each of them characterized by common spatial arrangement, prevalent permeability, and a degree of relative permeability restrained in a narrow range [41].

Limestones, dolomitic limestones, and dolomites constitute the Carbonate Complex that host the most important aquifers drained by the springs with major discharge amounts. It can be divided into three subcomplexes depending on the presence or absence of the karst process and forms (dolines and cavities) and the density of rock fracturing state; the hydraulic conductivity ranges from 10^{-4} m/s to 10^{-2} m/s [42], and the relative permeability varies from medium-high to very high, representing the favoured complex for the infiltration.

The Conglomerate Complex, mainly outcropping in the south-eastern part of the investigated area, consists of conglomerates and breccias. Characterized by a medium-high degree of relative permeability, it presents a discrete groundwater flow fed by the carbonate complexes. This complex stores part of the groundwater amount and allows the emergence of smaller springs.

The Calcarenite Complex, made of a gray well-layered calcarenite succession with frequent intercalations of marls, has a subordinate role in the local hydrogeological framework, which presents a medium degree of relative permeability due to the presence of the rock fractures.

The Detrital Complex, constituted by heterogeneous conglomerates and gravels with different cementation degrees, includes the detrital and clastic deposits that constitute the alluvial fans and the debris cones. Its hydraulic conductivity ranges from 10^{-7} m/s to 10^{-5} m/s with a medium degree of relative permeability [42].

The Fluviolacustrine Complex, characterized by a medium-low degree of relative permeability, comprehends clays, marly clays, layered clayey marls with sandy layers, and polygenic conglomerates rich in sandy matrix. It is largely made up by the quaternary deposits of the Mercure Basin that borders the carbonate hydrostructure along its southern boundary.

The Clayey-Marly Complex includes pelagic and chaotic sequences of varicoloured clays, marls, and marly limestone, belonging to the Sicilidi-Affinity and Lagonegresi Units and quartzites; clays and marls referable to the Frido Unit, in which even ophiolitic elements can be distinguished [43–45]; and arenaceous-pelitic alternation belonging to the Flysch of Albidona. This complex has a low degree of relative permeability, borders the carbonate hydrostructure, and plays an important hydrogeological role representing the limit of permeability in some parts of the system; the hydraulic conductivity is $<10^{-9}$ m/s [42].

The geometry of the carbonate hydrostructure and the underground watershed are mainly defined by the structural elements present throughout the entire hydrostructure, such as faults and thrust, tectonic deformation bands, and karst and fracturing state of rocks.

The assessment of the karst phenomena in the area was based mainly on the recognition of the surface karst forms; the entity of the underground karstic development is evinced considering the geomorphological context and the spring's emergency areas that leads to the consideration of the presence of evolved fractures and karstic conduits. The presence of the karst morphologies, on the dolomitic limestones, suggests a local prevalence of the calcareous component on the dolomite. They represent the surface trace of a developed underground karst network.

This specific hydrogeological setting bordered laterally by major faults and characterized by subsurface boundaries, due to tectonic elements, lithological arrangement, and development of karst network, influences the different groundwater flow directions and the emergence of numerous springs, distinguishing two aquifers with different hydrogeological and hydrodynamic characteristics (Figure 3).

The Lauria and La Spina-Zaccana aquifers, both characterized by the presence of important springs, located in the western and eastern parts of the carbonate massif, at altitudes between 315 m and 504 m a.s.l., represent strategic
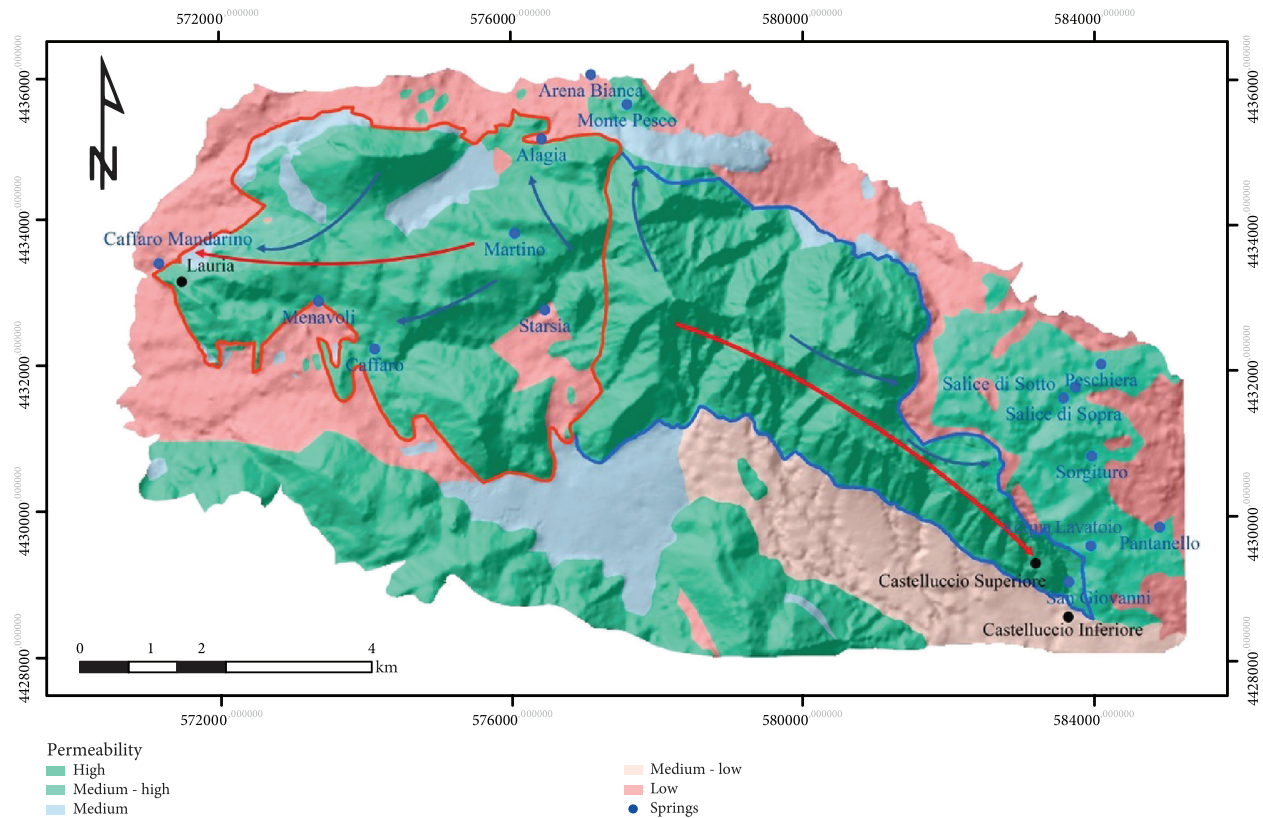
Figure 3: Hydrogeological map showing Lauria Aquifer (red line) and La Spina-Zaccana Mounts Aquifer (blue line) with relative permeability classes, main groundwater flow directions (red arrows and blue arrows represent, respectively, deep and shallow groundwater flow pathways), springs, and main urban areas (black circle).

water resources for the area and for the Basilicata region. Several other emergencies with smaller groundwater amounts are present along the border of the carbonate hydrostructure (Figure 3).

The groundwater flow, conditioned by different factors such as tectonic arrangement, rock fracturing degree, karst activity, and presence of the basal dolomite complex at the south-eastern part of the aquifer system, essentially occurs in two preferential directions.

The prevailing NE-SW and NW-SE directions are oriented towards the areas where the major springs emerge, most of which are not adequately exploited or even uncollected.

4.2. Hydrogeological Features of the Lauria and La Spina-Zaccana Aquifers.

The Lauria Aquifer is characterized by an evident stratigraphic-structural complexity. The carbonate structure is affected by a dense network of high angle direct faults, which develop the geometry of en-echelon from Lago La Rotonda to Campo del Galdo. This direct fault system shows a vertical fault throw of at least 400 meters and gets down the entire western block of the Lauria Ridge with respect to the La Spina-Zaccana Ridge.

The most evident consequence of this remarkable dislocation is represented by the difference of the lithological outcrops between the two blocks: in fact, while the limestones outcropping mainly characterizes the lowered western

block of the Lauria side, the eastern block is largely constituted by the outcrops of the deepest dolomitic limestones and dolomites.

In correspondence of this fault system, the distribution of the layered carbonate succession defines an anticlinal fold with the axial zone localized between Castello Starsia and La Spina Mount; it can be considered the tectonic structure that presumably corresponds to the hydrogeological watershed between the two aquifers.

Argillite-marly flysch and clayey-marly flysch bound, to the north and to the west, the carbonate aquifer, consisting limestones and dolomitic limestones. Argillite and marly limestones outcrop to the south, and the most markedly dolomitic terms emerge to the east characterized by an intense fracturing state. The groundwater pathways, influenced by the presence of different faults, has the preferential flow direction oriented NE-SW. It starts from the hydrogeological watershed with the La Spina-Zaccana aquifer and is directed towards the main emergencies located at W of the hydrostructure. The main springs, located in the municipality of Lauria, such as Caffaro-Mandarino, Caffaro, and Arena Bianca, reach a total capacity of about $845 \, \text{L s}^{-1}$ [46].

The three different important emergencies of Caffaro-Mandarino with the flow rate of about $0.81 \, \text{m}^3 \, \text{s}^{-1}$ [46], located on the edge of the carbonate structure, is tamponed by the clayey-marly flysch formations of the Sicilidi-Affinity Unit. The group of Caffaro-Mandarino springs represents

the delivery points of the deep aquifer groundwater flow. Nowadays, its discharge is partly used for hydroelectric purposes.

The Caffaro Spring did not naturally emerge, but the derivation of the draining tunnel was realized for a hydro-lectrical system; the flow rate of the Caffaro is equal to $25 \, L \, s^{-1}$ [46]. Some quantities of water flow in the detrital deposits or feed the minor springs: Alagia, Martino, and Montepesco, placing a different altitude, refer to shallow underground water circuits that characterize the variable regime of the small flow rates. Those positioned on average from 645 to 1120 m a.s.l. are located in two distinct areas enclosed between the northern slopes of Castello Starsia and the southern side of Serra Tornesiello. Starsia and Menavoli springs with $4 \, L \, s^{-1}$ flow rates are used for local needs (Figure 3). The presence of some springs at the northern edge of the hydrostructure is due to the underground water transfers of the carbonate rocks towards the flysch deposits in the most permeable areas and towards the detrital cover.

The La Spina-Zaccana aquifer constitutes the central-eastern portion of the northern area of the Lauria Mountains and consists of the two reliefs of La Spina and Zaccana Mounts.

The dolomites and dolomitic limestones represent the dominant geological formations and are constituted, at the bottom, by a monotonous succession of gray and micro- and macro-crystalline dolomites. Fluviolacustrine deposits of the Mercure Basin and a series of continental quaternary deposits, mainly present in the southern boundary of the aquifer and in some peripheral sectors of the La Spina-Zaccana ridge, are represented by coarse and subordinately fine clastic sediments, consisting of clays and marls.

Although dolomitic limestone and dolomite are considered part of a single succession in original stratigraphic continuity, a band of intense cataclastic deformation is evident at their contact, which is therefore to be considered of tectonic type. It has already been recognized in the study area [20, 47] and interpreted as a low-angle tectonic contact with a predominantly extensional or transtensive kinematics of a *younger on older* [48]. The carbonate aquifer is bounded almost in all directions by exclusively tectonic contacts of different nature and kinematics and stratigraphic places.

The north-western boundary of the hydrostructure is located in the anticlinal hinge zone of the Castello Starsia-La Spina Mount. At its north-eastern edge, however, the aquifer is bounded by a thrust, to places lowered by some normal faults, which superimposes the argillite-marly formations on the carbonates. Along the southern edge, the La Spina-Zaccana substructure is bounded by an important fault, indicated as Castelluccio Fault, with high inclination, oriented in the N120° direction and submerged towards SSO. It is formed in the Pleistocene with a left transcurrent kinematics subsequently reactivated as a direct fault in the upper Pleistocene.

The high and steep slope that characterizes the southern side of the La Spina-Zaccana ridge morphologically highlights the high rate of activity of this fault and its considerable vertical throw. Within its limits, the La Spina-Zaccana

morphostructure does not seem to be crossed by major faults, except for the NS subvertical direct fault present in the southern slope that intersects the Castelluccio Fault and which lowers the eastern sector.

The Castelluccio Fault acts as the morphostructural southern limit of the structure and from a hydrogeological point of view represents the superimposed permeability threshold of the San Giovanni spring front.

The La Spina-Zaccana carbonate aquifer represents significant groundwater resources, well fed and drained in large part from the San Giovanni spring; minor emergencies of less potentiality are scattered throughout the south-eastern sector of the structure (Figure 3).

Along the entire southern slope of the La Spina-Zaccana Ridge, the Castelluccio Fault places in tectonic contact the carbonate rocks of the aquifer with the Pleistocene fluviolacustrine deposits of the Mercure Basin. The geometry of the aquifer, its main hydrogeological characteristics, the underground water circulation, and the groundwater emergencies are closely connected to the geological, structural, and karst arrangement. The recharge area, essentially located at high altitudes of the hydrostructure, includes the main reliefs of the study area, towards the W-E direction.

The groundwater flow, predominantly, in the NW-SE direction, feeds the San Giovanni springs group, Acqua del Lavatoio and Pantanello springs along the eastern edge of Monte Zaccana. These springs have a total flow rate of about $580 \, L \, s^{-1}$ [46]. The San Giovanni spring front (at least 7 normal permanent springs) (mean discharge of $450 \, L \, s^{-1}$) [46], one of the most important groundwater resources of the Lucanian Apennines, is located along a steep slope at an altitude of between 480 m and 504 m. Groundwater is mainly, if necessary, exploited for drinking purposes and irrigation use. Other water emergencies, such as Peschiera, Salice Sopra, Salice Sotto, and Sorgituro, drain limited surficial aquifers characterized by shallow groundwater flow paths.

4.3. Sampling and Analytical Methods. Groundwater samples were collected from 15 springs, some of them partially used for drinking, irrigation, and hydroelectrical purposes, during a single field trip in May 2017. During the rainy season, another sampling was carried out only for isotopic analyses (November 2017).

The sampling sites, located mainly in the western and eastern sectors of the hydrostructure, were selected based on the complex hydrogeological geometry and hydrodynamic characteristics of the aquifers (Figure 3).

Groundwater springs were sampled to define the main hydrogeological and hydrogeochemical processes controlling the chemical properties. Physicochemical parameters including groundwater temperature, pH, and electrical conductivity were measured in situ. One filtered aliquot (using $0.45 \, \mu m$ cellulose acetate filters) and one filtered and acidified (with HNO_3) aliquot were collected and stored in low-density polyethylene bottles for laboratory analysis of major elements. The major elements were determined by ion chromatography, IC Metrohm 850 Professional. Cations (Na^+, K^+, Ca^{2+}, and Mg^{2+}) were separated by a Metrosep C 4 250/4.0 column using 3.0 mM HNO_3 as eluent and a flow

TABLE 1: Physicochemical parameters of the groundwater samples.

Spring name	Sample	Est	North	Altitude (a.s.l.)	Discharge (L/s)	pH	EC (μS/cm)	T (°C)
Alagia	P1	576401	4435186	920	2	7.2	550	10.9
Arena Bianca	P2	577083	4436071	735	11	7.7	383	11.6
Martino	P3	576032	4433888	1120	1	7.3	397	9.8
Montepesco	P4	577580	4435661	950	4	7.5	387	10.8
Caffaro	P5	574107	4432297	640	25	7.6	365	10.8
Caffaro M.	P6	571133	4433471	315	810	7.8	369	11.7
Menavoli	P7	573333	4432955	645	2	7.2	498	13.2
Starsia	P8	576448	4432836	835	4	7.4	535	12.7
Acqua Lavat.	P9	583972	4429592	705	4	7.7	430	10.2
Pantanello	P10	584918	4429849	630	16	7.5	425	11.4
Peschiera	P11	584111	4432091	910	4	7.5	390	11.4
Salice Sopra	P12	583759	4431779	925	5	7.5	372	13.4
Salice Sotto	P13	583594	4431623	940	4	7.6	365	13.1
San Giovanni	P14	583670	4429095	504	540	7.6	358	11.2
Sorgituro	P15	583982	4430826	875	3	7.6	365	10.8

Discharge data are from Basilicata Region [36]. The sampling sites are in WGS1984 UTM Coordinate System Zone 33N.

TABLE 2: Major element concentrations of the spring's groundwater sampled in the study area.

Sample	Na$^+$ (mg/L)	K$^+$ (mg/L)	Mg^{2+} (mg/L)	Ca^{2+} (mg/L)	Cl$^-$ (mg/L)	NO$_3^-$ (mg/L)	SO$_4^{2-}$ (mg/L)	HCO$_3^-$ (mg/L)	CS (meq/L)	AS (meq/L)	E (%)	SI calcite	SI dolomite
P1	4.1	0.5	11.8	62.0	4.5	1.0	2.8	251	4.3	4.3	-1.4	-0.3	-1.1
P2	6.1	0.4	13.4	62.8	8.5	4.4	7.6	252	4.5	4.6	-2.1	0.3	0.0
P3	4.4	0.6	8.2	60.1	5.8	0.1	4.6	232	3.9	4.1	-4.6	-0.2	-1.3
P4	3.6	0.5	11.1	58.0	4.4	1.2	3.3	240	4.0	4.1	-4.2	0.0	-0.6
P5	3.9	0.3	16.6	52.0	5.7	1.5	3.5	233	4.1	4.1	1.5	0.0	-0.3
P6	4.8	0.6	13.2	52.0	5.3	2.3	5.0	225	3.9	4.0	-1.6	0.5	0.5
P7	6.3	0.2	4.7	73.0	8.2	1.7	8.0	245	4.3	4.4	-3.0	-0.2	-1.3
P8	5.8	1.4	8.4	62.0	6.9	4.1	9.5	228	4.1	4.2	-2.9	0.0	-0.8
P9	3.9	0.2	18.6	52.8	5.6	1.8	4.6	245	4.3	4.3	1.0	0.2	0.0
P10	5.6	1.4	12.2	66.7	6.2	8.1	5.0	256	4.6	4.6	0.0	0.1	-0.4
P11	3.6	0.5	11.1	62.5	4.7	1.9	3.9	244	4.2	4.2	-1.0	0.0	-0.5
P12	3.6	1.5	12.9	74.2	3.8	0.1	0.8	297	5.0	5.0	-0.7	0.2	-0.1
P13	3.9	0.6	12.7	57.9	5.7	1.7	4.0	233	4.1	4.1	0.6	0.1	-0.2
P14	4.8	0.2	20.1	40.8	7.2	0.1	3.2	220	3.9	3.9	0.9	0.3	-0.3
P15	5.0	0.5	15.0	51.8	7.2	2.9	6.2	224	4.0	4.1	-0.2	0.0	-0.5

rate of 0.9 mL/min, whereas anions (F$^-$, Cl$^-$, NO$_3^-$, and SO$_4^{2-}$) by a Metrosep A supp7 250/40 column using 3.6 mM Na$_2$CO$_3$ as eluent at a flow rate of 0.7 mL/min. Alkalinity was determined by titration with 0.1 N HCl. The analytical precision was always better than 5% for each analysed species, and the ion balance (i.e., the difference between the cations and anions sum) was always within 3%.

The geochemical software PHREEQC 3.0 [49, 50] was used to calculate aqueous speciation of the investigated elements. Saturation index, defined as SI = log (IAP/Kt), IAP being the ion activity product of the mineral–water reaction and Kt the thermodynamic equilibrium constant at the measured temperature, were calculated by ion activities.

Thus, SI = 0 indicates a thermodynamic equilibrium state, and values >0 denote oversaturation and <0 undersaturation.

The field chemical composition of the analytical results and the saturation index (SI) values for calcite and dolomite are reported are listed in Tables 1 and 2.

Validation procedures characterize the analytical performance of laboratory tests in order to understand its capability and limitations. The limit of detection and the limit of quantitation (LOD and LOQ) are the parameters used to describe the analytical sensitivity of an analytical procedure.

The detection limit, LOD, represents the smallest concentration of an analyte in a sample that can be detected with reliable statistical certainty under the stated conditions of the

analytical test, with no guarantee about the bias or imprecision of the result.

The value is determined as the analyte concentration corresponding to the sample blank value plus three standard deviations:

$$LOD = X_{b1} + 3S_{b1}, \tag{1}$$

where X_{b1} is the mean concentration of the blank and S_{b1} is the standard deviation of the blank.

The LOQ is the lowest analyte concentration, determined with acceptable precision and accuracy under the stated conditions of the test, and corresponding to the sample blank value plus ten standard deviations as shown in the following equation:

$$LOD = X_{b1} + 10S_{b1}, \tag{2}$$

where X_{b1} is the mean concentration and S_{b1} is the standard deviation of the blank.

The weakness is that there is no objective evidence to prove that a low concentration of analyte will indeed produce a signal distinguishable from a blank (zero concentration) sample [51]. Results of the detection and quantification limits of the analyzed elements are expressed in Table 3.

To evaluate the interrelationships affecting the distribution of the major chemical elements, an R-mode factor analysis was performed.

Factor analysis provides a way to reduce the data to an easily interpretable form, by identifying chemical signatures expressed through statistically significant factors determined by the analysis.

R-mode factor analysis was undertaken by the Statgraphics Centurion XVI package [52], and factor component matrix is extracted (Table 4).

This matrix, showing the impact coefficient of the two extracted components, evidences the link between these components and the groups of variables.

The $^{18}O/^{16}O$ and $^{2}H/^{1}H$ ratios were determined by isotope ratio mass spectrometry (IRMS). Oxygen isotope measurements were carried out by using a Gas Bench peripheral coupled with a Thermo Delta V mass spectrometer. A TC-EA peripheral interfaced by means of a ConFlo IV with a Thermo Delta XP mass spectrometer was used for hydrogen isotopes. Results are expressed in terms of d-values (i.e., δD and $\delta^{18}O$) with respect to the Vienna Standard Mean Ocean Water (VSMOW) as follows:

$$\delta[‰] = \frac{R_{sample} - R_{VSMOV}}{R_{VSMOV}} \times 1000, \tag{3}$$

where R_{sample} is the stable-isotope ratio ($^{2}H/^{1}H$ or $^{18}O/^{16}O$) of the sample and R_{VSMOV} is the ratio for VSMOW. The analytical error for IRMS was ±0.1‰ for $\delta^{18}O$ and better than ±1‰ for δD. The isotopic data of the two sampling periods are reported in Table 5.

TABLE 3: Detection limit (LOD) and quantitation limit (LOQ) of the major element concentrations.

Element	LOD (mg/L)	LOQ (mg/L)
Na	0.28	0.94
K	0.18	0.67
Mg	0.15	0.49
Ca	0.17	0.56
Cl	0.48	1.61
SO	0.28	1.63
NO	0.1	1.14

TABLE 4: R-mode factor analysis results.

	Component 1	Component 2
EC	0.125	0.606
pH	-0.101	-0.503
Na^+	0.962	0.137
K^+	-0.005	0.606
Mg^{2+}	-0.318	-0.571
Ca^{2+}	0.093	0.956
Cl^-	0.859	-0.235
NO_3^-	0.490	0.223
SO_4^{2-}	0.923	0.039
HCO_3^-	-0.343	0.719

TABLE 5: Stable isotope composition of groundwater collected in two sampling periods.

Sample	$\delta^{18}O$	δD	$\delta^{18}O$	δD
	May 17		Nov 17	
P1	-8.1	-48	-8.8	-54
P2	-8.2	-47	-8.7	-53
P3	-8.2	-49	-8.9	-54
P4	-7.6	-45	-8.6	-53
P5	-7.7	-46	-8.4	-52
P6	-7.8	-46	-8.6	-51
P7	-7.5	-42	-8.4	-52
P8	-7.5	-45	-8.5	-50
P9	-7.5	-44	-8.3	-50
P10	-7.6	-44	-8.2	-52
P11	-7.7	-44	-8.3	-52
P12	-8.4	-52	-8.5	-53
P13	-7.8	-43	-8.4	-50
P14	-8.5	-52	-8.6	-53
P15	-8.6	-53	-8.6	-54

The isotope composition of O and H is reported in δ units per mil vs. the V-SMOW standard. The analytical error was ±0.1‰ for $\delta^{18}O$ and better than ±1‰ for δD.

5. Results and Discussion

5.1. Chemical Composition of Groundwater. Groundwater samples are characterized by low electrical conductivity
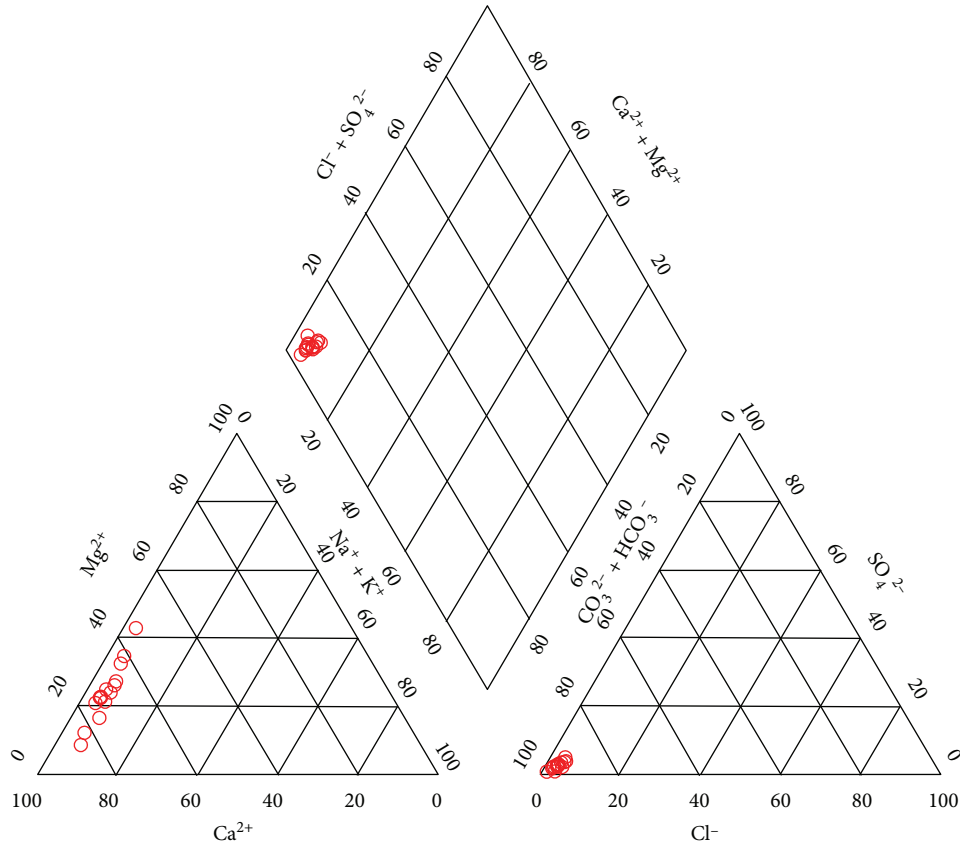
FIGURE 4: Piper diagram showing the groundwater hydrogeochemical facies.

(EC) values, ranging from 358 to 550 μS/cm, alkaline pH values (from 7.2 to 7.8) and temperature values between 9.8 and 13.4°C. The bicarbonate is the main anion in solution with concentrations ranging between 220 mg/L and 297 mg/L with an average value of 242 mg/L. Calcium and magnesium are the most abundant cations with average values of 59.2 and 12.7 mg/L, respectively.

NO_3 concentrations range from 0.1 mg/L to 8.1 mg/L and are lower than the maximum admissible concentrations defined by the Italian Law [53]. All the sampled groundwater records the following order of abundance in terms of cation and anion concentrations: $Ca^{2+}>Mg^{2+}>Na^+>K^+$ and $HCO_3^->Cl^->SO_4^{2-}>NO_3^-$. Magnesium and sulphates charge the greatest concentration variations.

The hydrogeochemical facies of groundwater, determined using the Piper diagram [54], shows that the investigated groundwater has a homogenous distribution with bicarbonate alkaline-earth composition (Figure 4).

To assess the role of the dissolution mechanisms of carbonate compounds the relationship of HCO_3^- to Ca^{2+} Mg^{2+} has been verified. The observation points tend to fall above $y = x$ (dissolution of carbonates), indicating that Ca^{2+} and Mg^{2+} ions would originate from calcite and dolomite mineral dissolution in the carbonate rock areas (Figure 5).

In consideration of the geological context in which the investigated springs occur, it is to be considered that this correlation is mainly due to the dissolution of the calcium

carbonate and in a minor way of the magnesium carbonate, dominant in these carbonate deposits.

The carbon dioxide of the soil reacts with water and carbonate rocks dissolving calcite and dolomite according to the following reactions:

$$CaCO_3 + 2CO_2 + 2H_2O = 2Ca^{2+} + 4HCO_3^-$$

$$CaMg(CO_3)_2 + 2CO_2 + 2H_2O = Ca^{2+} + Mg^{2+} + 4HCO_3^-$$

$$(4)$$
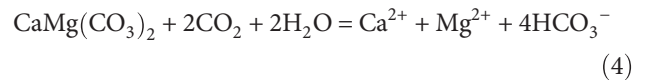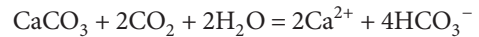
In Figures 6(a) and 6(b), the saturation indices (SI) for calcite and dolomite, expressed in logarithmic form, in relation to Mg/Ca ratio are shown. Most groundwater samples are saturated or nearly saturated with respect to calcite (Figure 6(a)). On the contrary, almost all of groundwater samples are undersaturated with respect to dolomite (Figure 6(b)).

The dolomite dissolution and concurrent precipitation of calcite maintain water-mineral equilibrium (dedolomitazion) and increase Mg/Ca ratios along flow paths. The scatter plot of Na^+ versus Cl^- (Figure 7) indicates that groundwater are well correlated ($r^2 = 0.75$) and show a Na/Cl ratio higher than seawater (Na/Cl = 0.86) and halite dissolution (Na/Cl = 1). The $Na^+/Cl^- > 1$ relationship may be
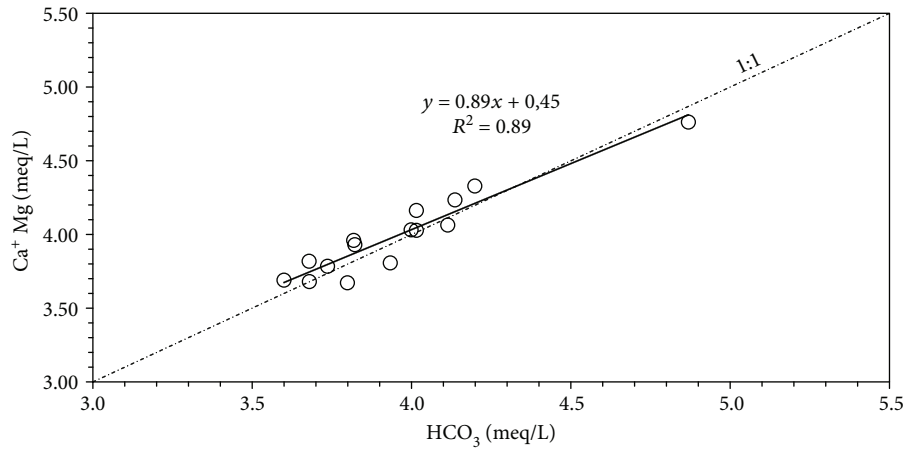
FIGURE 5: $(Ca^{2+}+Mg^{2+})$ vs. HCO_3^-. The dotted line shows the $(Ca + Mg)/HCO_3^- = 1$. The black line displays the significant correlation between selected variables.

(a)

(b)
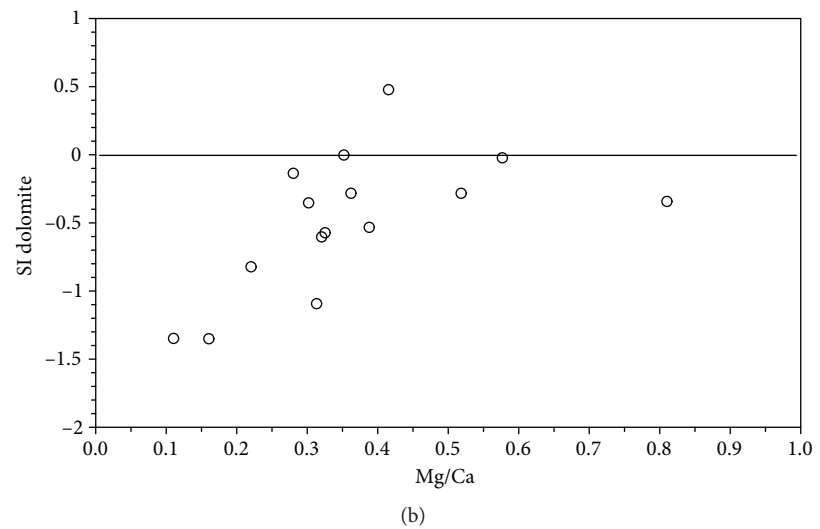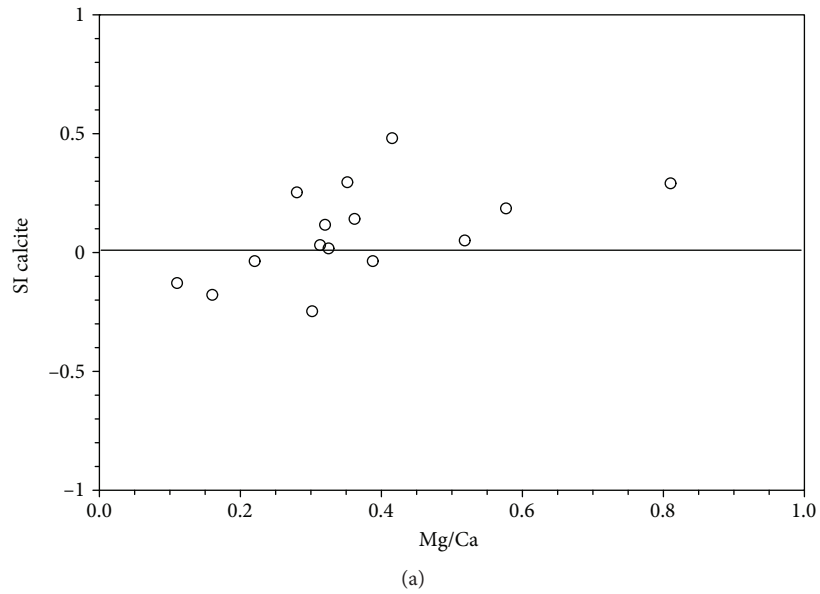
FIGURE 6: (a) Saturation index (S.I.) of calcite versus Mg/Ca ratio. (b) Saturation index (S.I.) of dolomite versus Mg/Ca ratio.
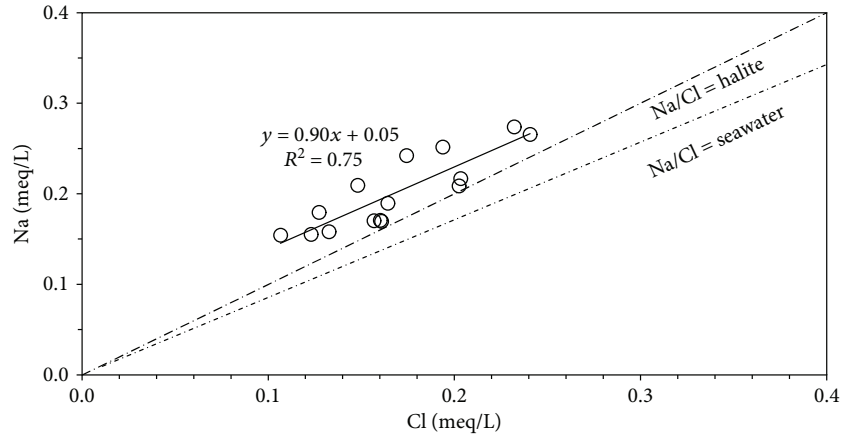
FIGURE 7: Na$^+$ vs. Cl$^-$ in meq/L. The reference lines of the Na/Cl ratio in halite and seawater are also displayed.
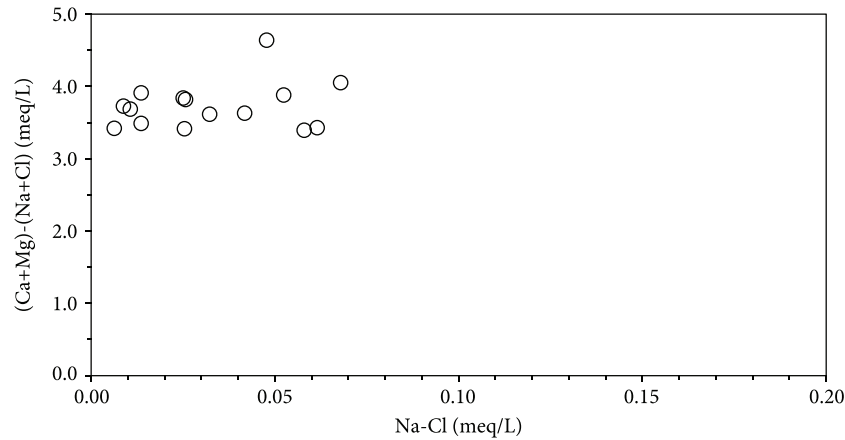
FIGURE 8: $[(Ca^{2+}+Mg^{2+})-(HCO_3^-+SO_4^{2-})]$ vs. (Na^+-Cl^-). The investigated water samples are not correlated highlighting that the ion exchange process does not take place.

interpreted as representative of the weathering of silicates (alkaline feldspar) or a process of ionic exchange.

In order to identify the possible process of ionic exchange, the graph of the relationship of $[(Ca^{2+}+Mg^{2+}) - (HCO_3^-+SO_4^{2-})]$ vs. (Na^+-Cl^-) has been considered (Figure 8). Ca^{2+} and Mg^{2+} concentrations are corrected by $HCO_3^-+SO_4^{2-}$, to exclude the contribution of ions from carbonates and silicates. Na^+ concentration is corrected by Cl^- to exclude Na^+ from atmospheric deposition [55].

Our data do not show a good correlation suggesting that the ionic exchange process is not possible. Therefore, the relative Na-excess is probably due to interaction of water with alkaline feldspar belonging to clastic rocks of the Frido Unit.

Factor analysis allowed verifying the important interdependences among the chemical elements. The factor component matrix (Table 4) determined by factor analysis explains the relationship between the components and the variables.

The analysis shows that component 1 is related to the sodium, sulphate, and chloride variables while electrical conductivity, calcium, potassium, and bicarbonates are linked to component 2.

The physical interpretation of the two factors is graphically evidenced in the two-component plot of Figure 9, where two main groups of variables related to physicochemical data of groundwater samples are shown and, even if they both fall within the positive value field, are anticorrelated.

In component 1, it is clear that the ions of Na^+, SO_4^{2-}, and Cl^-, even if characterized by low concentrations, have a high contribution in terms of correlation, indicating the interaction of water with silicate minerals of the arenaceous-pelitic flysch deposits. The loading of Na and Cl and their interrelation, can derive also, to a lesser extent, from the contribution of the sea spray provided by the high rainfall amounts of the study area, due to the orographic conditions and the nearness of the hydrostructure to the sea. The high permeability of the carbonate formations due to the intense fracturing state and karst processes promotes the infiltration of the precipitations into the groundwater system.

The results of component 2 indicate that the high loading factors of EC, Ca^{2+}, HCO_3^-, and K^+ can be associated with the dissolution of carbonate into the aquifer system, which increases the concentrations of these ions. Carbonate dissolution is the most important process affecting the ion concentrations of the groundwater of the samples. The loading factor of Mg^{2+} represents the processes related to the dissolution of the dolomites and dolomitic limestones.
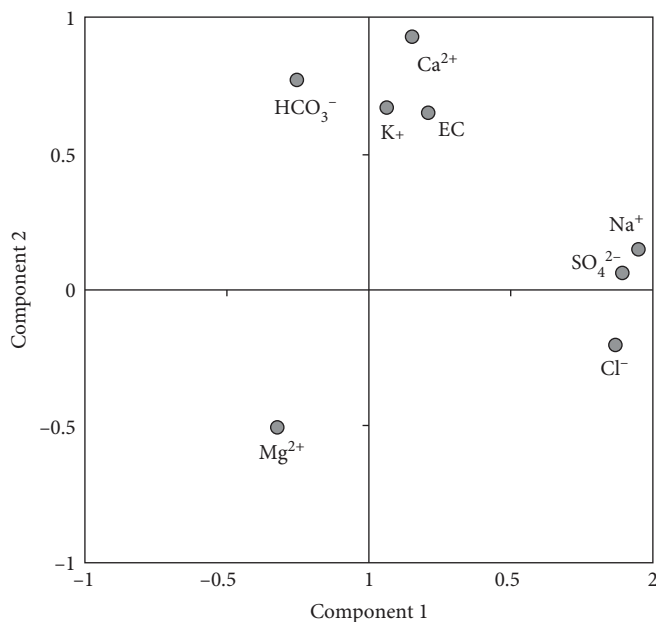
FIGURE 9: Factor score plot of components 1 and 2 in rotated space of the main analysed parameters.

Moreover, in the carbonate environments, in the presence of the arenaceous and marly flysch deposits, the effect of water-flysch interactions acts as the dissolution mechanisms of the silicates involving the release of detectable quantity of Ca^{2+}, HCO_3^-, Mg^{2+}, K^+, Na^+, and H_4SiO_4 [56, 57].

The factor scores of K^+ and NO_3^-, characterized by very low concentrations, do not have any discernible pattern, and the nitrate ion has no significant lithologic source; the correlation degree suggest that it may be associated mainly with zootechnical activity or surface runoff of fertilizer used for agricultural purposes.

5.2. δD and $\delta^{18}O$ Groundwater Data. Groundwater shows isotopic compositions ranging between -7.5‰ and –8.6‰ for oxygen and -42‰ and -54‰ for deuterium.

The δD and $\delta^{18}O$ relationship is plotted in Figure 10. All groundwaters plot between the Global Meteoric Water Line (GMWL) [58] and the Mediterranean Meteoric Water Line (MMWL) [59]. This indicated that groundwaters have a meteoric origin and secondary processes occurring after the precipitation (i.e., evaporation, evapotranspiration, and/or water–rock interaction) do not significantly change the isotope ratios of groundwater.

Most of the groundwater springs sampled in November 2017 show an enrichment in O and D heavier isotopes than do data measured in May 2017. The difference in $\delta^{18}O$ isotopic composition between the samplings is superior to the analytical error (0.1‰ and 1‰ for $\delta^{18}O$ and δD values, respectively). This is possible because in these springs, the contribution by seasonal rainfall is present, and this may be due to an aquifer with low water capacity and relatively short and shallow hydrogeological circuits through the sedimentary units. Only a limited number of groundwater (P10, P11, and P12 springs), sampled in November 2017, show isotopic values similar to data recorded in May 2017. These springs are not influenced by the seasonal variation of the

meteoric recharge. Therefore, under these conditions we may assume that these springs drain the deep aquifers characterized by deep groundwater flow pathways, where the temporal variations of the isotopic ratios are usually within the measurement error. In addition, these groundwaters, showing mean oxygen isotope ratios between -8.4‰ and -8.6‰, are similar to the springs, located at high altitudes >900 meters above sea level (a.s.l.), and pertaining to relatively short and shallow hydrogeological circuits. This finding allows estimating that the average altitude of the recharge areas for the major springs characterized by homogenous groundwater isotopic data ranges from 900 m to 1000 m a.s.l.

6. Conclusions

This study focused on the hydrogeological setting and groundwater hydrogeochemical assessment of the carbonate hydrostructure of the Lauria Mountains northern sector (southern Apennines). The complex hydrogeological environment and the hydrodynamic characteristics of the aquifer system reflect the geostructural peculiarities of the carbonate hydrostructure. According to the stratigraphic and tectonic setting, deep groundwater flow pathways feed the major springs. The presence of these important springs plays a considerable socioeconomic role for the interest of the entire territory in terms of water availability.

Results highlight that hydrogeochemical and stable isotopic investigations are useful to defining the hydrogeological conceptual model of the aquifer system and representing the essential tool to characterize groundwater chemical assessment. Hydrogeochemical analysis elucidates that the chemical compositions of groundwater depend from the lithology and from the hydrodynamic characteristics of the systems. It suggests that carbonate dissolution is the controlling factor for groundwater chemical properties. The factor
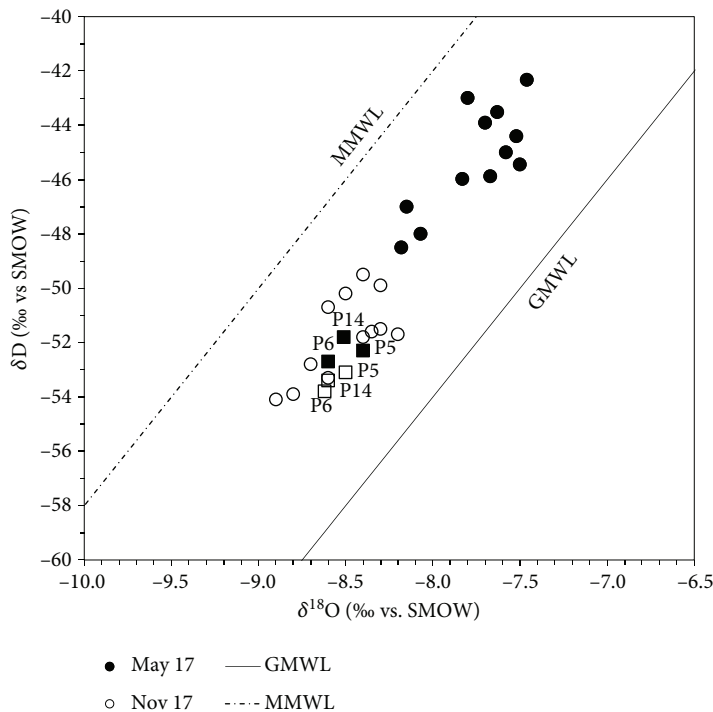
FIGURE 10: δ^{18}O and δD plot of local groundwater. For comparison, the global meteoric water line (GMWL) and the Mediterranean meteoric water line (MMWL) have been drawn. The filled and empty squares indicate the isotopic data of P6, P14, and P5 springs sampled in May 2017 and November 2017, respectively.

analysis has demonstrated a greater usefulness in interpreting the hydrogeochemical data relating to water–rock interaction processes with carbonate rocks and silicate minerals.

The main aim of this study was to achieve a deeper understanding of the hydrogeological system and groundwater hydrogeochemical characteristics of the carbonate hydrostructure, using a hydrogeological and hydrogeochemical integrated approach, even in hydrogeological systems with limited data availability, finalized at identifying available groundwater resources.

At present, it is possible to argue that considerable groundwater amounts can be used for supplementary and substitutive uses, or to compensate for water emergencies, through sustainable and opportune management actions and strategies.

The current changes in hydrogeology should be faced by improved focus on monitoring techniques and exploitation of information; therefore, the relevance of this carbonate hydrostructure requires further and more detailed knowledge. The findings indicate that effort should be directed, in the future, to the monitoring of the springs discharge, to the detailed isotopic study of rainfall and groundwater, for a better understanding of the preferential groundwater flow directions, of recharge time, taking into account the impact of climate change, in the perspective of protecting these resources from depletion and contamination.

Data Availability

The data used to support the findings of this study are included within the article.

Disclosure

Conflicts of Interest

The authors declare that there is no conflict of interest regarding the publication of this paper.

References

[1] S. Eden and R. G. Lawford, "Using science to address a growing worldwide water dilemma for the 21st century," in *Water: Science, Policy and Management. Water Resources Monograph 16,* Lawford, Ed., Publisher AGU, 2003.

[2] C. J. Vörösmarty, P. B. McIntyre, M. O. Gessner et al., "Global threats to human water security and river biodiversity," *Nature*, vol. 467, no. 7315, pp. 555–561, 2010.

[3] M. M. Mekonnen and A. Y. Hoekstra, "Four billion people facing severe water scarcity," *Science Advances*, vol. 2, no. 2, article e1500323, 2016.

[4] C. J. Vörösmarty, P. Green, J. Salisbury, and R. B. Lammers, "Global water resources: vulnerability from climate change and population growth," *Science*, vol. 289, no. 5477, pp. 284–288, 2000.

[5] T. Distefano and S. Kelly, "Are we in deep water? Water scarcity and its limits to economic growth," *Ecological Economics*, vol. 142, pp. 130–147, 2017.

[6] R. G. Taylor, B. Scanlon, P. Döll et al., "Ground water and climate change," *Nature Climate Change*, vol. 3, no. 4, pp. 322–329, 2013.

[7] European Commission, "Directive 2000/60/EC of the European Parliament and of the Council of 23 October 2000 establishing a framework for community action in the field of water policy," *Official Journal of the European Communities*, vol. 2000, 2000.

[8] European Commission, "Directive 2006/118/EC of the European Parliament and of the Council of 12 December 2006 on the protection of groundwater against pollution and deterioration," *Official Journal of the European Communities*, vol. 2006, 2006.

[9] Decreto legislativo 3 aprile 2006, *Norme in materia ambientale*, Gazzetta Ufficiale, 2006.

[10] L. W. Mays, "Groundwater resources sustainability: past, present, and future," *Water Resources Management*, vol. 27, no. 13, pp. 4409–4424, 2013.

[11] W. J. Cosgrove and D. P. Loucks, "Water management: current and future challenges and research directions," *Water Resources Research*, vol. 51, no. 6, pp. 4823–4839, 2015.

[12] I. Clark and P. Fritz, *Environmental Isotopes in Hydrology*, Lewis Publishers, New York, 1997.

[13] G. Vandenschrick, B. van Wesemael, E. Frot et al., "Using stable isotope analysis (δD–$\delta 18O$) to characterise the regional hydrology of the Sierra de Gador, south east Spain," *Journal of Hydrology*, vol. 265, no. 1-4, pp. 43–55, 2002.

[14] W. M. Edmunds, "Geochemistry's vital contribution to solving water resource problems," *Applied Geochemistry*, vol. 24, no. 6, pp. 1058–1073, 2009.

[15] I. Cartwright, T. R. Weaver, D. I. Cendón et al., "Constraining groundwater flow, residence times, inter-aquifer mixing, and aquifer properties using environmental isotopes in the southeast Murray Basin, Australia," *Applied Geochemistry*, vol. 27, no. 9, pp. 1698–1709, 2012.

[16] A. L. Herczeg, F. W. J. Leaney, M. F. Stadler, G. L. Allan, and L. K. Fifield, "Chemical and isotopic indicators of point-source recharge to a karst aquifer, South Australia," *Journal of Hydrology*, vol. 192, no. 1-4, pp. 271–299, 1997.

[17] L. Yin, G. Hou, X. Su et al., "Isotopes (δD and $\delta 18O$) in precipitation, groundwater and surface water in the Ordos Plateau, China: implications with respect to groundwater recharge and circulation," *Hydrogeology Journal*, vol. 19, no. 2, pp. 429–443, 2011.

[18] S. Prada, J. V. Cruz, and C. Figueira, "Using stable isotopes to characterize groundwater recharge sources in the volcanic island of Madeira, Portugal," *Journal of Hydrology*, vol. 536, pp. 409–425, 2016.

[19] B. D'Argenio, T. Pescatore, and P. Scandone, "Schema geologico dell'Appennino meridionale (Campania e Lucania)," in *Atti del convegno "Moderne vedute sulla geologia dell'Appennino"*, vol. 183, pp. 49–72, Quaderni Accademia Nazionale Lincei, 1973.

[20] M. Schiattarella, "Tettonica della Catena del Pollino (confine calabro-lucano)," *Memorie Società Geologica Italiana*, vol. 51, pp. 543–566, 1996.

[21] E. Perri and M. Schiattarella, "Evoluzione tettonica quaternaria del bacino di Morano Calabro (Catena del Pollino), Calabria settentrionale," *Bollettino Società Geologica Italiana*, vol. 116, pp. 3–15, 1997.

[22] M. Schiattarella, "Quaternary tectonics of the Pollino Ridge, Calabria-Lucania boundary, Southern Italy," in *Continental Transpressional and Transtensional Tectonics*, R. E. Holdsworth, R. A. Strachan, and J. F. Dewey, Eds., vol. 135, no. 1pp. 341–354, Geological Society, London, 1998.

[23] F. Russo and M. Schiattarella, "Osservazioni preliminari sull'evoluzione morfostrutturale del bacino di Castrovillari (Calabria settentrionale)," *Studi Geologici Camerti*, vol. 1992/1, pp. 271–278, 1992.

[24] E. Turco, R. Maresca, and P. Cappadona, "La tettonica plio-pleistocenica del confine calabro-lucano: modello cinematico," *Memorie Società Geologica Italiana*, vol. 45, pp. 519–529, 1990.

[25] M. Schiattarella, M. M. Torrente, and F. Russo, "Analisi strutturale ed osservazioni morfostratigrafiche nel bacino del Mercure (confine calabro-lucano)," *Il Quaternario, Italian Journal of Quaternary Sciences*, vol. 7, pp. 613–626, 1994.

[26] D. Gioia and M. Schiattarella, "Caratteri morfotettonici dell'area del Valico di Prestieri e dei Monti di Lauria (Appennino Meridionale)," *Il Quaternario, Italian Journal of Quaternary Sciences*, vol. 19, no. 1, pp. 129–142, 2006.

[27] E. Patacca and P. Scandone, "Geology of the Southern Apennines," *Bollettino Società Geologica Italiana*, vol. 7, pp. 75–119, 2007.

[28] P. Scandone, "The preorogenic history of the Lagonegro basin (southern Apennines)," in *Geology of Italy*, C. Squyres, Ed., pp. 305–315, The Earth Sciences Society of the Libyan Arab Republic, 1975.

[29] P. Scandone, "Studi di geologia lucana: Carta dei terreni della serie calcareo-silico-marnosa e note illustrative," *Bollettino della Società dei Naturalisti in Napoli*, vol. 81, pp. 225–300, 1972.

[30] P. Scandone, "Studi di geologia lucana: la serie calcareo-silico-marnosa e i suoi rapporti con l'Appennino calcareo," *Bollettino Società Naturalisti in Napoli*, vol. 7766, pp. 1–175, 1967.

[31] E. Marsella, "I terreni lagonegresi tra San Fele e la Val d'Agri. Evoluzione tettonico-sedimentaria (Trias superiore-Giurassico)," in *Tesi di Dottorato in Geologia del Sedimentario*, Università di Napoli, 1988.

[32] F. Mostardini and S. Merlini, "Appennino centro meridionale. Sezioni geologiche e proposta di modello strutturale," *Memorie Società Geologica Italiana*, vol. 35, pp. 177–202, 1986.

[33] L. Ogniben, "Schema introduttivo alla geologia del confine calabro-lucano," *Memorie Società Geologica Italiana*, vol. 8, pp. 435–763, 1969.

[34] S. D. Knott, "The Liguride Complex of Southern Italy – a Cretaceous to Paleogene accretionary wedge," *Tectonophysics*, vol. 142, no. 2-4, pp. 217–226, 1987.

[35] S. D. Knott, "Structure, kinematics and metamorphism in the Liguride Complex, southern Apennines, Italy," *Journal of Structural Geology*, vol. 16, no. 8, pp. 1107–1120, 1994.

[36] S. Laurita and G. Rizzo, "Blueschist metamorphism of metabasite dykes in the serpentinites of the Frido Unit, Pollino Massif," *Rendiconti Online della Società Geologica Italiana*, vol. 45, pp. 129–135, 2018.

[37] G. Rizzo, M. T. C. Sansone, F. Perri, and S. Laurita, "Mineralogy and petrology of the metasedimentary rocks from the Frido Unit (southern Apennines, Italy)," *Periodico di Mineralogia*, vol. 85, pp. 153–168, 2016.

[38] G. Papani, M. T. De Nardo, G. Bettelli, D. Rio, C. Tellini, and L. Vernia, *Note Illustrative della Carta Geologica d'Italia alla*

scala 1:50.000 e Foglio 521 LAURIA, ISPRA, Servizio Geologico d'Italia, 2016.

[39] G. Bonardi, F. O. Amore, G. Ciampo, P. De Capoa, P. Miconnet, and V. Perrone, "Il Complesso Liguride Auct.: stato delle conoscenze e problemi aperti sulla sua evoluzione pre-appenninica ed i suoi rapporti con l'Arco Calabro," *Memorie Società Geologica Italiana*, vol. 4, pp. 17–35, 1988.

[40] F. Canora, M. A. Musto, and F. Sdao, "Groundwater recharge assessment in the carbonate aquifer system of the Lauria Mounts (southern Italy) by GIS-based distributed hydrogeological balance method," in *Computational Science and Its Applications–ICCSA 2018, Lecture Notes in Computer Science*, O. Gervasi, Ed., Springer, 2018.

[41] M. Civita, "Proposte operative per la legenda delle carte idrogeologiche," *Bollettino Società Naturalisti in Napoli*, vol. 82, pp. 1–12, 1973.

[42] F. Sdao and G. D'Ecclesiis, "Idrogeologia dei Monti di Lauria (Basilicata)," in *Atti del 3° Convegno Nazionale Protezione e Gestione Acque Sotterranee per il III Millennio*, P. Bologna, Ed., vol. 2, pp. 175–183, Quaderni di Geologia Applicata, Parma, 1999.

[43] M. C. Dichicco, A. De Bonis, G. Mongelli, G. Rizzo, and R. Sinisi, "μ-Raman spectroscopy and X-ray diffraction of asbestos' minerals for geo-environmental monitoring: the case of the southern Apennines natural sources," *Applied Clay Science*, vol. 141, pp. 292–299, 2017.

[44] M. Dichicco, S. Laurita, R. Sinisi, R. Battiloro, and G. Rizzo, "Environmental and health: the importance of Tremolite Occurence in the Pollino Geopark (Southern Italy)," *Geosciences*, vol. 8, no. 3, p. 98, 2018.

[45] G. Rizzo, S. Laurita, and U. Altenberger, "The Timpa delle Murge ophiolitic gabbros, southern Apennines: insights from petrology and geochemistry and consequences to the geodynamic setting," *Periodico di Mineralogia*, vol. 87, pp. 5–20, 2018.

[46] Landsystem, *Piano di Risanamento delle Acque della Regione Basilicata: Censimento dei corpi idrici*, Regione Basilicata, 1990.

[47] L. Ferranti, J. S. Oldow, and M. Sacchi, "Pre-Quaternary orogen-parallel extension in the Southern Apennine belt, Italy," *Tectonophysics*, vol. 260, no. 4, pp. 325–347, 1996.

[48] A. Ietto and B. D'Argenio, "Some accounts on thrust and subsequent extensional tectonics in the Pollino Mountains. Southern Apennines," *Rendiconti Online Società Geologica Italiana*, vol. 13, pp. 121–124, 1990.

[49] D. L. Parkhurst and C. A. J. Appello, "User's guide to PHREEQC (version 2)—a computer program for speciation, batch-reaction, one-dimensional transport, and inverse geochemical calculations," *US Geological Survey Water-Resources Investigations*, pp. 99–4259, 1999, Report.

[50] D. L. Parkhurst and C. A. J. Appello, "Description of input and examples for PHREEQC version 3: a computer program for speciation, batch-reaction, one-dimensional transport, and inverse geochemical calculations," in *Techniques and Methods, Book 6, chapter A43*, p. 497, U.S. Geological Survey, 2013.

[51] A. Shrivastava and V. B. Gupta, "Methods for the determination of limit of detection and limit of quantitation of the analytical methods," *Chronicles of Young Scientists*, vol. 2, no. 1, pp. 21–25, 2011.

[52] Statgraphics® Centurion XVI User Manual, *StatPoint Technologies, Inc*, 2009.

[53] Decreto legislativo 2 febbraio 2001, *Attuazione della direttiva 98/83/CE relativa alla qualità delle acque destinate al consumo umano*, Gazzetta Ufficiale, 2001.

[54] A. M. Piper, "A graphic procedure in the geochemical interpretation of water-analyses," *Transactions of the American Geophysical Union*, vol. 25, no. 6, pp. 914–923, 1944.

[55] A. Biswas, B. Nath, P. Bhattacharya et al., "Hydrogeochemical contrast between brown and grey sand aquifers in shallow depth of Bengal Basin: consequences for sustainable drinking water supply," *Science of The Total Environment*, vol. 431, pp. 402–412, 2012.

[56] E. Merlak, *Solubilità della silice nell'interazione acqua-flysch del carso Triestino*, vol. 44, Atti e Memorie della Commissione Grotte E. Boegan, 2014.

[57] M. Amanti, M. Buchetti, D. Centioli et al., "Hydrogeochemical features of spring waters in the Sheet N. 348 "Antrodoco" area," *Periodico di Mineralogia*, vol. 81, no. 3, pp. 269–299, 2012.

[58] H. Craig, "Isotopic variations in meteoric waters," *Science*, vol. 133, no. 3465, pp. 1702-1703, 1961.

[59] J. R. Gat and I. Carmi, "Evolution of the isotopic composition of atmospheric waters in the Mediterranean Sea area," *Journal of Geophysical Research*, vol. 75, no. 15, pp. 3039–3048, 1970.

Research Article

Inferred Industrial and Agricultural Activities Impact on Groundwater Quality of Skhira Coastal Phreatic Aquifer in Southeast of Tunisia (Mediterranean Region)

Samira Melki [ID], **Amina Mabrouk El Asmi, and Moncef Gueddari**

Laboratory of Geochemistry and Environmental Geology, Department of Geology, Faculty of Sciences of Tunis, University of Tunis El Manar, 2092 Tunis, Tunisia

Correspondence should be addressed to Samira Melki; melkisamiralefi@hotmail.fr

In Tunisia, it has been proven through various previously published studies that agricultural overexploitation and urban and industrial activities increase the risk of groundwater quality deterioration. The present study is a new research to be added to groundwater appraisal and comes to assess groundwater quality of the phreatic Skhira aquifer in relation to surrounding anthropic activities and also tries to evaluate potential risk threatenings of the local population. For that, 20 water well samples covering the phreatic aquifer were analyzed for physical and chemical parameters, major cations and anions, nutrient elements, fluorine, and some trace metal elements. Results show that the area close to the phosphogypsum storage site is the zone which is the most affected by industrial activity. This area corresponds to the upstream part of the aquifer, in terms of the trending flow, and records the highest conductivity values, high $H_2PO_4^-$, F^-, SO_4^{2-}, and Zn^{2+} concentrations. Groundwater samples in this area are also characterized by a relatively low hydrogen potential (acid pH). High NO_3^- are recorded especially upstream of the aquifer and are thought to be caused by high fertilizer use. Overall, most analyzed samples do not meet the World Health Organization norms and therefore are not suitable as drinking waters. In addition, well water use for irrigation represents a medium to high sodicity and alkanization risk. The current study sheds light on the increasing deterioration risk of the aquifer and is an awakening call for decision-makers to imply means for urgent solutions.

1. Introduction

Either worldwide or on a regional or a local scale, groundwater pollution is gaining momentum and is fastly wide spreading. The main causes are related to overexploitation, increase in urban and industrial activities and a more generalized irrigation [1]. Such pollution induced a hydraulic disequilibrium in terms of demand but also a remarkable increase in water cost. Several Mediterranean countries are already facing a situation of severe water quality degradation [2]. In Tunisia, a country with an arid climate, over most of its territory, exploitable water resources became progressively limited and unable to satisfy the increasing demand especially for agricultural use and industrial development [3]. This water crisis deepened with time and is unfortunately forecasted to worsen in the future. Tunisia depends heavily on waterfall

and at the same time is subject to various natural and anthropic processes which are rendering the water crisis even worst. In fact, from the South, the Saharan dunes are in a continuous progression towards the North and forest areas are shrinking as a response to urban expansion. To this, we add an agriculture centered on continuous water irrigation, a low-citizen awareness of water importance and moderate use, and an alarming worldwide climate change which is foreseen. All these are combined factors making Tunisia subject to a tense water crisis which would become critical if practical solutions are not applied in the near future. In addition, current mobilized waters may face more shortage due to phreatic aquifer overexploitation, exploitation of nonrenewable underground deep aquifers, the siltation of dams, and overall pollution which may affect all these resources. On the other hand, groundwater resources of the Mediterranean

coastal plains in the southern bank of the basin (Middle East and North Africa) show a qualitative and quantitative deterioration worsening with time [4].

In Tunisia, water aquifers constitute an important part of water resources with a hydric potential representing 42% of total volume, estimated at 4840 million m^3 [5]. However, seawater intrusion due to overexploitation, agricultural activity, and industrial discharges may lead to the degradation of groundwater quality and reduced opportunities for their use. The assessment of the availability and quality of these waters is becoming essential and crucial in the integrated management of water resources.

In the southeast of Tunisia, the Skhira region is marked by a high aridity with a deficiary hydric balance. The economic activities in this region are diverse and have steadily increased over the last twenty years. Since 1980, the introduction of new hydraulic-agricultural practices in the Skhira area had greatly damaged the natural environment through the increasing of exploitation wells [6]. There are currently over 600 wells, the majority of which are abandoned or are transformed into deep boreholes [7]. Several previous studies have shown that irrigation in arid zones leads to, inescapably, major soil and groundwater degradation.

Industrial activities in the Skhira region are mainly focused on production of chemical fertilizers and phosphoric acid, by transformation of natural phosphates. This production generates, in addition to gaseous and particulate emissions into the atmosphere, a big quantity of liquid discharges and huge amounts of phosphogypsum which is stored on site [8, 9]. These discharges have an effect on the surrounding environment, especially soil, and on the quality of surface and underground waters [10]. The phreatic aquifer of Skhira provides an important water resource, widely exploited to satisfy the growing social and economic needs in the region. Thus, periodic monitoring of groundwater quality is essential. Within this context, this study is aimed at assessing the phreatic aquifer water quality through specific parameters, in particular the physical-chemical measurements, major cations and anions, the nutrient elements, fluorine, and some trace metal elements. This will help to identify the various factors and phenomena that govern their spatial variation and to evaluate the groundwater suitability for human consumption and irrigation purposes.

2. Presentation of the Study Area

The study area is located in the south-east part of Tunisia, on the northern coast of the Gulf of Gabes, at 75 km south of the Sfax City and at 60 km north of the Gabes City (Figure 1). The study area is located between $34°20'$ and $34°54'$ north latitude and between $10°02'$ and $10°42'$ east longitude. Agriculture is the main economic activity in the Skhira region, reinforced by phosphate industry. The Skhira region is under the combined influence of a Saharan climate, hot and dry to the Southwest, and a Mediterranean climate, relatively wet and temperate to the North. It is characterized by scarce rains becoming reasonably abundant during the cold period between the months of November and April and totally drought between the months of May and October. The average annual precipitation is around 180 mm. The mean annual temperature is 23°C [11].

Geologically, the outcrops of the Skhira region consist mainly of sandy-clay sediments termed the Segui formation, rich in gypsum at the top with some thin silty sand levels [12]. This formation is Miocene-Pliocene to Early Quaternary in age (Figure 2(a)). The Skhira aquifer, the current case study, is constituted by sandy horizons either of upper Miocene-Pliocene sediments in the downstream part or of lower Pliocene-Villafranchien sediments in the upstream side (Figure 2(b)). In shallow areas, the aquifer is represented by permeable sandy and silty Quaternary sediments [13].

The Skhira aquifer is limited by the Bir Ali Ouedrane aquifer in the north, Sebkhat Naouel in the west, the Gabes-North aquifer in the south, and by the sea to the east (Figure 1). This aquifer is mainly recharged by meteoric waters. The piezometric level varies from 40 m in the upstream side to 10 m near the coast [14]. Groundwater flows in a northwest to southeast direction, with a hydraulic gradient of $5.15.10^{-3}$ [15].

3. Materials and Methods

3.1. Sampling. Chemical characterization and spatial variation monitorings of Skhira groundwater quality were performed in order to identify the polluting elements from phosphogypsum waste in the industrial area and from the overfertilization related to agricultural activities. A spatial monitoring of different parameters of groundwater evaluation was carried out in January 2014. Samples were taken from 20 wells, which cover most of the Skhira phreatic aquifer. We have to be precise that samples were selected only from wells still in use and only those equipped with a pumping system allowing water to be renewed. Abandoned wells were not included in this study as we believe that they do not represent the current status of the aquifer. For that, water sampling at different depths was performed using a submersible pump while respecting the sampling standards. We proceeded to water renewal by sufficient pumping, accompanied by pH, conductivity, and dissolved oxygen content control. Sampling was carried out when the values of these parameters are believed to have been stabilized. Temperature, pH, dissolved oxygen content, and conductivity were measured in situ using calibrated portable digital meters. Samples taken were acidified using a 0.1 $NHNO_3$ and kept at 4°C until final laboratory analyses [16].

3.2. Analytical Methods. All geochemical analyses were carried out at the Environment and Geochemistry Laboratory of the Faculty of Sciences of Tunis. Laboratory analyses concerned the nutrient elements (nitrates, nitrites, ammoniacal nitrogen, and orthophosphates), major elements (Na^+, K^+, Ca^{2+}, Mg^{2+}, Cl^-, SO_4^{2-}, and HCO_3^-), fluorine, and some trace elements (Zn^{2+}, Al^{3+}, Cu^{2+}, and Fe^{3+}). Anions and cations in solution were analyzed by the following ion chromatography technique: the aqueous sample is injected on an anion or cation column to separate the desired ions according to their charges and their sizes. For example, fluorides, chlorides,
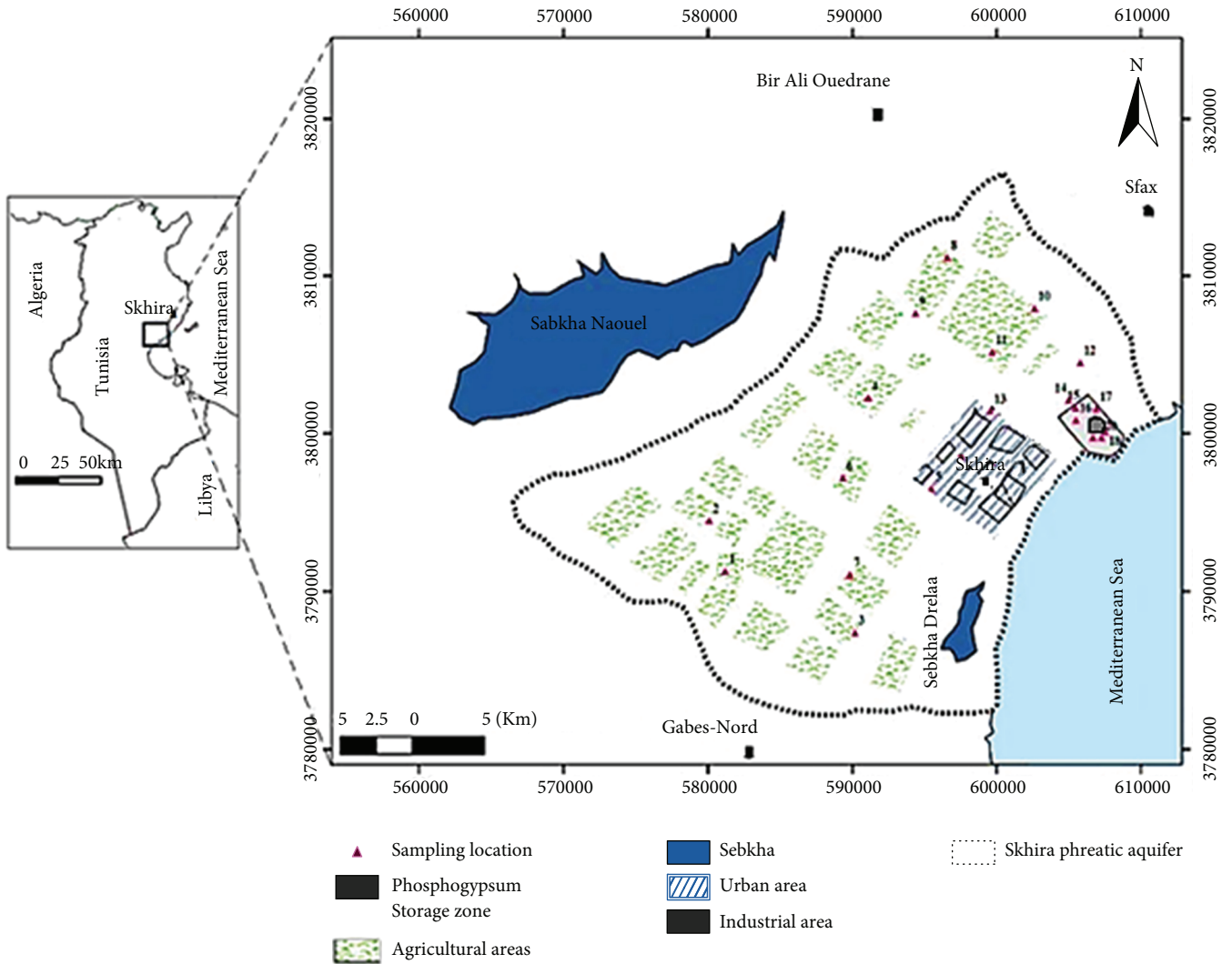
Figure 1: Location map of the study area showing location sampled for groundwater analysis.

bicarbonates, nitrites, nitrates, phosphates, and sulphates in solution are separated on an anionic column and quantified by means of a conductimetric detector positioned at the column outlet [17].

3.3. Chemical Methods. The evaluation of water quality of the Skhira aquifer was determined using different software (AquaChem 2014.2 and XLSTAT 2013 for Windows) and several methods such as geochemical methods combined with GIS. In order to calculate the thermodynamic equilibrium of the Skhira groundwater in relation to associated minerals in the reservoir rock and in the unsaturated zone sediments, we used the PHREEQC program which allows the determination of various coefficient activities on the basis of different established chemical laws (Debye-Huckel's simple law, Debye-Huckel's extended law, and Water and Debye-Huckel's law). This program takes into account kinetic laws in some reactions and allows simulating certain phenomena at the water-sediment interface of the unsaturated zone [18].

3.4. Statistical Analysis. In this study, geostatical modeling was applied to all gathered physical and chemical data on all studied wells of the Skhira aquifer. This modeling combines the SIG tool to geostatical techniques. The interpolation of ordinary "Krigeag" shows a good prediction of the average error close to zero. After applying different variogram models for each groundwater quality parameter of the current study, the error was calculated using cross-validation and is listed in Table 1. The best found kriging parameters were selected from the cross-validation results. The groundwater quality prediction maps (Figures 3–5) show the concentration distribution from the cross-validation process. This geostatical approach generated spatial previsions for nonsampled points through estimation of the lowest error [19].

Multivariate statistical analysis of the experimental data has been performed using XLSTAT. In this study, only the principal component analysis (PCA) and Pearson correlation matrix analysis were undertaken. The application of PCA offers a clearer understanding of groundwater quality and enables comparison of the different waters as well as

(a)

(b)
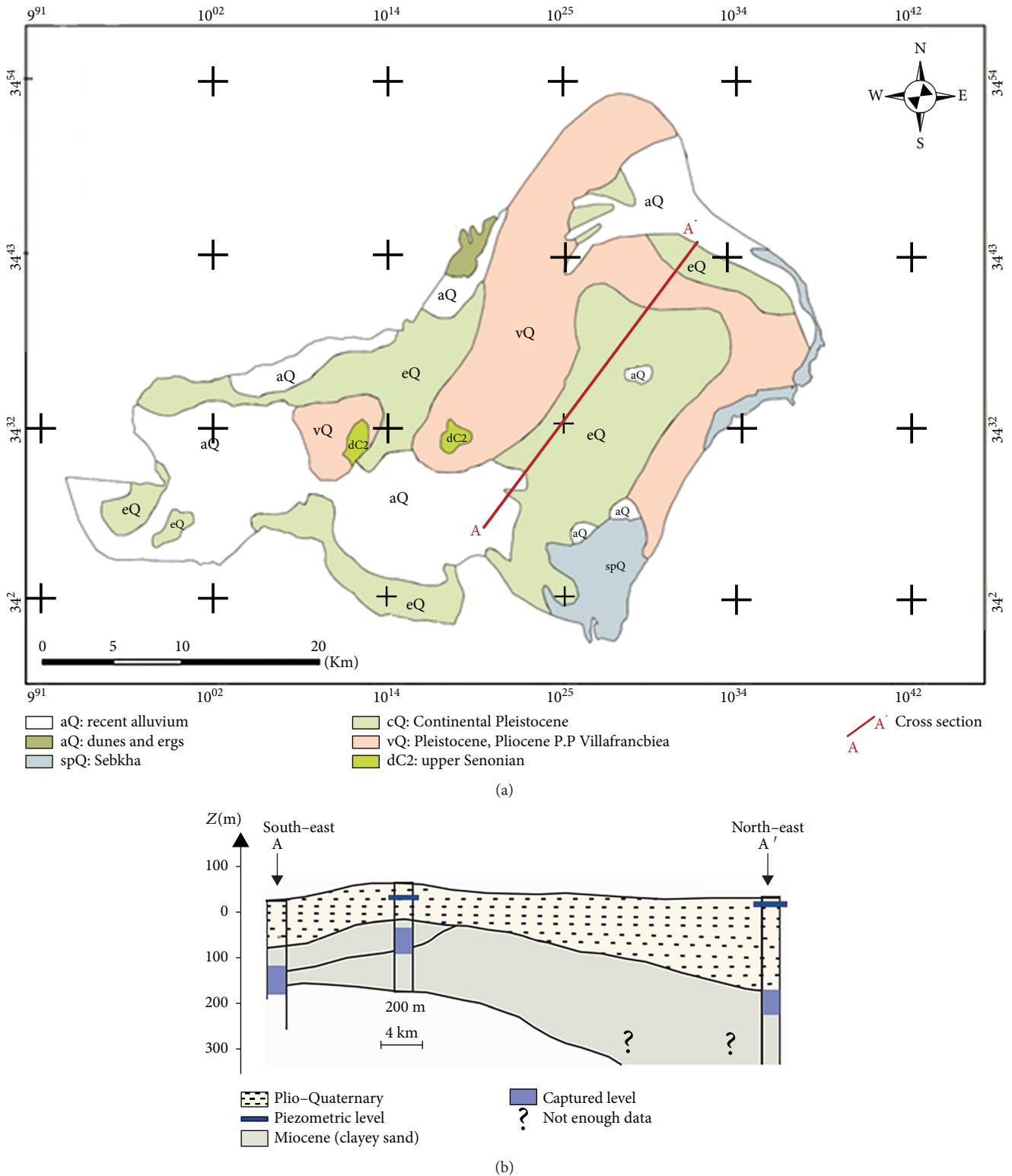
FIGURE 2: Geologic map of the Skhira region (a) ([42], modified) and schematic cross section along A-A′ (b) ([14], modified).

their geochemical correlations [20]. The combination of different established elements (samples and parameters) was used to assess the spatial variation of the groundwater chemical composition and to identify the most common pollution sources.

4. Results and Discussion

4.1. Groundwater Geochemical Characteristics. Results of the physical and chemical parameter analyses of 20 water samples collected from the Skhira aquifer are given in Table 2.

TABLE 1: Fitted parameters of variogram for groundwater quality prediction maps.

Parameters	ME	RMSE	AKSE	MSPE	RMSP
pH	-0.0013	0.225	0.2317	-0.00219	0.9499
EC	-2.803	127	130.9	-0.0117	0.66
NO_3	0.315	11.07	12.75	-0.0021	0.91
H_2PO_4	-1. 483	21.92	22.42	-0.0633	1.66
$SO_4{}^2$	-0.957	18.21	17.28	-0.0205	0.87
F	-0.044	1.33	2.06	0.0300	0.69

ME: mean error; RMSE: root mean squared error; AKSE: average kriging standard error; MSPE: mean standardized prediction error; RMSP: root mean square standardized prediction.

The Skhira aquifer temperatures are little variable with values ranging between 10.1 and 11.8°C. This little variation could be related to the thermic equilibrium between geological strata and infiltrated water.

The groundwater sample pH is overall neutral, with values ranging between 6.45 and 7.19. The lowest values are found within samples SK18 and SK19 which are under the direct influence of gypsum-rich infiltrated waters supplied from the industrial zones where phosphoric acid is processed (Figure 3(a)). These supplied phosphogypsum leachates have a low pH of 2.7 [21]. Water sample electrical conductivity (EC) values range from 2820 to 17200 μS/cm. The EC spatial repartition shows that the most charged waters with dissolved salt are those collected close to the phosphogypsum storage zone. A general increase in EC is observed following the water flow trends which are from south-west to south-east and from north-west to north-east (Figure 3(b)). This increase is related to the water-sediment interaction of the unsaturated zone and to gypsiatic water infiltration. The latter shows an electric conductivity of 19000 μS/cm [21]. However, we have to emphasize that based on [14, 22–24], salinity around the Skhira coast has increased with time from 1-4 mg/L to 2-10 mg/L between 1994 and 2013. This increase is intimately related to water overexploitation of the aquifer. Such increase suggests a marine intrusion, still to be thoroughly investigated in the future using isotopic signatures.

The dissolved O_2 contents range between 1.2 and 6.1 mg/L. The lowest value was recorded in the water sample collected from the SK18 piezometer, located near the gypsatic water storage ponds. The magnitude of the spatial variation of these levels would be dependent on the thickness of the unsaturated zone, the recharge rate, temperatures acting on the solubility of oxygen, and the upstream-downstream mixing effect [25].

$H_2PO_4{}^-$ is found to be the dominant form of inorganic phosphorus dissolved in analyzed waters, with contents ranging between 1.23 and 33.67 mg/L. This is the most stable form of orthophosphate at pH values between 2.2 and 7.2 [26]. The richest water samples in H_2PO4^- are those collected from SK17 and SK18 piezometers, which are located close to the phosphogypsum dump of the Skhira industrial zone (Figure 4(a)). The low contents are recorded at the upstream side of the aquifer. The spatial variation of these levels is related to the infiltration of phosphogypsum leaching waters and to diffusion according to the flow direction of the aquifer.

Nitrogen is present in natural waters as a particulate dissolved organic form and as a dissolved inorganic form [27]. Dissolved inorganic nitrogen (DIN) analyses targeted nitrates (NO_3^-), nitrites (NO_2^-), and ammoniacal nitrogen (NH_4^+). In the Skhira aquifer, the DIN contents range between 5.79 and 130.7 mg/L for NO_3^-, from 0.01 to 0.08 mg/L for NO_2^-, and from 0.01 to 0.14 mg/L for NH_4^+. The highest NO_3^- contents are measured in piezometers located in the central and northwestern parts of the aquifer (Figure 4(b)). These zones correspond to irrigated perimeters overinseminated by nitrogen fertilizers. The most charged waters in NO_2^- and NH_4^+ are those collected from wells drilled in the industrial zone. We note a positive correlation between NO_3^- and O_2 (Figure 6(a)) combined to a negative correlation between NO_2^- and O_2 (Figure 6(b)) and also between NH_4^+ and O_2 (Figure 6(c)). This implies that oxygen content variation is the driving mechanism of nitrogen distribution in the aquifer. In fact, the most nitrate-rich waters are found to be the most oxygenated, which explains the stability of NO_3^- ions and their predominance over other forms of dissolved inorganic nitrogen. The spatial distribution of nitrate levels would be monitored by physical-chemical parameters and environmental factors related to soils that control NH_4^+ nitrification of chemical fertilizers and/or soil organic matter degradation [28]. However, this distribution is also guided by the unsaturated zone thickness and lithology which ensures nitrate transfer to the saturated zone [29, 30].

The negative correlation between nitrogen (DIN) and orthophosphates (Figure 6(d)) suggests that these two elements do not share the same origin. The nitrogen origin of the Skhira aquifer waters would be mainly related to agricultural activity and the infiltration of organic matter-rich water, as is the case of the water sample collected from SK18 wells.

Figure 7 presents the major element contents with the following predominance order:

(i) $Na^+ > Ca^{2+} > Mg^{2+} > K^+$, for cation

(ii) $Cl^- > SO_4^{2-} > HCO_3^-$, for anion

The Cl^- contents range between 18.44 and 100.19 meq/L and is the dominant anion for the Skhira aquifer. The Na+ contents range from 17.82 to 165 meq/L and is the dominant cation. The Ca^{2+} contents vary from 12.48 to 34 meq/L, Mg^{2+} contents are between 8.4 and 44.08 meq/L, and SO_4^{2-} contents are between 15.62 and 142.66 meq/L, while HCO_3^-
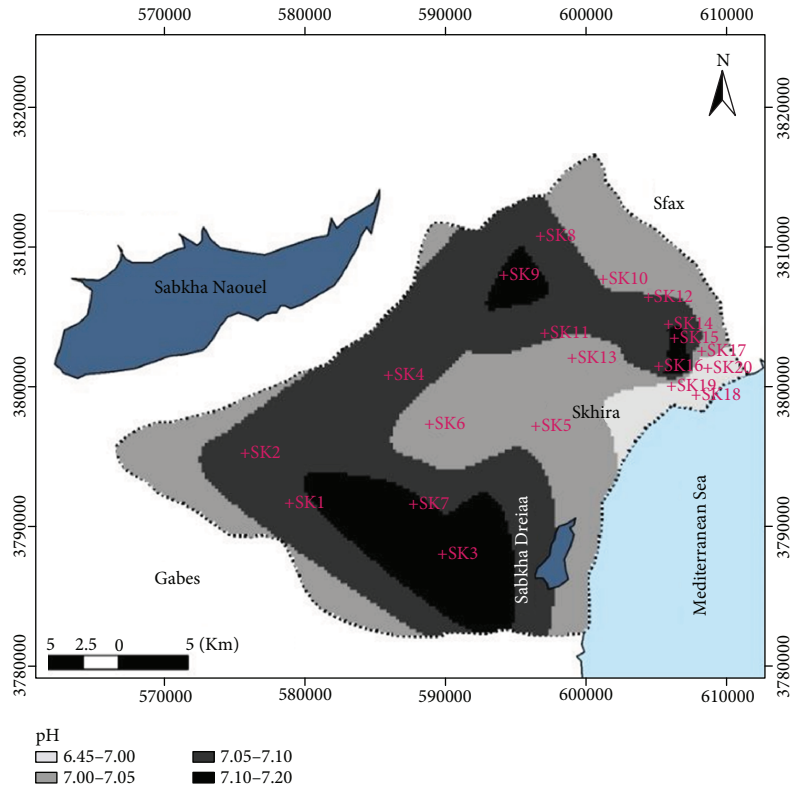
(a)
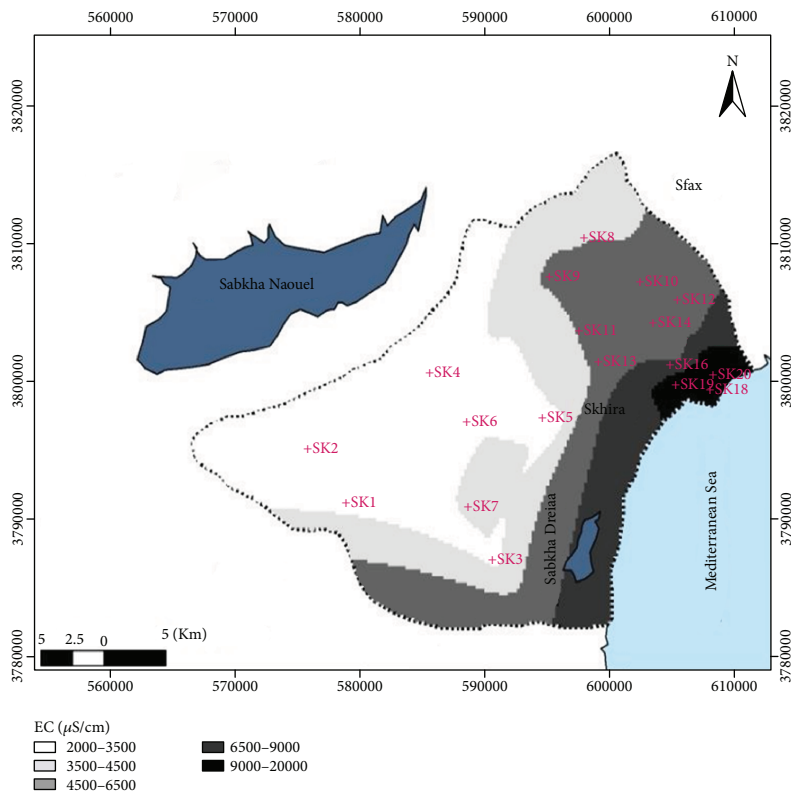
(b)

Figure 3: Spatial distribution maps of pH (a) and electrical conductivity (b) in groundwaters of the Skhira aquifer. See mean error (ME) and root mean square error (RMSE) in Table 1.
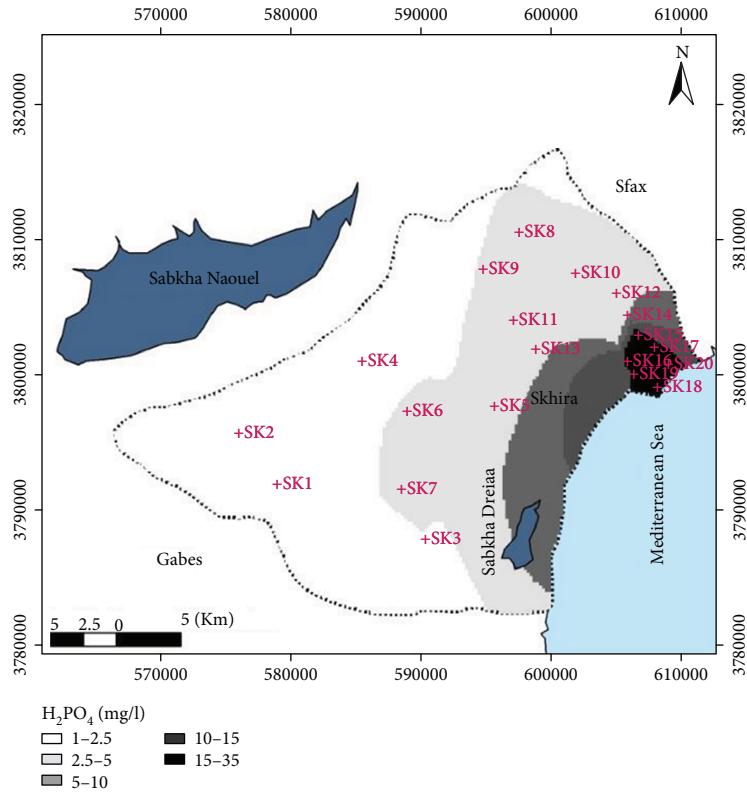
(a)
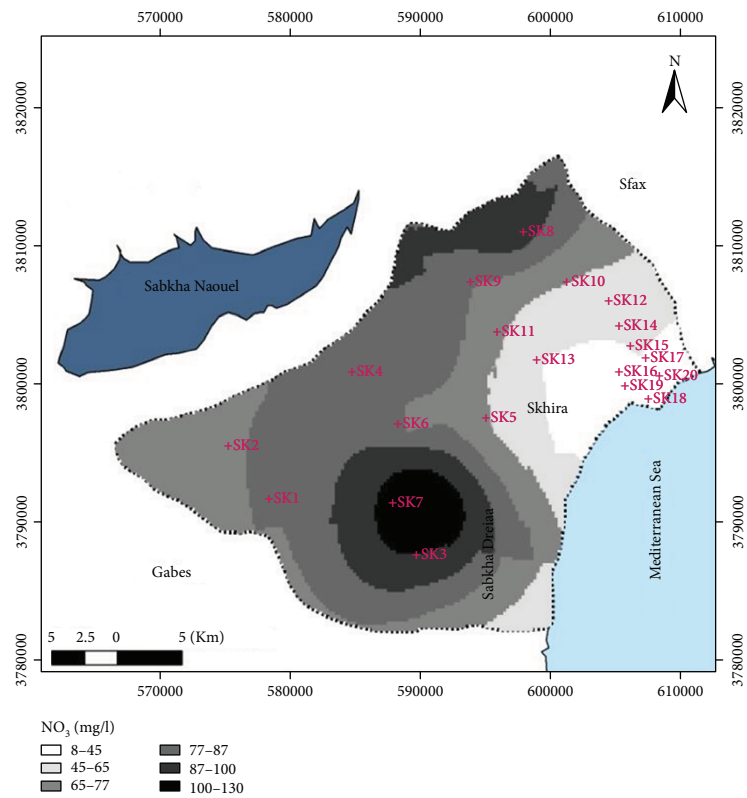
(b)

FIGURE 4: Spatial distribution maps of orthophosphates (a) and nitrates (b) in groundwaters of the Skhira aquifer. See mean error (ME) and root mean square error (RMSE) in Table 1.
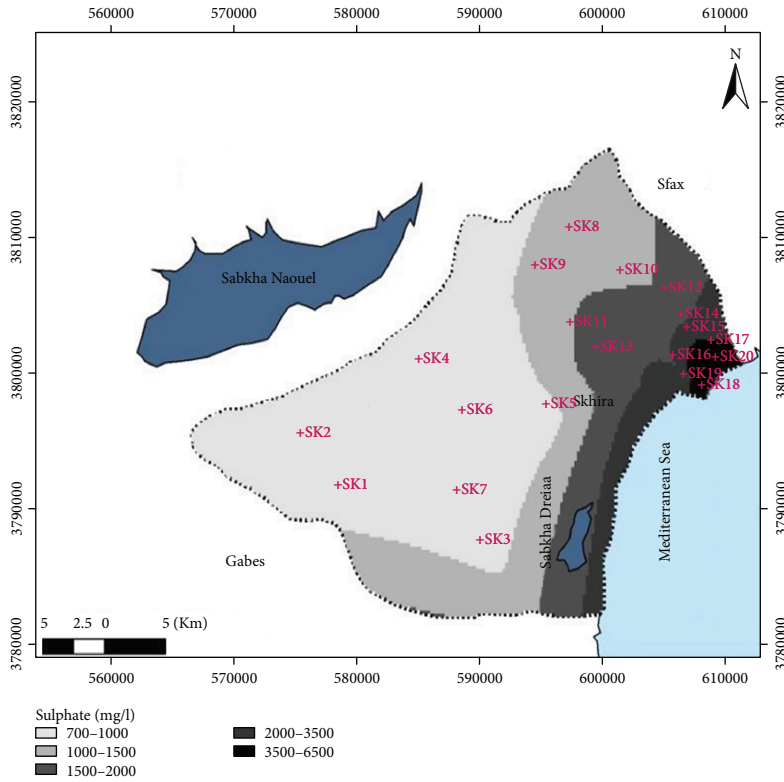
(a)
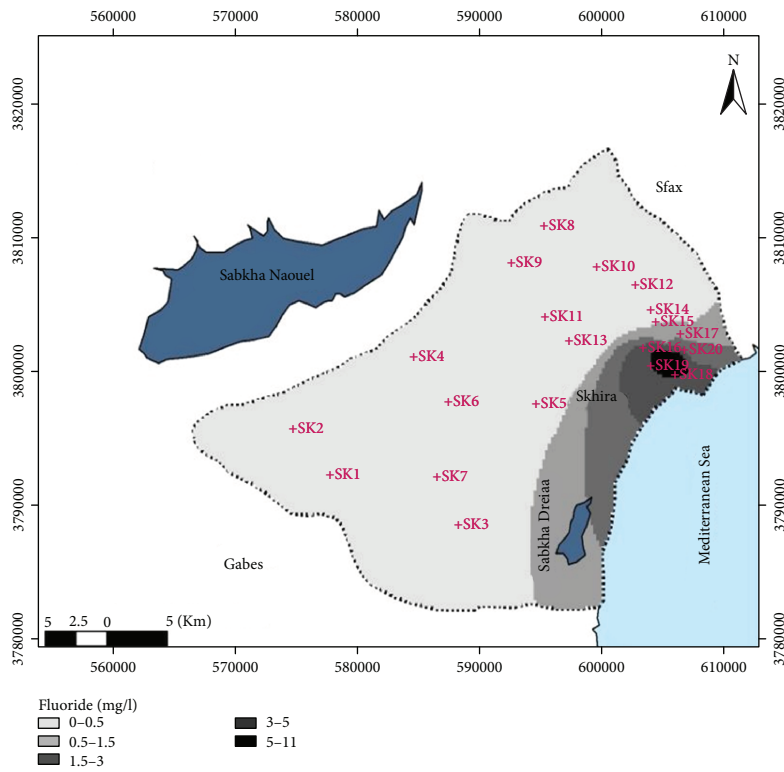
(b)

FIGURE 5: Spatial distribution maps of sulphate (a) and fluoride (b) in groundwaters of the Skhira aquifer. See mean error (ME) and root mean square error (RMSE) in Table 1.

Table 2: Physical and chemical results of water samples of the Skhira phreatic aquifer.

Samples	T (°C)	pH	CE (μS/cm)	O_2 dissolved	Na	Cl	K	Ca	Mg	HCO_3	SO_4	NO_3	NO_2	NH_4	H_2PO_4	F	Al	Fe	Zn	Cu
SK1	11.2	7.17	2820	6.1	447	654	12	256	144	101	750	90.1	0.01	0.02	1.23	0.03	0.12	0.04	0.04	<0.01
SK2	10.1	7.17	2870	5.9	467	672	15	264	136	104	766	83.7	0.01	0.05	1.43	0.05	0.05	0.03	0.04	<0.01
SK3	11.4	7.19	3210	5.8	498	698	16	291	176	113	900	96.7	0.03	0.03	1.76	0.07	0.12	0.04	0.15	<0.01
SK4	11.1	7.15	3312	5.6	410	759	15	378	189	120	920	86	0.01	0.03	1.98	0.05	0.11	0.02	0.06	<0.01
SK5	11	7.13	3356	5.7	454	786	24	305	197	133	940	63.9	0.02	0.04	2.63	0.04	0.13	0.05	0.16	<0.01
SK6	10.8	7.1	3450	5.7	659	806	14	301	101	135	1075	74.3	0.01	0.02	2.8	0.04	0.13	0.04	0.32	<0.01
SK7	11.8	7.18	4506	6.7	763	1033	16	354	211	124	1127	130.7	0.01	0.01	4.9	0.08	0.14	0.14	0.3	<0.01
SK8	11.4	7.01	4557	5.9	770	1098	25	317	258	144	1232	98.3	0.01	0.05	2.7	0.06	0.14	0.03	0.29	<0.01
SK9	10.8	7.15	4789	5.4	794	1101	17	378	175	147	1322	76.8	0.01	0.07	2.45	0.05	0.14	0.41	0.3	<0.01
SK10	10.9	7.09	4980	5.4	803	1243	14	454	201	154	1453	63	0.02	0.03	2.78	0.07	0.12	0.06	0.41	<0.01
SK11	11.3	7.05	4988	5.3	898	1283	24	472	198	156	1642	55.6	0.02	0.02	2.89	0.08	0.12	0.04	0.29	<0.01
SK12	11.7	7.19	5023	5.3	1033	1321	12	453	211	153	1759	55	0.03	0.02	4.27	0.04	0.07	0.02	0.28	<0.01
SK13	11	7.11	5124	5.2	1024	1387	13	489	212	155	1899	45	0.02	0.04	4.5	0.07	0.13	0.27	0.36	<0.01
SK14	10.8	7.12	5250	5.2	1107	1454	11	402	190	177	2027	39.7	0.01	0.12	4.2	1.1	0.12	0.42	0.37	<0.01
SK15	11.2	7.16	6260	5.2	1601	1462	27	466	225	140	2265	42.38	0.02	0.021	18	3.5	0.13	0.02	0.41	<0.01
SK16	11.3	7.12	8300	5.1	1603	1545	43	404	201	260	2009	31.21	0.01	0.075	16	3	0.15	0.37	0.31	<0.01
SK17	10.7	7.06	8940	5.1	1933	1535	25	557	245	162	3110	45.89	0.01	0.1	33.67	1.9	0.15	0.35	0.47	<0.01
SK18	11.8	6.45	17200	1.2	3795	3552	59	675	529	1690	6848	5.79	0.08	0.12	21.67	10.3	0.18	0.78	0.51	<0.01
SK19	11.2	6.94	12840	4.5	1618	1730	24	619	370	165	2675	25.64	0.02	0.12	16.5	5	0.14	0.54	0.37	<0.01
SK20	11.2	7.03	9740	4.6	1827	1690	22	680	355	262	3584	24.14	0.02	0.14	17.67	3.3	0.13	0.65	0.39	<0.01

*Units in mg/L except pH and EC (μS/cm).

(a)

(b)

(c)

(d)
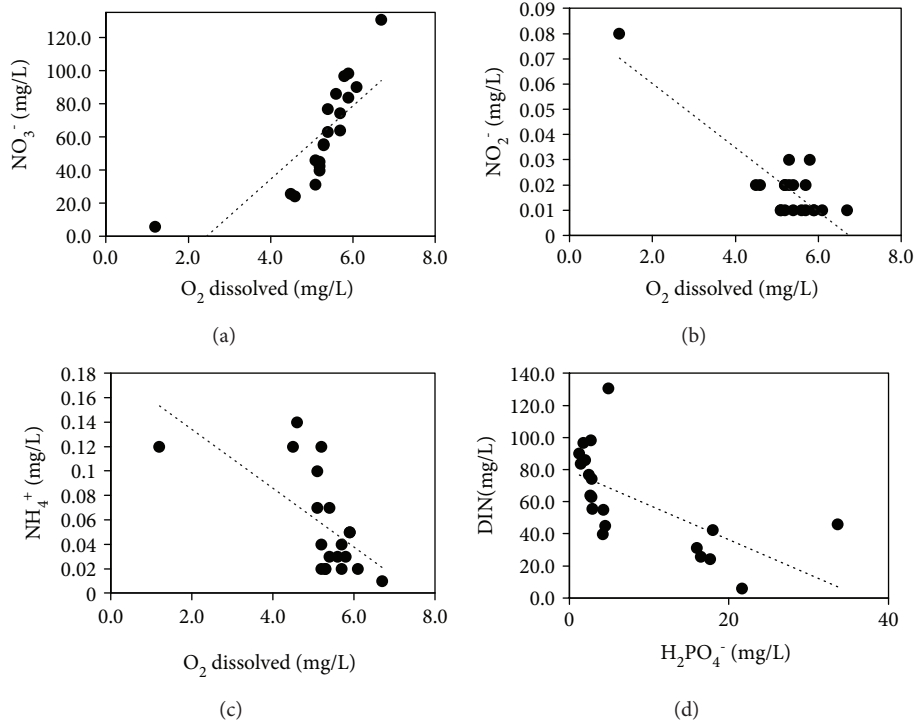
FIGURE 6: Bivariate plot of O_2 dissolved versus NO_3^- (a), NH_4^+ (b), and NO_2^- (c). Bivariate plot of H_2PO_4 versus DIN (NO_3^-+NH_4^++NO_2^-) (d).
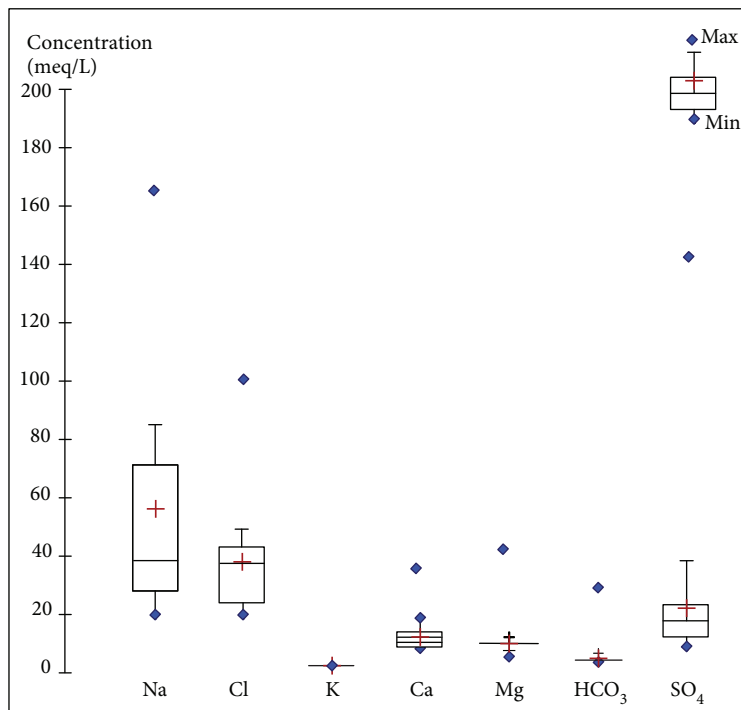
FIGURE 7: Box plot of major elements of the Skhira aquifer.

contents are between 1.65 and 27.7 meq/L. These elements form the bulk of the mineralization of the Skhira aquifer. As has already been shown through EC measurements, waters with the highest dissolved salts are those collected

from wells located in the coastal zone and also north-east of the aquifer, in the industrial zone.

The high sulphate contents recorded downstream (Figure 5(a)), north-east of the aquifer, and near the

TABLE 3: Saturation indices (SI) of $CaCO_3$, $CaSO_4 \cdot 2H_2O$, and CaF_2 in the Skhira phreatic aquifer.

Samples	SK1	SK2	SK3	SK4	SK5	SK6	SK7	SK8	SK9	SK10	SK11	SK12	SK13	SK14	SK15	SK16	SK17	SK18	SK19	SK20
Is calcite	-0.38	-0.37	-0.28	-0.19	-0.26	-0.31	-0.2	-0.38	-0.16	-0.14	-0.17	-0.13	-0.13	-0.16	-0.17	-0.01	-0.09	0.14	0.03	0.05
Is gypsum	-0.6	-0.58	-0.52	-0.42	-0.49	-0.43	-0.41	-0.44	-0.32	-0.24	-0.2	-0.2	-0.15	-0.2	-0.4	-0.23	0	0.17	-0.02	0.1
Is fluoride	-0.85	-3.24	-2.98	-3.17	-3.46	-3.42	-2.85	-3.18	-3.21	-2.88	-2.77	-3.41	-2.89	-0.58	0.43	0.26	-0.07	1.2	0.78	0.42

(a)

(b)

(c)
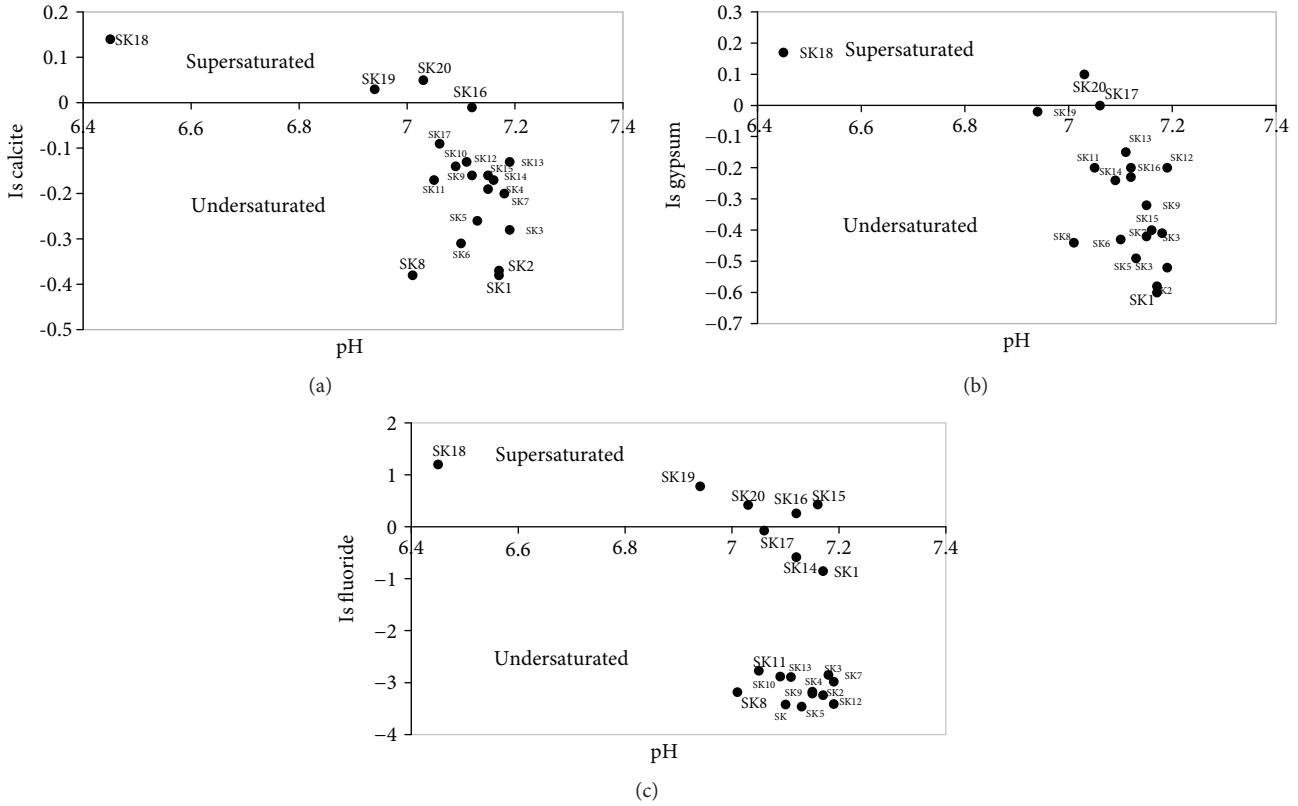
FIGURE 8: Saturation indexes of $CaSO_4 \cdot 2H_2O$ (SI) versus pH (a). Saturation indexes of $CaCO_3$ (SI) versus pH (b). Saturation indexes of CaF_2 (SI) versus pH (c).

phosphogypsum dump could have an atmospheric origin in relation to the emission of sulfur gases, SO_2, and H_2S [31].

In our study, we tested the saturation state with respect to calcite and gypsum. The considered dissolution reactions and the solubility product constant values (T = 25°C and P = 1 atm) are as follows [32]:

$$\text{Calcite}: CaCO_3 + H^+ \leftrightarrow Ca^{++} + HCO_3^- \qquad \log K = 1,71.$$

$$\text{Gypsum}: CaSO_4.2H_2O \leftrightarrow Ca^{++} + SO_4^{2-} + 2H_2O \quad \log K = -4,61.$$

$$(1)$$
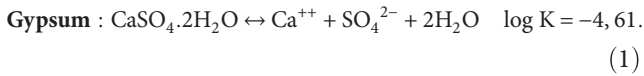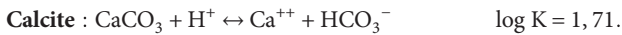
The water saturation indices of the study area with respect to calcite vary from -0.38 to 0.14 (Table 3). Their variations according to pH show that slightly acidic waters are supersaturated with respect to $CaCO_3$ (Figure 8(a)), which confirms the influence of pH on the solubility of this mineral [32].

The saturation indices for gypsum vary from -0.6 to 0.17 (Table 3). Water saturation in regard to gypsum near the industrial zone (SK17, SK18, and SK20; Figure 8(b)) is mainly related to phosphogypsum acid leachate percolation, which favors the solubility of the mineral during infiltration through the unsaturated zone sediments. These results show that the dissolution of gypsum and calcite in the north-east part of the aquifer, normally accelerated in most acidic waters, has led to the increase in calcium and sulphate concentrations in these waters, exceeding the solubility

thresholds of the two minerals [32]. In the rest of the aquifer and under natural recharge conditions, gypsum and calcite undersaturation states may reflect that the dissolution of these two minerals locally controls the total water saline load.

The main source of fluoride in groundwater is the dissolution of fluoride-rich minerals, particularly apatite and fluorine [33]. The groundwater fluoride contents are governed by various factors like temperature, pH, salinity, the amount of fluoride in the host rock, the presence or absence of complexes or colloids, and the solubility of fluorinated minerals [34]. In addition, the F^- anion is not included in adsorption processes or ionic exchanges (as these two mechanisms are only relevant for cations). This leaves only the precipitation-dissolution mechanism as the controlling factor for F^- contents. In the Skhira aquifer, the fluorine contents vary between 0.03 and 10.3 mg/L. The highest contents are measured in water samples collected from piezometers located around the phosphogypsum dump, in particular that of Sk18 (Figure 5(b)) where gypsatic waters are held and are heavily charged in F- with concentrations reaching even 3500 mg/L [21]. Saturation states of fluorite (CaF_2) levels were tested, taking into account the following dissolution equation ($T = 25°C$ and $P = 1$ atm) [33]:

$$\text{Fluorite}: CaF_2 \leftrightarrow Ca^{++} + 2F^- \quad \log K = -10,96. \qquad (2)$$
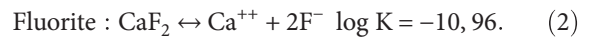
The saturation indices for fluorite vary from -3.46 to 1.2 (Table 3). Based on water saturation index calculations, it is

TABLE 4: Pearson correlation matrix of water quality variables of the Skhira phreatic aquifer.

Variables	T (°C)	pH	EC	O$_2$	Na	Cl	K	Ca	Mg	HCO$_3$	SO$_4$	NO$_3$	NO$_2$	NH$_4$	H$_2$PO$_4$	F	Al	Fe	Zn
T°C	1	-0.2622	0.3448	-0.2821	0.3502	0.4080	0.3888	0.2748	0.4795	0.3992	0.3418	-0.0142	0.5064	-0.0976	0.0988	0.3494	0.4027	0.1394	0.2339
pH		1	-0.7796	0.8479	-0.7591	-0.8097	-0.7664	-0.5462	-0.8120	-0.8756	-0.7994	0.4963	-0.7304	-0.5314	-0.3805	-0.8257	-0.6325	-0.6563	-0.4568
CE			1	-0.8847	0.9442	0.9293	0.7763	0.8600	0.9259	0.7627	0.9332	-0.7574	0.6726	0.7391	0.7654	0.9451	0.5974	0.8518	0.6886
O$_2$				1	-0.9138	-0.9429	-0.7757	-0.7448	-0.8569	-0.9169	-0.9445	0.7765	-0.8609	-0.6214	-0.5593	-0.9120	-0.4843	-0.7497	-0.5753
Na					1	0.9694	0.8191	0.8144	0.8719	0.8404	0.9822	-0.7565	0.7355	0.6561	0.7937	0.9400	0.5921	0.7910	0.7367
Cl						1	0.7911	0.8118	0.8950	0.8804	0.9718	-0.7494	0.7946	0.6268	0.6491	0.9164	0.5742	0.7873	0.7403
K							1	0.4933	0.7222	0.7998	0.7665	-0.5573	0.6597	0.4191	0.6068	0.8376	0.6343	0.5586	0.4502
Ca								1	0.8257	0.5216	0.8390	-0.7900	0.5231	0.6795	0.7293	0.7321	0.4329	0.7656	0.7563
Mg									1	0.7866	0.9052	-0.6217	0.7538	0.6721	0.6137	0.8894	0.5483	0.7700	0.5879
HCO3										1	0.8721	-0.5042	0.8999	0.4324	0.4061	0.8448	0.5001	0.6209	0.4372
SO4											1	-0.7516	0.7864	0.6853	0.7283	0.9238	0.5593	0.8114	0.7054
NO3												1	-0.4840	-0.6834	-0.6368	-0.7192	-0.3187	-0.6955	-0.6246
NO2													1	0.2728	0.2972	0.7513	0.3292	0.4579	0.3828
NH4														1	0.6081	0.6419	0.3867	0.9012	0.4966
H2PO4															1	0.6968	0.5216	0.6157	0.6625
F																1	0.5649	0.7649	0.5731
Al																	1	0.5732	0.6085
Fe																		1	0.6062
Zn																			1

TABLE 5: Summary of the PCA results including the loadings of the eigenvalues.

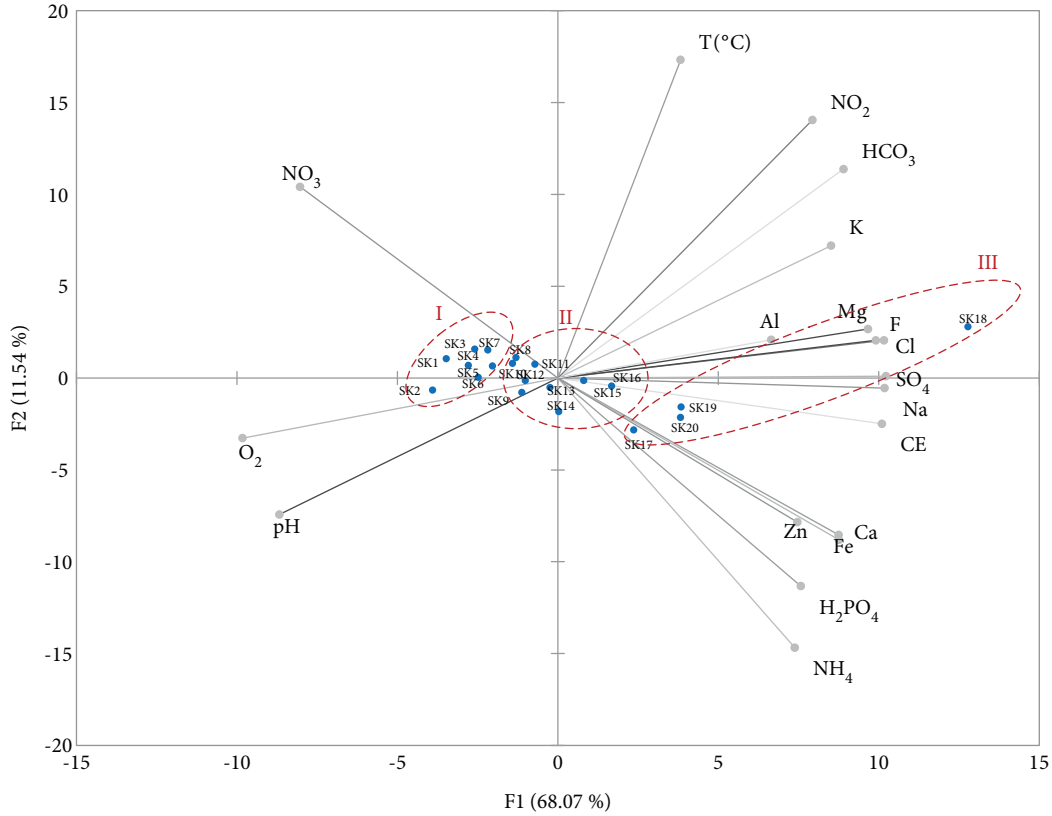|	F1	F2	F3	F4	F5	F6	F7
Eigenvalues	10.89	1.85	1.07	0.69	0.53	0.38	0.26
Variance explained (%)	68.07	11.54	6.71	4.29	3.32	2.39	1.62
Cumulative variance (%)	68.07	79.62	86.33	90.62	93.94	96.33	97.97

FIGURE 9: Spatial distribution of the variables and individuals in the axis system F.

found that samples selected from the industrial zone are the only waters saturated to oversaturated with respect to fluorine. Away from the phosphogypsum storage zone, water samples are found undersaturated with respect to fluorine, in response to mixing with infiltration meteoric waters, and the greater distance from fluorine supply by the phosphogypsum dump. We note that waters saturated with respect to fluorine are also found saturated with respect to calcite and gypsum indicating a spatial dependency related to the phosphogypsum storage zone. Away from this zone, waters become undersaturated in fluorine, calcite, and gypsum. Furthermore, the most acid waters are found saturated with respect to fluorine [35] (Figure 8(c)).

The aluminum contents range between 0.05 and 0.18 mg/L. The highest aluminum concentrations are recorded in the water sample collected from the SK18 piezometer, described above as having the lowest pH value and therefore favorable to the solubility of the element [35]. The iron contents in the analyzed waters range between 0.02 and 0.78 mg/L. The highest concentrations are also

recorded at the SK18 piezometer, where the salinity is peaking and the pH is the lowest. Zinc speciation in water depends on many factors such as pH, the amount of dissolved material, and redox potential. A low pH is necessary to maintain the zinc in solution [36]. Zinc concentrations in analyzed water samples vary between 0.04 and 0.51 mg/L. The highest value characterizes the water sampled near the gypsum collection basins, where zinc contents reach up to 4 mg/L [21]. All analyzed Skhira phreatic aquifer water samples show copper concentrations below detection limit which is around 0.01 mg/L. The absence of trace elements or their presence at very low concentrations in the analyzed groundwater samples compared to those detected in the gypsatic waters can be explained by the sequestering function of soils overlying the unsaturated zone [37].

4.2. Statistical Study. Table 4 includes all correlation coefficients between all studied variables. A very good positive correlation is noted between electrical conductivity and major elements. These elements constitute the main mineralization

TABLE 6: Water quality of the Skhira aquifer with respect to WHO standards [44] and Tunisian standards [45].

Parameters	WHO (2011)	NT.09.14 (2012)	Number of samples exceeding the recommended value		% of samples exceeding the recommended value	
			WHO	NT.09.14	WHO	NT.09.14
T°C	—	25	—	0	—	0
pH	6.5 to 8.5	6.5 to 8.5	1	1	5	5
EC (μS/cm)	1500	1500	20	20	100	100
Na (mg/L)	200	—	20	—	100	—
Cl (mg/L)	250	600	20	20	100	100
K (mg/L)	30	—	2	—	10	—
Ca (mg/L)	200	300	20	20	100	100
Mg (mg/L)	150	150	20	20	100	100
HCO_3 (mg/L)	380	—	1	—	5	—
SO_4 (mg/L)	250	600	20	20	100	100
NO_3 (mg/L)	45	45	13	13	65	65
NO_2 (mg/L)	3	3	0	0	0	0
F (mg/L)	1.5	1.7	6	6	30	30
Al (mg/L)	0.2	0.2			0	0
Zn (mg/L)	3	3	0	0	0	0

of the Skhira aquifer. In addition, the predominance of dissolved inorganic nitrogen depends heavily on dissolved oxygen contents. For that, NO_3 is found in oxygenated waters whereas NH_4^+ and NO_2 are associated with oxygen-poor waters. We note also that calcium bears a geochemical behavior similar to sulphates and fluorine which indicates that the element is associated with SO_4 and F^-. The negative correlations between metallic trace elements and pH show that increasing the water's pH induces lowers trace metallic contents and their rather association to the particular phase.

Taking into consideration all the gathered geochemical results of the Skhira phreatic aquifer, a statistical analysis through principal component analysis (PCA) was carried out. The results show that the explanation percentages are distributed unequally according to several axes (Table 5). The first two axes represent 79.6% of the total variance with 68.1% for the F1 axis and 11.5% for the F2 axis. The main plane is generated by axes F1 and F2 because they contain the maximum of information. We note that conductivity and Na^+, Cl^-, SO_4^{2-}, and Ca^{2+} concentrations and, to a lesser extent, Mg^{2+} and HCO_3^- contents do present a fairly good correlation (Figure 9). They are well distributed on either side of axis F1, forming a single group. These variables form the bulk of the Skhira phreatic aquifer mineralization. The F2 axis can be assimilated to pH, dissolved O_2, and nitrates, a result which is consistent with the stability conditions of nitrate (Eh and pH). In the F1-F2 axes, the data projection helps distinguish three clusterings: the first group (I) is composed of the least dissolved salt-rich waters and corresponds to the upstream side of the study area; the second group (II) is composed by the most mineralized waters within the downstream area of the study zone, probably influenced by marine intrusion; and the third group (III) is composed of

TABLE 7: Groundwater classification according to electrical conductivity [38].

Type of water	EC (μS/cm)	Number of samples	% of samples
Non-saline water	<700	0	0
Slightly saline	700-3000	2	10
Medium saline	3000-6000	12	60
Highly saline	>6000	5	25
Very saline	>14000	1	5
Brine	>42000	0	0

TABLE 8: Irrigation quality of groundwater based on sodium percentage % Na [39].

%Na	Class	Number of samples	% of samples
0-20	Excellent	0	0
20-40	Good	0	0
40-60	Permissible	16	80
60-80	Doubtful	4	20
>80	Unsuitable	0	0

waters overcharged with very high contents in major elements and fluorine and cauterizing the north-east area of the study zone.

4.3. Quality Assessment of Skhira Aquifer Waters for Potability and Irrigation. The evaluation of the potential uses of the Skhira aquifer waters for human consumption was based on the comparison of the obtained chemical results with the Tunisian (NT.09.14) Norms and the
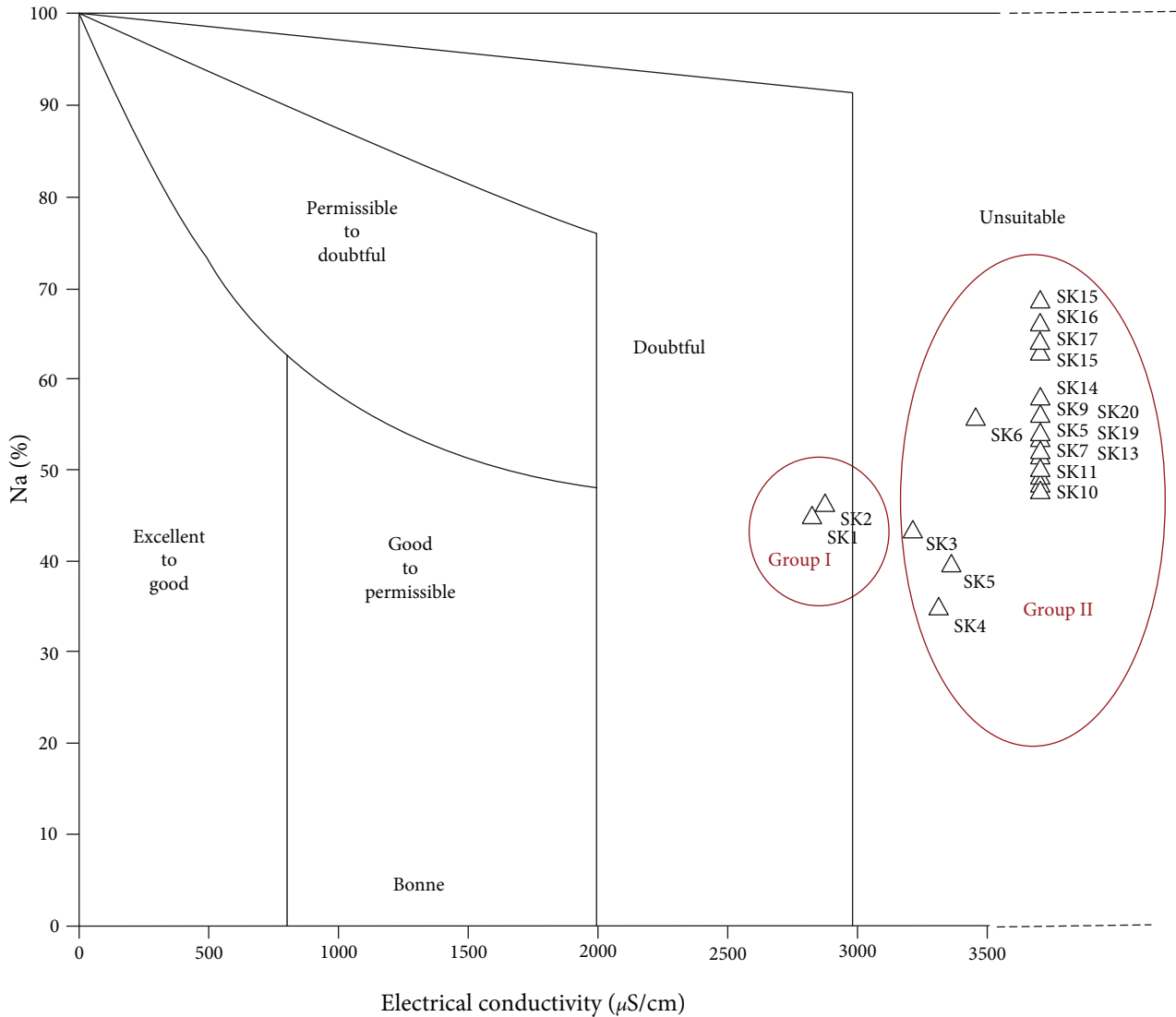
FIGURE 10: Wilcox diagram for the Skhira phreatic aquifer [43].

International Standards of Potability Norms set by the World Health Organization (WHO). This assessment reveals that most analyzed water samples do not meet both standard norms and can be considered not suitable for drinking especially at the downstream side of the aquifer (Table 6). These waters cannot be used for human consumption without special treatment.

The main parameters used to assess water quality intended for irrigation are electrical conductivity, sodium content expressed in percent, and residual alkalinity [38]. The saline load of irrigation water, assessed through conductivity, conditions the osmotic pressure which, when too high, renders water absorption by the plants difficult [38]. As shown in (Table 7), around 60% of water samples have a medium salinity.

The mobility of sodic clays is usually increased when sodium concentrations are increased rendering soils harder and more coherent. This leads to soil permeability decrease and therefore a decrease in water mobility, hence becoming

less available to plants' roots. The effect of sodium, carried by irrigation waters on soils, is estimated via the percentage of sodium.

%Na can be calculated using the following formula [39]:

$$\%Na = 100 * (Na + K)/(Ca + Mg + Na + K), \qquad (3)$$

where contents are expressed in meq/L.

%Na in the Skhira aquifer ranges between 45 and 68% (Table 8). Most groundwater samples with 40 to 60% Na are permissible for irrigation purposes. However, the SK 15, SK16, SK17, and SK18 piezometers, located in the industrial area, are doubtful for irrigation. Wilcox used the percentage of Na content (%) as a function of the electrical conductivity (EC) to evaluate the suitability of water for irrigation. The projection of the different analyzed samples on the diagram allows the distinction of two water groups (Figure 10):

(1) Group I: low-quality waters, which are moderately mineralized. They occur in the center and west parts of the aquifer

(2) Group II: it includes highly mineralized waters with an extremely high risk of salinization and the highest percentage of sodium content. This group characterizes waters sampled from piezometers located in the downstream part of the aquifer

Alkalinity measures the ability of water to neutralize acids. The neutralizing power of water is mainly related to the presence of HCO_3^- and CO_3^{2-} ions. As a result, alkalinity can be expressed as follows [40]:

$$
\begin{aligned}
\text{Alc}(\text{meq/L}) &= 2\left(CO_3^{2-}\right) + \left(HCO_3^-\right) - \left(H^+\right) + \left(OH^-\right) \\
&= 2\left(Ca^{2+}\right) + 2\left(Mg^{2+}\right) + \left(K^+\right) + \left(Na^+\right) \\
&\quad - 2\left(SO_4^{2-}\right) - \left(Cl^-\right)
\end{aligned} \tag{4}
$$

After the precipitation of alkaline-earth carbonates, the residual sodium carbonate (RSC) has the following expression [40]:

$$
\text{Alc}_{\text{RSC}}(\text{meq/L}) = 2\left(CO_3^{2-}\right) + \left(HCO_3^-\right) - 2\left(Ca^{2+}\right) - 2\left(Mg^{2+}\right) \tag{5}
$$

If the residual alkalinity is positive, a risk of alkalization may affect irrigated soils. If it is negative, after the precipitation of alkaline-earth carbonates, the soil water would follow a neutral saline pathway [41]. The residual alkalinity of the Skhira aquifer waters is negative (Table 9), removing the risk of soil degradation by alkalinization in case these waters would be used for irrigation.

5. Conclusion

Water quality monitoring shows that the influence of industrial activities, especially phosphate treatment, concerns mainly the downstream part north-east of the aquifer where the water is acidic and highly charged in SO_4^{2-}, $H_2PO_4^-$, and F⁻. The waters sampled in the upstream portion are only influenced by the natural conditions of supply and the water-sediment interaction of the unsaturated zone.

The spatial distribution of nitrates would be controlled, in addition to the excessive use of nitrogen fertilizers, by physical and chemical factors.

Comparison of the analyzed water's chemical results with national and international standards indicates that the majority of these waters do not meet the potability criteria. However, and for irrigation purposes, the majority of analyzed samples present a medium sodicity and alkalinization. Their use for irrigation requires a good drainage and a reasonable organic matter addition.

Based on the outcome of this study, we recommend that urgent remedial solutions have to be given to the area close to the phosphogypsum dump which seems to be the major cause of the current aquifer water degradation. An impermeable barrier has to be foreseen to stop highly charged water

Table 9: Alkalinity and residual sodium carbonate (RSC) of selected groundwater samples.

Samples	Alkalinity (meq/L)	RSC (meq/L)
SK1	19.64	-47.94
SK2	18.88	-47.36
SK3	23.31	-56.58
SK4	27.77	-67.33
SK5	22.35	-61.15
SK6	8.42	-44.72
SK7	28.05	-68.53
SK8	26.51	-72.34
SK9	15.78	-64.56
SK10	18.57	-76.38
SK11	15.25	-77.64
SK12	15.13	-77.96
SK13	10.84	-81.69
SK14	5.19	-68.97
SK15	18.78	-81.80
SK16	17.41	-69.64
SK17	8.33	-93.88
SK18	63.35	-127.96
SK19	34.27	-120.86
SK20	10.16	-122.87

infiltration from this site to the aquifer. Furthermore, the use of the Skhira groundwater for drinking has to be preceded by proper treatment. The same water can be used for irrigation with a special care given to minimize the alkanization and sodicity.

Data Availability

We have to emphasize that all data (physical and chemical parameters, major cations and anions, nutrient elements, fluorine, and some trace metal elements) used to support the findings of this study are included within the article and will be accessible to readers.

Conflicts of Interest

The authors declare that they have no conflicts of interest.

References

[1] A. Shahbazi and A. Esmaeli-Sar, "Groundwater quality assessment in north of Iran: a case study of the Mazandaran Province," *World Sciences Journal*, vol. 5, pp. 92–97, 2009.

[2] M. A. Massoud, M. D. Scrimshaw, and J. N. Lester, "Qualitative assessment of the effectiveness of the Mediterranean action plan: wastewater management in the Mediterranean Region," *Ocean and Coastal Management*, vol. 46, no. 9-10, pp. 875–899, 2003.

[3] R. Trabelsi, K. Abid, K. Zouari, and H. Yahyaoui, "Groundwater salinization processes in shallow coastal aquifer of Djeffara

plain of Medenine, Southeastern Tunisia," *Environmental Earth Sciences*, vol. 66, no. 2, pp. 641–653, 2012.

[4] H. Bouzourra, R. Bouhlila, L. Elango, F. Slama, and N. Ouslati, "Characterization of mechanisms and processes of groundwater salinization in irrigated coastal area using statistics, GIS, and hydrogeochemical investigations," *Environmental Science and Pollution Research*, vol. 22, no. 4, pp. 2643–2660, 2015.

[5] DGRE, *Annuaires d'Exploitation des Nappes Phréatiques*, Direction Générale des Ressources en Eaux, Tunis, Tunisia, 2010.

[6] GEREP, *Etude d'impact sur l'environnement de l'usine projetée d'acide phosphorique Tifert dans le site de Skhira*, 2007.

[7] CRDA, *Commissariat régional du développement agricole de Sfax, Rapport annuaire*, 2008.

[8] S. Melki and M. Gueddari, "Impact assessment of phosphogypsum leachate on groundwater of Sfax-Agareb (Southeast of Tunisia): using geochemical and isotopic investigation," *Journal of Chemistry*, vol. 2018, Article ID 2721752, 10 pages, 2018.

[9] R. Ben Amor and M. Gueddari, "Major ion geochemistry of Ghannouch–Gabes coastline (at Southeast Tunisia, Mediterranean Sea): study of the impact of phosphogypsum discharges by geochemical modeling and statistical analysis," *Environmental Earth Sciences*, vol. 75, no. 10, p. 851, 2016.

[10] P. M. Rutherford, M. J. Dudas, and R. A. Samek, "Environmental impacts of phosphogypsum," *Science of the Total Environment*, vol. 149, no. 1-2, pp. 1–38, 1994.

[11] INM, *National Institute of Meteorology, Climate Data Report for the Period 2005–2015*, 2015.

[12] S. Melki, *Modélisation de la variation spatio-temporelle de la qualité des eaux des nappes de Sfax-Agareb, de Skhira et de Gabès-Nord au niveau des sites du GCT, [Ph.D. thesis]*, University of Tunis El Manar, Tunis, Tunisia, 2018.

[13] Y. P. Illy, *Etude des ressources hydrauliques de la région de Sidi M'hadheb. Etude hydrogéologiques préliminaire*, Bureau d'inventaire des ressources hydrauliques, Industrie et Energie, Tunis, Tunisia, 1968.

[14] N. Ben Cheikh, *Etude des relations hydrodynamiques entre la nappe profonde de Sfax et les systèmes aquifères méridionaux (Menzel Habib et Gabès Nord): Origines et mécanismes de minéralisation des eaux souterraines, [Ph.D. thesis]*, ENIS, Sfax, Tunisia, 2013.

[15] M. A. Maliki, M. Krimissa, J. L. Michelot, and K. Zouari, "Relation entre nappes superficielles et aquifère profond dans le bassin de Sfax (Tunisie)," *Comptes Rendus de l'Académie des Sciences - Series IIA - Earth and Planetary Science*, vol. 331, no. 1, pp. 1–6, 2000.

[16] J. Rodier, *L'analyse de l'eau. Eaux naturelles, eaux résiduaires, eau de mer*, Dunod, 8th edition, 2005.

[17] S. Melki and M. Gueddari, "Contribution of isotopic and geochemical tools for impact assessment of phosphogypsum on the groundwater quality of Skhira aquifer, in the southeast of Tunisia," in *43rd IAH CONGRESS*, Montpellier, France, 2016.

[18] H. C. Helgeson and D. H. Kirkham, "Theoretical prediction of the thermodynamic behavior of aqueous electrolytes at high pressures and temperatures; II, Debye-Huckel parameters for activity coefficients and relative partial molal properties," *American Journal of Science*, vol. 274, no. 10, pp. 1199–1261, 1974.

[19] D. G. Krige, "A statistical approach to some basic mine valuation problems on the Witwatersrand," *Journal of the Southern African Institute of Mining and Metallurgy*, vol. 52, pp. 119–139, 1951.

[20] A. Kharroubi, F. Tlahigue, B. Agoubi, C. Azri, and S. Bouri, "Hydrochemical and statistical studies of the groundwater salinization in Mediterranean arid zones: case of the Jerba coastal aquifer in Southeast Tunisia," *Environmental Earth Sciences*, vol. 67, no. 7, pp. 2089–2100, 2012.

[21] GCT, *Caractérisation environnementale des sites des usines de Sfax, de Skhira et de Gabès. Rapport interne*, 2011.

[22] A. Maliki, *Etude hydrogéologique de la nappe phréatique de Djebeniana et de Skhira et de la nappe profonde de Sfax*, DEA, 1994.

[23] M. B. Marzouk, *Situation de l'exploitation des nappes phréatiques du Gouvernorat de Sfax*, A/RE de Sfax, 2000.

[24] R. T. Chtourou, *Contribution à l'étude de la salinisation des nappes phréatiques côtières. Cas du système de Sfax-Mahdia, [Ph.D. thesis]*, ENIS, Sfax, Tunisia, 2008.

[25] O. Atteia, *Chimie et pollution des eaux souterraines*, Lavoisier, Paris, France, 2015.

[26] W. Stumm and I. J. Morgn, *Aquatic Chemistry: an Introduction Emphasizing Chemical Equilibria in Natural Waters*, John Wiley & Sons, Hoboken, NJ, USA, 2nd edition, 1981.

[27] G. Copin-Montegut, *Chimie de l'eau de mer*, de l'institut océanographique, Paris, France, 1995.

[28] A. Landreau and J. C. Roux, *Répartition et Évolution des Teneurs en Nitrates dans les Eaux Souterraines en France, Note Technique*, BRGM, Orléans, France, 1981.

[29] I. Alami, M. Zeraouli, M. Addou, A. Mokhtari, and A. Soulaymani, "Évaluation de la pollution nitrique de la nappe phréatique de la," *Afrique Science: Revue Internationale des Sciences et Technologie*, vol. 3, no. 3, pp. 378–390, 2007.

[30] B. Tlili-Zrelli, M. Gueddari, and R. Bouhlila, "Spatial and temporal variations of water quality of Mateur Aquifer (Northeastern Tunisia): suitability for irrigation and drinking purposes," *Journal of Chemistry*, vol. 2018, Article ID 2408632, 15 pages, 2018.

[31] A. Chafai, A. Maalej, and K. Medhioub, "Etude de la variabilité des constituants de l'aérosol dans la ville de Sfax (Tunisie)," in *Pollution Atmosphérique*, pp. 121–129, Revue, 2000.

[32] M. Gueddari, *Géochimie et thermodynamique des évaporites continentals, étude du lac Natron en Tanzanie et du Chott El Jrid en Tunisie, [Ph.D. thesis]*, University of Louis Pasteur, Strasbourg, France, 1984.

[33] C. A. J. Appelo and D. Postma, *Geochemistry, Groundwater and Pollution*, Balkema, Rotterdam, Netherlands, 2nd edition, 1993.

[34] S. Melki and M. Gueddari, "Impact assessment of phosphogypsum on the groundwater of Sfax-Agareb Aquifer, in Southeast of Tunisia," in *19th International Conference on Energy, Water and Environment (ICEWE 2017)*, vol. 11, p. 23, Istanbul, Turkey, 2017.

[35] T. Chernet, Y. Travi, and V. Valles, "Mechanism of degradation of the quality of natural water in the Lakes Region of the Ethiopian rift valley," *Water Research*, vol. 35, no. 12, pp. 2819–2832, 2001.

[36] Y. Travi, *Hydrologie et Hydrochirnie des aquiferes du Sénégal, Hydrogéochimie du fluor dans les eaux souterraines, Mémoire N095*, Institut de géologie, Université Louis Pasteur de Strabourg et Centre de Géochimie de la surface, CNRS, Strabourg, France, 1993.

[37] J. C. Germon, "Les fonctions épuratrices du sol et leurs limites," in *Sol Interface Fragile*, P. Stengel and S. Gelin, Eds., pp. 187–201, INRA, Paris, France, 1998.

[38] W. P. Kelly, "Permissible composition and concentration of irrigation water," in *Proceedings of the American Society of Civil Engineers*, pp. 607–609, Reston, VA, USA, 1940.

[39] T. Y. Stigter, S. P. J. van Ooijen, V. E. A. Post, C. A. J. Appelo, and A. M. M. Carvalho Dill, "A hydrogeological and hydrochemical explanation of the groundwater composition under irrigated land in a Mediterranean environment, Algarve, Portugal," *Journal of Hydrology*, vol. 208, no. 3-4, pp. 262–279, 1998.

[40] A. Al Droubi, "Géochimie des sels et des solutions concentrées par évaporation. Modèle thermodynamique de simulation. Application aux sols salées du Tcahd," Institut de Géologie – Université Louis-Pasteurp, Strasbourg, France, 1976.

[41] A. Phocaides, *Technical Handbook on Pressurized Irrigation Techniques*, Food and Agriculture Organization of the United Nation, FAO, Rome, Italy, 2007.

[42] S. Hafdhi, *Etude hydrochimique et isotopique des eaux souterraines de Skhira: Modélisation des processus géochimiques*, PFE, ENIS, Sfax, Tunisia, 2013.

[43] L. V. Wilcox, *Classification and Use of Irrigation Water*, US Department of Agriculture, Washington, DC, USA, 1955.

[44] WHO, *Guidelines for Drinking-Water Quality*, World Health Organization, Geneva, Switzerland, 4th edition, 2011.

[45] SONEDE, *Rapport mensuel du laboratoire, NT.09.44*, 2012.

Research Article

Boron Isotopes in the Mount Vulture Groundwaters (Southern Italy): Constraints for the Assessment of Natural and Anthropogenic Contaminant Sources

Michele Paternoster [1,2]

^{1}*Department of Sciences, University of Basilicata, Viale dell'Ateneo Lucano 10, 85100 Potenza, Italy*
^{2}*Istituto Nazionale di Geofisica e Vulcanologia, Sezione di Palermo, Via Ugo La Malfa 153, 90146 Palermo, Italy*

Correspondence should be addressed to Michele Paternoster; michele.paternoster@unibas.it

The Mt. Vulture volcanic aquifer is an important reservoir of effervescent mineral water in southern Italy. This area is included in the Vulture Regional Park and is located on a popular tourist route for its high scenic and ecological value. Unfortunately, signs of anthropogenic impact have recently increased. Among minor elements, boron and its isotopes are considered useful environmental tracers since different anthropogenic and natural sources can be distinguished. In this study, B content and (δ^{11}B) isotope composition were determined in the Mt. Vulture groundwaters. The groundwater chemistry is strongly influenced by input of CO_2-rich volcanic gases, and two different hydrofacies are observed. The first water type (BAW) has bicarbonate alkaline and alkaline-earth composition and relatively low salinity, whereas the second one (HSW) has bicarbonate-sulphate alkaline composition and higher salinity. The HSW are enriched in boron and have low δ^{11}B values (from –9.6‰ to –4.3‰) similar to those measured in the local magmas suggesting that B contents in these waters are influenced by prolonged interaction between local meteoric water and volcanic rocks. As to BAW, a wide variability in B concentrations (from 14 μg/l to 769 μg/l) and B isotope composition (from -16.1‰ to +23‰) has been observed. A possible anthropogenic input is thought to be responsible for such variability. The water samples with high B concentrations and negative δ^{11}B values (−12.2‰ to −16.1‰) are probably influenced by agricultural activities; for water samples characterized by positive δ^{11}B values (from +5.8‰ to +7.9‰) and low B contents, a slight contamination by sewage effluents cannot be excluded. These conclusions are also supported by B/Cl molar ratios ($7.8E-3$ to $1.6E-2$) different from those of the HSW group ($1.1E-2$ to $7.0E-2$). This study highlights that also in the Mt. Vulture volcanic area B isotopes coupled to the B/Cl ratio can be a useful tool for the assessment of natural and anthropogenic contaminant sources.

1. Introduction

The Mt. Vulture basin is one of the most significant aquifer systems of southern Italy. Its groundwater is an important and valuable resource for potable and mineral water supply and agricultural and industrial uses. In the last years, to satisfy the intensifying water demand, groundwater extraction has been gradually increased. However, signs of anthropogenic impact, especially nitrogen contamination, have recently become evident [1]. Assessing the processes controlling groundwater quality is essential for an effective water resource management and protection, especially in the

Mt. Vulture area which has an important role for both the local economy and water supply of the whole Basilicata Region. Usually, an isotopic approach can provide information on the type of pollution and on its possible origin. Among minor elements, boron and its isotopes are considered useful environmental tracers for this purpose. Boron is geochemically very mobile and soluble, and in the aqueous environment, it may be as both borate ion $(B(OH)_4^-)$ and boric acid (H_3BO_3). Typically, low-saline groundwaters and rivers have low B concentrations (<100 μg/l), whereas saline groundwaters may show high concentrations up to several tens of μg/l [2]. The World Health Organization (WHO)

recommends an upper limit of 500 μg/l in drinking water [3]. The drinking water standard of the European Community [4, 5] and Italian legislation [6] is two times this recommended value. The B dissolved in groundwaters is generally derived by natural sources, related to hydrothermal water sources, weathering of igneous rocks, and leaching from sedimentary deposits of marine and nonmarine origin and seawater intrusion [7, 8]. However, anthropogenic boron input due to manufacturing of glass, ceramics, leather, fertilizers, cosmetics, detergents, etc., as well as municipal wastewater and sewage effluent producing a significant environmental impact, have been demonstrated in surface water and groundwater [8–10]. At lower temperatures, boron can be removed from solution by absorption onto clay minerals and incorporation into secondary minerals [8, 9]. Boron has two natural stable isotopes, ^{11}B and ^{10}B, with abundances of 19.8% and 80.2%, respectively. The boron isotope geochemistry has been used in defining magmatic and hydrothermal processes [11, 12], low-temperature geochemical processes [13], paleo-ocean pH reconstruction [14, 15], and global biogeochemical cycles [16]. In addition, several studies have demonstrated the ability of boron isotopes to detect distinct anthropogenic boron sources in surface water and groundwater systems [17–20]. However, it is not always possible to distinguish agricultural signatures from urban effluents and natural sources only by means of B isotopes because values may overlap. Consequently, other chemical elements or elemental ratios have to be considered along with the B isotope to assess the contaminant sources carefully [20–22]. The B/Cl molar ratio is thought to be a geochemical tracer significantly useful for this purpose. For example, B/Cl values tend to be rather homogeneous for fluids derived from a common reservoir [20, 22], denoting it as a useful tool to discriminate B's origin. With this in mind, the paper focuses on the occurrence and distribution of boron and of its isotopes in the Mt. Vulture groundwaters in order to evaluate B's origin and to distinguish between natural and anthropogenic contaminant sources.

2. Study Area

Mt. Vulture is a Pleistocene stratovolcano composed mainly of pyroclastic deposits and lava flows ranging in composition from foidite, basanites, to phonolites with several intermediate rock types [23, 24]. These products have a strongly silica-undersaturated character with alkaline potassic to ultrapotassic affinities [25]. This volcano is located at the eastern border of the Apennine compressive front, at the western margin of the Apulia foreland (Figure 1). Volcanic activity started at 742 ± 12 ka and continued, interrupted by long-lasting quiescence periods, up to 142 ± 11 ka [26]. In the peripheral sectors of Mt. Vulture, fluviolacustrine deposits of Pliocene and lower Pleistocene age are outcropping (Fiumara di Atella Super-synthem, [27]). The volcanic products lie over Pleistocene gravel and clay, in subhorizontal layers that cover the intensely deformed flysch sediments of Miocene age. The oldest pre-Miocene bedrock units consist principally of deep-sea sediments belonging to units ranging from early Triassic to lower-middle Miocene [28].

The Mount Vulture aquifer, mainly hosted by volcanic rocks, consists of interconnected multilayered aquifer systems, locally confined [29]. The groundwater flow pathways are conditioned by structural hydraulic parameters, anisotropy features of the aquifer, and the existing fracture network [29, 30]. The tectonic discontinuities act as deep preferential groundwater flow and promote the mineralization processes of groundwater occurring within two independent hydrogeological basins, the Monticchio–Atella basin (southern area) and the Melfi–Barile basin (north-eastern area) [31].

The volcano hosts numerous springs and wells emerging at different elevations, especially in the south-eastern and western sectors (Figure 1). The western area of Mt. Vulture is mainly characterized by forests, pastures, and uncultivated fields. Beech forests are widespread at higher altitudes while oak and chestnut trees are found at lower altitudes. Some industrial plants for mineral water extraction are present in a limited area near the Monticchio Bagni site. In the south-eastern area, there are two small villages as well as industrial plants and the agricultural activities are principally related to farming [1].

3. Sampling and Analysis

Waters from 34 springs and operating wells, owned by both companies and private individuals and used for irrigation and drinking water supply, were collected during a single field trip between January and March 2009. The wells have depths between 30 and 250 meters and were drilled into volcanic products (pyroclastic and effusive rocks). The sampling sites were selected based on a previous hydrogeological, hydrogeochemical study [31, 33] and tectonic setting of the investigated area. Waters are mainly located in the Monticchio–Atella basin, fourteen sampling sites in the western sector (Monticchio Bagni area), nineteen in the south-eastern area (near the Atella and Rionero in Vulture village), and only one sample in the north-eastern area of the Melfi–Barile basin. In addition, a single sample of meteoric water, collected at the Monticchio Bagni area in a rain gauge for one month of observation (March 2009), was analyzed.

B concentrations were measured by inductively coupled plasma-mass spectrometry (Element Finnigan) at the Activation Laboratory of Actlabs (Ontario, Canada). The determination of B was performed using the external standard calibration method, employing NIST and SLRS standard reference materials for calibration. The precision of the analytical results, estimated by running triplicate analyses every 10 samples, was 2-5%. The accuracy of the results (±5%) was obtained by analyzing certified reference materials from the Merck Calibration Laboratory. Samples for B isotopic composition were filtered in the field using 0.45 mm filters. Boron isotopic composition was determined by negative-ion thermal-ionization mass spectrometry (N-TIMS), direct loading procedure at the Isotope Science Laboratory of University of Calgary (ISL-UC), following the methods described by Gaillardet [34]. The external reproducibility of $\pm 1\delta$ ($2\sigma_{mean}$ corresponding to $2s/n^{0.5}$, where $n = 3$ replicate analyses) for the B isotope measurements was
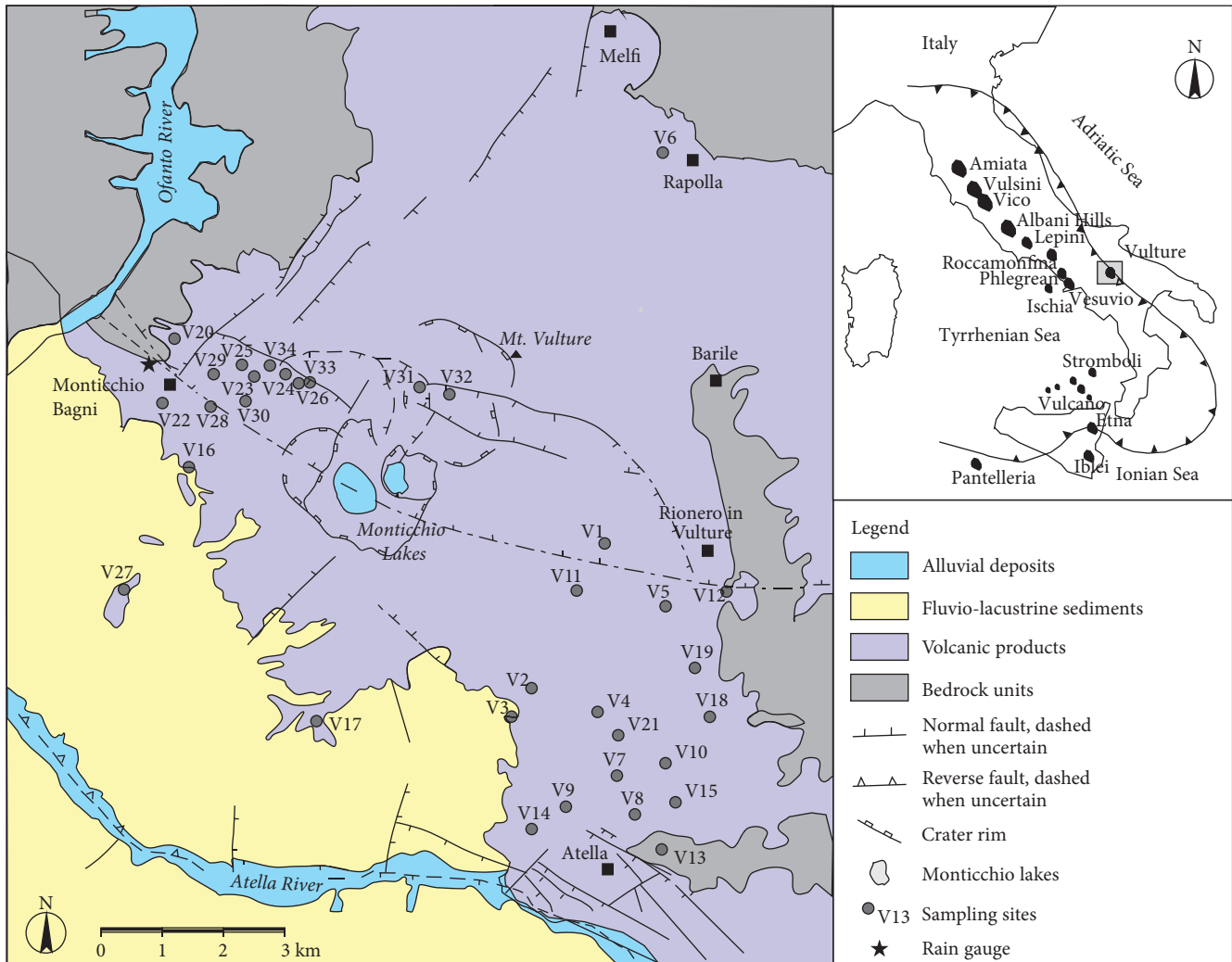
Figure 1: Geological sketch map of the Mt. Vulture area (modified from Giannandrea et al. [32]). The localization of sampling sites (grey circles), rain gauge (star), and code of the water samples are shown.

determined by replicate analyses of the NIST-SRM 951 standard. The B isotopic composition was measured with an average analytical precision (2σ) of $\pm 1\delta$‰. The boron isotopic compositions are expressed as per mil differences relative to mean $^{11}B/^{10}B$ ratios of 4.00125 determined for the NIST-SRM 951 boric acid standard.

4. Results and Discussion

4.1. Groundwater Chemistry. According to previous papers [1, 33, 35], in the Mt. Vulture area two different types of groundwater are distinguished on the basis of physical-chemical parameters and concentrations of dissolved chemical components. Most of the investigated waters have a bicarbonate alkaline-earth and alkaline composition (Figure 2). These waters show temperatures ranging from 8.8°C to 19.9°C and electrical conductivity (EC) from 140 to 1940 μS/cm. Bicarbonate is generally the main anion in solution with concentrations ranging between 66 and 1763 mg/l with an average value of about 508 mg/l [33, 35].

During basalt weathering, CO_2 is converted into bicarbonate, showing a positive correlation with the concentration of major and minor elements. The composition of bicarbonate alkaline-earth and alkaline waters (hereafter BAW) is principally due to low-temperature leaching of the host volcanic rocks [35]. The other investigated waters are bicarbonate–sulphate–alkaline (hereafter HSW) in composition and show high salinity [31, 33, 35] and 1183 to 16,400 μs/cm EC values that are higher than in the previous group. The temperature values range from 15.1 to 17.4°C. Such high-salinity springs are enriched in sodium and sulphate with respect to average groundwater composition and have the highest concentration of dissolved CO_2 that are likely due to the ongoing active, magmatic-mantle outgassing [36–38]. The HSW group is related to prolonged water circulation in alkali and feldspathoid-rich pyroclastic layers interbedded with clay deposits [33]. Previous studies [1] revealed an inhomogeneous distribution of NO_3 concentrations in the Mt. Vulture area. In the western portion, N input has been associated with an organic soil component only. In the south-eastern part, a
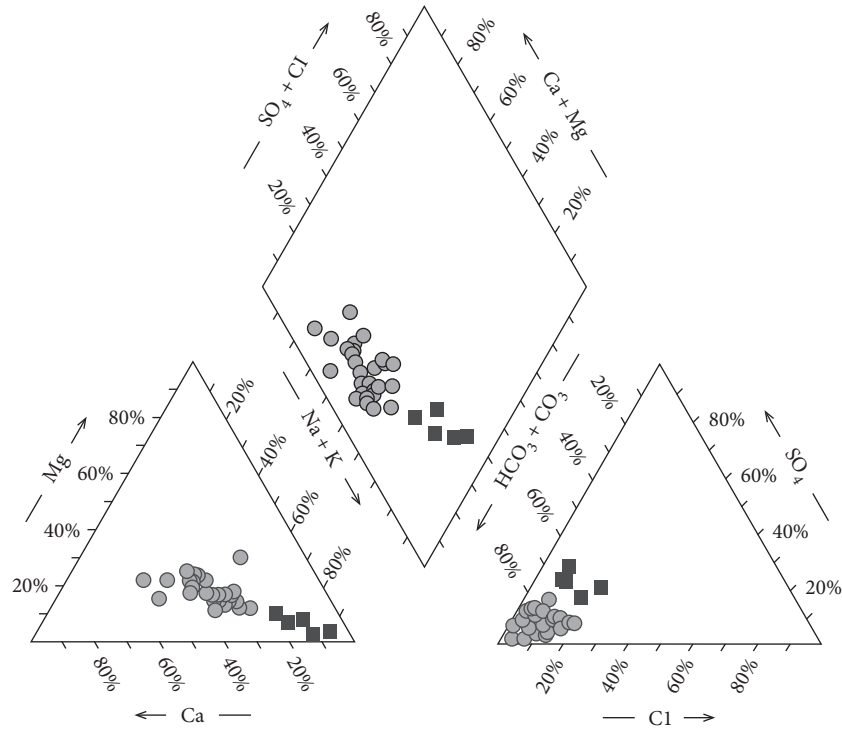
Figure 2: Piper diagram. Circles are for bicarbonate alkaline-earth and alkaline water (BAW) while squares represent the bicarbonate-sulphate-alkaline waters (high-salinity water, HSW). Data are from Parisi et al. [31, 33].

possible anthropogenic contamination (mainly derived from use of inorganic fertilizer) has been documented. Relative to groundwater origin, stable isotopic data of $\delta^{18}O$ and δD highlight that these groundwaters are meteoric in origin and they are not significantly affected by seasonal variations [39]. According to the local vertical isotopic gradient (0.17‰ for $\delta^{18}O$/100 m) defined by Paternoster et al. [39], the meteoric recharge altitude of Mt. Vulture groundwaters is between 800 and 1200 meters above sea level.

4.2. B Concentrations and Isotopes. Boron contents and $\delta^{11}B$ isotopic values of the studied waters show a wide variability (Table 1). Boron concentrations range from 14 to 5130 μg/l, with an average value of 556 μg/l (Figure 3(a)). BAW samples of the western area range from 14 to 652 μg/l, with the only V30 sample having B contents higher than those in the WHO guideline (500 μg/l). BAW samples from the south-eastern area have B concentrations between 45 and 769 μg/l. V01 and V20 samples record B concentrations higher than those in the WHO guideline. The highest B concentrations (from 746 to 5130 μg/l) were observed in the HSW samples. Among these, V6, V14, and V17 samples have B contents higher than the maximum admissible concentration (1000 μg/l) by drinking water Directive 98/83/EC [5] and the Italian legislation [6]. Generally, the Mt. Vulture groundwaters have higher B concentrations compared with those in other volcanic systems in Italy [40, 41]. The $\delta^{11}B$ values range from −16.1‰ to +23‰ (Figure 3(b)). BAW samples from the western area have $\delta^{11}B$ values from −6.6‰ to −1.6‰. Among these, only two samples (V31

and V32) show both a significant enrichment in heavier boron isotopes (+17.8‰ and +23‰, respectively) and the lowest B concentrations (18 μg/l and 14 μg/l, respectively), similar to the local meteoric water (RW, Table 1) analyzed in this study ($\delta^{11}B = +26‰$ and $B = 12\,\mu$g/l). In the south-eastern area, based on B contents and $\delta^{11}B$ values, two BAW subsets can be identified: (a) groundwaters having B contents lower than 70 μg/l and positive $\delta^{11}B$ values (from +5.8‰ to +7.9‰), (b) groundwaters with B concentrations higher than 70 μg/l and negative $\delta^{11}B$ values (from −16.1‰ to −1.9‰) (Figures 3(a) and 3(b)). Finally, HSW have the highest B contents (from 746 to 5130 μg/l) and low $\delta^{11}B$ values (from −9.6‰ to −4.3‰).

4.3. Origin of Boron. In nature, different B reservoirs exist (mantle-derived volcanic rocks: −10‰ < $\delta^{11}B$ < 0‰, marine carbonates: +10‰ < $\delta^{11}B$ < +30‰, altered oceanic crustal rocks: 0‰ < $\delta^{11}B$ < +25‰, old continental rocks and siliciclastic sediments: −15‰ < $\delta^{11}B$ < +5‰, seawater: $\delta^{11}B$ ∼ +40‰) with wide ranges of B isotope composition that sometimes overlap each other [41]. According to D'Orazio et al. [42], the Mt. Vulture volcanic rocks display negative $\delta^{11}B$ values (ranging between −9.6‰ and −5.6‰) that are strongly consistent with values of the HSW group (−9.6‰ and −4.3‰) suggesting that the water-volcanic rock interaction is the main process controlling the chemical composition of the HSW samples. The aforementioned silica-undersaturated volcanic products are thought to represent the main source of B also in the BAW group

TABLE 1: B concentration and isotopic composition of the Mt. Vulture groundwaters.

Sample no.	Long. (north)	Lat. (east)	Elevat.	Type	CH	T* (°C)	EC* (μS/cm)	pH*	δ11B (‰)	B (μg/L)	B/Cl [1]
V1	4531210	555380	545	W	BAW	13	350	6.6	−5.1	504	4.8E − 02
V2	4528490	554302	544	W	BAW	15.2	237	6.8	−2.7	261	6.6E − 02
V3	4528250	554060	600	W	BAW	17.2	233	7.5	+7.9	59	1.4E − 02
V4	4528240	555360	545	W	BAW	15	304	6.1	+5.8	67	1.6E − 02
V5	4535826	556800	686	W	BAW	13.3	202	5.8	+7.6	54	1.0E − 02
V6	4536694	557091	365	S	HSW	17	2910	6.5	−4.3	2210	3.4E − 02
V7	4526900	556320	490	W	BAW	15.3	607	6.1	−13.1	275	9.0E − 03
V8	4526817	556303	490	W	BAW	14.1	478	6.9	−12.7	233	1.2E − 02
V9	4526707	556342	490	W	BAW	13.8	430	6.9	−2.2	175	3.1E − 02
V10	4526605	556340	483	W	BAW	16	291	7.0	+6.7	60	1.0E − 02
V11	4531235	555467	555	W	BAW	13.1	234	6.2	+6.3	57	1.2E − 02
V12	4534820	557160	519	W	BAW	15.7	265	6.5	+7.6	45	7.8E − 03
V13	4525820	555300	474	S	BAW	15.7	763	5.9	−4.5	451	3.9E − 02
V14	4525900	555260	461	S	HSW	15.1	16,4	6.9	−5.8	3470	1.1E − 02
V15	4526955	556359	487	W	BAW	14.7	896	5.9	−9	463	6.3E − 02
V16	4531940	548200	575	S	HSW	15.2	1183	5.9	−6.9	746	6.7E − 02
V17	4526867	551828	449	S	HSW	17	4350	6.5	−9.4	5130	7.0E − 02
V18	4527726	556960	550	W	BAW	15	370	5.9	−1.9	118	1.2E − 02
V19	4527739	556970	552	W	BAW	16.1	362	6.3	−12.2	213	1.4E − 02
V20	4537726	548012	554	W	BAW	18.5	1717	6.3	−16.1	769	1.3E − 02
V21	4526870	556607	493	W	BAW	16.1	435	6.1	−7.1	144	2.3E − 02
V22	4532983	547976	547	S	HSW	17.4	2149	6.2	−9.6	923	5.8E − 02
V23	4533314	549828	566	W	BAW	16.8	750	5.9	−1.6	264	2.7E − 02
V24	4533306	550031	565	W	BAW	18.1	1480	6.0	−5.2	470	3.9E − 02
V25	4533379	549532	657	W	BAW	14	351	6.1	−3.9	91	1.3E − 02
V26	4532938	551154	690	W	BAW	19.5	1147	6.0	−6.1	146	1.2E − 02
V27	4530603	547666	682	W	BAW	18.9	698	5.9	−5.4	246	2.4E − 02
V28	4532832	549658	650	W	BAW	19.9	1346	6.1	−6.6	498	3.4E − 02
V29	4533100	549100	644.	W	BAW	19.5	918	5.9	−4.9	355	2.7E − 02
V30	4533672	549815	555	W	BAW	19.6	1940	6.2	−6.6	652	3.9E − 02
V31	4532900	551950	885	S	BAW	9.6	206	7.6	+17.8	18	2.6E − 03
V32	4533066	552194	960	S	BAW	8.8	140	7.0	+23	14	2.5E − 03
V33	4532966	551315	780	W	BAW	15.8	369	5.9	−4.6	84	9.5E − 03
V34	4532930	550040	735	W	BAW	16.5	448	5.7	−4.9	102	1.3E − 02
R35	rainwater								+26	12	

Notes: Elevat.: elevation in meters above sea level; S: spring; W: well; CH: chemical hydrofacies; BAW: bicarbonate alkaline-earth and alkaline water; HSW: bicarbonate–sulphate–alkaline water; EC: electric conductivity measured at 25°C; n.m.: not measured. The location of the sampling point is provided in UTM Zone 33 coordinates using the European Datum of 1950. *Data from Parisi et al. [31, 33], [1]Cl data from Parisi et al. [31, 33].

although the B isotope composition of some BAW samples is different. However, based on hydrogeological issue, the Mt. Vulture volcanic products clearly host all the analyzed groundwaters suggesting a negligible contribution from the other rocks (such as flysch sediments and basement rocks) occurring in the studied area. In order to assess the B origin in the BAW group, a mixing model between the local meteoric water and volcanic-hosted end-member (HSW) has been taken into account. The mixing model can be quantitatively estimated by means of the following equations:

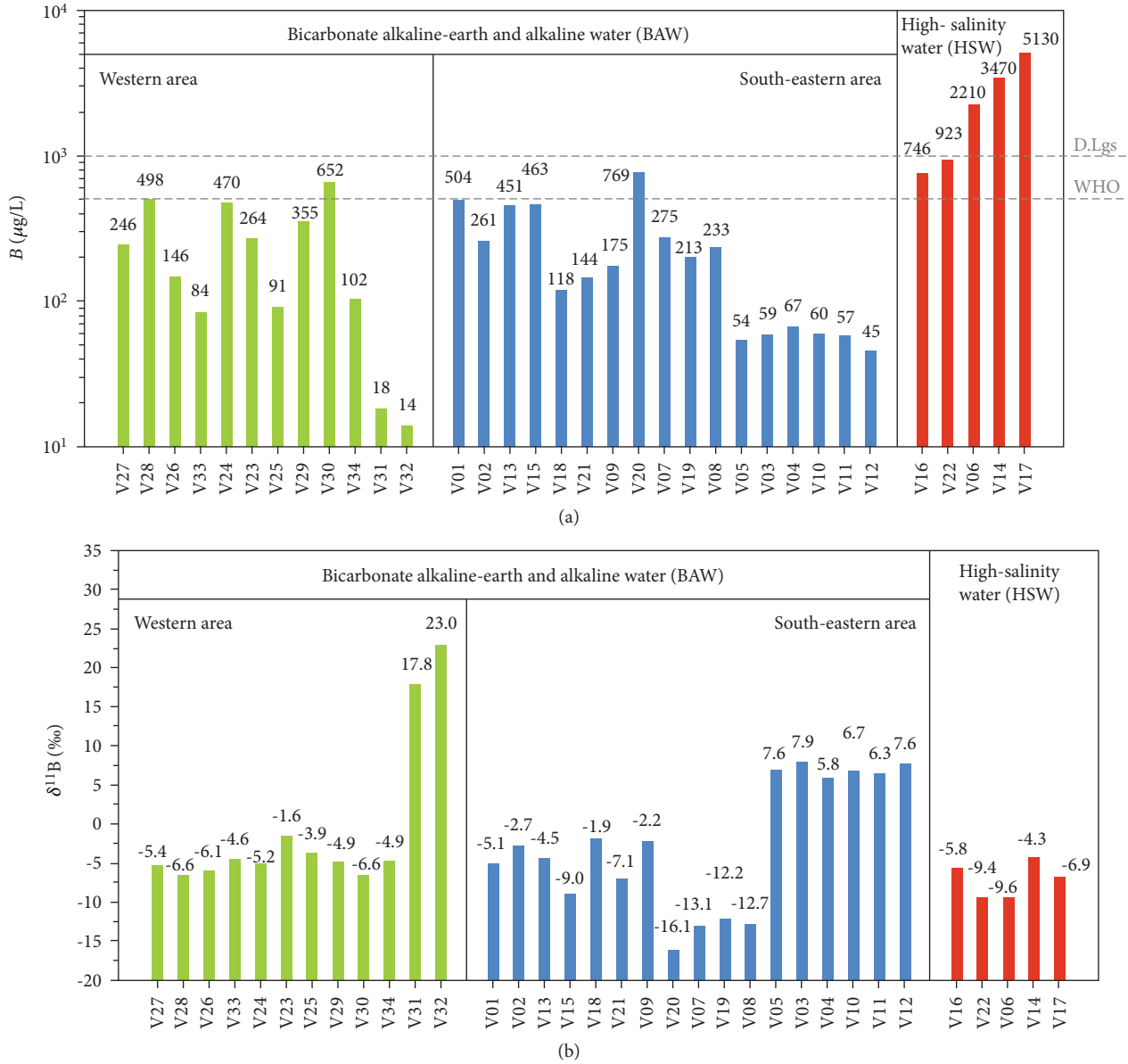$$B_{\mathrm{mix}} = B_c \times f + B_d \times (1 - f), \qquad (1)$$

FIGURE 3: Boron concentrations (a) and $\delta^{11}B$ values (b) of the Mt. Vulture groundwaters divided into bicarbonate alkaline-earth and alkaline (BAW) and bicarbonate-sulphate-alkaline (high-salinity water (HSW)) water types.

$$\delta^{11}B_{\text{mix}} = \left(\delta^{11}B_c \times \frac{B_c}{B_{\text{mix}}} \times f + \delta^{11}B_d \times \frac{B_d}{B_{\text{mix}}} \times (1-f) \right),$$

$$(2)$$

where B_{mix}, B_c, and B_d, as well as $\delta^{11}B_{\text{mix}}$, $\delta^{11}B_c$, and $\delta^{11}B_d$ are the B concentrations and isotopic values of mixing water, local meteoric water, and HSW group, respectively. f is the mixing ratio. For calculations, the composition of the local meteoric water sample (RW, $\delta^{11}B = +26‰$, $B = 12\,\mu g/l$) and the highest and lowest $\delta^{11}B$ values of the HSW group were used. In Figure 4, the ML1 and ML2 mixing curves are shown along with investigated water samples. BAW samples of the western area are concentrated in a narrow range within the two mixing curves, suggesting B is mainly sourced from host

volcanic rocks. V31 and V32 samples, enriched in heavier B isotopes, fall close to the local meteoric water end-member. Regarding the BAW samples from the south-eastern area, because of their compositional variability, groundwaters fall in different fields suggesting more B sources. Some water samples, similar to the western area BAW samples, lie between the two mixing curves denoting a natural B source due to water-volcanic rock interaction. The V7, V8, V19, and V20 samples, depleted in heavy B isotopes (from −16.1‰ to −12.2‰) and with B concentrations between 213 and 769 $\mu g/l$, are far from both ML1 and ML2 mixing curves falling near the MLA mixing curve between local meteoric water and water-soluble anthropogenic boron end-member consisting of synthetic Ca-borate fertilizers
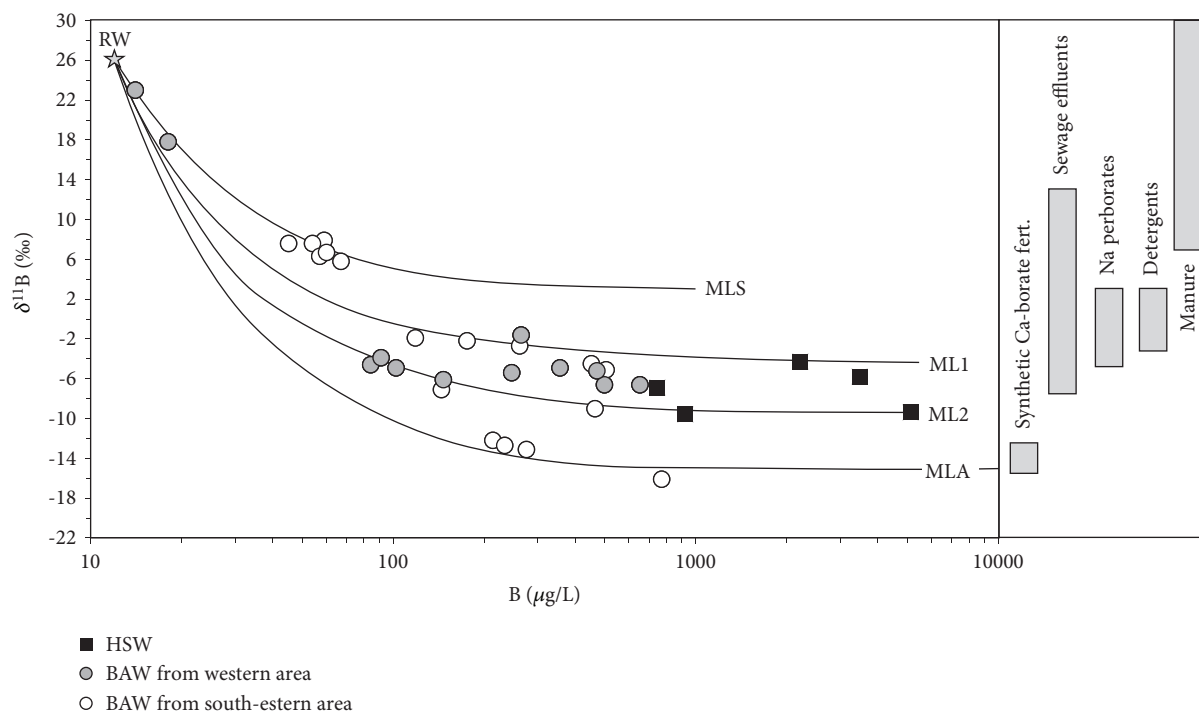
FIGURE 4: $\delta^{11}B$ (‰) versus B content (μg/l) binary plot. ML1 and ML2 curves indicate the mixing between local meteoric end-member (rainwater = RW, $\delta^{11}B$ = +26‰; B = 12 μg/l) and range of isotopic values of the HSW group ($\delta^{11}B$ = −4.3‰ and −9.6‰; B = 5130 μg/l). The MLA curve represents the hypothetical mixing behavior between local meteoric water and water-soluble anthropogenic boron compounds (synthetic Ca-borate fertilizers, average $\delta^{11}B$ value of -13.5‰ and B = 30 mg/l, [21]). The MSA mixing curve is drawn with following data (RW, and sewage effluents with average $\delta^{11}B$ value of +2.6‰ and B = 1000 μg/l; from Barth [43], Xue et al. [44], and Vengosh et al. [9]). Ranges of $\delta^{11}B$ of sewage effluents (−7.7‰ to +12.9‰; [9, 43, 44]), sodium perborates (−4.8‰ to +3.1‰; [2]), detergents (−2.9‰ to +3.1‰; [2]), synthetic Ca-borate fertilizers (−15‰ to −12.1‰; [21]), and manure (+6.9‰ to +42.1‰, [17, 44]) are shown for comparison.

(Figure 4). The Ca-borate and Na-borate fertilizers are the most used synthetic compounds in the agricultural activities and along with sodium perborate, municipal wastewaters, sewage effluents, and landfill leachates represent the main anthropogenic contaminants in the groundwater and shallow water [2, 9]. According to Mongelli et al. [1], in the study area agricultural activities are widely practiced suggesting for these water samples an anthropogenic B origin mainly associated with use of synthetic Ca-borate fertilizers.

As to BAW samples with low B values (less than 70 μg/l), a marked enrichment in ^{11}B is evident (Figure 4). These water samples do not fit the ML1, ML2, and MLA mixing curves, but their path is approximated by a new mixing curve (MLS). The MLS curve is between local meteoric water and groundwater contaminated by sewage effluents ($-7.7‰ < \delta^{11}B < +12.9‰$, Xue et al. [44], Vengosh et al. [9]). The B/Cl ratio also supported this finding. Several studies have revealed that B/Cl ratios tend to be rather homogeneous for fluids derived from a common reservoir [20, 21, 45]. In groundwater contaminated by domestic wastewater, sewage effluents, and other anthropogenic sources (mainly from Na- or Ca–borates), the B/Cl ratios coupled to a distinctive B isotopic signature allow us to distinguish different contaminant sources [20, 21]. For the studied groundwaters, the B/Cl molar ratios were calculated based on Cl data from Parisi et al. [31, 33] and range between

$7.0E − 2$ and $2.5E − 3$ (Table 1). As shown in Figure 5 ($\delta^{11}B$ vs B/Cl molar), most of the investigated water samples fall in the field of groundwater in nonmarine aquifers [21]. Two different groups of water samples deviate from the general trend of the measured B/Cl values. In detail, the water samples with low B isotopic values show B/Cl values falling in the range of groundwater contaminated by synthetic Ca-borate fertilizers; the water samples with high B isotopic values are in the field of sewage-contaminated groundwater, although other anthropogenic contaminant sources (i.e., municipal wastewater) cannot be excluded because of overlapping between ranges of their B isotopic values (+5.3‰ to +20.5‰, [2, 46]).

5. Conclusions

B concentration and isotope composition of Mt. Vulture groundwaters were determined to assess B's origin and to distinguish between natural and anthropogenic contaminant sources. In the study area, two water types have been identified. The first type, named high-salinity water (HSW), is characterized by the highest B contents (from 746 to 5130 μg/l), and low $\delta^{11}B$ values (from −9.6‰ to −4.3‰), similar to those measured by D'Orazio [42] in the local magmas (from −9.6‰ to−5.6‰), suggesting that prolonged water-volcanic rock interaction is the main B source. The
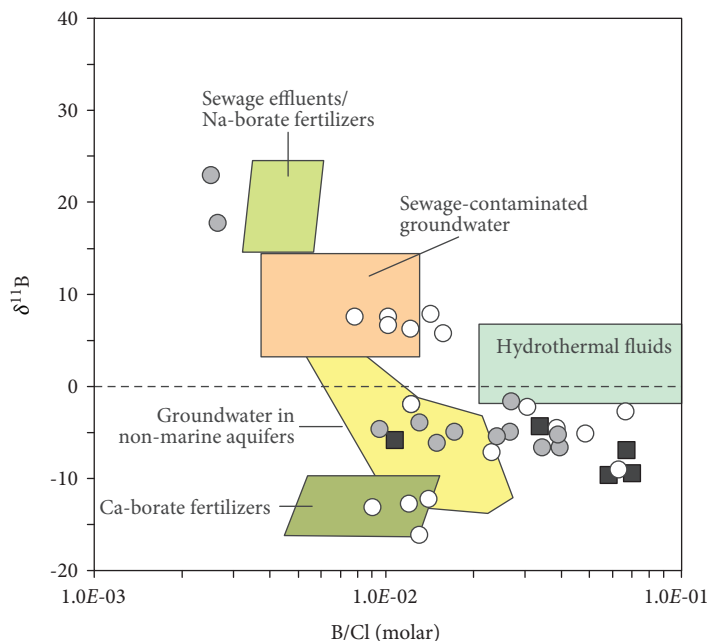
FIGURE 5: Pattern of typical ranges of δ^{11}B and B/Cl values of potential contamination sources, after Vengosh et al. [21]. Symbols are as in Figure 4.

second water type, named bicarbonate alkaline-earth and alkaline waters (BAW), records a wide variability in the B contents and isotopic values. The δ^{11}B values of the BAW group suggest that boron is mainly derived from leaching of volcanic rocks, although a contribution from local anthropogenic contaminants cannot be excluded for two BAW subsets. The water samples with high B concentrations and the lowest δ^{11}B values can be probably affected by water-soluble anthropogenic boron compounds consisting of synthetic Ca-borate fertilizers; other samples with high B isotopic values show B/Cl values, different from those of the HSW group, falling in the field of sewage-contaminated groundwater. This manuscript highlights that the B isotopes coupled to the B/Cl ratio in the Mt. Vulture volcanic area allow generally to define B's origin and evaluate natural and anthropogenic contaminant sources.

Data Availability

The data used to support the findings of this study are available from the corresponding author upon request.

Disclosure

Preliminary data of this manuscript were presented at the Premier International Conference on Energy, Minerals, Water, The Earth (June 16-21, 2018, Vancouver, Canada).

Conflicts of Interest

The author declares that there is no conflict of interest regarding the publication of this paper.

References

[1] G. Mongelli, M. Paternoster, and R. Sinisi, "Assessing nitrate origin in a volcanic aquifer using a dual isotope approach," *International journal of Environmental Science and Technology*, vol. 10, no. 6, pp. 1149–1156, 2013.

[2] S. R. Barth, "Utilization of boron as a critical parameter in water quality evaluation: implications for thermal and mineral water resources in SW Germany and N Switzerland," *Environmental Geology*, vol. 40, no. 1-2, pp. 73–89, 2000.

[3] World Health Organization and International Programme on Chemical Safety, "Boron in drinking-water: Background document for development of who guidelines for drinking-water quality," in *Guidelines for Drinking-Water Quality. Vol. 2, Health Criteria and Other Supporting Information*, World Health Organization, Geneva, 2nd edition, 1998, http://www.who.int/iris/handle/10665/38551.

[4] E. Weinthal, Y. Parag, A. Vengosh, A. Muti, and W. Kloppmann, "The EU drinking water directive: the boron standard and scientific uncertainty," *European Environmental*, vol. 15, no. 1, pp. 1–12, 2005.

[5] EU Directive, 1998/83/EC, *Council Directive of 3 November 1998 on the Quality of Water Intended for Human Consumption 1998 Official Journal of the European Union L33032*, 1998.

[6] Decreto legislativo 31/2001, *Decreto legislativo 2 febbraio 2001, n. 31, attuazione della direttiva 98/83/CE relativa alla qualità*

delle acque destinate al consumo umano, Gazzetta Ufficiale n. 52, 2001.

[7] W. Kloppmann, G. Bianchini, A. Charalambides et al., "Boron contamination of water resources in the Mediterranean region: distribution, social impact, and remediation," in *Final Report Section 6 of Project "Boremed"*, Contract EVKI-CT-2000-00046 (European Union), 2004, http://boremed.brgm.fr.

[8] M. Pennisi, R. Gonfiantini, S. Grassi, and P. Squarci, "The utilization of boron and strontium isotopes for the assessment of boron contamination of the Cecina River alluvial aquifer (central-western Tuscany, Italy)," *Applied Geochemistry*, vol. 21, no. 4, pp. 643–655, 2006.

[9] A. Vengosh, K. G. Heumann, S. Juraske, and R. Kasher, "Boron isotope application for tracing sources of contamination in groundwater," *Environmental Science & Technology*, vol. 28, no. 11, pp. 1968–1974, 1994.

[10] W. Kloppmann, E. Petelet-Giraud, C. Guerrot, L. Cary, and H. Pauwels, "Extreme boron isotope ratios in groundwater," *Procedia Earth and Planetary Science*, vol. 13, pp. 296–300, 2015.

[11] A. Vengosh, A. Starinsky, Y. Kolodny, and A. R. Chivas, "Boron isotope geochemistry of thermal springs from the northern Rift Valley, Israel," *Journal of Hydrology*, vol. 162, no. 1-2, pp. 155–169, 1994.

[12] S. Tonarini, M. Dantonio, M. A. Di Vito, G. Orsi, and A. Carandente, "Geochemical and B–Sr–Nd isotopic evidence for mingling and mixing processes in the magmatic system that fed the Astroni volcano (4.1–3.8 ka) within the Campi Flegrei caldera (southern Italy)," *Lithos*, vol. 107, no. 3-4, pp. 135–151, 2009.

[13] N. Muttik, K. Kirsimäe, H. E. Newsom, and L. B. Williams, "Boron isotope composition of secondary smectite in suevites at the Ries crater, Germany: boron fractionation in weathering and hydrothermal processes," *Earth and Planetary Science Letters*, vol. 310, no. 3-4, pp. 244–251, 2011.

[14] Y. Liu, W. G. Liu, Z. C. Peng et al., "Instability of seawater pH in the South China Sea during the mid-late Holocene: evidence from boron isotopic composition of corals," *Geochimica et Cosmochimica Acta*, vol. 73, no. 5, pp. 1264–1272, 2009.

[15] G. J. Wei, M. T. McCulloch, G. Mortimer, W. Deng, and L. Xie, "Evidence for ocean acidification in the Great Barrier Reef of Australia," *Geochimica et Cosmochimica Acta*, vol. 73, no. 8, pp. 2332–2346, 2009.

[16] W. H. Schlesinger and A. Vengosh, "Global boron cycle in the Anthropocene," *Global Biogeochem Cycles*, vol. 30, no. 2, pp. 219–230, 2016.

[17] D. Widory, E. Petelet-Giraud, P. Négrel, and B. Ladouche, "Tracking the sources of nitrate in groundwater using coupled nitrogen and boron isotopes: a synthesis," *Environmental Science & Technology*, vol. 39, no. 2, pp. 539–548, 2005.

[18] M. Pennisi, G. Bianchini, A. Muti, W. Kloppmann, and R. Gonfiantini, "Behaviour of boron and strontium isotopes in groundwater–aquifer interactions in the Cornia Plain (Tuscany, Italy)," *Applied Geochemistry*, vol. 21, no. 7, pp. 1169–1183, 2006.

[19] A. Nigro, G. Sappa, and M. Barbieri, "Boron isotopes in groundwater: evidence from contamination and interaction with terrigenous–evaporitic sequence, east-central Italy," *Geochemistry: Exploration, Environment, Analysis*, vol. 18, no. 4, pp. 343–350, 2018.

[20] E. Dotsika, D. Poutoukis, W. Kloppmann, C. Guerrot, D. Voutsa, and T. H. Kouimtzis, "The use of O, H, B, Sr and S isotopes for tracing the origin of dissolved boron in groundwater in Central Macedonia, Greece," *Applied Geochemistry*, vol. 25, no. 11, pp. 1783–1796, 2010.

[21] A. Vengosh, Y. Kolodny, and A. J. Spivack, "Ground-water pollution determined by boron isotope systematic," in *Application of Isotope Techniques to Investigate Groundwater Pollution*, pp. 17–38, IAEA, 1998, IAEA-TECDOC-1046.

[22] S. R. Barth, "Geochemical and boron, oxygen and hydrogen isotopic constraints on the origin of salinity in groundwaters from the crystalline basement of the Alpine Foreland," *Applied Geochemistry*, vol. 15, no. 7, pp. 937–952, 2000.

[23] L. Beccaluva, M. Coltorti, P. Di Girolamo et al., "Petrogenesis and evolution of Mt. Vulture alkaline volcanism (southern Italy)," *Mineralogy and Petrology*, vol. 74, no. 2-4, pp. 277–297, 2002.

[24] G. Mongelli, M. Paternoster, G. Rizzo, M. T. Cristi Sansone, and R. Sinisi, "Trace element geochemistry of the Mt Vulture carbonatites, southern Italy," *International Geology Review*, vol. 55, no. 12, pp. 1541–1552, 2013.

[25] M. De Fino, L. La Volpe, A. Peccerillo, G. Piccarreta, and G. Poli, "Petrogenesis of Monte Vulture volcano (Italy): inferences from mineral chemistry, major and trace element data," *Contributions to Mineralogy and Petrology*, vol. 92, no. 2, pp. 135–145, 1986.

[26] A. Büettner, C. Principe, I. M. Villa, and D. Bocchini, "39Ar–40Ar geochronology of Monte Vulture," in *La Geologia del Monte Vulture*, C. Principe, Ed., pp. 73–86, Grafiche Finiguerra, Lavello, Italy, 2006.

[27] P. Giannandrea, L. La Volpe, C. Principe, and M. Schiattarella, "Unità stratigrafiche a limiti inconformi e storia evolutiva del vulcano medio-pleistocenico di Monte Vulture (Appennino meridionale, Italia)," *Bollettino della Società Geologica Italiana (Italian Journal of Geosciences)*, vol. 125, pp. 67–92, 2006.

[28] C. Principe and P. Giannandrea, "Stratigrafia ed evoluzione geologica del vulcano Vulture (Basilicata, Italia). Rapporti fra vulcanismo ed ambienti sedimentari. Cinematiche collisionali: tra esumazione e sedimentazione," 81° riunione estiva della Società Geologica Italiana, Torino, 2002.

[29] G. Spilotro, F. Canora, F. Caporale, R. Caputo, M. D. Fidelibus, and G. Leandro, "Hydrogeology of M. Vulture," in *La Geologia del Monte Vulture (a cura di Claudia Principe)*, C. Principe, Ed., pp. 123–132, Grafiche Finiguerra, 2006.

[30] G. Mongelli, M. Paternoster, G. Rizzo, and R. Sinisi, "Trace elements and REE fractionation in subsoils developed on sedimentary and volcanic rocks: case study of the Mt. Vulture area, southern Italy," *International Journal of Earth Sciences*, vol. 103, no. 4, pp. 1125–1140, 2014.

[31] S. Parisi, M. Paternoster, C. Kohfahl et al., "Groundwater recharge areas of a volcanic aquifer system inferred from hydraulic, hydrogeochemical and stable isotope data: Mount Vulture, southern Italy," *Hydrogeology Journal*, vol. 19, no. 1, pp. 133–153, 2011.

[32] P. Giannandrea, L. La Volpe, C. Principe, and M. Schiattarella, *Carta geologica del Monte Vulture alla scala 1:25.000*, Litografia Artistica Cartografica, Firenze, 2004.

[33] S. Parisi, M. Paternoster, F. Perri, and G. Mongelli, "Source and mobility of minor and trace elements in a volcanic aquifer system, Mt. Vulture (southern Italy)," *Journal of Geochemical Exploration*, vol. 110, no. 3, pp. 233–244, 2011.

[34] J. Gaillardet, D. Lemarchand, C. Göpel, and G. Manhès, "Evaporation and sublimation of boric acid: application for boron purification from organic rich solutions," *Geostandards and Geoanalytical Research*, vol. 25, no. 1, pp. 67–75, 2001.

[35] M. Paternoster, S. Parisi, A. Caracausi, R. Favara, and G. Mongelli, "Groundwaters of Mt. Vulture volcano, southern Italy: Chemistry and sulfur isotope composition of dissolved sulfate," *Geochemical Journal*, vol. 44, no. 2, pp. 125–135, 2010.

[36] A. Caracausi, M. Martelli, P. M. Nuccio, M. Paternoster, and F. M. Stuart, "Active degassing of mantle-derived fluid: a geochemical study along the Vulture line, southern Apennines (Italy)," *Journal of Volcanology and Geothermal Research*, vol. 253, pp. 65–74, 2013.

[37] A. Caracausi, M. Paternoster, and P. M. Nuccio, "Mantle CO_2 degassing at Mt. Vulture volcano (Italy): relationship between CO_2 outgassing of volcanoes and the time of their last eruption," *Earth and Planetary Science Letters*, vol. 411, pp. 268–280, 2015.

[38] A. Caracausi and M. Paternoster, "Radiogenic helium degassing and rock fracturing: a case study of the southern Apennines active tectonic region," *Journal of Geophysical Research: Solid Earth*, vol. 120, no. 4, pp. 2200–2211, 2015.

[39] M. Paternoster, M. Liotta, and R. Favara, "Stable isotope ratios in meteoric recharge and groundwater at Mt. Vulture volcano, southern Italy," *Journal of Hydrology*, vol. 348, no. 1-2, pp. 87–97, 2008.

[40] M. Battistel, S. Hurwitz, W. C. Evans, and M. Barbieri, "The chemistry and isotopic composition of waters in the low-enthalpy geothermal system of Cimino-Vico Volcanic District, Italy," *Journal of Volcanology and Geothermal Research*, vol. 328, pp. 222–229, 2016.

[41] M. Pennisi, W. P. Leeman, S. Tonarini, A. Pennisi, and P. Nabelek, "Boron, Sr, O, and H isotope geochemistry of groundwaters from Mt. Etna (Sicily)—hydrologic implications," *Geochimica et Cosmochimica Acta*, vol. 64, no. 6, pp. 961–974, 2000.

[42] M. D'Orazio, F. Innocenti, S. Tonarini, and C. Doglioni, "Carbonatites in a subduction system: the Pleistocene alvikites from Mt. Vulture (southern Italy)," *Lithos*, vol. 98, no. 1-4, pp. 313–334, 2007.

[43] S. Barth, "Application of boron isotopes for tracing sources of anthropogenic contamination in groundwater," *Water Research*, vol. 32, no. 3, pp. 685–690, 1998.

[44] D. Xue, J. Bottea, B. De Baets et al., "Present limitations and future prospects of stable isotope methods for nitrate source identification in surface- and groundwater," *Water Research*, vol. 43, no. 5, pp. 1159–1170, 2009.

[45] D. M. Shaw and N. C. Sturchio, "Boron-lithium relationships in rhyolites and associated thermal waters of young silicic calderas, with comments on incompatible element behaviour," *Geochimica et Cosmochimica Acta*, vol. 56, no. 10, pp. 3723–3731, 1992.

[46] R. L. Bassett, P. M. Buszka, G. R. Davidson, and D. Chong-Diaz, "Identification of groundwater solute sources using boron isotopic composition," *Environmental Science & Technology*, vol. 29, no. 12, pp. 2915–2922, 1995.

Research Article

Groundwater Quality Assessment in a Karst Coastal Region of the West Aurunci Mountains (Central Italy)

Giuseppe Sappa [ID]**, Silvia Iacurto** [ID]**, Flavia Ferranti** [ID]**, and Francesco M. De Filippi** [ID]

Department of Civil, Building and Environmental Engineering (DICEA), Sapienza University of Rome, Rome 00184, Italy

Correspondence should be addressed to Giuseppe Sappa; giuseppe.sappa@uniroma1.it

This paper presents the results of a groundwater quality assessment carried out in the karst coastal region of the West Aurunci Mountains (Central Italy). 55 spring and 18 well water samples, collected from 2016 to 2018, were analysed to study the main processes controlling the hydrogeochemical evolution and groundwater quality properties. In the study area, groundwater samples are mostly characterized by a Ca-HCO$_3$ facies, indicating that the groundwater hydrogeochemical evolution is mainly controlled by the carbonate mineral dissolution/precipitation. The cationic and anionic concentrations confirm that groundwater samples belong to the order of Ca^{2+} > Mg^{2+} > Na$^+$ > K$^+$ and HCO$_3^-$ > Cl$^-$ > SO$_4^{2-}$, respectively. Well water samples show, over time, an increasing mineralization with respect to the spring water samples. In more detail, the enrichment of Ca^{2+}, Na$^+$, and Cl$^-$ in well water samples is mainly due to the dissolution of calcite, dolomite, and halite minerals and secondly to a probable ion exchange related to seawater intrusion. Seawater intrusion, probably affecting the chemical composition of well water samples, was studied using ionic ratios, graphical approaches, and specific indices, such as the BEX index. Results suggest that carbonate weathering, ion exchange, and seawater intrusion in this karst coastal region are the major factors controlling groundwater geochemistry. This study shows that groundwater quality assessment, based on hydrogeochemical investigation techniques, has been a useful tool to characterize and model carbonate aquifers in Central Italy, with the aim of achieving proper management and protection of these important water resources.

1. Introduction

Karst aquifers cover more than 30% of the European land mass [1], where carbonate lithologies occupy about 35% of the territory. Groundwater resources coming from karst aquifers give, in some countries, up to 50% to the drinking water supply [2]. For a large part of the Mediterranean region, karst springs play an essential role in the water supply. During the Mediterranean long dry summer months, karst springs provide fresh and high-quality water, which has been an important resource for human development in this region since antiquity [3]. Specifically, in Italy, the karst carbonate aquifers of the Central Apennines represent the larger groundwater resource. These aquifers are very complex systems: each one has its own distinctive characteristics. Karst aquifer peculiarities make them strategic resources which, however, are not yet properly exploitable, because of objective difficulties that are found in their study [4]. The

use of groundwater resources is increasing due to population rise, economic growth, intensified agricultural development, and the loss of surface water due to contamination [5]. In those countries with an extensive coastline, such as Italy, the high drinking water demand can lead to an uncontrolled groundwater exploitation of coastal aquifers [6, 7]. Coastal aquifers are major sources for freshwater supply in many countries around the world, especially in arid and semiarid zones and particularly because almost 70% of the world population lives in coastal areas [8, 9]. The main consequence of this groundwater overexploitation is seawater intrusion and, because of it, water salinization, which has become the most widespread form of groundwater contamination both in the Mediterranean regions of Europe [10–13] and in lots of coastal areas of the world [9, 14–18].

The quality of coastal aquifers is controlled by the variations of hydrochemical processes like seawater intrusion, geogenic process (weathering, ion exchange, and water-rock

TABLE 1: The location of the spring and the well water sampling survey.

Sample codes	Name	Location of sampling survey	Latitude	Longitude	Elevation (m a.s.l.)
TUL	Tulliola well	Formia	41°15′8.21″	13°35′2.23″	20
TER	Terenzia well	Formia	41°15′8.04″	13°34′59.06″	20
MAZ	Mazzoccolo Spring	Formia	41°15′44.10″	13°36′50.83″	18
CAP	Capodacqua di Spigno Spring	Spigno Saturnia	41°17′36.46″	13°42′42.18″	35

interaction), and anthropogenic activities (agriculture, industry, and urbanization). The salinization is the result of concomitant processes related to both seawater intrusion and water-rock interaction, which in some cases are virtually indistinguishable [19]. Hence, several studies usually combine the hydraulic and the hydrogeochemical approach, because understanding the hydrochemical characteristics of coastal groundwater could provide guidance for sustainable groundwater management [20]. In the present work, the karst coastal region of the West Aurunci Mountains has been chosen as the study area for the groundwater quality assessment.

73 groundwater samples were collected from 2016 to 2018 and analysed to evaluate the main geochemical processes controlling the groundwater evolution in this hydrogeological system. With the aim of identifying the potential seawater intrusion in this coastal region, several water quality indicators and some diagrams, which use hydrochemical parameters, have been applied in this case study [21–30].

2. Study Area

In this study, two main karst springs of the West Aurunci Mountains and 2 wells (Table 1), belonging to the "25 Ponti" wellfield, which is going to be exploited for drinking purposes, were examined based on the physical-chemical data availability. The study area is located in Italy, in the Southern Latium Region, and involves the competence territory of the Formia, Gaeta, and Spigno Saturnia municipalities, for a total of about 10 ha (Figure 1).

The Mazzoccolo Spring comes out inside the inhabited area of the Formia municipality less than 1 km from the shoreline (Figure 1). The Capodacqua di Spigno Spring is on the other hand at the base of the La Civita Mountain slopes, about 2 km away from the city and about 4 km from the shoreline. The new "25 Ponti" wellfield, at last, is out of the Formia city centre, about 500 m from the coast.

3. Geological and Hydrogeological Setting

The Aurunci Mountains, together with the Lepini and Ausoni Mountains, belong to the pre-Apennines of Latium and form the carbonate platform of the Volsci Ridge, separated from the Apennine ridge by the Latina Valley. The Aurunci Mountains mostly consist of massive dolomitic limestone and dolomite layers, deposited on the carbonate platform with a thickness of about 3000 meters [31]. The stratigraphic succession of the carbonate platform, from the bottom to the top, is generally characterized by a calcareous-dolomitic series and by a carbonate series with detrital-organogenic limestone, in which Pliocene sea deposits overlap (Figure 2) [32]. Above these deposits, marine lagunal subtidal limestone (Middle Liassic-Upper Jurassic) rarely and poorly dolomitized occurs.

The presence of layers containing rubble stones and oolitic deposits suggests the occurrence of a depositional environment. In the same way, the lower Cretaceous deposits suggest the onset of a carbonate platform depositional system ranging from a tidal flat to a lagoon. The analysis of textural parameters and vertical organisation of the lithofacies allows the recognition a cyclic organisation, arranged in shoaling upward sequences [33]. The Volsci Ridge is a structure in the Apennine direction, which on the northeastern edge is overthrust on the terrigenous deposits of the Latina Valley, while on the south western edge, it is characterized by direct faults that lower towards the Tyrrhenian Sea. The overthrust presents an Apennine trend up to Esperia, where it changes direction and follows the edge of the Western Aurunci.

Downstream of the Mazzoccolo Spring, geognostic data indicated the presence of a direct fault, which cuts the outcrop of the Pliocene calcarenites, with the presence (between the coast and the spring) of clayey silts with Quaternary piroclastite. As for the Capodacqua di Spigno Spring, a direct fault cuts the high part of the Spigno Saturnia area. In the Miocene formations, in contact with the carbonates, there are direct faults with an anti-Apennine direction, which delineate a mild Quaternary tectonic pit, characterized by extensive alluvial deposits. In addition, next to the spring, there is a circular shape of alluvial deposits, with a diameter of about 200 meters, which suggests a past phenomenon of a sinkhole, which most likely originated from the collapse of a large karst cavity in the buried carbonate substrate [32].

Karst depressions (superficial and subsurficial) originate from chemical processes related to the contact between rainwater and some types of carbonate rocks, i.e., the limestone, the dolomitic limestone, and the dolomites, which are part of the carbonate series previously described. Although dolomite has a lower solubility than calcite, in the series, the two minerals alternate, so in the studied area, the superficial karst forms are widespread in the hydrogeological basin, except in those areas with high slopes, usually associated with the fault lines. The Western Aurunci area is a karst area without a true hydrographic network, and therefore, the genesis of the existing valleys, within the relief, appears more affected by the faults than the runoff. Surface hydrology is reduced by many absorption points, which rapidly drain rainwater into the subsoil. The Aurunci Mountains are composed of two distinct hydrogeological units: the Western
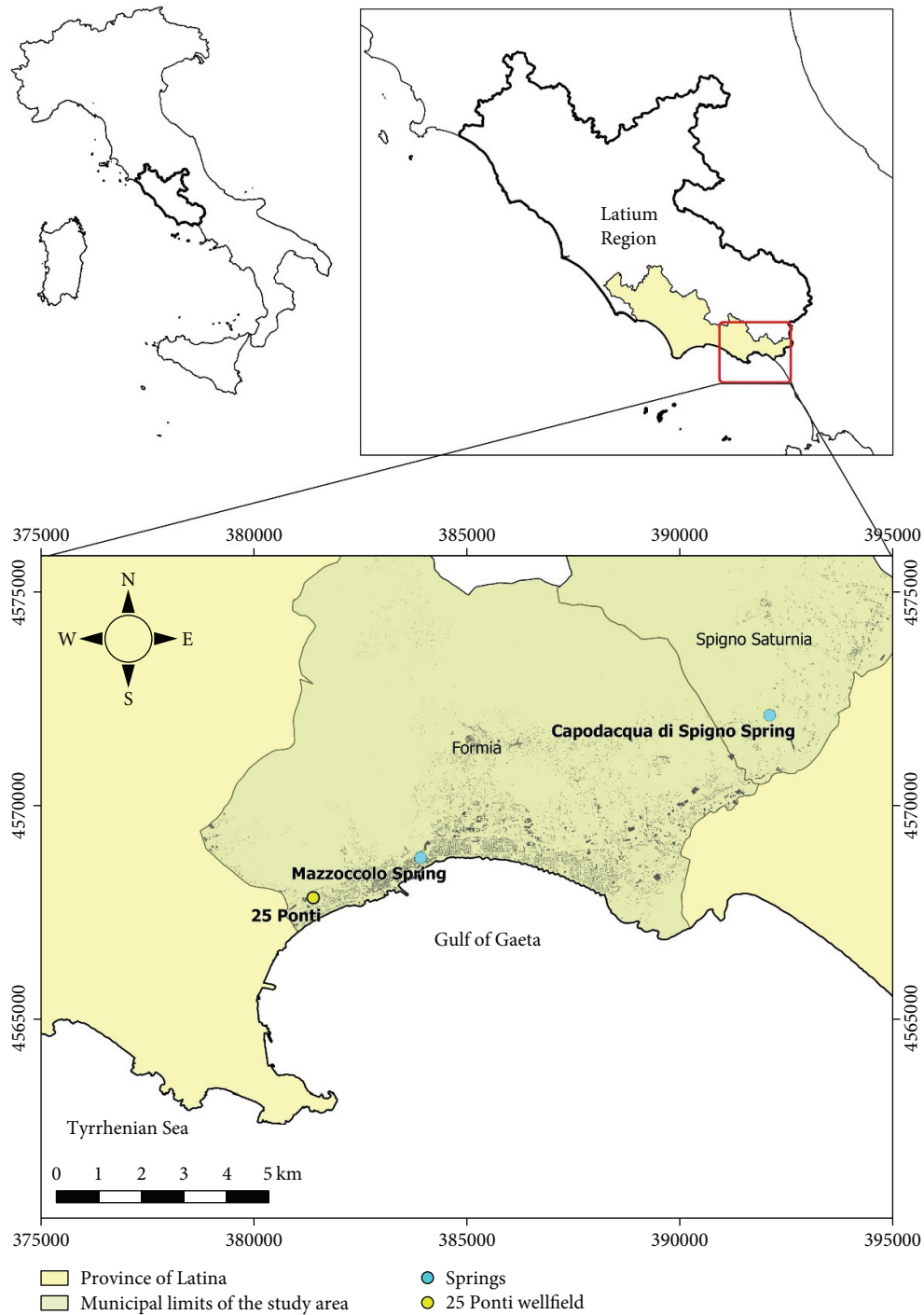
Figure 1: Geographical framework of the study area.

Aurunci Unit, belonging to the Ausoni-Aurunci system, and the Eastern Aurunci Unit, separated from the western one by a marly-arenaceous flysch complex [32]. The Western Aurunci hydrogeological unit, as previously described, is made up of dolomitic limestone and dolomites of the Jurassic and Cretaceous ages, which houses an important karst aquifer, giving rise to springs. The most important ones are the Mazzoccolo and Capodacqua di Spigno (Figure 3), which show, respectively, an active recharge of about 17 and

$37 \, m^3$/year, averaged over 40 years of observations, whereas feeding areas have been estimated at about $30 \, km^2$ and $60 \, km^2$, respectively [34]. The Eastern Aurunci hydrogeological carbonate structure is surrounded by relatively less-permeable sediments, including the Frosinone flysch, the Roccamonfina vulcanite, and the Garigliano Plain alluvial deposits [32, 35]. The Mazzoccolo Spring flows from the base of Pliocene conglomerates, which is tectonically in contact with the limestone. This spring is located at an altitude of
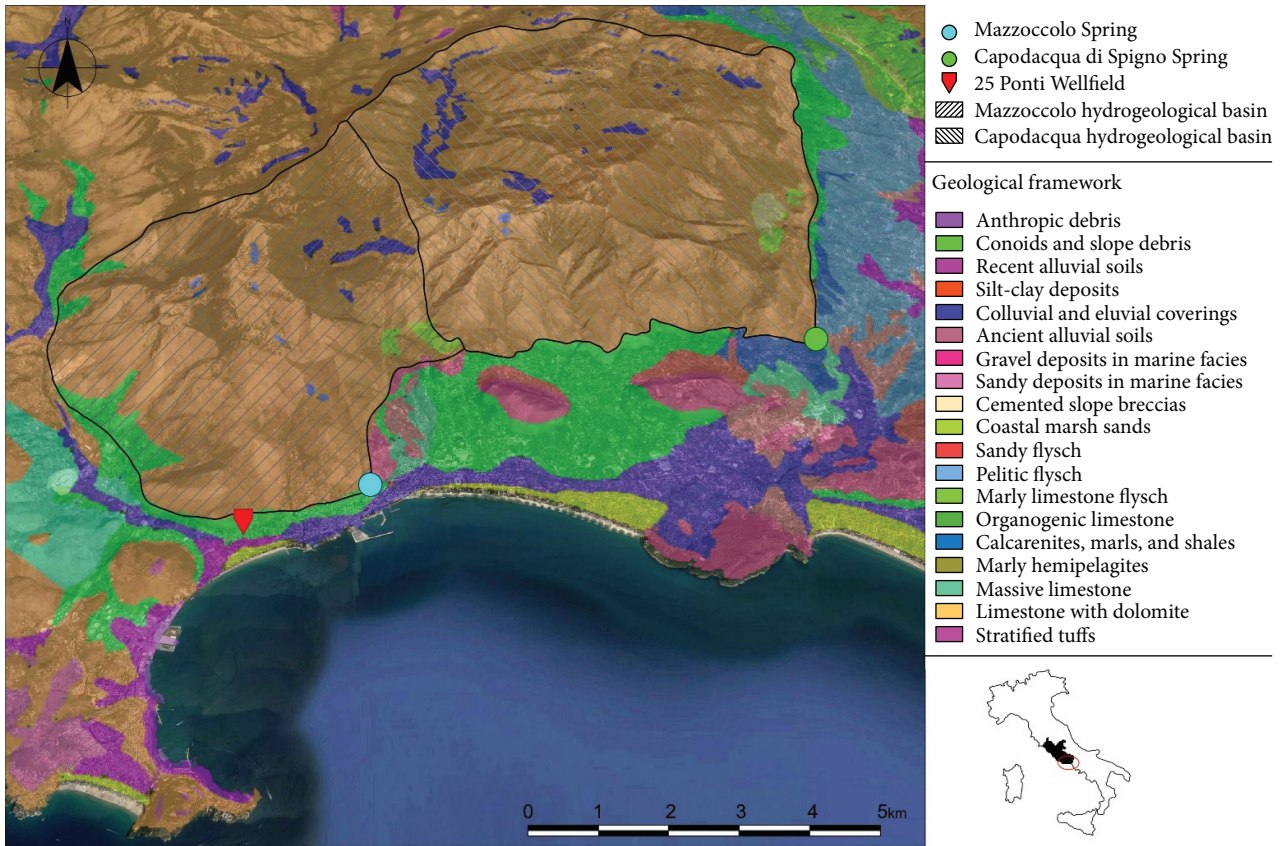
Figure 2: Geological framework of the study area.
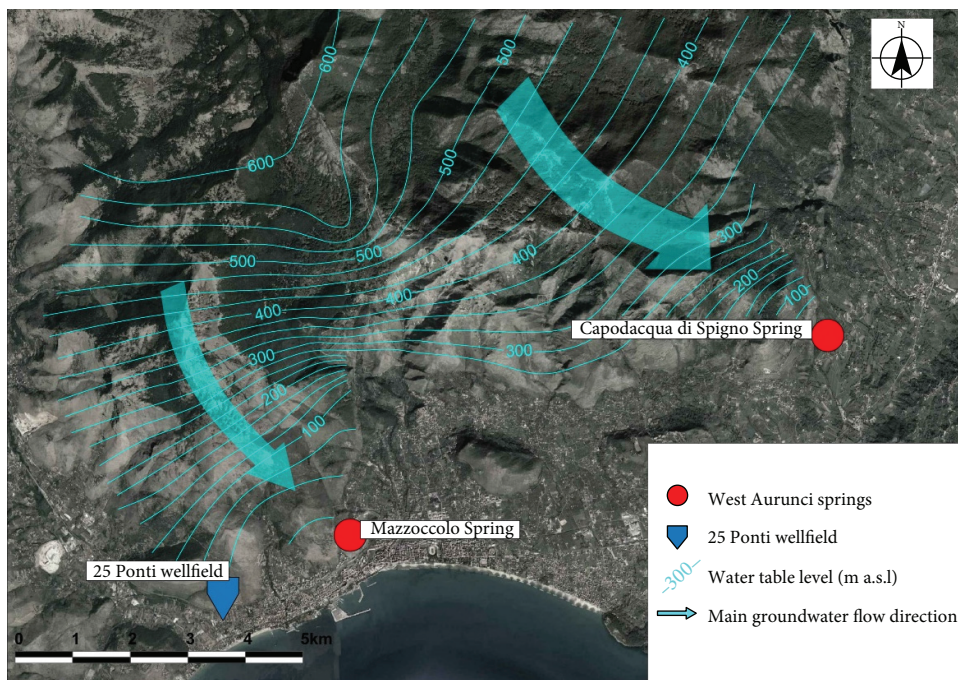
Figure 3: Subsurface hydrology of the West Aurunci karst aquifer (modified from [32]).

11.5 m a.s.l., where rocks present fractures due to the intersection of numerous faults [36]. The local geological setting of the study area is characterized by conglomeratic limestone on the hills (Mola Mountain), surrounded by clayey sands and alluvial deposits of debris. The abundance of groundwater is due to the permeability of the limestone (highly

FIGURE 4: Geological cross section from the "25 Ponti" wellfield to the coastline.

fractured and deep karst), which stores a significant quantity of groundwater. In this area, the top of the saturated zone presents considerable differences in the level (Figure 3) [4, 32].

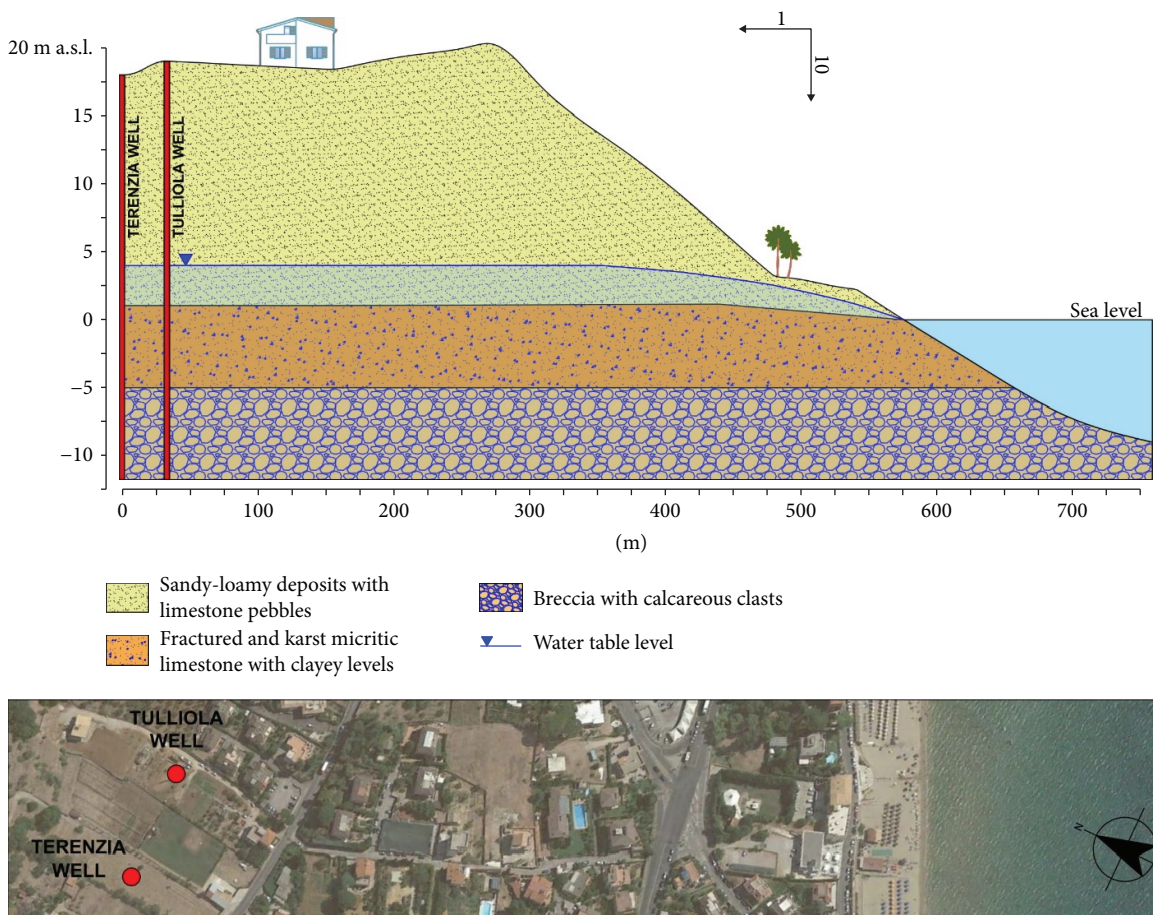The Capodacqua di Spigno Spring is located at an altitude of about 35 m a.s.l., on the eastern edge of the Aurunci Mountains. The spring water comes out from the permeable limestone of the La Civita Mountain and the Castello Mountain and flows above the upper Miocene clays, at the lowest point of the limestone-clay contact [37, 38].

The general groundwater flow direction of the aquifer is towards the SE, but there are also important local flows along the two faults that delimit the carbonate series outcropping, especially the one to the east, which seems to represent the main water conduit towards the spring.

The "25 Ponti" area, where the Tulliola and Terenzia wells are located, is about 1 ha. The geology is locally characterized by the presence of a top layer made of silty-sandy deposits (about 17 m), a central layer made of fractured and karst micritic limestone (about 8 m), and a bottom layer made of breccia with calcareous clasts (more than 50 m). The bottom layer consists of the saturated part of the aquifer, since the water table level is about 4 m a.s.l. and the wells are about 500 m away from the coastline (Figure 4).

In this area, the hydrogeological context allows huge groundwater drainage towards the sea, estimated in flow rates of about 3-4 m³/s and confirmed by the presence of several small submarine springs.

4. Materials and Methods

The monitoring activities were conducted from 2016 to 2018. 73 groundwater samples were collected from 2 karst springs and 2 wells, extensively used for drinking purposes (Table 1). Descriptive statistics of the analysed parameters in water samples are reported in Table 2. The Mazzoccolo (28 samples) and Capodacqua di Spigno (27 samples) springs have been monitored monthly from January 2016 to January 2018. The Tulliola well was realized in July 2017; for this reason, water samples have been collected monthly only from August 2017 to December 2017 (16 samples). In fact, during this period, the well has been used at increasing flow rates to monitor the effects of groundwater exploitation on the karst coastal aquifer quality (Table 3). The Terenzia well has been completed in June 2018, and the related water samples have been collected during a slug test made in July 2018 (2 samples). As regards chemical analyses, bicarbonate was determined in the lab by titration with 0.1 N HCl. The chemical composition was determined using standard analytical methods [39]. All the analyses of major cations and anions were carried out by the laboratory of the local water supply agency, using a Dionex

TABLE 2: Descriptive statics of analysed parameters in the groundwater samples.

Sample codes	Parameters	EC (μS/cm)	Na$^+$ (mg/l)	K$^+$ (mg/l)	Ca^{2+} (mg/l)	Mg^{2+} (mg/l)	Cl$^-$ (mg/l)	SO$_4$$^{2+}$ (mg/l)	HCO$_3$$^-$ (mg/l)
TUL	Minimum	607.00	16.70	0.30	62.90	9.80	42.80	27.20	244.00
	Maximum	858.00	36.70	12.40	120.60	17.80	137.30	32.30	475.80
	Mean	728.13	26.44	2.08	95.57	13.94	78.14	29.98	371.34
	STD	87.83	6.57	2.85	17.49	2.29	37.64	1.21	70.01
TER	Minimum	1102.00	55.00	1.40	133.30	32.90	196.00	69.20	573.40
	Maximum	1146.00	58.00	2.00	140.10	34.10	218.30	69.60	597.80
	Mean	1124.00	56.50	1.70	136.70	33.50	207.15	69.40	585.60
	STD	31.11	2.12	0.42	4.81	0.85	15.77	0.28	17.25
MAZ	Minimum	280.00	2.10	0.10	31.10	1.00	6.60	2.90	97.60
	Maximum	313.00	5.10	8.20	59.40	11.90	11.80	4.30	244.00
	Mean	302.50	3.91	0.95	48.55	7.48	8.08	3.56	185.61
	STD	6.89	0.89	1.68	7.14	2.60	1.26	0.36	30.50
CAP	Minimum	258.00	2.00	0.10	33.60	1.00	5.30	2.50	109.80
	Maximum	325.00	4.20	8.50	59.30	10.00	9.30	3.80	219.60
	Mean	290.89	3.34	0.82	47.52	7.22	6.75	3.13	181.19
	STD	17.71	0.65	1.58	7.71	2.59	1.15	0.34	28.45

TUL: Tulliola well; TER: Terenzia well; MAZ: Mazzoccolo Spring; CAP: Capodacqua di Spigno Spring.

TABLE 3: Average flow rates and cumulated water volumes exploited in the Tulliola well.

Date	$Q_{average}$ (l/s)	V_{cum} (m^3)
September 2017*	17.00	22032
October 2017	36.68	98246
November 2017	37.74	97822
December 2017	36.96	98997

*Exploitation start date: 18/09/2017.

ICS-1000 Ion Chromatograph, calibrated through repeated analysis of five working cation and anion standards, with concentrations within the range of analyses.

5. Results and Discussion

5.1. Hydrogeochemical Facies. Results coming from analyses show that the Mazzoccolo and Capodacqua di Spigno spring water samples are characterized by a cationic composition mainly dominated by Ca^{2+} and Mg^{2+}, with the abundance order of Ca^{2+} > Mg^{2+} > Na$^+$ (meq/l). This water composition reflects the geological nature of the hydrogeological basins to which both springs refer. The Tulliola and Terenzia well water samples are more mineralized, with the abundance order of Ca^{2+} > Mg^{2+} ≈ Na$^+$ (meq/l) (Figure 5). The anionic composition order is HCO$_3$$^-$ > Cl$^-$ > SO$_4$$^{2-}$ (in meq/l), suggesting the potentially different nature of the groundwater and related flow paths. A high variability between minimum and maximum values is specific for the Tulliola well (Figure 5). As shown in Table 2, the electrical conductivity (EC) of the Mazzoccolo and Capodacqua di Spigno springs ranges between 280 μS/cm and 313 μS/cm and between 258 μS/cm and 325 μS/cm, respectively. The lowest value of
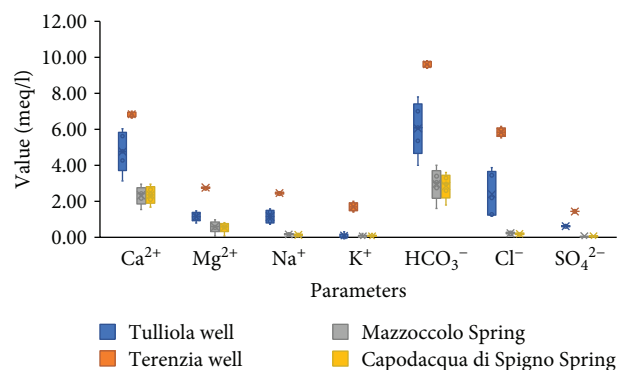

FIGURE 5: Boxplot of the major composition in the spring and well water samples.

EC was recorded for both springs in April 2017, at the end of the rainy season. The EC values of the Tulliola well water range between 607 μS/cm and 858 μS/cm, respectively, at the beginning and at the end of the water withdrawal, whereas the Terenzia well shows a higher EC value, beyond the value of 1100 μS/cm.

In Figure 6, the Cl$^-$ concentration in the Tulliola well water samples is represented, with respect to the operating flow rates from September 2017 to December 2017. The comparison between the increase of the Cl$^-$ content and the total water volume extracted from the well, starting from 18th September, clearly highlights the flow rate influence on groundwater quality changes (Figure 6). The Piper diagram [40] shows that Ca^{2+} and HCO$_3$$^-$ are the dominant ions in the study area (Figure 7). All spring and well water samples show a Ca-HCO$_3$ facies, due to the carbonate dissolution process, related to the presence of limestone and dolomitic limestone outcropping in the study area. The Na-Cl water
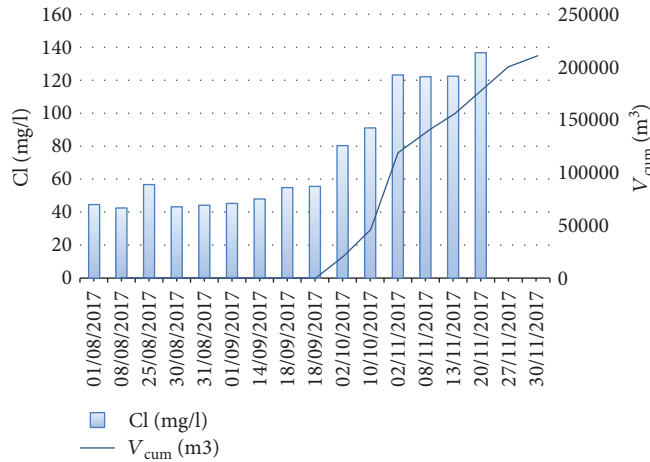
FIGURE 6: Comparison between the Cl concentration and water cumulated volume of the Tulliola well.

Explanation
▲ Tulliola well samples   ● Mazzoccolo Spring samples
△ Terenzia well samples   ○ Capodacqua di Spigno Spring

FIGURE 7: Piper trilinear diagram showing hydrogeochemical facies of the groundwater.

types are majorly present in the coastal aquifers where groundwater salinity is high. The sample distribution in the Piper diagram shows that the wells' groundwater (the Tulliola and Terenzia wells) slightly moves from freshwater (the Mazzoccolo and Capodacqua di Spigno springs) to Na-Cl facies, which represented the saline water type (Figure 5). The different hydrochemical facies between these different water resources may reflect on the higher Cl⁻ concentrations in the coastal area, due to seawater intrusion. When seawater intrusion occurs, the seawater undergoes chemical changes due to the cation exchange reactions.

5.2. *Geochemical Modeling*. Groundwater geochemistry is controlled by water-rock interactions [41, 42]. To identify

TABLE 4: Statistical summary of saturation indices of minerals in groundwater using PHREEQC. BEX index and some ionic ratios of interest in the study area.

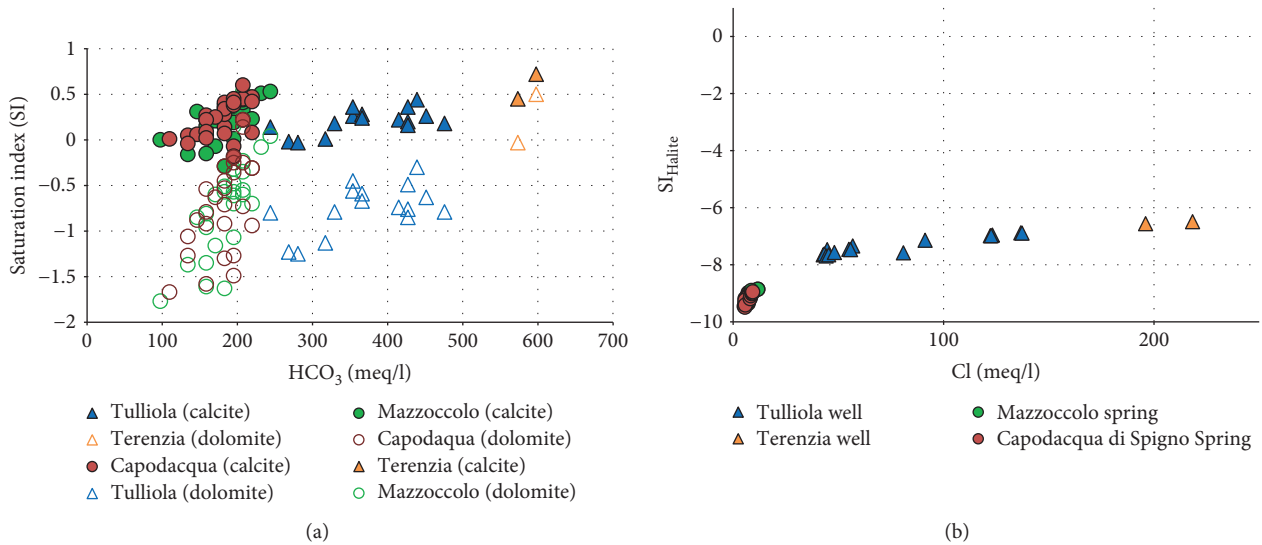| Sample codes	Parameters	Calcite	Dolomite	Halite	Na/Cl (meq/l)	Cl/HCO$_3$ (meq/l)	BEX (*BEX$_d$)
TUL	Minimum	-0.030	-1.250	-7.690	0.400	0.155	-1.393
	Maximum	0.440	-0.300	-6.880	0.942	0.553	1.083
	Mean	0.203	-0.752	-7.333	0.583	0.353	-0.012
	STD	0.134	0.269	0.306	0.164	0.126	0.810
TER	Minimum	0.450	-0.030	-6.560	0.410	0.588	-2.825*
	Maximum	0.720	0.500	-6.490	0.433	0.628	-2.419*
	Mean	0.585	0.235	-6.525	0.421	0.608	-2.622*
	STD	0.191	0.375	0.049	0.016	0.028	0.287*
MAZ	Minimum	-0.290	-1.770	-9.360	0.450	0.051	-0.028
	Maximum	0.530	0.530	-8.860	1.092	0.118	1.111
	Mean	0.229	-0.661	-9.058	0.751	0.077	0.565
	STD	0.216	0.571	0.142	0.171	0.015	0.250
CAP	Minimum	-0.180	-1.670	-9.490	0.533	0.065	0.047
	Maximum	0.600	0.220	-8.950	1.109	0.553	0.083
	Mean	0.229	-0.714	-9.204	0.772	0.428	0.065
	STD	0.201	0.504	0.137	0.155	0.205	0.010

FIGURE 8: Saturation index (SI) values for the carbonate and evaporite minerals for the spring and well water samples. Calcite and dolomite saturation indices versus HCO$_3^-$ (a); halite saturation index versus Cl$^-$ (b).

these processes, geochemical modeling and the saturation index of spring and well water samples were studied, in order to investigate groundwater interaction with carbonate rocks. The saturation indices (SI) referring to groundwater samples, with respect to different mineral phases (i.e., calcite, dolomite, and halite), were calculated using the geochemical software PHREEQC [43] (Table 4). The positive and negative SI values represent the thermodynamic potential for precipitation and dissolution, respectively. Equilibrium is indicated when SI = 0; the groundwater is supersaturated when SI > 0, which shows that precipitation is needed to achieve equilibrium. If s, the groundwater is undersaturated: this fact indicates that dissolution is required to reach equilibrium.

Groundwater saturation with respect to calcite suggests that this carbonate mineral is the main component in the host rock. However, the lower calcite saturation has influenced groundwater chemical composition. All water samples are undersaturated in the halite mineral, indicating that groundwater dissolves most likely the halite along the flow paths, hence leading to an increase of Na$^+$ and Cl$^-$ concentrations [44].

The results of the geochemical model suggest that more than half of the spring water samples are saturated with respect to calcite and undersaturated with respect to dolomite (Figure 8(a)). The saturation with respect to calcite and dolomite reflects a great dissolution and strong

mineralization along groundwater flow paths. The high dissolution rate for carbonate rocks allows for waters close to saturation with respect to the calcite and dolomite and evaporite mineral halites to remain undersaturated, resulting in continued dissolution along the flow paths. This indicates that the groundwater is able to dissolve gypsum and halite along the flow paths; hence, the concentrations of Ca^{2+}, SO_4^{2-}, Na^+, and Cl^- in the solution would increase.

Spring water has great variability in calcite and dolomite saturation indices. The calcite and dolomite saturation indices of samples coming from both springs present great variability, instead of those related to well water (Figure 8(a)). The Terenzia well water samples are saturated with respect to both calcite and dolomite, whereas the Tulliola well water samples are saturated with calcite and undersaturated with dolomite. The diagram representing the halite saturation index with respect to Cl^- (Figure 8(b)) highlights that all the groundwater samples are undersaturated with halite, with saturation index values that generally show a growing trend related to the increasing concentration of Cl^-. This trend is clear both in the Tulliola well samples, with the flow rates increasing, and in the Terenzia well samples, but not in the groundwater spring samples. The effects of seawater encroachment in the well water have been evaluated studying different ionic ratios and relationships. For example, the Na/Cl ratio values, lower than the seawater value (0.88), generally suggest seawater encroachment [24, 25, 45].

The Na/Cl ratios for the analysed samples range from 0.40 to 0.94 in well water and from 0.45 to 1.11 in spring water (Table 4). For the well water samples, the Na/Cl ratios show a decreasing trend as the Cl^- concentration increases (Figure 9). In the Tulliola well, the Na/Cl ratios clearly decreased along the period of the well exploitation, proportionally to the extracted flow rate, suggesting first evidence of a seawater intrusion in this system as a consequence of the well exploitation. This hypothesis is confirmed by the Na/Cl ratio of the Tulliola water sample, collected before the pumping (01/08/2017), which has a value higher than the Mediterranean seawater ratio (0.88). In spring water samples, the Na/Cl ratios show high variability, which is not related to a Cl^--increasing concentration. The lower values of the Na/Cl ratios in well water samples, with respect to the Mediterranean seawater ratio, are also due to the deficit of Na^+ resulting from the cation exchange process with Ca^{2+} occurring during seawater intrusion [24].

This is quite evident examining Figures 10(a) and 10(b), where Na^+ and Ca^{2+} clearly deviated (respectively, with a negative and a positive trend) from their conservative expected values indicated by the freshwater-saline water mixing line.

The Cl/HCO_3 ionic ratio is useful to characterize the origin of salinity in the groundwater and to classify the rate of seawater intrusion [14, 23, 41]. The Cl/HCO_3 ratio ranges from 0.16 to 0.63 in well water and from 0.05 to 0.55 in spring water (Table 4). According to the classification shown in Figure 11, all groundwater samples fall in the "not affected" field, with higher values for the Terenzia well samples, close to the "slightly affected" one. As regards samples collected in the two springs, they fall far from the line that separates
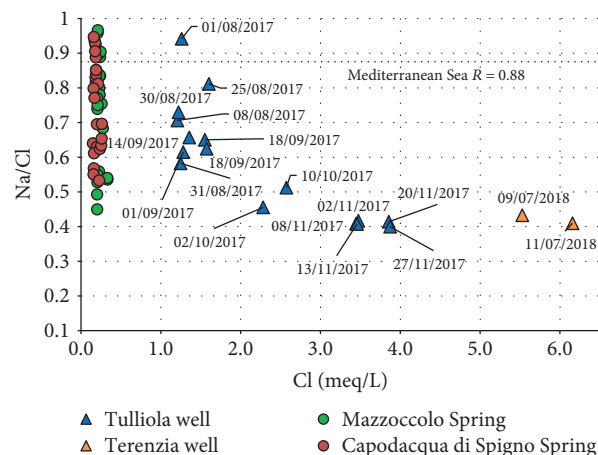

Figure 9: Scatter plot of Cl vs. Na/Cl.

the "not affected" from the "slightly affected" area. It is interesting, however, to note how the samples of the Tulliola well are approaching this line with the progress of time, i.e., with the increase of the flow rate.

5.3. Seawater Intrusion Assessment. The Base Exchange Index (BEX) is frequently used in regional hydrochemical surveys in order to indicate whether an aquifer is salinizing or freshening or it has been freshened or salinized in the past [22]. In this study, the BEX index has been calculated to investigate if well water samples were affected by seawater intrusion.

According to Stuyfzand, using the relation between sodium, potassium, and magnesium to chloride, the process of salinization and freshening of groundwater can be identified with the help of a positive or negative value of the BEX index [46, 47] according to

$$BEX = Na + K + Mg - 1.0716 \cdot Cl \, (meq/L). \tag{1}$$

For dolomitic aquifers, Stuyfzand [46] has suggested another index (BEX_d) which is expressed by the following:

$$BEX_d = Na + K - 0.8768 \cdot Cl \, (meq/L). \tag{2}$$

These parameters represent the difference between principal marine cations, which are found in one water sample, and the expected values of these for seawater. The BEX represents the trend of groundwater salinization or freshening: a positive value represents freshening, a negative value indicates salinization, and a value equal zero represents no base exchange [46–48]. The BEX index was calculated according to equation (1) for all groundwater samples, except for the Terenzia well water samples, saturated in the dolomite mineral, for which equation (2) has been applied (Table 4). All spring water values are positive, confirming the absence of seawater intrusion (Figure 12). Tulliola well BEX indices point out a salinization trend (BEX < 0) from the half of September 2017, due to the extensive pumping which caused a slight seawater intrusion (Figure 12). The Terenzia well water samples show the most negative value of the BEX_d indices, confirming the seawater intrusion in the study area.
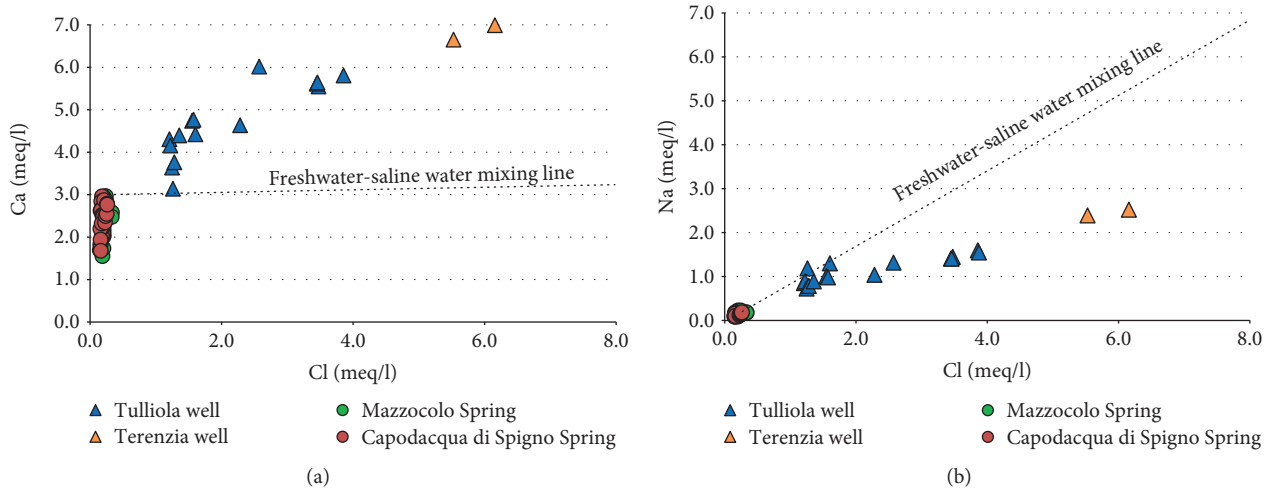
(a)

(b)

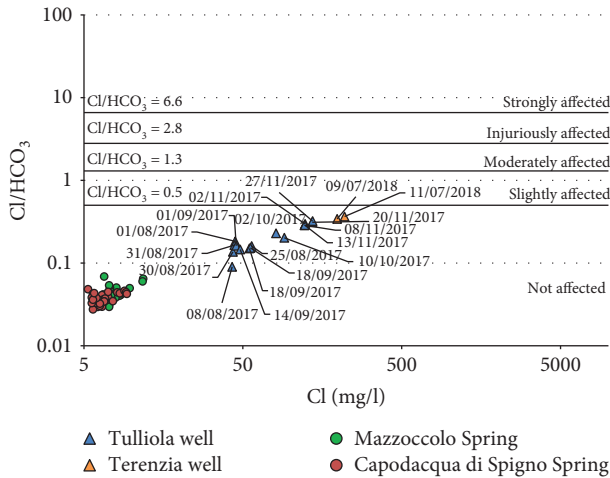Figure 10: Scatter plot of Cl vs. Ca (a) and Na (b).

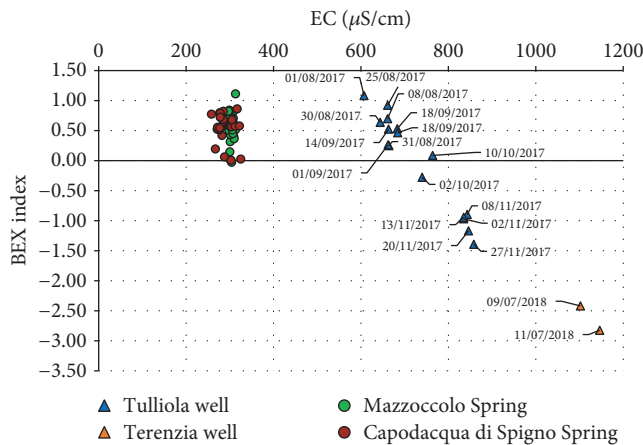Figure 11: Scatter plot of Cl vs. the Cl/HCO$_3$ ratio.

Figure 12: Scatter plot of electrical conductivity (EC) vs. the BEX index.
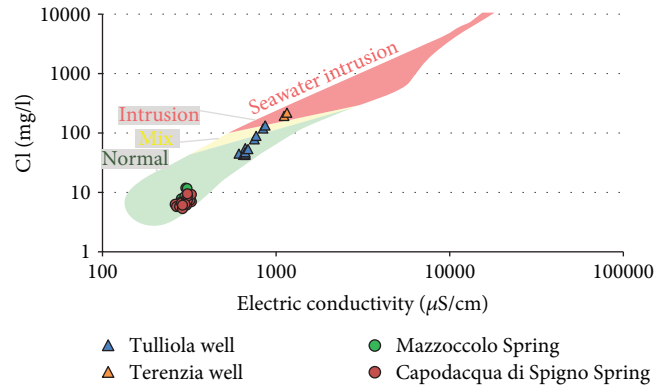
Figure 13: Chloride-EC bivariate plot to define mixing and seawater intrusion (based on Kelly approach, (2006)).

Similar considerations can be made using some graphical representations, specific for groundwater analysis, which allow to better understand the ongoing processes in the aquifer. Figure 13 shows a plot based on the approach outlined by Kelly [27], in which the correlation between chloride concentrations and the electrical conductivity of groundwater samples collected is represented.

All groundwater samples, collected in the Mazzoccolo and Capodacqua di Spigno springs, fall in the green area, which delimits the "normal" conditions, showing no trend related to the sampling date. On the contrary, for groundwater samples collected in the Tulliola well, the proportional increase of both values suggest a slight seawater intrusion in the area. In particular, water samples collected before the Tulliola well exploitation (August 2017) fall into the green area, whereas those collected during October 2017 and November 2017 fall in the yellow and red areas, respectively, confirming the slightly negative effect of the pumping to groundwater quality. The two water samples collected in the Terenzia well, before and after the slug test, fall into the red area, which defines the "intrusion" conditions.

FIGURE 14: Hydrochemical Facies Evolution Diagram (HFE-D) for groundwater samples.

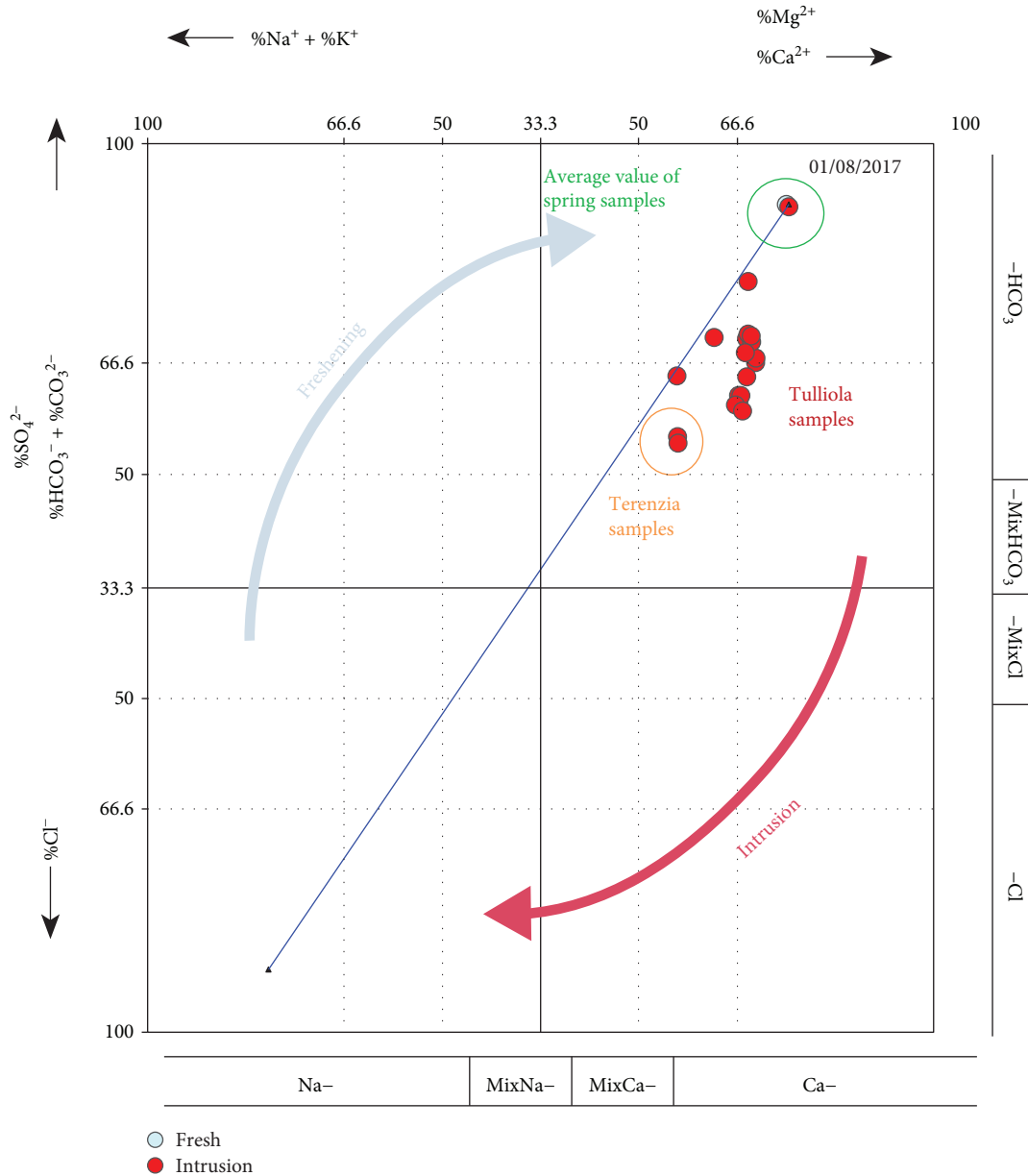The negative effect of the pumping to groundwater quality is also confirmed plotting the Hydrochemical Facies Evolution Diagram (HFE-D), proposed by Giménez-Forcada and Sánchez San Román [49]. This diagram has been specifically created in order to better highlight the main processes occurring in coastal aquifers, involving seawater intrusion evolution, through a detailed study of the groundwater hydrochemical facies evolution [49].

The abscissa represents, separately, the percentages of Na^+ and Ca^{2+} in meq/l. In the diagram setup, in order to identify direct and reverse ion exchange reactions, for water samples containing a percentage of Ca^{2+} greater than that of Na^+, only the Ca^{2+} percentage is represented and vice versa. Calcium and sodium percentage values, between 0% and 33%, are not represented with the aim to draw the lines

of evolution facies, and Mg^{2+} is not integrated into the diagram due to its irregular behaviour in exchange processes. The ordinates represent the percentage of anions. In particular, the chloride percentage characterizes seawater, and the bicarbonate or sulphate percentage (depending on their dominance in freshwater) characterizes the recharge water.

Freshwater generally corresponds to the heterotopic facies Ca-HCO_3/SO_4, whereas the Na-Cl facies identify saline or seawater. Seawater intrusion is suggested by an early increase in salinity and a reverse exchange of Na-Ca, which is recognized by the characteristic Ca-Cl facies. Finally, this type of water evolves towards facies that are closer to seawater (Na-Cl).

To build up this diagram, an excel macro, courtesy of the same authors [49], was applied. In Figure 14, data

related to the Tulliola and Terenzia well water samples are represented in the Hydrochemical Facies Evolution Diagram (HFE-D).

The blue line represents the binary mixing of freshwater with seawater. Data, coming from collected water samples, appear on the right and beneath the mixing line, falling in the field of Mg-Ca-HCO$_3$ facies (Figure 14). In order to investigate the possible seawater intrusion into the "25 Ponti" area, a single point, given by the mean values of all spring water samples, was added to the HFE-D. This point (blue colour) represents groundwater not affected by saline intrusion (i.e., freshwater), but in the plot, it is not easily recognizable due to the closeness to the Tulliola well sample collected in 01/08/2017. This evidence confirms that, before the pumping, the Tulliola well groundwater chemical characteristics were similar to the spring water characteristics. The other water samples collected in the Tulliola well during August 2018 fall along the mixing line. On the contrary, the rest of the Tulliola water samples show a tendency toward Ca-MixHCO$_3$ composition (Figure 14), highlighting an increase in salinity, maybe due to the development of reverse exchange reactions, related with the groundwater exploitation. Water samples collected in the Terenzia well are plotted below the mixing line, closer than those of the Tulliola well, suggesting a more mineralized water.

6. Conclusions

Results coming from a groundwater quality assessment, carried out in the karst coastal region of the West Aurunci Mountains (Central Italy), have been presented here, as these karst carbonate aquifers well represent some typical hydrogeological frameworks in the southern part of the Latium Region.

Groundwater samples, collected from two springs and two wells, exploited for drinking purposes, were analysed to study the main processes controlling the hydrogeochemical evolution and water quality properties.

The geochemical modeling shows that all groundwater samples belong to the Ca-HCO$_3$ hydrogeochemical facies, highlighting a different mineralization between spring and well water samples.

The Mazzoccolo and Capodacqua di Spigno springs present similar geochemical characteristics, related to the carbonate dissolution process occurring in the aquifer.

On the contrary, the proximity to the coastline of the "25 Ponti" wellfield and the higher values of EC, Na$^+$, and Cl$^-$, measured in well water samples, suggest a potential seawater intrusion phenomenon.

In order to evaluate its severity, ionic ratios, graphical approaches, and specific indices have been used. In the Tulliola well, all the geochemical parameters analysed clearly change over time, proportionally to the flow rate exploited from the well, approaching the values obtained for the Terenzia well samples. In fact, the two water samples collected in the Terenzia well, before and after the slug test, show the highest mineralization most likely related to seawater intrusion.

The results obtained confirm that carbonate coastal aquifers are very vulnerable; therefore, they require continuous and systematic monitoring, in order to achieve a sustainable groundwater exploitation even in times of emergency.

Data Availability

The data used to support the findings of this study have been included within the supplementary information file.

Conflicts of Interest

The authors declare that there is no conflict of interest regarding the publication of this paper. The authors' employer is the Department of Civil, Building and Environmental Engineering (DICEA), Sapienza University of Rome.

Acknowledgments

Supplementary Materials

Supplementary 1. Supplementary Table 1: analysed parameters in the groundwater samples: Tulliola well (TUL), Terenzia well (TER), Mazzoccolo Spring (MAZ), and Capodacqua di Spigno Spring (CAP). The Mazzoccolo (28 samples) and Capodacqua di Spigno (27 samples) springs have been monitored monthly from January 2016 to January 2018. The Tulliola well water samples have been collected monthly only from August 2017 to December 2017 (16 samples). The Terenzia well water samples have been collected in July 2018 (2 samples). Supplementary 2. Supplementary Table 2: the groundwater sample saturation indices (SI), with respect to different mineral phases (i.e., calcite, dolomite, and halite). The SI were calculated using the geochemical software PHREEQC. (Supplementary Materials)

References

[1] S. Foster, R. Hirata, and B. Andreo, "The aquifer pollution vulnerability concept: aid or impediment in promoting groundwater protection?," *Hydrogeology Journal*, vol. 21, no. 7, pp. 1389–1392, 2013.

[2] B. Andreo, J. Vías, J. J. Durán, P. Jiménez, J. A. López-Geta, and F. Carrasco, "Methodology for groundwater recharge assessment in carbonate aquifers: application to pilot sites in southern Spain," *Hydrogeology Journal*, vol. 16, no. 5, pp. 911–925, 2008.

[3] C. Caetano Bicalho, C. Batiot-Guilhe, J. L. Seidel, S. van Exter, and H. Jourde, "Geochemical evidence of water source characterization and hydrodynamic responses in a karst aquifer," *Journal of Hydrology*, vol. 450-451, pp. 206–218, 2012.

[4] F. Banzano, *Caratterizzazione del flusso in acquiferi carbonatici fratturati dell'Italia centrale per la gestione e la protezione delle risorse idriche sotterranee, [Ph.D.*

Thesis] in Earth Sciences, XXIV Cycle, Sapienza University of Rome, 2014.

[5] G. Sappa and G. Luciani, "Groundwater management in Dar Es Salam coastal aquifer (Tanzania) under a difficult sustainable development," *WSEAS Transactions on Environment and Development*, vol. 10, pp. 465–477, 2014.

[6] B. Capaccioni, M. Didero, C. Paletta, and L. Didero, "Saline intrusion and refreshening in a multilayer coastal aquifer in the Catania Plain (Sicily, Southern Italy): dynamics of degradation processes according to the hydrochemical characteristics of groundwaters," *Journal of Hydrology*, vol. 307, no. 1-4, pp. 1–16, 2005.

[7] G. Sappa and G. Luciani, "Sustainability of groundwater management in the coastal plain of Dar Es Salaam (Tanzania)," *Rendiconti online della Società Geologica Italiana*, vol. 35, pp. 264–267, 2015.

[8] R. Casa, M. Rossi, G. Sappa, and A. Trotta, "Assessing crop water demand by remote sensing and GIS for the Pontina Plain, Central Italy," *Water Resources Management*, vol. 23, no. 9, pp. 1685–1712, 2009.

[9] R. H. Kim, J. H. Kim, J. S. Ryu, and D. C. Koh, "Hydrogeochemical characteristics of groundwater influenced by reclamation, seawater intrusion and land use in the coastal area of Yeonggwang, Korea," *Geosciences Journal*, 2018.

[10] J. D. Gomez, J. A. Lopez Geta, and E. Garrido Schneider, "The state of seawater intrusion in Spain," in *Coastal aquifers intrusion technology, Mediterranean countries*, J. A. Lopez-Geta, J. D. Gomez, J. A. Orden, G. Ramos, and L. Rodriguez, Eds., vol. 14, pp. 169–185, IGME, 2003.

[11] M. Argamasilla, J. A. Barbera, and B. Andreo, "Factors controlling groundwater salinization and hydrogeochemical processes in coastal aquifers from southern Spain," *Science of the Total Environment*, vol. 580, pp. 50–68, 2017.

[12] V. De Montety, O. Radakovitch, C. Vallet-Coulomb, B. Blavoux, D. Hermitte, and V. Valles, "Origin of groundwater salinity and hydrogeochemical processes in a confined coastal aquifer: case of the Rhône delta (Southern France)," *Applied Geochemistry*, vol. 23, no. 8, pp. 2337–2349, 2008.

[13] M. Antonellini, P. Mollema, B. Giambastiani et al., "Salt water intrusion in the coastal aquifer of the Southern Po Plain, Italy," *Hydrogeology Journal*, vol. 16, no. 8, pp. 1541–1556, 2008.

[14] A. Ekhmaj, Y. Ezlit, and M. Elaalem, "The situation of seawater intrusion in Tripoli, Libya," *International Conference on Biological, Chemical and Environmental Sciences (BCES)*, 2014, pp. 1–3, Penang, Malaysia, June 14-15.

[15] P. M. Barlow and E. G. Reichard, "Saltwater intrusion in coastal regions of North America," *Hydrogeology Journal*, vol. 18, no. 1, pp. 247–260, 2010.

[16] G. Kanagaraj, L. Elango, S. G. D. Sridhar, and G. Gowrisankar, "Hydrogeochemical processes and influence of seawater intrusion in coastal aquifers south of Chennai, Tamil Nadu, India," *Environmental Science and Pollution Research*, vol. 25, no. 9, pp. 8989–9011, 2018.

[17] J. Mahlknecht, D. Merchán, M. Rosner, A. Meixner, and R. Ledesma-Ruiz, "Assessing seawater intrusion in an arid coastal aquifer under high anthropogenic influence using major constituents, Sr and B isotopes in groundwater," *Science of The Total Environment*, vol. 587-588, pp. 282–295, 2017.

[18] A. K. Mohanty and V. V. S. G. Rao, "Hydrogeochemical, seawater intrusion and oxygen isotope studies on a coastal region

in the Puri District of Odisha, India," *CATENA*, vol. 172, pp. 558–571, 2019.

[19] Q. Ge, X. Liang, M. Jin, J. Li, and Y. Liu, "Origin and geochemical processes of porewater in clay-rich deposits in the North Jiangsu Coastal Plain, China," *Geofluids*, vol. 2017, Article ID 8715080, 13 pages, 2017.

[20] G. Mongelli, S. Monni, G. Oggiano, M. Paternoster, and R. Sinisi, "Tracing groundwater salinization processes in coastal aquifers: a hydrogeochemical and isotopic approach in the Na-Cl brackish waters of northwestern Sardinia, Italy," *Hydrology and Earth System Sciences*, vol. 17, no. 7, pp. 2917–2928, 2013.

[21] P. Zhou, M. Li, and Y. Lu, "Hydrochemistry and isotope hydrology for groundwater sustainability of the coastal multilayered aquifer system (Zhanjiang, China)," *Geofluids*, vol. 2017, Article ID 7080346, 19 pages, 2017.

[22] A. H.-D. Cheng and D. Ouazar, "Analytical solutions," in *Seawater Intrusion in Coastal Aquifers—Concepts, Methods and Practices*, J. Bear, A. H.-D. Cheng, S. Sorek, D. Ouazar, and I. Herrera, Eds., vol. 14, pp. 163–191, Springer, Dordrecht, the Netherlands, 1999.

[23] S. Najib, A. Fadili, K. Mehdi, J. Riss, and A. Makan, "Contribution of hydrochemical and geoelectrical approaches to investigate salinization process and seawater intrusion in the coastal aquifers of Chaouia, Morocco," *Journal of Contaminant Hydrology*, vol. 198, pp. 24–36, 2017.

[24] J. Klassen, D. M. Allen, and D. Kirste, *Chemical Indicators of Saltwater Intrusion for the Gulf Islands, British Columbia*, Department of Earth Sciences, Simon Fraser University, Final report submitted to BC Ministry of Forests, Lands and Natural Resource Operations and BC Ministry of Environment, 2014.

[25] N. Alfarrah and K. Walraevens, "Groundwater overexploitation and seawater intrusion in coastal areas of arid and semi-arid regions," *Water*, vol. 10, no. 2, p. 143, 2018.

[26] P. J. Sajil Kumar, "Deciphering the groundwater-saline water interaction in a complex coastal aquifer in South India using statistical and hydrochemical mixing models," *Modeling Earth Systems and Environment*, vol. 2, no. 4, pp. 1–11, 2016.

[27] D. J. Kelly, "Development of seawater intrusion protection regulations," in *Session 6 1st SWIM-SWICA Joint Saltwater Intrusion Conference*, pp. 135–145, Cagliari-Chia Laguna, Italy, September 24-29, 2006.

[28] E. Giménez-Forcada, "Dynamic of sea water interface using hydrochemical facies evolution diagram," *Groundwater*, vol. 48, no. 2, pp. 212–216, 2010.

[29] L. Tulipano, V. Cotecchia, and M. D. Fidelibus, "An example of the multitracing approach in studies of karstic and coastal aquifers," in *Proceedings of the International Symposium and Field Seminar on Hydrogeological Processes in Karst Terranes*, pp. 381–389, Antalya, Turkey, 1993.

[30] S. Jorreto, F. Sola, Á. Vallejos et al., "Evolution of the geometry of the freshwater-seawater interface in a coastal aquifer affected by an intense pumping of seawater," *Geogaceta*, vol. 62, pp. 87–90, 2017.

[31] C. Boni and P. Bono, *Carta Idrogeologica del Territorio della Regione Lazio—Scala 1:250.000*, Regione Lazio, Assessorato alla Programmazione, Ufficio Parchi e Riserve, Università degli Studi di Roma "La Sapienza", Roma, Italy, 1988.

[32] A. M. Baldi, A. Marzocchi, F. Ricci et al., "La torbidità alle captazioni idropotabili dei monti Aurunci," in *Aquifer Vulnerability and Risk, 4th Congress on the Protectionand Management of Groundwater*, pp. 1–25, Parma, Italy, 21-22-23 September, 2005.

[33] D. Rossi, S. Bigi, M. Del Castello, and P. Di Manna, "The structure of the Aurunci Mountains (Southern Lazio): a balanced cross section and its restoration," *Bollettini Società Geologica Italiana*, vol. 1, pp. 151–159, 2002.

[34] G. Sappa, F. Ferranti, S. Iacurto, and F. M. D. Filippi, "Effects of climate change on groundwater feeding the Mazzoccolo and Capodacqua di Spigno Springs (Central Italy): first quantitative assessments," in *18th International Multidisciplinary Scientific GeoConference SGEM*, pp. 219–226, Albena, Bulgaria, 2018.

[35] B. Accordi, A. Biasini, C. Caputo et al., "Geologia e Dissesti del Territorio Montano della Regione Lazio," in *Carta della Montagna, vol. 2, Monografia Regionale No. 12 Lazio, Ministero di Agricoltura*, pp. 55–101, Roma, Italy, 1976.

[36] P. Celico, "Schema Idrogeologico dell'Appennino Carbonatico Centro-Meridionale," *Memorie e Note dell'Istituto di Geologia Applicata*, vol. 14, pp. 1–97, 1978.

[37] N. Ialongo, *Studio idrogeologico Sorgente Mazzoccolo*, Relazione idrogeologica. Amministrazione comunale di Formia, 1983.

[38] C. Bergomi, V. Catenacci, G. Cestari, M. Manfredini, and V. Manganelli, *Note illustrative della Carta Geologica d'Italia alla scala 1:100.000, Foglio 171 Gaeta e Vulcano di Roccamonfina*, Poligrafica & Cartevalori, Ercolano (Napoli), Italy, 1969.

[39] APHA, *Standard Methods for the Examination of Water and Wastewater*, APHA, Washington, DC, USA, 19th edition, 1995.

[40] A. M. Piper, "A graphic procedure in the geochemical interpretation of water-analyses," *Transactions of the American Geophysical Union*, vol. 25, no. 6, pp. 914–923, 1944.

[41] S. Ergul, F. Ferranti, and G. Sappa, "Arsenic in the aquifer systems of Viterbo Region, Central Italy; distribution and geochemistry," *Rendiconti Online Società Geologica Italiana*, vol. 24, pp. 116–118, 2013.

[42] G. Sappa, F. Ferranti, F. de Filippi, and G. Cardillo, "Mg^{2+} based method for the Pertuso Spring discharge evaluation," *Water*, vol. 9, no. 1, p. 67, 2017.

[43] D. L. Parkhurst and C. A. J. Appello, *User's Guide to PHREEQC (Version 2)—a Computer Program for Speciation, Batch-Reaction, One-Dimensional Transport, and Inverse Geochemical Calculations*, US Geological Survey Water-Resources Investigations, Report, 99-4259, 1999.

[44] W. Stumm and J. J. Morgan, *Chemical Equilibria and Rates in Natural Waters*, John Wiley and Sons, New York, NY, USA, 1996.

[45] M. Sudaryanto and W. Naily, "Ratio of major ions in groundwater to determine saltwater intrusion in coastal areas," in *Global Colloquium on GeoSciences and Engineering 2017*, Bandung, Indonesia, 18-19 October, 2017.

[46] P. J. Stuyfzand, "A new hydrochemical classification of water types: principles and application to the coastal dunes aquifer system of the Netherlands," in *Proceedings of the 9th Salt Water Intrusion Meeting*, pp. 641–655, Delft 12-16 May, Delft University of Technology, 1986.

[47] P. J. Stuyfzand, "A new hydrochemical classification of water types. J. regional characterization of water quality," in *Proceedings of the Baltimore symposium, IAHS 182*, pp. 89–98, Baltimore, MD, USA, 1989.

[48] P. J. Stuyfzand, "Base exchange indices as indicators of salinization or freshening of (coastal) aquifers," in *Proceedings of the 20th Salt Water Intrusion Meeting*, pp. 262–265, Naples, FL, USA, 2008.

[49] E. Giménez-Forcada and F. J. Sánchez San Román, "An excel macro to plot the HFE-diagram to identify sea water intrusion phases," *Groundwater*, vol. 53, no. 5, pp. 819–824, 2015.

Research Article

Geochemical Modeling of Water-Rock Interaction in the Granulite Rocks of Lower Crust in the Serre Massif (Southern Calabria, Italy)

Carmine Apollaro [ORCID]

University of Calabria, Department of Biology, Ecology and Earth Sciences (DIBEST), 87036 Rende, Italy

Correspondence should be addressed to Carmine Apollaro; apollaro@unical.it

To simulate the evolution of groundwaters interacting with granulitic rocks of the lower crust exposed in the southern sector of the Calabrian region, reaction path modeling was performed by means of the EQ3/6 software package version 8.0a. Low-salinity waters issuing from granulite have Na–Cl to Na-HCO$_3$ composition, about neutral pH (mean value of 6.7), outlet temperatures of 7.7 to 14.2°C, oxidant redox potentials from 100 to 182 mV, and electrical conductivity from 72.1 to 196.9 μS/cm. The mineral constituents of local granulite are plagioclase, amphibole, biotite, clinopyroxene, garnet, and orthopyroxene. Simulations were carried at constant temperature of 11.8°C (which reproduces the average temperature of local groundwaters) fixing the fugacity of CO$_2$ at 10$^{-2.4}$ bar (mean value), 10$^{-2.0}$ bar (mean value +1 σ), and 10$^{-2.8}$ bar (mean value -1 σ). The analytical contents of major elements in groundwaters were satisfactorily reproduced by modeling and are fully consistent with the secondary minerals produced by weathering processes affecting the same rocks.

1. Introduction

The chemical composition of natural water is derived from many different sources of solutes, including aerosols and gases from the atmosphere, erosion and weathering of soil and rocks, and dissolution or precipitation reactions occurring below the land surface. However, human activities play an important and not negligible role on the chemical composition of natural waters. Some of the processes of dissolution or precipitation of minerals can be closely evaluated by means of principles of chemical equilibrium whereas other processes are irreversible and require consideration of reaction mechanisms and rates [1–4]. During water rock-interaction, the major, minor, and trace constituents are leached from primary minerals and enriched into local groundwaters. At the same time, during the progressive dissolution of the rocks, the aqueous solution may attain saturation with respect to different secondary solid phases, potentially acting as sinks of various elements and species [5–9]. For these reasons, the fate of the chemical components

of interest during weathering of rocks is a rather complex theme, whose understanding requires the use of reaction path modeling [10–20]. In this work, the EQ3/6 software package, version 8.0a [21], was used to study the weathering processes that occurred on the granulite rocks of the Serra Massif. Reaction path modeling was performed using some needful information, comprising (i) relevant thermodynamic and kinetic data, (ii) chemical composition and abundance of each primary solid phase of interest, (iii) chemical composition of the initial aqueous solution, and (iv) chemical composition of the aqueous solution during water–rock interaction. Items (i) to (iii) are needed to implement reaction path modeling, whereas item (iv) is used to evaluate its validity, through comparison of computed results with analytical data.

2. Geological Background

The Calabrian belt, known as the Calabrian-Peloritan Arc [22], belongs to a fold belt linking the NW-SE Apennines
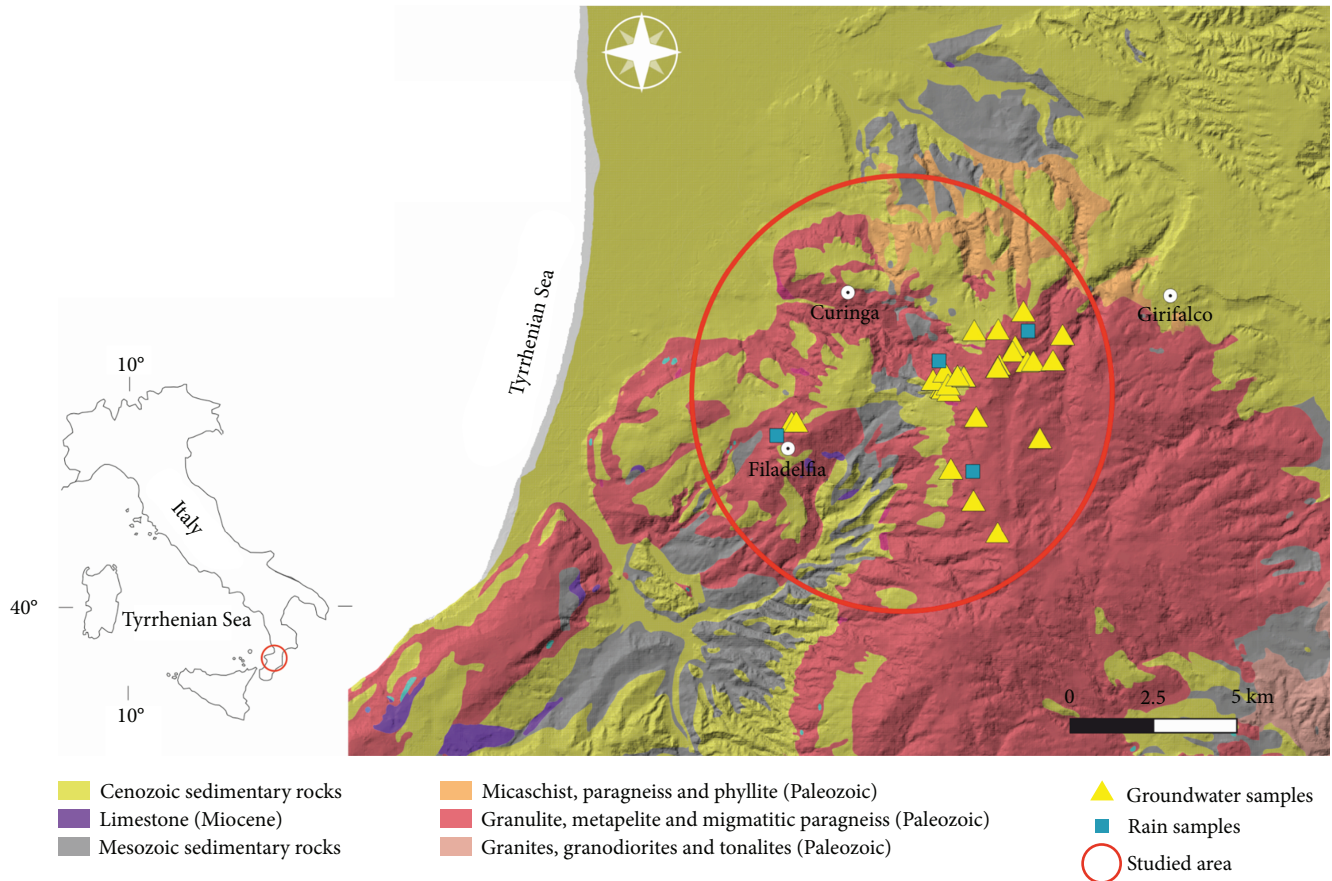
FIGURE 1: Simplified geological map of the study area also showing the location of spring water and rainwater samples.

structure with W-E-trending structures of Sicily and Northern African Maghrebian regions [23].

On the basis of radiometric, petrological, and seismic data [24], the Calabrian Peloritan Arc (CPA) has been considered to have a pre-Hercynian lower crustal segment thrust into the middle crust during the Hercynian orogeny and uplifted during the Europe-Apulia collision in Oligocene-Early Miocene ([22, 25] and references therein).

CPA is divided into two main sectors: (i) the northern sector, in which fall the Sila Massif and Coastal Chain, and (ii) southern sector, in which fall Aspromonte and Serre Massifs. The two sectors are separated by a strike-slip tectonic line cross along the Catanzaro trough [26]. The study areas fall in the Serre Massif which is made up mainly of high- and low-grade metamorphic rocks that discontinuously overlay the late Hercynian granitoids, granodiorites, and tonalites. All the sequences are sometimes covered by unmetamorphosed Cenozoic sedimentary deposits [27]. In the studied area (Figure 1), granulite-facies crop up extensively. These rocks can be associated with two distinct tectonic units belonging to the Monte Gariglione and Polia-Copanello complexes of the Sila Unit ([22, 28]; Bonardi et al., 2001). The two lithostratigraphic units [29] consist in (i) the lower unit mainly made up of metabasic rocks, predominantly layered metagabbro, and meta-anorthosite with small and subordinate ultramafic bodies and in (ii) the upper unit made up of migmatitic aluminous paragneiss,

orthopyroxene-bearing felsic granulite, and marbles that sometimes include quartz monzo-gabbronorite sills and/or dikes. Surrounding the investigated area, the granulite-facies rocks and phyllonitic rocks are separated by the Curinga-Girifalco Line of Alpine age [29].

3. Methods

3.1. Water Sampling and Analytical Techniques. A total of 30 spring water samples and 4 local rainwaters were collected in the study area (Figure 1) and analyzed for major components. During the collection samples, unstable parameters, such as temperature, pH, and oxidation-reduction potential (Eh) as well as electrical conductivity (EC), were measured in the field by using portable instruments. Total alkalinity was also determined in the field by acidimetric titration utilizing HCl 0.01 N as titrating agent. Waters were filtered in situ through a $0.4\,\mu m$ pore-size polycarbonate membrane filter (Nuclepore). Samples for the determination of anions were stored without further treatment. Samples for the determination of cations were acidified, by addition of suprapure acid (1% HNO_3) after filtration and stored. New polyethylene bottles were used for all the samples. In the laboratory, the concentrations of Na^+, K^+, Mg^{2+}, Ca^{2+}, F^-, Cl^-, SO_4^{2-}, and NO_3^- were determined by high-performance liquid chromatography (HPLC, Dionex DX 1100). All the chemical data were determined in the laboratory of the Department of

TABLE 1: Chemical-physical parameters of groundwater samples coming from the study.

Code	Temp °C	pH	Eh (mV)	Cond (μs/cm)	Na (mg/L)	K (mg/L)	Ca (mg/L)	Mg (mg/L)	Alk Tot (mg/L)	SO$_4$ (mg/L)	Cl (mg/L)	NO$_3$ (mg/L)	SiO$_2$ (mg/L)	F (mg/L)
1	13.30	6.8	123.0	193.9	14.6	1.9	11.2	4.7	60.5	8.1	20.0	16.5	20.3	0.1
2	12.80	6.0	120.0	92.8	8.3	1.1	2.5	1.4	12.8	6.8	11.8	1.2	10.8	0.1
3	12.50	6.7	100.0	118.5	10.4	0.9	4.0	2.9	23.6	5.3	16.1		19.3	0.1
4	12.40	6.7	102.0	100.7	8.5	0.9	3.1	2.8	15.1	6.2	13.0		15.0	0.1
5	12.10	6.5	107.0	103.6	10.0	1.1	3.6	1.9	22.8	4.3	15.1		14.8	0.1
6	12.10	6.0	128.0	105.9	9.3	1.1	4.0	2.1	18.1	12.1	12.4	1.1	11.8	0.0
7	11.80	6.7	107.0	147.4	11.2	1.2	6.0	2.7	19.9	8.5	19.7	0.6	15.8	0.1
8	12.20	6.8	121.0	125.0	12.0	1.0	5.0	2.2	37.2	3.6	12.9		25.3	0.1
9	12.60	6.2	133.0	106.1	9.3	1.1	3.6	2.0	20.5	4.3	15.1	4.1	24.5	0.1
10	12.40	6.3	117.0	92.6	8.5	0.9	2.6	1.6	11.9	7.4	13.3	0.7	13.8	0.1
11	12.30	6.3	121.0	123.2	9.8	1.1	5.4	3.6	33.5	5.0	14.5	3.3	17.0	0.1
12	12.50	6.8	110.0	133.8	9.6	0.8	6.6	3.5	39.7	3.0	9.2	2.4	22.3	0.1
13	11.40	7.2	103.0	140.3	10.9	1.1	7.9	3.1	38.9	6.0	13.6	1.1	28.5	0.1
14	11.40	6.3	131.0	109.3	10.7	1.1	3.1	1.5	13.8	4.3	18.5	1.9	18.5	0.1
15	11.30	6.3	138.0	72.1	7.1	0.4	1.8	0.8	7.4	4.0	11.0	0.2	13.5	0.0
16	11.20	6.5	129.0	86.5	8.2	0.6	2.4	1.0	11.3	4.3	12.0	0.7	15.8	0.0
17	10.90	6.9	118.0	126.8	10.9	1.0	5.3	2.0	27.9	3.1	14.9	0.4	37.5	0.1
18	11.90	7.1	110.0	112.1	9.0	0.8	4.2	2.5	26.7	5.9	11.9	2.2	53.5	0.1
19	10.30	7.2	108.0	110.4	8.9	0.9	4.8	2.3	21.1	4.0	14.9	0.0	41.8	0.1
20	9.60	6.4	138.0	92.1	8.1	1.0	2.5	1.7	17.3	3.4	12.7	1.0	26.5	0.1
21	11.50	8.2	111.0	177.6	9.0	2.2	9.5	7.1	41.7	17.4	11.2		35.3	0.1
22	9.60	7.3	100.0	101.4	9.7	0.8	4.1	2.2	21.6	5.0	13.3	3.9	23.8	0.1
23	12.40	6.3	105.0	92.8	7.7	0.9	4.6	1.9	27.5	5.0	9.1	0.9	22.5	0.1
24	7.70	6.8	135.0	116.5	9.0	0.9	6.2	2.4	32.2	4.5	13.2	3.0	31.3	0.1
25	10.40	6.2	140.0	86.6	7.4	0.7	2.9	1.3	14.5	4.4	11.3	0.5	11.3	0.0
26	11.70	7.1	100.0	127.1	9.6	0.9	5.4	2.9	35.4	3.1	8.1	1.3	13.2	0.1
27	11.80	7.1	102.0	196.9	13.5	1.5	8.6	5.0	35.7	3.4	28.5	0.6	16.5	0.1
28	13.30	6.4	168.0	108.2	8.6	0.9	2.6	1.5	15.8	4.1	12.8		11.6	0.1
29	13.10	6.3	182.0	97.3	8.1	0.7	2.5	1.4	15.9	4.8	10.8		11.3	0.1
30	14.20	6.6	158.0	115.3	9.5	0.9	3.0	2.0	21.0	3.8	14.3		14.7	0.1

TABLE 2: Chemical-physical parameters of rainwater samples coming from the study area.

	pH	Ca (mg/L)	Mg (mg/L)	Na (mg/L)	K (mg/L)	HCO$_3$ (mg/L)	SO$_4$ (mg/L)	Cl (mg/L)	SiO$_2$ (mg/L)
Rain 1	5.62	2.60	0.60	6.80	0.31	7.42	3.65	10.49	9.65
Rain 2	6.50	1.30	0.33	6.20	0.94	10.1	4.56	9.40	9.33
Rain 3	6.20	2.30	0.35	12.40	1.40	5.62	3.26	13.20	5.64
Rain 4	6.33	0.90	0.30	8.60	0.60	6.98	4.23	12.41	7.10

Biology, Ecology and Earth Sciences of the University of Calabria, and are reported in Tables 1 and 2.

3.2. Chemical Characterization of Rocks and Minerals. The mineralogical and chemical characteristics of the granulite considered as a dissolving reactant in this work is based on the study of Apollaro et al. [30] who collected and analyzed several granulite samples from the lower crust exposed in the southern sector of the Calabrian region.

Apollaro et al. [30] carried out modal analyses on granulite-bearing plagioclase rock lithotypes (e.g., [31, 32]) to determine the volume percentages of main and accessory minerals by optical microscopy of thin sections using a mechanical stage. Granulite rocks have a coarse-grained

texture and are plagioclase-rich (60%) with minor amounts of amphibole (10%), biotite (10%), clinopyroxene (8%), garnet (8%), and orthopyroxene (4%).

3.3. Geochemical Modeling. Reaction path modeling of progressive dissolution of granulite in rainwater was carried out by means of the software package EQ3/6, version 8.0a [21], utilizing the thermodynamic database of Wolery and Jove-Colon [33]. Three simulations were performed in kinetic (time) mode, under a closed system with secondary solid phases and an open system with CO_2, adopting different, constant P_{CO_2} values ($10^{-2.0}$, $10^{-2.4}$, and $10^{-2.8}$ bar) and at constant temperature of 11.8°C (which reproduces the average temperature of local groundwaters).

Based on the mineralogical and petrographic data, the dissolving granulite was considered to be constituted by plagioclase, amphibole, biotite, clinopyroxene, garnet, and orthopyroxene. Kinetic parameters and surface area were specified for each primary (dissolving) solid phase because reaction path modeling was performed in time mode (Table 3). Kinetic parameters were obtained from the compilation and critical review of available laboratory dissolution experiments [34]. Thermodynamic data of some minerals such as anorthite, K-feldspar, albite, annite, phlogopite, muscovite, 1.4 nm clinochlore, magnesite, calcite, rhodochrosite, siderite, witherite, strontianite, and aragonite were evaluated by a review work of Helgeson et al. [35]. Thermodynamic data of clay minerals (Mg, Na, K, and Ca end members of beidellite, saponite, and montmorillonite) and 1.4 nm chamosite and celadonites were calculated by Wolery and Jove-Colon [33] and references therein. Those of vermiculites such as Me-Al vermiculites, Me-Fe vermiculites, Me-Mg-Al vermiculites, and Me-Mg-Fe vermiculites with Me=Na, K, Mg, and Ca were evaluated by Apollaro et al. [36, 37]. From Perri et al. [38], thermodynamic data of illite were obtained, and those of ferrihydrites are from the work of Majzlan et al. [39].

Four chemical analyses of rainwaters collected in the study area (Table 2) were used to compute the chemical composition of the initial aqueous solution (mean value).

4. Water Chemistry

4.1. Water Classification. Low-salinity waters issuing from granulite have about neutral pH (mean value of 6.7), outlet temperatures of 7.7° to 14.2°C, oxidant redox potentials from 100 to 182 mV, and electrical conductivity from 72.1 to 196.9 μS/cm. Based on the triangular plots of major anions and major cations (Figure 2), the waters show a Na-Cl to Na-HCO_3 composition.

In the binary diagram of pH vs. P_{CO_2} (Figure 3(a)), most of the waters are within the soil range (0.002–0.04 bar; [40]); only 2 samples are positioned below the lower soil threshold.

Therefore, in the area, CO_2 is prevailingly contributed by biogenic shallow sources, such as the decay of organic matter and root respiration occurring in the rhizosphere. The plot of the calcite saturation index vs. pH (Figure 3(b)) shows that undersaturation with calcite is a common condition for all waters.

TABLE 3: Geometrical surface areas and masses of solid phases of interest.

Mineral	Vol %	Initial surface area (cm^2)	Vm (cm^3/mol)	Mass (mole)
Plagioclase	60	84000	100.11	13.98462
Amphibole	10	14000	139.2	1.67625
CPX	8	11200	100.25	1.86201
OPX	4	5600	138.665	0.67309
Garnet	8	11200	272.92	0.68396
Biotite	10	14000	152.27	1.53237
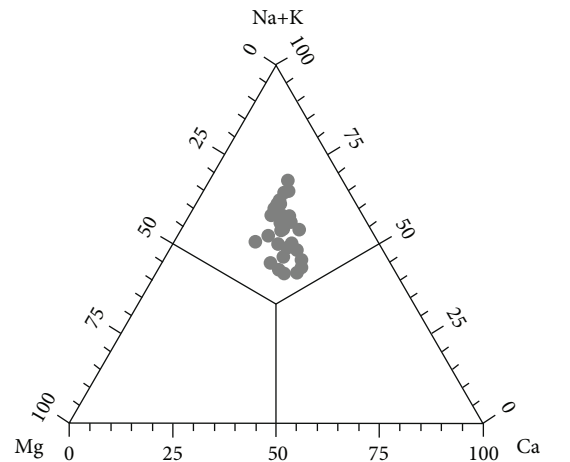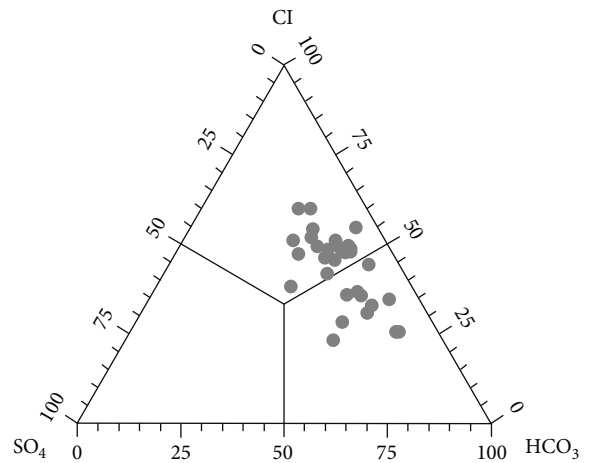
FIGURE 2: Triangular plots of major anions and major cations for the 30 groundwater samples from the study area.

5. Interpretation of Reaction Path Modeling

Analytical data of the groundwaters from the granulitic aquifer of the lower crust exposed in the southern sector of the Calabrian region were compared with results of reaction path modeling. For the waters of interest, alkalinity is used as a reaction progress variable (Xi) instead of pH for the following reasons [13]: (i) the progressive
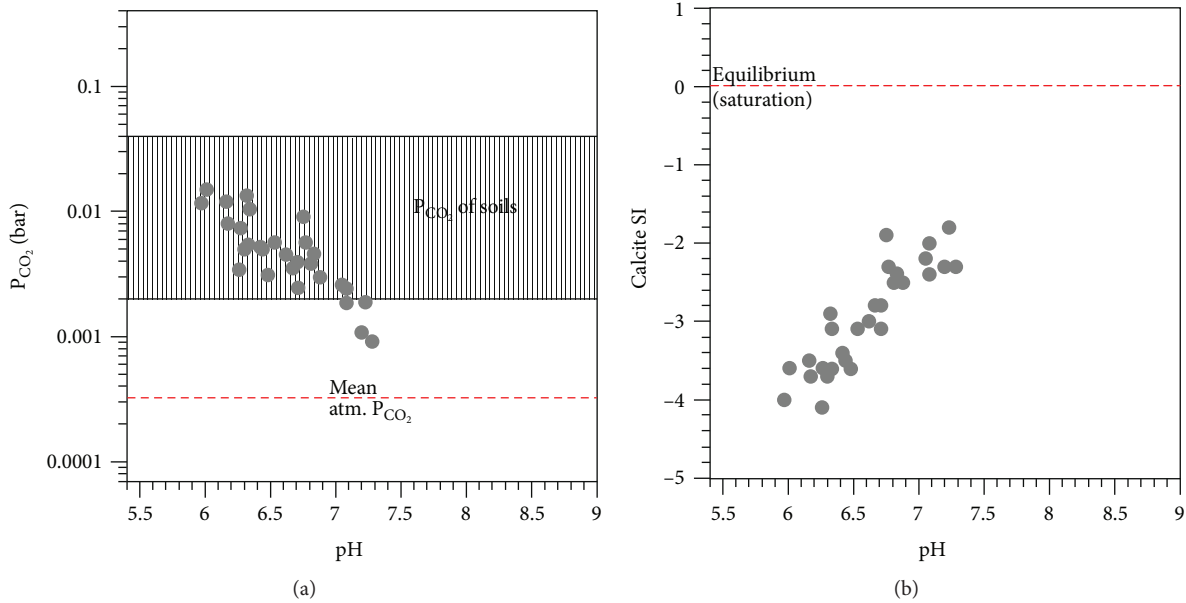
(a)

(b)

FIGURE 3: (a) Correlation diagram of pH vs. P_{CO_2} also showing the range of soil P_{CO_2} [40] and the mean atmospheric P_{CO_2} value. (b) Correlation diagram of pH vs. calcite saturation index.

dissolution of primary solid phases, driven by conversion of aqueous CO_2 to HCO_3^- ion, causes a continuous increase in alkalinity, (ii) precipitation of calcite, which would cause a decrease in alkalinity, is limited (see Section 4.1), and (iii) the alkalinity consumption due to acidity produced by oxidative dissolution of pyrite is negligible, as indicated by the generally low SO4 concentrations.

Indeed, during water-rock interaction, due to the appearance of different secondary mineral assemblages acting as pH buffers (e.g., [41–44]), pH changes are quite irregular and less continuous.

Figure 4 shows a close-to-linear relation between Xi and alkalinity, with a good correspondence for all different pCO$_2$ values considered.

The simulations show a progressive dissolution dominated by plagioclase followed by a minor amount of amphibole, clinopyroxene, and biotite and negligible amounts of orthopyroxene and garnet for all the investigated pCO$_2$ (Figure 5).

As already shown by Apollaro et al. [30], the differences in the type and amount, along the reaction path of the secondary minerals (Figure 6), mainly reflect the different dissolutions of primary minerals and, therefore, a different contribution during the reaction, of chemical elements.

The two main secondary solid phases forming during granulite dissolution, appearing at alkalinity close to 5 mg HCO$_3$/L, are kaolinite and vermiculites with minor amount of hydroxides. Kaolinite, vermiculites, and hydroxides act as sinks of Al, Si, and Fe released by primary dissolved minerals. Carbon dioxide partial pressure has a significant influence on the first appearance of product phases for all these minerals except kaolinite. The lower the pCO$_2$, the earlier all the secondary phases begin to precipitate.
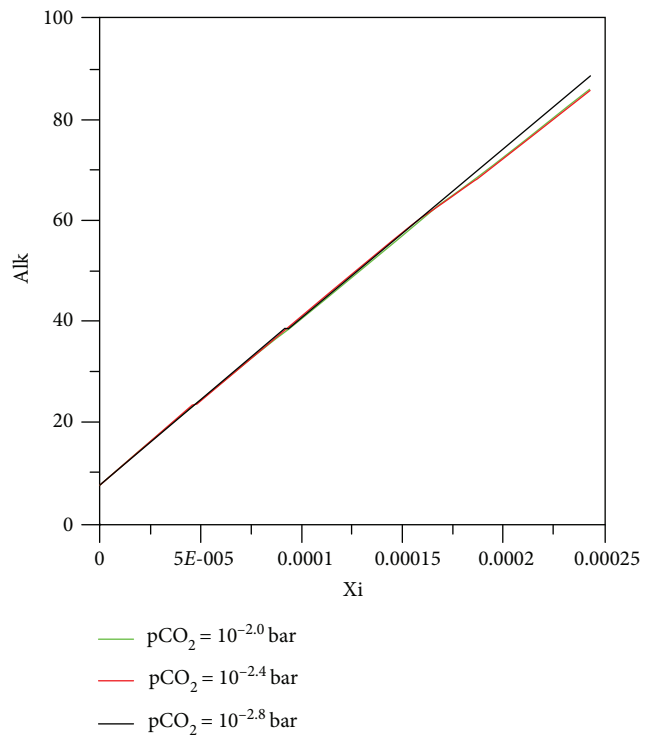

FIGURE 4: Plot of alkalinity vs. the reaction progress variable showing the results of reaction path modeling for the dissolution of granulite under different fCO$_2$ values (see legend).

Consistently with the undersaturation with calcite, there is no solid carbonate.

5.1. The Aqueous Solution. The theoretical path of granulite dissolution, at constant pCO$_2$ of $10^{-2.0}$, $10^{-2.4}$, and $10^{-2.8}$ bar,
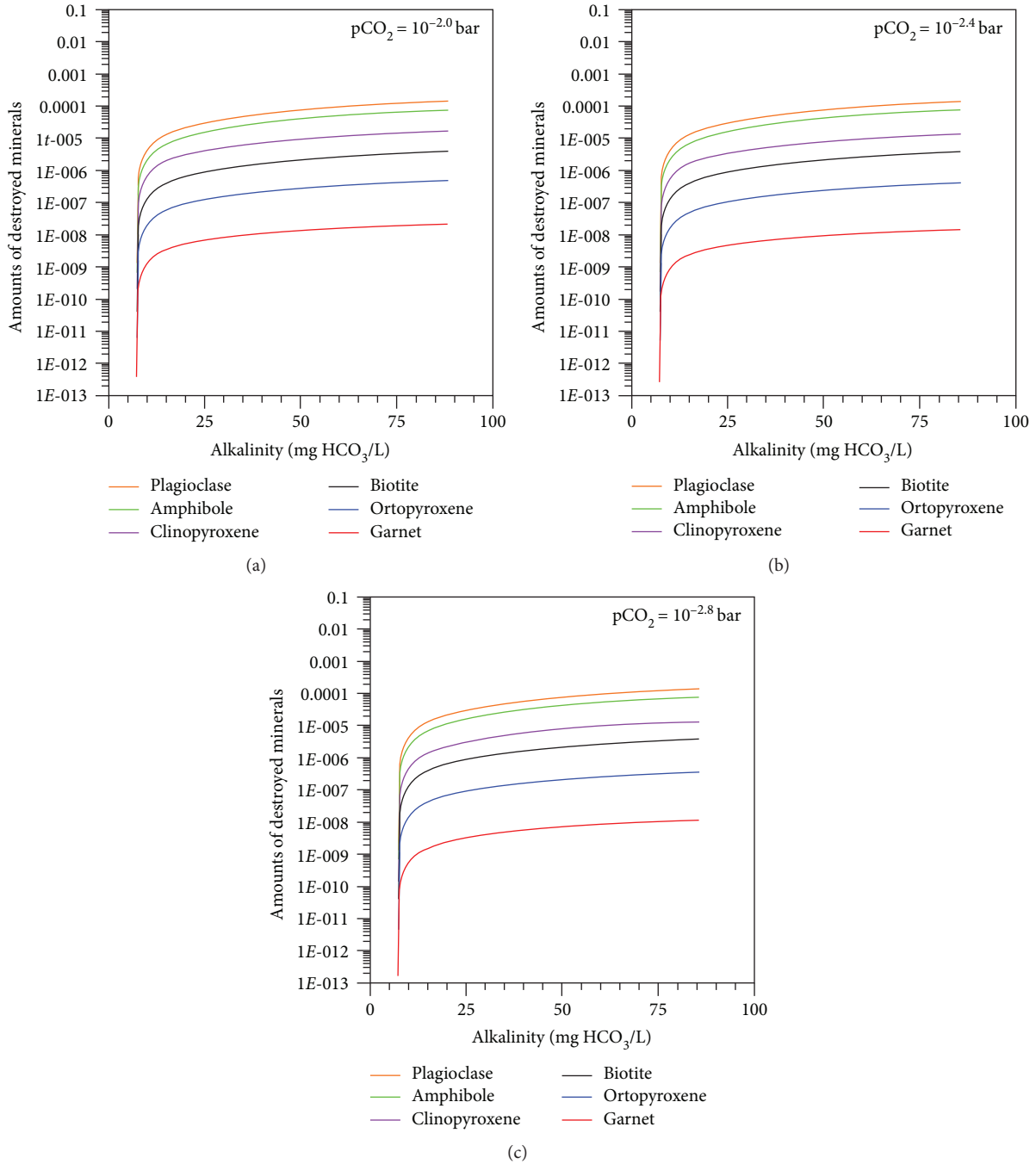
(a)

(b)

(c)

FIGURE 5: Moles of destroyed solid reactants against alkalinity, showing the results of reaction path modeling for the dissolution of granulite: (a) pCO$_2$ of $10^{-2.0}$ bar, (b) pCO$_2$ of $10^{-2.4}$ bar, and (c) pCO$_2$ of $10^{-2.8}$ bar.

indicates that the water-rock interaction is dominated by dissolution of plagioclase, amphibole, and clinopyroxene and much less from biotite, orthopyroxene, and garnet (Figure 5). The concentration of aqueous Ca and Mg (Figure 7) increases owing to dissolution of plagioclase, amphibole, and clinopyroxene, and the amount of Ca and Mg incorporated in precipitating secondary minerals is negligible. Variable pCO$_2$ does not affect the Ca/HCO$_3$ and Mg/HCO$_3$ ratio at the three pCO$_2$ values, and there is a very

good agreement between reaction path modeling results and the analytical data (Figure 7).

The binary plots of Na versus alkalinity and K versus alkalinity (Figure 8) highlight that the dissolved Na and K concentrations increase slightly through the whole simulation, since the amounts of Na and K contributed by dissolution of plagioclase and biotite are minimal, and a part of K and Na is incorporated in the vermiculites at all pCO$_2$ (Figure 6). As already shown by Apollaro
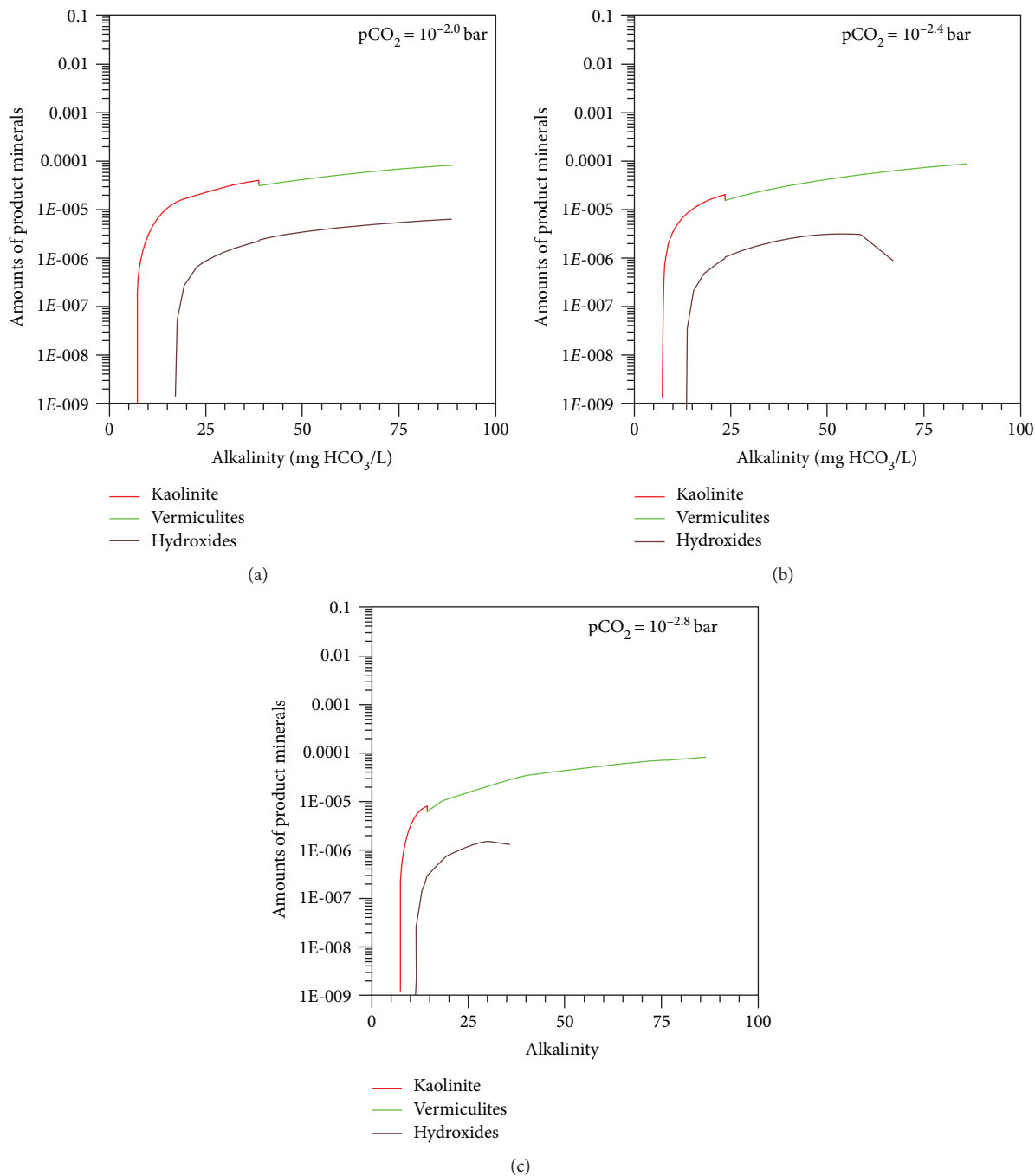
(a)

(b)

(c)

FIGURE 6: Moles of solid product phases against alkalinity, showing the results of reaction path modeling for the dissolution of granulite (a) pCO_2 of $10^{-2.0}$ bar, (b) pCO_2 of $10^{-2.4}$ bar, (c) pCO_2 of $10^{-2.8}$ bar.

et al.,[13] Na and K versus alkalinity plots in low TDS groundwaters are poorly informative because these two alkali metals are probably controlled by varying contributions of atmospheric-marine salts rather than the water-rock interaction.

The binary plots of SiO_2 versus alkalinity (Figure 9) highlight that the concentration of aqueous SiO_2 increases during the dissolution of granulite because all minerals present in the rocks contain SiO_2 and the amount of SiO_2 incorporated in precipitating kaolinite and vermiculite is

subordinate. Similar to Ca and Mg, variable pCO_2 does not affect the SiO_2/HCO_3 ratio and there is a very good agreement between analytical data and results of reaction path modeling.

6. Conclusion

Geochemical prospecting carried out in the granulitic rocks exposed in the southern sector of the Calabrian region (Southern Italy) has allowed identification of several springs
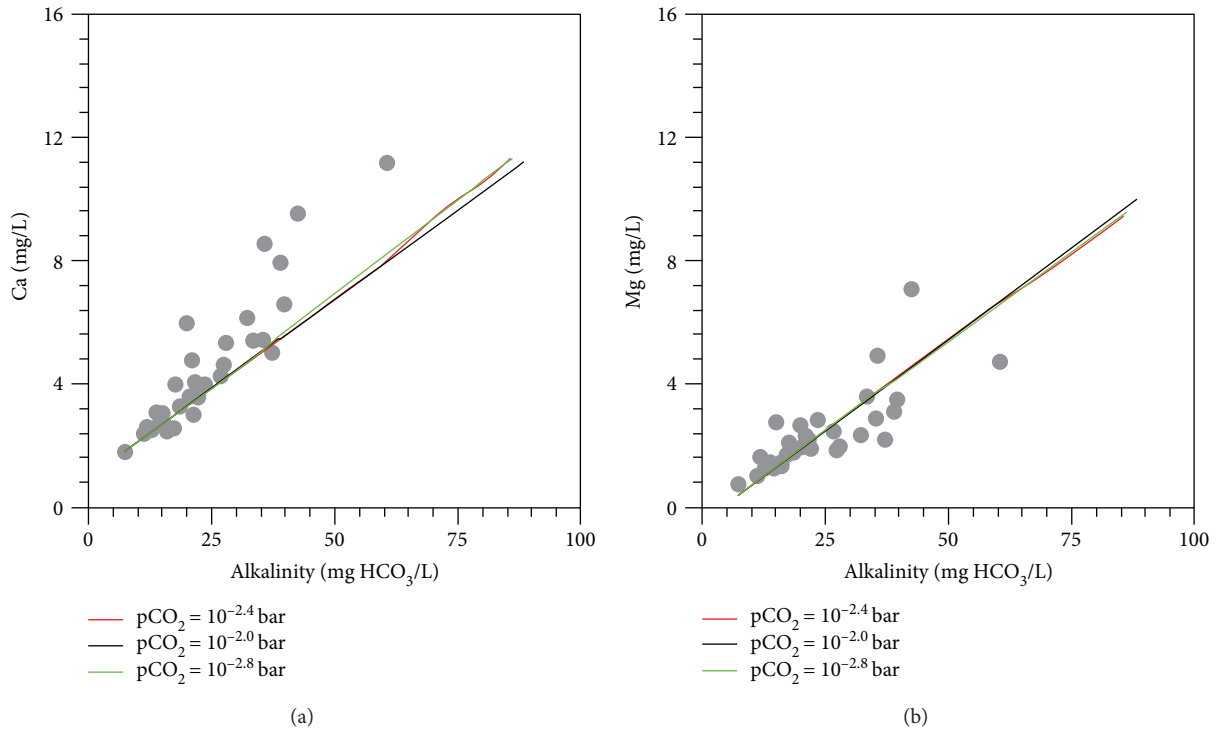
(a)

(b)

Figure 7: Plots of (a) Ca and (b) Mg vs. alkalinity showing the analytical data from groundwaters interacting with granulitic rocks of the lower crust as well as the results of reaction path modeling for granulite dissolution under different pCO_2 (see legend).

(a)

(b)
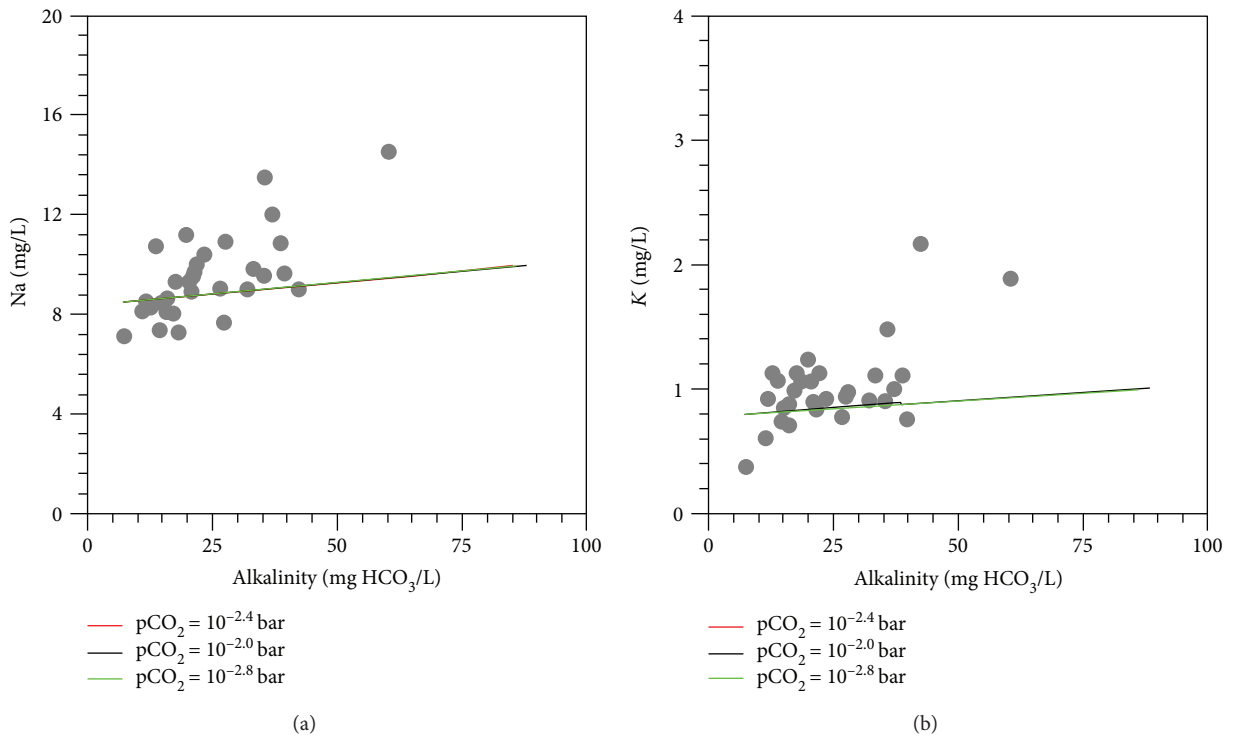
Figure 8: Plots of (a) Na and (b) K vs. alkalinity showing the analytical data from groundwaters interacting with granulitic rocks of the lower crust as well as the results of reaction path modeling for granulite dissolution under different pCO_2 (see legend).

hosted in a very extensive shallow hydrogeological metamorphic complex. To evaluate the irreversible water-rock mass exchanges occurring during the evolution of rainwaters to groundwaters, a reaction path modeling in kinetic (time) mode was performed, under a closed system with secondary solid phases and an open system with CO_2, adopting

FIGURE 9: Plots of SiO_2 vs. alkalinity showing the analytical data from groundwaters interacting with granulitic rocks of the lower crust as well as the results of reaction path modeling for granulite dissolution under different pCO_2 (see legend).

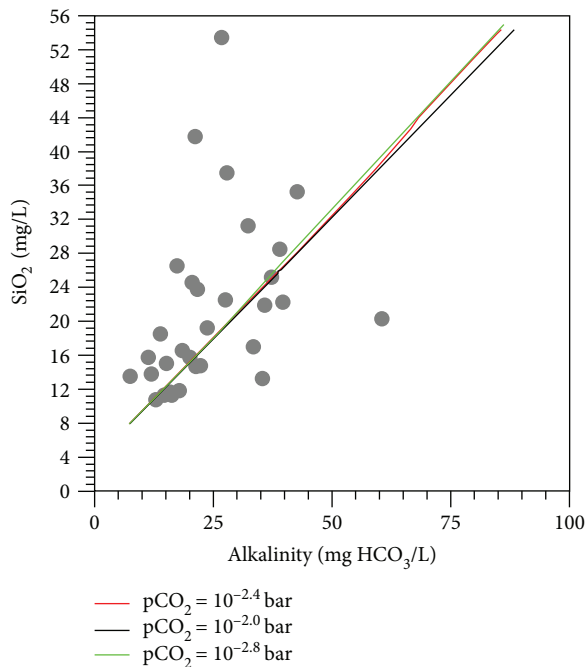different, constant pCO_2 values ($10^{-2.0}$, $10^{-2.4}$, and $10^{-2.8}$ bar) and at constant temperature of $11.8°C$.

The secondary (product) solid phases that were allowed to precipitate are kaolinite, vermiculite solid mixture, and hydroxide solid mixture according to the general understanding of chemical weathering and the results obtained by Apollaro et al. [30] who studied the weathering processes affecting the same rocks.

The results of reaction path modeling show that the release of major dissolved constituents to shallow groundwaters is mainly controlled by weathering of plagioclase accompanied by minor amounts of amphibole, clinopyroxene, and biotite and negligible amounts of orthopyroxene and garnet. Computed contents of key dissolved components (Ca, Mg, Na, K, and SiO_2) are comparable with analytical data, although not all the details are reproduced, probably due to insertion in the model of the average composition of primary minerals, in spite of their nonnegligible chemical variations and to the fact that some elements such as Na and K are controlled by varying contributions of atmospheric-marine salts rather than the water-rock interaction.

Since the frequent worldwide occurrence of this type of rock, it can be said that this kind of research is of widespread interest and these results can be transferred to other sites where granulite rocks occur.

Data Availability

The manuscript is a data self-contained article, whose results were obtained from the laboratory analysis, and the entire data is presented within the article. However, if any additional information is required, these are available from the corresponding author upon request to the e-mail apollaro@unical.it

Conflicts of Interest

The author declares that he has no conflicts of interest.

References

[1] C. A. J. Appelo and D. Postma, *Geochemistry, Groundwaters and Pollution*, A.A. Balkema, Rotterdam, 1999.

[2] E. K. Berner and R. A. Berner, *Global Environment: Water, Air, and Geochemical Cycles*, Prentice Hall, Upper Saddle River, 1996.

[3] D. Hem, *Study and Interpretation of the Chemical Characteristics of Natural Water U.S. Geological Survey*, Water Supply Paper 2254, 1970.

[4] D. Langmuir, *Aqueous Environmental Geochemistry*, Prentice Hall, Upper Saddle River, 1997.

[5] C. Apollaro, L. Marini, and R. De Rosa, "Use of reaction path modeling to predict the chemistry of stream water and groundwater: a case study from the Fiume Grande valley (Calabria, Italy)," *Environmental Geology*, vol. 51, no. 7, pp. 1133–1145, 2007.

[6] C. Apollaro, L. Marini, R. de Rosa, P. Settembrino, F. Scarciglia, and G. Vecchio, "Geochemical features of rocks, stream sediments, and soils of the Fiume Grande Valley (Calabria, Italy)," *Environmental Geology*, vol. 52, no. 4, pp. 719–729, 2007.

[7] I. Guagliardi, C. Apollaro, F. Scarciglia, and R. De Rosa, "Influence of particle-size on geochemical distribution of stream sediments in the Lese river catchment, southern Italy," *Biotechnology, Agronomy, Society and Environment*, vol. 17, no. 1, pp. 43–55, 2013.

[8] I. Guagliardi, G. Buttafuoco, C. Apollaro, A. Bloise, R. De Rosa, and D. Cicchella, "Using gamma-ray spectrometry and geostatistics for assessing geochemical behaviour of radioactive elements in the Lese catchment (southern Italy)," *International Journal of Environmental Research*, vol. 7, pp. 645–658, 2013.

[9] F. Scarciglia, R. De Rosa, G. Vecchio, C. Apollaro, G. Robustelli, and F. Terrasi, "Volcanic soil formation in Calabria (southern Italy): the Cecita Lake geosol in the late Quaternary geomorphological evolution of the Sila uplands," *Journal of Volcanology and Geothermal Research*, vol. 177, no. 1, pp. 101–117, 2008.

[10] M. Accornero and L. Marini, "The double solid reactant method for modeling the release of trace elements from dissolving solid phases: I. Outline and limitations," *Environmental Geology*, vol. 55, no. 8, pp. 1627–1635, 2008.

[11] C. N. Alpers and D. K. Nordstrom, "Geochemical modeling of water-rock interactions in mining environments," in *The Environmental Geochemistry of Mineral Deposits, Chapter: 14*, G. S. Plumlee and M. J. Logsdon, Eds., pp. 289–324, Society for Economic Geologists, 1999.

[12] C. Apollaro, M. Accornero, L. Marini, D. Barca, and R. de Rosa, "The impact of dolomite and plagioclase weathering on the chemistry of shallow groundwaters circulating in a granodiorite-dominated catchment of the Sila Massif (Calabria, Southern Italy)," *Applied Geochemistry*, vol. 24, no. 5, pp. 957–979, 2009.

[13] C. Apollaro, L. Marini, T. Critelli et al., "Investigation of rock-to-water release and fate of major, minor, and trace elements in the metabasalt–serpentinite shallow aquifer of Mt. Reventino (CZ, Italy) by reaction path modelling," *Applied Geochemistry*, vol. 26, no. 9-10, pp. 1722–1740, 2011.

[14] J. Bruni, M. Canepa, G. Chiodini et al., "Irreversible water–rock mass transfer accompanying the generation of the neutral, Mg–HCO3 and high-pH, Ca–OH spring waters of the Genova province, Italy," *Applied Geochemistry*, vol. 17, no. 4, pp. 455–474, 2002.

[15] F. Cipolli, B. Gambardella, L. Marini, G. Ottonello, and M. Vetuschi Zuccolini, "Geochemistry of high-pH waters from serpentinites of the Gruppo di Voltri (Genova, Italy) and reaction path modeling of CO2 sequestration in serpentinite aquifers," *Applied Geochemistry*, vol. 19, no. 5, pp. 787–802, 2004.

[16] T. Critelli, G. Vespasiano, C. Apollaro, F. Muto, L. Marini, and R. De Rosa, "Hydrogeochemical study of an ophiolitic aquifer: a case study of Lago (Southern Italy, Calabria)," *Environment and Earth Science*, vol. 74, no. 1, pp. 533–543, 2015.

[17] H. C. Helgeson, "Evaluation of irreversible reactions in geochemical processes involving minerals and aqueous solutions: I. Thermodynamic relations," *Geochimica et Cosmochimica Acta*, vol. 32, no. 8, pp. 853–877, 1968.

[18] H. C. Helgeson, R. M. Garrels, and F. T. Mackenzie, "Evaluation of irreversible reactions in geochemical processes involving minerals and aqueous solutions: II. Applications," *Geochimica et Cosmochimica Acta*, vol. 33, no. 4, pp. 455–481, 1969.

[19] B. Merkel, B. Planer-Friedrich, and D. K. Nordstrom, *Groundwater Geochemistry: a Practical Guide to Modeling of Natural and Contaminated Aquatic Systems*, Springer Verlag, 2008.

[20] C. Zhu and G. M. Anderson, *Environmental Applications of Geochemical Modeling*, Cambridge University Press, UK, 2002.

[21] T. W. Wolery and R. L. Jarek, "Software user's manual," in *EQ3/6, Version 8.0. Sandia National Laboratories—U.S*, Department of Energy Report, 2003.

[22] M. L. Amodio, G. Bonardi, V. Colonna et al., "L'arco Calabro-Peloritano nell'orogene Appenninico Maghrebide," *Memorie della Società Geologica Italiana*, vol. 17, pp. 1–60, 1976.

[23] E. Maccarrone, A. Paglionico, G. Piccarreta, and A. Rottura, "Granulite-amphibolite facies metasediments from the Serre (Calabria, Southern Italy): their protoliths and the processes controlling their chemistry," *Lithos*, vol. 16, no. 2, pp. 95–111, 1983.

[24] V. Schenk, "U-Pb and Rb-Sr radiometric dates and their correlation with metamorphic events in the granulite-facies basement of the serre, Southern Calabria (Italy)," *Contributions to Mineralogy and Petrology*, vol. 73, no. 1, pp. 23–38, 1980.

[25] R. Cirrincione, E. Fazio, P. Fiannacca, G. Ortolano, A. Pezzino, and R. Punturo, "The Calabria Peloritani Orogen, a composite terrane in Central Mediterranean; its overall architecture and geodynamic significance for a pre-Alpine scenario around the Tethyan basin," *Periodico di Mineralogia*, vol. 84, pp. 701–749, 2015.

[26] C. Tansi, F. Muto, S. Critelli, and G. Iovine, "Neogene-Quaternary strike-slip tectonics in the central Calabrian Arc (southern Italy)," *Journal of Geodynamics*, vol. 43, no. 3, pp. 393–414, 2007.

[27] F. Ietto, F. Perri, and F. Cella, "Geotechnical and landslide aspects in weathered granitoid rock masses (Serre Massif, southern Calabria, Italy)," *Catena*, vol. 145, pp. 301–315, 2016.

[28] D. Dietrich, S. Lorenzoni, P. Scandone, E. Zanettin-Lorenzoni, and M. Di Pierro, "Contribution to the knowledge of the tectonic units of Calabria; relationships between composition of K-white micas and metamorphic evolution," *Bollettino della Società Geologica Italiana*, vol. 95, no. 1-2, pp. 193–217, 1976.

[29] V. Schenk, "Petrology of Felsic Granulites, Metapelites, Metabasics, Ultramafics, and Metacarbonates from southern Calabria (Italy): prograde metamorphism, uplift and cooling of a former lower crust," *Journal of Petrology*, vol. 25, no. 1, pp. 255–296, 1984.

[30] C. Apollaro, F. Perri, E. Le Pera, F Ilaria, and T. Critelli, *Chemical and Minero-Petrographical Changes on Granulite Rocks Affecting by Weathering Processes*, Front Earth Science, 2019.

[31] G. Rizzo, E. Piluso, and L. Morten, "Phlogopite-bearing ultramafic rocks from the Serre massif, Calabrian Peloritan Arc, southern Italy: an example of hybridization between hydrous siliceous melts and peridotites?," *Geologica Acta*, vol. 3, pp. 81–96, 2004.

[32] G. Rizzo, E. Piluso, and L. Morten, "Tonalitic to trondhjemitic dykes within metabasic lower-crust rocks, Serre Massif, Calabrian-Peloritan arc," *Bollettino Società Geologica Italiana*, vol. 4, pp. 45–52, 2005.

[33] T. W. Wolery and C. Jove-Colon, *Qualification of Thermodynamic Data for Geochemical Modeling of Mineral-water Interactions in Dilute Systems*, Sandia National Laboratories Report, 2007, ANL-WIS-GS-000003 REV 01.

[34] L. Marini, *Geological Sequestration of Carbon Dioxide - Thermodynamics, Kinetics, and Reaction Path Modeling*, Developments in Geochemistry, 2007.

[35] H. C. Helgeson, J. M. Delany, H. W. Nesbitt, and D. K. Bird, "Summary and critique of the thermodynamic properties of rock-forming minerals," *American Journal of Science*, vol. 278, pp. 1–229, 1978.

[36] C. Apollaro, L. Marini, T. Critelli, and R. De Rosa, "The standard thermodynamic properties of vermiculites and prediction of their occurrence during water–rock interaction," *Applied Geochemistry*, vol. 35, pp. 264–278, 2013.

[37] C. Apollaro, L. Marini, T. Critelli et al., "Modeling of the impact of dolomite and biotite dissolution on vermiculite composition in a gneissic shallow aquifer of the Sila Massif (Calabria, Italy)," *Applied Geochemistry*, vol. 35, pp. 297–311, 2013.

[38] F. Perri, F. Scarciglia, C. Apollaro, and L. Marini, "Characterization of granitoid profiles in the Sila Massif (Calabria, southern Italy) and reconstruction of weathering processes by mineralogy, chemistry, and reaction path modeling," *Journal of Soils and Sediments*, vol. 15, no. 6, pp. 1351–1372, 2015.

[39] J. Majzlan, A. Navrotsky, and U. Schwertmann, "Thermodynamics of iron oxides: part III. Enthalpies of formation and stability of ferrihydrite ($\sim$Fe(OH)$_3$), schwertmannite ($\sim$FeO(OH)$_{3/4}$(SO$_4$)$_{1/8}$), and ε-Fe$_2$O$_3$," *Geochimica et Cosmochimica Acta*, vol. 68, no. 5, pp. 1049–1059, 2004.

[40] G. A. Brook, M. E. Folkoff, and E. O. Box, "A world model of soil carbon dioxide," *Earth Surface Processes and Landforms*, vol. 8, no. 1, pp. 79–88, 1983.

[41] B. W. Christenson and C. P. Wood, "Evolution of a vent-hosted hydrothermal system beneath Ruapehu Crater Lake, New Zealand," *Bulletin of Volcanology*, vol. 55, no. 8, pp. 547–565, 1993.

[42] L. Marini and G. Ottonello, Eds., *Atlante degli acquiferi della Liguria*, vol. 3, Le acque dei complessi ofiolitici, Pisa, 2003, bacini: Arrestra, Branega, Cassinelle, Cerusa, Erro, Gorzente, Leira, Lemme, Lerone, Orba, Piota, Polcevera, Rumaro, Sansobbia, Stura, Teiro, Varenna, Visone. Pacini Editore,.

[43] M. H. Reed, "Hydrothermal alteration and its relationships to ore fluids composition," in *Geochemistry of Hydrothermal Ore Deposits*, H. L. Barnes, Ed., pp. 303–365, Wiley, 1997.

[44] C. Apollaro, I. Fuoco, G. Brozzo, and R. De Rosa, "Release and fate of Cr (VI) in the ophiolitic aquifers of Italy: the role of Fe (III) as a potential oxidant of Cr (III) supported by reaction path modelling," *Science of the Total Environment*, vol. 660, pp. 1459–1471, 2019.

Research Article

Groundwater Quality on the Adriatic Karst Island of Mljet (Croatia) and Its Implications on Water Supply

Staša Borović ⬥, **Josip Terzić, and Marco Pola** ⬥

Department of Hydrogeology and Engineering Geology, Croatian Geological Survey, Zagreb 10000, Croatia

Correspondence should be addressed to Staša Borović; sborovic@hgi-cgs.hr

Water supply of the islands is a global challenge, especially in the countries which have highly indented coastlines with numerous islands. The island of Mljet in Croatia was investigated due to its unique source of water supply: desalination of water from brackish lakes—*blatinas*—fed by groundwater and connected to the sea by karst conduits. Water sampling and chemical analyses were performed during hydrological minimum and maximum with regard to groundwater levels in 2005/2006 and minimum in 2016. A total of 13 samples were analysed within the study: 10 samples were taken from blatinas, 1 from pit well, and 2 from borehole wells. All waters sampled from the lakes are of Na-Cl type. The seawater percentage in the lakes used to extract feed water for desalination plants, calculated by conservative mixing approach, is relatively low (0.7-9.8%) and varies in correlation with hydrological seasons. Low proportion of seawater is an essential factor of cost minimisation in desalination by the installed reverse osmosis (RO) plants. Daily monitoring of total dissolved solids in the feed water was introduced in May 2016, and its results were analysed in the context of precipitation—a sole source of island aquifer recharge. Maximum concentrations were observed during September and interpreted to be caused by a combination of natural and anthropogenic pressure during the summer tourist season. Minimum concentrations were expected after the rainy season in the cold part of the year but were observed in June instead. Due to a short observation period and untypical distribution of precipitation in the same time interval, the data can only be considered indicative. An unusual pattern of sulphate anion concentrations, which cannot be attributed solely to fresh- and seawater mixing, was observed in one of the blatinas, but its origin could not be determined based on available data. Taking into account all the presented data on groundwater quality, climate change predictions, the connection of water supply system to the mainland and problems with the effluent treatment, it is clear that the main future challenge will be the creation of an island-wide sustainable water management plan followed by continuous monitoring and research.

1. Introduction

Islands make up about 1/6 of the land area on Earth [1]. The majority of that area is composed of large islands such as Greenland, New Guinea, Borneo, Madagascar, Sumatra, or Honshu. They also house a significant proportion of the world population, ca. 700 million or 10% [2], with the most populous being Java, Honshu, Great Britain, Luzon, and Sumatra. However, there are many small ($<1000 \, km^2$) and very small islands ($<100 \, km^2$ or width $\leq 3 \, km$) [3], many of which are distant from the mainland. According to [4], forty islands in the Mediterranean region can be classified as small, and far more as very small islands, according to mentioned UNESCO classification [3]. Unlike large islands, they often

lack single or multiple resources and are therefore faced with a specific set of challenges. It is their strategic interest to reach self-sufficiency in different aspects, especially regarding water and energy supply. Such strategies often combine both aspects in the systems including desalination and utilization of renewable energy sources. Twenty islands worldwide are trying to achieve an absolute water and energy self-sufficiency, out of which ten have already succeeded [2, 5].

Desalination is a source of water supply in many regions worldwide, with the predominance of arid and coastal areas, as well as small and/or remote islands. There are approximately 24,000 desalination plants in more than 150 countries, and the number is continuously growing by about

500 plants annually. Over half of them are situated in the Middle East, followed by 17% in North America and 10% in Europe. Two-thirds of all installed desalination plants use RO technology [6].

Croatia has one of the most indented coastlines on a global scale (indentation index being 3.4 [7]), comprising 79 islands, 525 islets, and 642 rocks and rocks awash, which makes a total of 1,246 [8]. It can be characterized as concordant coastline, i.e., the beds of different rock types are folded into ridges, which are oriented parallel to the coastline. Concordant coastlines can be present as two different types, one of which is designated the Dalmatian type coast [9], after the Croatian region of Dalmatia, where the island of Mljet is also situated (Figure 1). A typical feature is that the islands, straights, and peninsulas are elongated parallel to the shoreline, and elongated shape obviously has implications to the possibility of fresh water accumulation in the island aquifers.

At the beginning of the 2000s, a bulk research program was performed on several small (even for the Adriatic Sea scale) islands in the northern part of Dalmatia. The program comprised geological and hydrogeological mapping, surface geophysical research (mostly electric resistivity tomography and seismic refraction profiling), and borehole drilling with pumping tests and hydrochemical research. The main purpose was to extract brackish groundwater with the lowest possible proportion of seawater in order to minimise the cost of desalination by RO plants. Results were limited to a few positive boreholes, but the experience gained was significant for further studies, e.g., [10–12], and numerous unpublished technical reports. Unfortunately, the program was stopped and has not been renewed since.

Among 66 permanently inhabited Croatian islands [8], ten have secured their water supply from their own resources (partially or completely). Several studies have been performed on these and some other islands [13, 14]. RO desalination plants exist on the islands of Dugi otok, Lastovo, and Mljet (Figure 1). While all of these islands use brackish water from drilled wells, the latter gets the majority of feed water from specific natural brackish lakes—*blatinas*. Being that the blatinas are the main water source used for public water supply, the quality of their water and groundwater in connected aquifers is paramount for the island's self-sufficiency. Taking that into account, the main goal of the presented study is to establish a scientific basis for understanding these unique natural phenomena and their connection with the groundwater in the surrounding karst aquifers. The obtained results can be used to improve water supply of the island of Mljet, despite other possible solutions, since the complete (or partial) water supply from its own resource is a very important present and future task.

2. History of Hydrogeological Studies on the Island of Mljet

The island of Mljet has a surface of $98 \, \text{km}^2$. It is elongated in WNW-ESE direction and has an indentation index of 3.81 [10], which is calculated as the ratio between the actual coastline length and the circumference of the circle with the area equal to the island surface area [7]. It is a part of southern
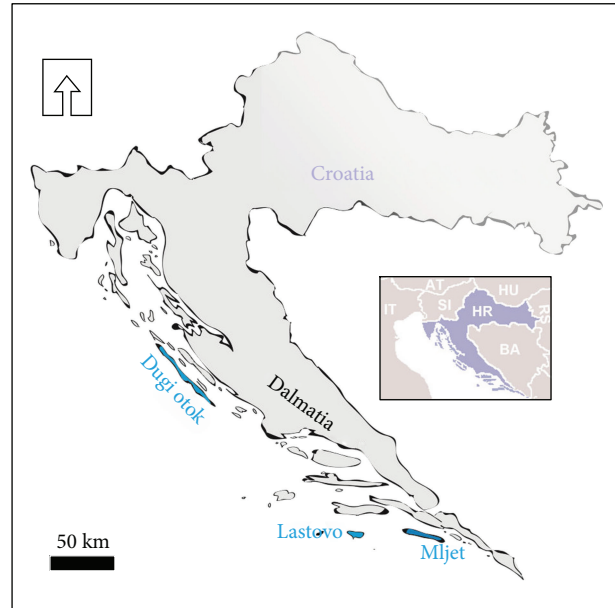

FIGURE 1: Position of Croatia on the Adriatic coast of SE Europe and the island of Mljet in S Dalmatia region (AT: Austria; BA: Bosnia and Herzegovina; HR: Croatia; HU: Hungary; IT: Italy; RS: Serbia; SI: Slovenia).

Dalmatian island archipelago and is characterized by a semiarid variety of Mediterranean climate, i.e., Csa according to Köppen classification [15].

The earliest data about the hydrogeological research of the island of Mljet come from [16] and were conducted in order to ensure local water supply. At that time, the population of the island was small, and rainwater harvesting tanks were mostly used. The authors described lowdischargefreshwater springs and proposed geophysical research which would determine the locations for two exploration-exploitation wells targeting dolomites in the vicinity of Babino Polje. At the same time, the blatinas were deemed unfit for water supply purposes and no further research was recommended. However, construction of a dug well next to blatina in Blatsko polje was proposed; the location of which would be determined by detailed hydrogeological mapping and geophysical research.

In 1971, four exploration wells were drilled on the island [17]. The investor, the local government, chose the locations and drilled the wells without prior hydrogeological research and supervision. Unsurprisingly, the wells did not show any significant yield (maximum was 0.2 l/s).

Hydrogeological research and pumping tests at a few localities were conducted by [18] in order to secure water for the temporary water supply using RO desalination plants, as a transitional solution until the regional Neretva-Pelješac-Korčula-Lastovo (NPKL) pipeline is extended from the mainland to Mljet island. The research has shown favourable conditions, and RO desalination plants were installed in Sobra, Blato, and Kozarica (Figures 2 and 3). After that, an additional well in Blato was drilled and tested in 2000 [21]. It had very good characteristics so the temporary water supply was improved. Similar procedure increased

(a)

(b)
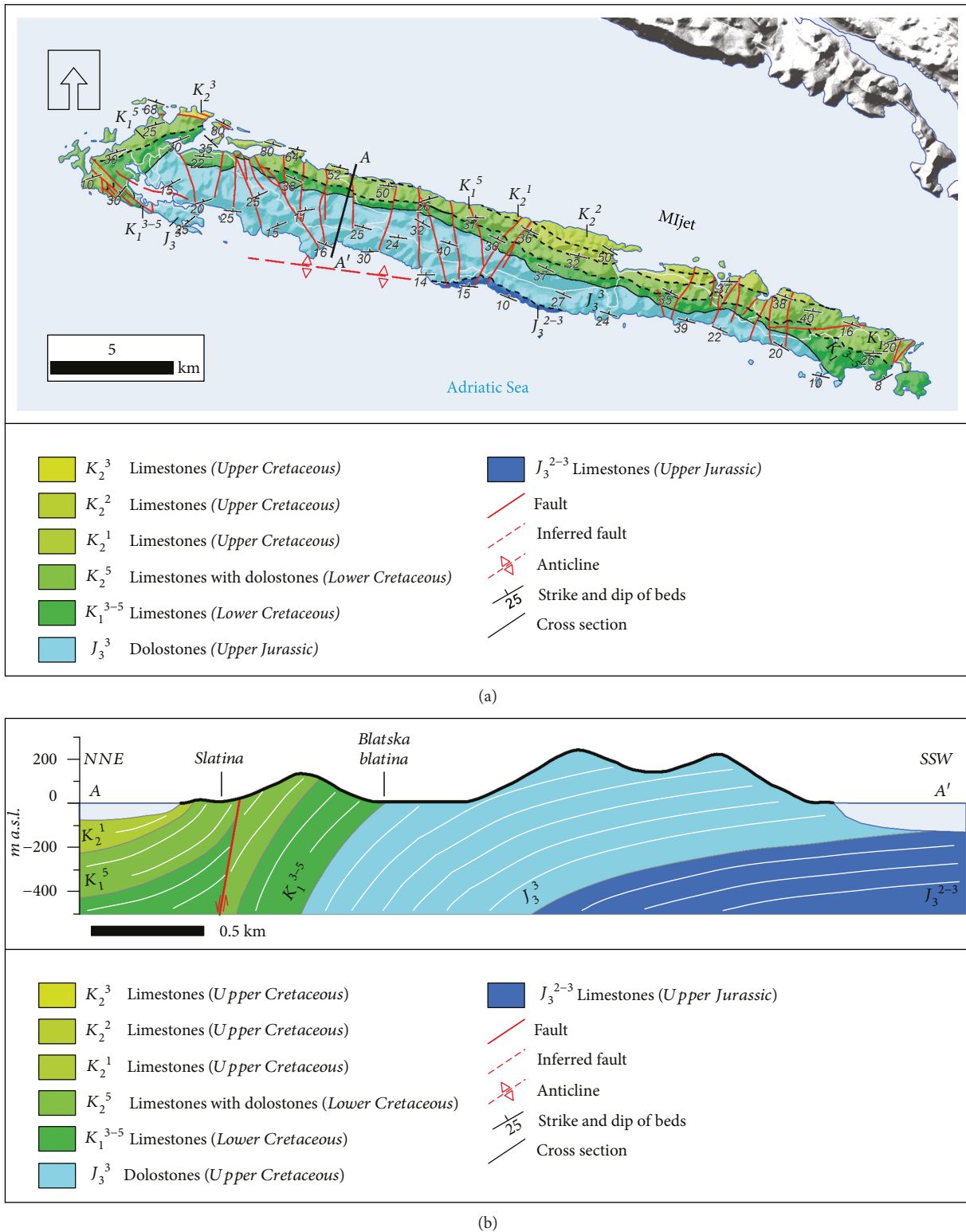
Figure 2: Geological map (a) and cross section (b) of the island of Mljet (modified after [19, 20]).

the intake capacity in Sobra in 2002 [22]. Sobra desalination plant is situated close to the coast so it discharges its effluent into the sea, while the one in Blato is in the central part of the island so the effluent is disposed of in the same karst polje.

Although a branch of NPKL pipeline to the island of Mljet (NPKLM) was partially constructed several years ago, it was put into operation only recently and the water supply for the settlements is still secured using desalination of brackish water from lakes and wells. The supply exceeds demand

FIGURE 3: Hydrogeological map of the island of Mljet (modified after [19, 20]).

by far during the cold part of the year. In the warm period of the year, the island population multiplies due to tourism activity, which is characteristic of many Mediterranean islands [23]. At the same time, the groundwater level is at its minimum, so the desalination plants usually cover 90% of the demand, while the rest of the demand is met using water carrier ships.
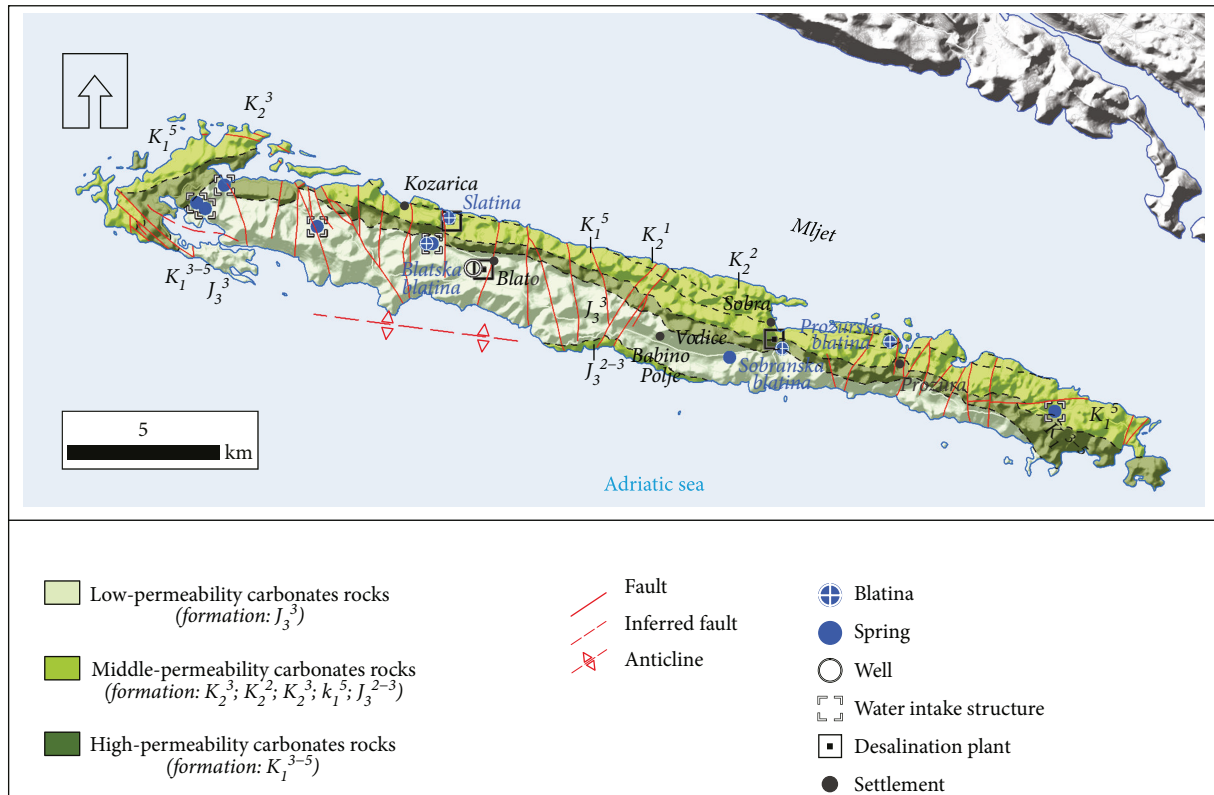
3. Geological and Hydrogeological Settings

3.1. Structural Setting and Lithostratigraphy. Structural fabric of Mljet is basically simple: it is a monocline dipping toward NNE, probably a northern limb of an overturned anticline (Figure 2). Its strike is WNW-ESE, and the axis is supposed to be off the SW shore of the island, i.e., the whole overturned southern limb is submerged under the sea [19]. The only prominent fault is a reverse fault along the SW shore of the island, which is also submerged. It is a marginal fault which penetrated deep in the lower structural units of the Dinarides inside the Adriatic (Vis-Lastovo-Mljet fault), while the fault contact with the Adria microplate is about 10 km off the SW coast of Mljet (Vis-southern Adriatic fault; [10, 24]). The majority of faults have normal and high angle strike relative to the fold axis. Although numerous, they are not very persistent, so the dominant fold structure is mostly preserved.

Chronostratigraphic units are presented according to [19]. The oldest deposits on Mljet are of Jurassic age, and they crop out on the SSW limb of the island (Figure 2). Kimmeridgian-Tithonian deposits (J_3^{2-3}) are fine-grained limestones, deposited mechanically (calclutite), with high

$CaCO_3$ content, and their thickness is around 250 m. However, the most characteristic Jurassic deposits are Tithonian dolostones with rare occurrences of interlayered limestone (J_3^3). Dolomitization process destroyed the majority of primary limestone structures, but in some localities, calclutites were identified. The thickness of the deposits is around 800 m.

Lower Cretaceous deposits also extend in a WNW-ESE belt along the northern shore of the island (Figure 2). Barremian and Aptian deposits (K_1^{3-5}) lay transgressively on the Malmian deposits. They are mechanically deposited calclutites and calcarenites. Calclutites are composed of up to 98% $CaCO_3$, and biocalcarenites contain well-sorted material. Thickness is up to 400 m. Albian limestones (K_1^5) have different fossil content, contain dolomite interlayers, and are around 200 m thick.

Upper Cretaceous deposits extend all along the northern coast of the island (Figure 2). They are lithologically very similar to Lower Cretaceous deposits but can be distinguished by micro- and macrofossil content. Cenomanian and Turonian deposits (K_2^1 and K_2^2, respectively) are present on Mljet itself, while Senonian (K_2^3) are submerged, but can be found on the islets off the northernmost coast of Mljet.

Tertiary deposits are not present on Mljet, and the Quaternary is represented by *terra rossa* and eolian sands in small karst poljes.

3.2. Hydrogeological Setting. The abovementioned Jurassic and Cretaceous limestones and dolostones can be characterized by different hydrogeological properties and functions
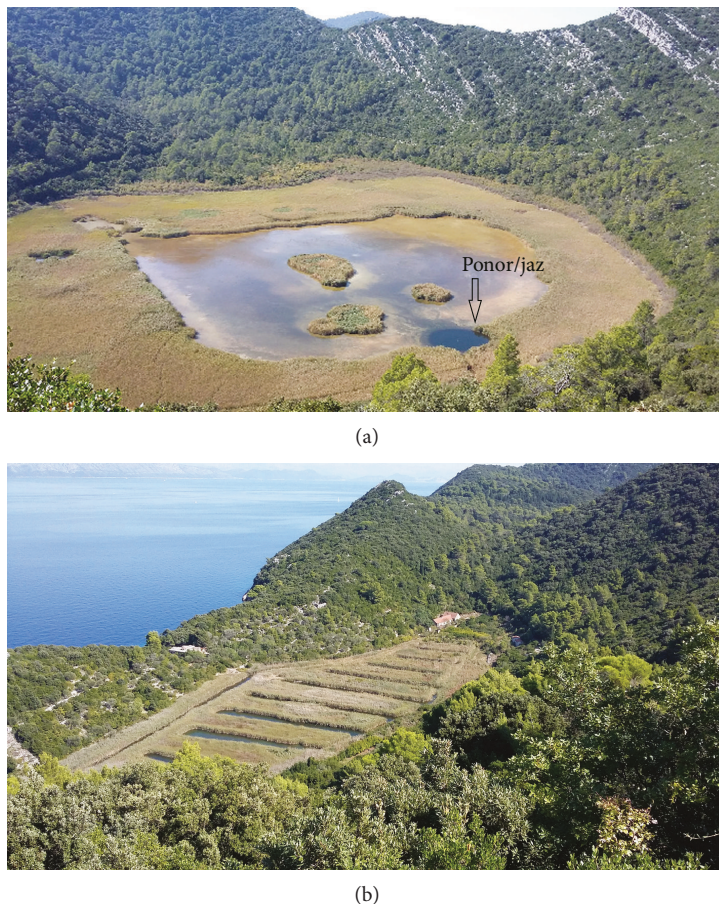
(a)

(b)

FIGURE 4: Blatska blatina in Blato—situated furthest from the sea (a) and blatina Slatina in Kozarica—closest to the sea both laterally and vertically and with known conduit toward the sea (b).

(Figure 3). The dominant type of porosity is secondary porosity induced by fracturing. In limestones, the fracturing was followed by intense karstification, which is far less pronounced in the dolostones. It is important to point out that in the Dinaric karst, the karstification is much deeper than it would be expected when observing present-day sea level. The mean sea level was over 100 meters lower than today at the end of the last glacial maximum, thus making the base of karstification lower as well [25–28]. Such sequence of events obviously caused the existence of karst channels below present-day sea level, which has a significant impact on flow in karst aquifers [29]. On the surface, the limestone is more prone to corrosion which results in typical karst forms, while the dolomite is predominantly mechanically weathered into milder morphological forms. On the islands of such size, relatively lower permeability of the rock mass (dolomitic limestones or dolostones) is more suitable for fresh or brackish water accumulation in the underground than the highly karstified limestones. That is the case because in the highly permeable rock mass, total seawater intrusion would occur and there would be no aquifers or lenses of fresh groundwater significant in the context of providing public water supply.

Because of the permeability contrast between Jurassic (predominantly) dolostones and Cretaceous (predominantly) limestones, the dolostones represent a relative hydrogeological barrier on the island [30, 31]. Monocline structure dipping toward NNE, combined with the island's elongated shape and zonal arrangement of geological units with dolostones in the SW and limestones in the NE, causes the water which infiltrates into carbonate rock mass to flow toward the NE and discharge along the NE coast in the concentrated form of vruljas (submarine springs) and coastal springs of increased salinity [18], as well as via diffuse discharge, i.e., seepage [10]. Although dolomitic rocks are declared a relative barrier, their persistent fracturing produces a bulk hydraulic conductivity that is one order of magnitude lower than the karstified limestones. This combination of factors makes them adequate for (1) preventing significant seawater penetration into island aquifer from the S and (2) generating slower flux through dolostone rock mass, thereby creating certain groundwater storage which slowly discharges toward the northern parts in dry seasons due to aforementioned structural, geological, and morphological reasons. In such conditions, the blatinas and karst aquifers can exist in both dolomites and limestones. If the island consisted exclusively of karstified limestone rock masses of high hydraulic conductivity, there would be no possibility to prevent an almost immediate discharge of the infiltrated water (and groundwater) during rain periods due to the short distance between the infiltration area and the sea. Furthermore, seawater would extensively intrude
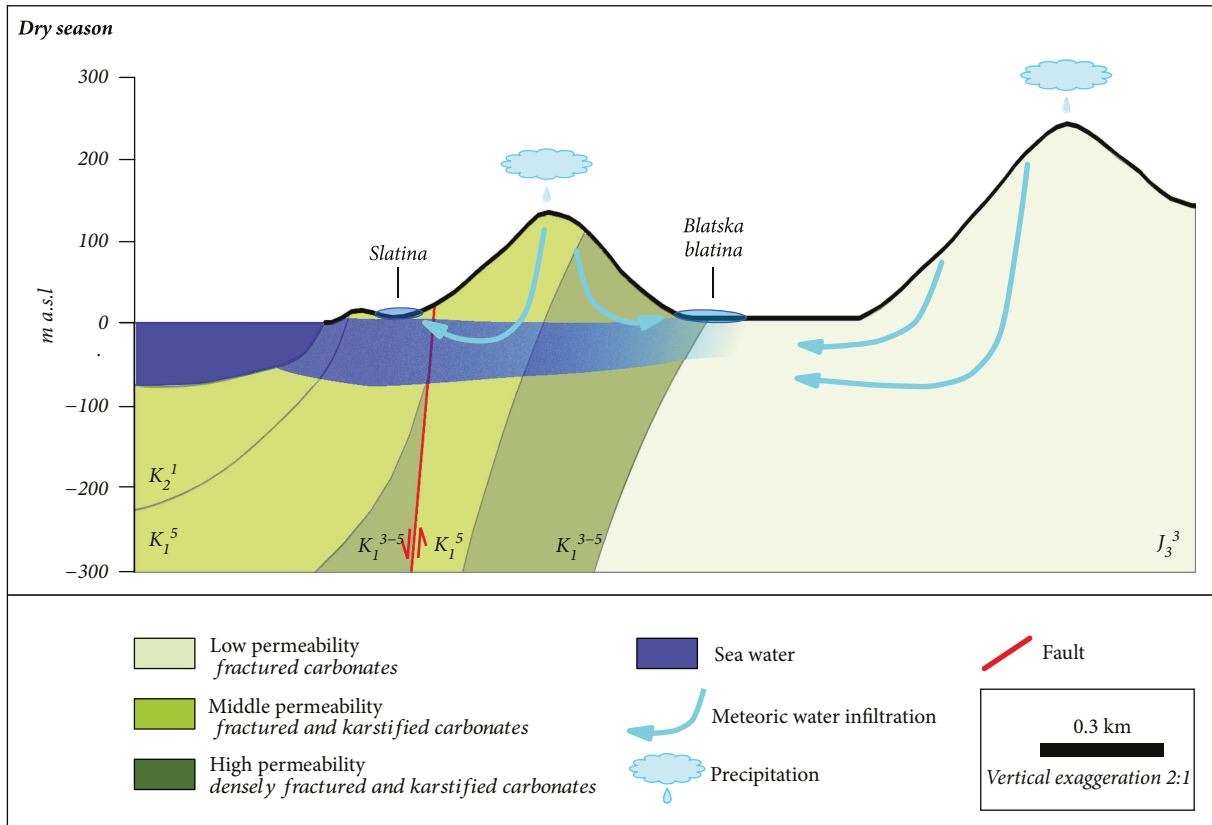
(a)
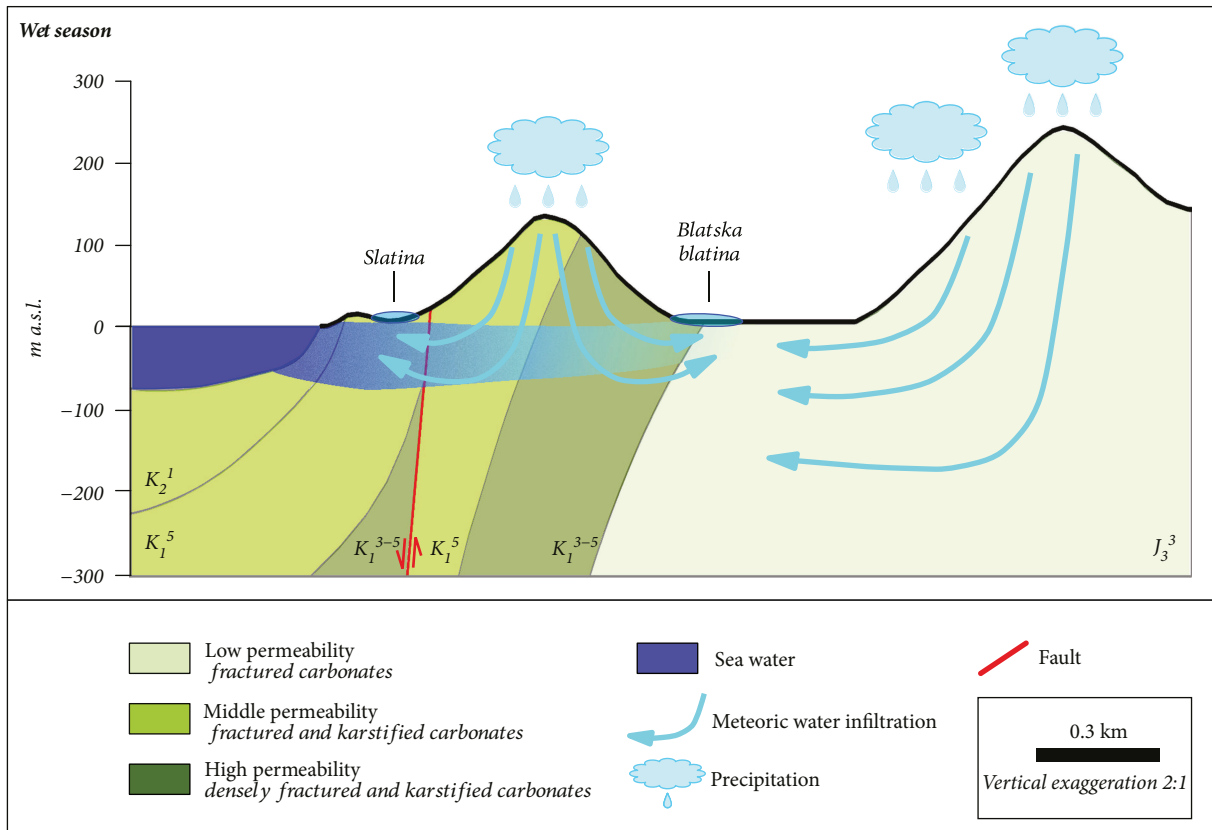
(b)

FIGURE 5: Conceptual models of blatinas during dry (a) and wet (b) periods.

the rock masses during dry periods inhibiting its prolonged mixing with freshwater.

Although there are some minor permanent and intermittent freshwater springs on the island, the most impressive phenomenon from the hydrogeological point of view is the *blatinas* (Figure 4). These are marshy brackish lakes situated next to ponor (swallow hole) of karst polje (as in Blatsko polje) or submerged sinkholes (as in Sobra, Kozarica, and Prožura).

Each *blatina* has ponor, locally named *jaz*—a deep shaft that continues through the unexplored karst conduits and has contact with the sea, which is evident from the regular appearance of eels in blatinas. Jaz functions as an estavelle connected to the sea. During low groundwater levels, the seawater/freshwater transition zone progresses deeper inland and penetrates the aquifer, causing an increase in groundwater salinity which also reaches blatinas. During high groundwater levels, fresh water sinks into jaz and pushes the mixing zone toward the sea, causing a decrease in blatina salinity. Functioning of blatinas during different hydrological seasons is schematised in Figure 5.

Even though in the Adriatic there are islands of similar size, shape and hydrological parameters (as summarized by [4, 10] into a hydrological size index), blatinas appear exclusively on Mljet. It is a consequence of a characteristic combination of hydrogeological and morphological features, i.e., of the facts that (1) the altitudes of polje and sinkholes are very close to sea level and (2) polje and sinkholes are connected to the sea by macroscopic size karst conduits.

4. Methodology

Water samples were collected during two separate campaigns. A set of samples was collected during hydrological minimum (autumn of 2005) and hydrological maximum (spring 2006), with regard to groundwater levels, at different kinds of hydrogeological features: blatinas, pit well, and drilled wells. These samples were analysed in the hydrochemical laboratory of the Croatian Geological Survey. The electrical conductivity (EC), total dissolved solids (TDS), pH, and temperature (T), as well as the alkalinity of all the samples, were measured in situ. Contents of sulphate, nitrate, bromide, potassium, sodium, calcium, and magnesium were analysed using LabAlliance ion chromatography apparatus. Chloride content was determined by the addition of dilute mercuric nitrate solution to acidified water in the presence of diphenylcarbazone indicator. Data quality was assessed by calculating the charge balance between the sum of cations and the sum of anions, expressed in meq/l, which was always ±5%.

Another sampling was conducted in 2016 from Sobranska blatina. This sample was analysed by NALCO Water laboratory in Leiden, The Netherlands, certified to ISO 9001 standard.

TDS of feed water from Sobranska blatina was monitored on a daily basis by the operator of the desalination plant in Sobra from May 2016 to June 2018 and

monthly average TDS values were calculated as the arithmetic mean.

The data from sampling campaigns in 2005/2006 were subjected to mathematical multivariate technique (R-mode factor analysis) together with samples from numerous Adriatic islands [12]. The result was a "minimum" mathematical model which ignores minor influences and nonlinear effects present in the data spread [32]. Through this technique, the multivariate relationships were reduced to simple correlations with a number of mutually uncorrelated and independent factors. In that way, data structure hidden from direct observation can be recognized and explained as natural processes in the system. Such analysis is often used in hydrogeological and environmental studies for estimating the source of pollution and for various similar purposes [33–37]. For this purpose, software STATISTICA 7.0 was used.

All precipitation data were obtained from the Meteorological and Hydrological Service of Croatia which has a climatological station on the island of Mljet. Precipitation was also recorded on a daily basis and afterwards summed into monthly precipitation.

5. Results and Discussion

5.1. Hydrochemical Facies. Hydrochemical analyses from water sampling during hydrological minimum 2005, maximum 2006, and minimum 2016 are displayed in Table 1 and Figure 6.

It is visible that the nontreated waters during the hydrological minimum do not satisfy the prescribed criteria for drinking water. All of the samples exceed maximal allowed concentrations of sodium and chloride ions, as well as EC, which is in accordance with all known facts about the genesis and functioning of blatinas. Also, in Blato wells and Prožurska blatina, the sulphate ion concentrations exceed maximum values.

High nitrate ion concentrations were also observed in blatinas, especially during higher groundwater levels. That is attributed to the leaching of the nitrates from soil on arable land in karst poljes and from the epikarst zone during a rainy period of the year. Also, in such marshy lakes, a significant amount of nitrogen is present in living plants and animals, as well as in their detritus. Ammonification and nitrification occur during their decomposition, which additionally increases the nitrate content in the waters.

The Piper diagram (Figure 6) illustrates the hydrochemical facies of analysed waters. It is visible that 11 out of a total of 13 analysed samples exhibit a sodium-chloride facies. Water from Vodice spring is (Ca, Mg)-HCO$_3$ type during both dry and wet seasons and its composition reflects the Jurassic dolomite aquifer from which the water originates (Figures 2 and 3). Water from wells in Blato is the only one which changes the type seasonally: during the hydrological maximum, it exhibits a mixed-HCO$_3$ type facies, although clearly much higher concentrations of calcium and magnesium cations are present than in other analysed waters.

TABLE 1: Physicochemical parameters and major ion composition of waters from localities on the island of Mljet in different seasons (values in **bold italics** are exceeding maximum values for drinking water; localities marked by an asterisk are not a part of the water supply system).

	Sampling point	Elevation (m a.s.l.)	EC (μS/cm)	T (°C)	pH	Ca^{2+}(mg/l)	Mg^{2+}(mg/l)	Na^+(mg/l)	K^+(mg/l)	HCO_3^-(mg/l)	Cl^-(mg/l)	SO_4^{2-}(mg/l)	NO_3^-(mg/l)
MIN 2005	Spilja intake structure—Sobra	4	*2,860*	15.7	7.4	153	53.2	*329*	9.8	399	*660*	90	1.9
	Blato wells	28	*8,120*	15.9	7.66	160	117	*1,574*	*76*	410	*2,240*	*300*	0
	Slatina	0.5	*6,930*	22.1	7.5	118	111	*1,096*	*70*	450	*1,950*	190	0
	Prožurska blatina*	0.5	*32,000*	*26.1*	7.79	75	200	*5,582*	*102*	310	*9,640*	*1,600*	0
MAX 2006	Spilja intake structure—Sobra	4	1,527	15.7	7.61	66.4	20.9	185	3.1	215	*340*	50	0
	Sobranska blatina	3	1,529	16.2	7.82	66.4	20.9	195	3.1	215	*380*	51	0
	Blato wells	28	877	14.7	7.59	76.8	25.4	46	2.1	285	86	43	29
	Blatska blatina	2	2,010	14.6	8.23	78.4	25.1	*380*	3.2	285	*754*	46.9	39
	Kozarica intake structure	1	*5,620*	15.2	7.24	126.4	90.8	*728*	3.4	510	*1,436*	50.1	32
	Slatina	0.5	*6,550*	14.7	7.26	127.6	90.6	*891*	3.4	510	*1,781*	42.5	22
	Prožurska blatina*	0.5	*17,170*	19.6	8.5	171.2	338.9	*2,520*	*52*	580	*4,889*	*430*	0
	Vodice spring*	103	762	14.4	7.55	80.8	35.2	24	1.2	290	47.6	11.2	0
MIN 2016	Spilja intake structure—Sobra	4	*3,300*	—	8.2	140	61	*410*	*15*	280	*790*	100	<10
	Drinking water		2,500	25	6.6-9.5	n/a	n/a	200	12	n/a	250	250	50

Sources: data for 2005 and 2006 [10]; standards for drinking water [38]. Abbreviations: MIN: hydrological minimum; MAX: hydrological maximum; both with respect to groundwater levels.
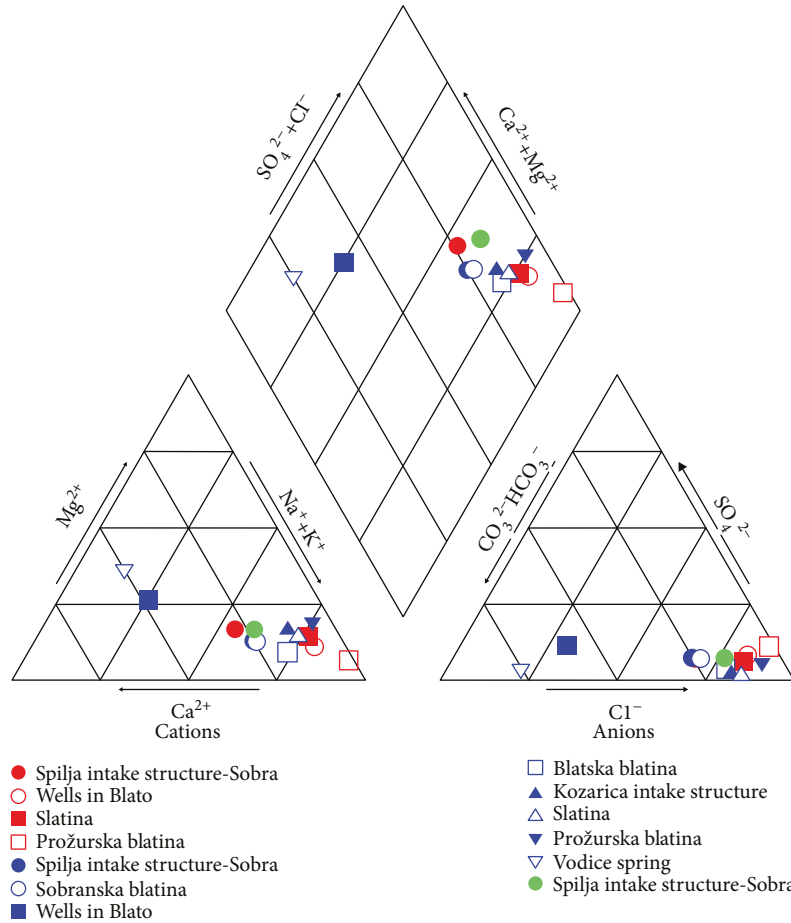
Figure 6: Piper diagram constructed from major ion compositions of samples shown in Table 1 (red symbols: MIN 2005; blue symbols: MAX 2006; green symbol: MIN 2016).

During the drilling, Musladin [21] reported that the well is in limestone rock up to its final depth of 38 m, but the water composition suggests that contact with dolomite exists, and probably in close proximity, as suggested by geological setting (Figure 2(b)).

5.2. Seawater Percentage. The percentage of seawater (SP) was calculated according to conservative mixing approach [39], from measured concentrations of Cl^- ions, using the simplified form of the equation according to [12]:

$$SP = 0.005[Cl^-]. \qquad (1)$$

Equation (1) is a theoretical linear equation describing the relation of seawater percentage in the sample to chloride anion content in the sample valid for coastal mixing (transition) zone. The equation is simplified by the following assumptions: (i) concentration of chloride anions in rainwater is zero; (ii) concentration of chloride anions in the seawater is constant; and (iii) the only source of chlorides in groundwater is mixing with seawater. Notwithstanding these simplifications, the equation is adequate for orientation purposes, especially in the context of other necessary simplifications while considering karstified carbonate aquifers and island aquifers.

Table 2: SP in the samples from different locations and in different seasons on the island of Mljet.

	Location	SP (%)
	Spilja intake structure—Sobra	3.3
MIN 2005	Wells in Blato	11.2
	Slatina	9.8
	Prožurska blatina	48.2
	Spilja intake structure—Sobra	0.7
	Sobranska blatina	1.9
	Wells in Blato	0.4
	Blatska blatina	3.8
MAX 2006	Kozarica intake structure	7.2
	Slatina	8.9
	Prožurska blatina	24.4
	Vodice	0.2
MIN 2016	Spilja intake structure—Sobra	4.0

Source: data for 2005 and 2006 from [10]. Abbreviations as in Table 1.

As can be observed in Table 2, the lowest percentage was recorded in the natural spring of Vodice (0.2%), and the wells in Blato (0.4%), which was expected. Blatinas generally have

TABLE 3: Factor scores. Specific objects are described by three dominant factors/processes.

	MIN 2005				MAX 2006		
Location	F1	F2	F3	Location	F1	F2	F3
Spilja intake structure—Sobra	-0.125	*0.725*	0.497	Spilja intake structure—Sobra	-0.329	-1.023	0.478
Wells in Blato	*1.267*	*0.786*	0.768	Sobranska blatina	-0.362	-1.034	0.767
Slatina	*0.810*	*1.044*	1.740	Wells in Blato	-0.201	-0.654	*-0.578*
Prožurska blatina	**5.140**	-0.637	1.059	Blatska blatina	0.038	-0.842	-0.418
Dominant process in the system (in italics)				Kozarica intake structure	0.583	**0.857**	-0.878
				Slatina	0.680	**0.780**	*-0.689*
Very dominant process in the system (in bold italics)				Prožurska blatina	**2.295**	1.903	2.328
				Vodice spring	-0.434	-0.580	0.320

Source: [10]. Abbreviations as in Table 1.

TABLE 4: Measured and theoretical sulphate anion concentrations in mg/l.

	Measured	Calculated from SP	Calculated from [Cl$^-$]
Wells in Blato (MIN 2005)	300	302	307
Prožurska blatina (MIN 2005)	1,600	1,301	1,269
Prožurska blatina (MAX 2006)	430	659	652

Abbreviations as in Table 1.

higher SP, which is logical due to their proven conduit connections to the sea: Sobranska blatina (1.9%), Blatska blatina (3.8%), and Slatina (9%). The highest SP was recorded in Prožurska blatina (24.4–48.2%, depending on the season), which is not included in the water supply system. That would not be economically feasible due to the fact that the energy consumption for RO desalination, and consequentially the cost, increases exponentially with water salinity.

5.3. *Multivariate Factor Analysis.* The hydrochemical data from 79 samples from various Croatian Adriatic islands were subjected to multivariate analysis technique of factor analysis [12], which has shown that 13 hydrochemical variables can be grouped into three factors, which represent 84% of the total variance of the system when considering Adriatic karst islands in general. Those are F1: mixing of fresh groundwater and surrounding seawater (58%); F2: carbonate dissolution (18%); and F3: anthropogenic influence, i.e., nitrate contamination (8%).

In the blatinas of Mljet (Table 3), due to connection to the sea, F1 factor was significantly loaded for all analysed samples, although salinity varies from almost potable brackish water in Sobra and Blato, to almost 50% of seawater during dry season in Prožura, where F1 is strongly emphasized in any hydrological moment. In Prožurska blatina, there is also a high influence of F2 during hydrological maximum, pointing to more intense carbonate dissolution in the shallow epikarst zone during rainfall. Wells in Blato and Slatina in Kozarica have a high impact of F3 during hydrological maximum, interpreted as anthropogenic contamination, i.e., leaching of nitrates of agricultural origin by precipitation. F3 was especially emphasized as negative (with respect to initially negative variable loading) in Prožura during high groundwater levels, pointing to excessive nitrogen degradation in these hydrological circumstances. The interesting

conclusion is spatial (regional) domination of limestone dissolution (F2) and pollution (F3) during the rainy season, when washing out from the soil and epikarstic belt is present. The risk of pollution is relatively low during the dry season in the summer, and human influence on groundwater was reflected in significant slowing down of the process of ammonia volatilization during the dry season. At higher groundwater levels, this process is strongly highlighted. Highly positive values of the bipolar F3 process in Kozarica and Prožura are probably a consequence of high air temperature in the summer. In the same study [12], multivariate cluster analysis resulted with only two clusters, described as (1) marine cluster (presented by sodium and chloride ions) and (2) lithogeochemical (all other parameters). Therefore, presented factor analysis seems much more appropriate for this kind of data and gives deeper insight into this complex natural system.

5.4. *Excess Sulphate Anion Content.* Sulphate anion values above the limit for drinking water (Table 1) can be analysed in the context of Tables 2 and 3. It is assumed that the principal source of sulphates in Mljet aquifer is seawater, because in the geological model (Figure 2), there is no record of sulphate rocks (such as gypsum or anhydrite). Since no evaporite rocks are present on the island, it was analysed if the sulphate anion concentration is proportional to the seawater percentage in corresponding samples (Table 4). The sulphate anion concentration in seawater was adopted from [40] to be 2700 mg/l. Such analysis shows that in the case of wells in Blato, the discrepancy of measured from calculated value is -0.7%, i.e., it almost absolutely corresponds to the conservative mixing of fresh- and seawater, when measurement error and seawater chemistry variations are taken into account. However, in the case of Prožurska

FIGURE 7: Elements of Sobra desalination system (satellite imagery adopted from Google Earth), with embedded photograph of Sobranska blatina taken from the location of a desalination plant in September 2016 in the bottom-left corner.

blatina, the discrepancy was +18.7% during the hydrological minimum and -53.3% during the maximum.

For the purpose of the mentioned factor analysis, equations of linear correlation with corresponding coefficients of correlation for various measured parameters were calculated for the sample set from multiple Adriatic karst islands. The authors have determined a correlation factor of $r = 0.91$ between sulphate and chloride anions for the equation $[SO_4^{2-}] = 13.1[Cl^-] + 16.1$ [12]. A similar result was obtained by applying that calculation (the last column of Table 4). That means that applying either literature value for seawater composition or the correlation derived from numerous Adriatic islands, it is not possible to explain the sulphate concentrations measured in Prožurska blatina by conservative mixing model. Obviously, increased ion concentrations during the dry season could be the result of excess evaporation and decreased concentrations of high precipitation during the wet season. If that were the case, the regularity would also be present with other sea-derived ions, especially chloride, which is not observed.

5.5. Temporal TDS and Precipitation Analysis. TDS, determined in [10] to have a functional relationship to chloride anion concentrations ($r = 1$), was monitored at Sobranska blatina, which provides the majority of the feed water for desalination (Figure 7).

The hydrochemical composition of water from blatinas is dependent on rainfall, both directly at the lake surface and, mostly, indirectly by infiltration into aquifers and subsequently through fresh groundwater flow. The summary TDS and precipitation data, resulting from a two-year monitoring on a daily basis, are presented graphically in Figure 8 as monthly averages.

It can be observed that maximum TDS values occur regularly in September. That is the consequence of two
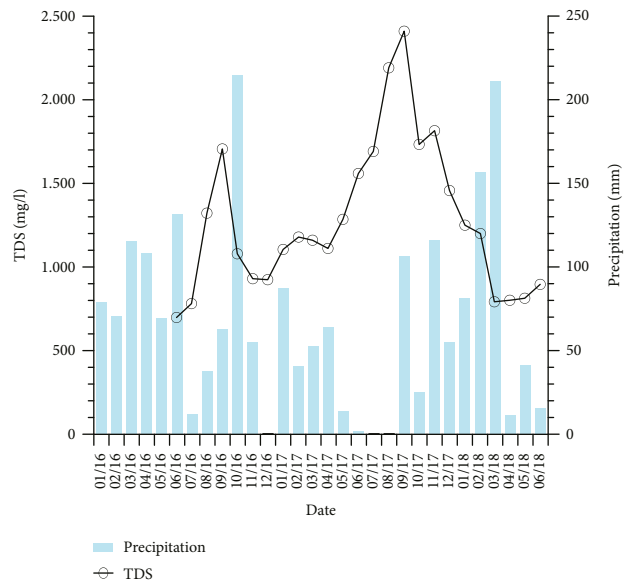

FIGURE 8: Monthly average values of TDS in Sobranska blatina and precipitation on the island of Mljet calculated from diurnal observations.

interacting factors: natural (low precipitation) and anthropogenic (increased pumping due to summer tourist season). Minimal TDS values in the Mediterranean climate area are expected after the rainy season, during the spring. However, monitoring data suggest that the lag is longer and the minimum can be expected in June (as in the cases of 2016 and 2018). In 2017 the minimum TDS was recorded in January, which is assumed to be an outlier.

However, a two-year monitoring period is far too short to determine hydrological patterns of such a complex system which is also disturbed by human activities.

What can be done is a comparison to the referent climatological period of 1981-2000 at the climatological station on Mljet. In that period, the average annual rainfall was 743 mm, with a minimum of 579 mm in 1991 and a maximum of 1099 mm in 1996. Using that as a reference, the rainfall in 2016 was 956 mm, and in 2017 it was only 562 mm. Also according to the reference climatological period, December is a month with the highest average precipitation, and in December 2016 the precipitation was zero. Extremely low rainfall can account for the fact that during 2017 with the usual pumping quantities, TDS of Sobranska blatina never fell under 1,000 mg/l.

5.6. Predicted Impact of Climate Change. According to Lang's rain factor (f), which is a quotient of annual average rainfall in mm and temperature in °C, a climate can be considered semiarid if f is in the range of 40-60, while it is arid if the factor is lower than 40 [15]. Since the average temperature in the referent period was 16.3°C, the rain factor for Mljet was 45.6, i.e., the island experiences semiarid climate, closer to arid than to semihumid part of the spectrum. In the referent 20-year period, a variability in annual precipitation is visible, with the maximum being almost twice the minimum precipitation ($\min_{1991}: \max_{1996} = 1: 1.9$). According to the 2017 data, the minimal precipitation values display a decreasing trend.

Generally, most climate models for the Mediterranean region predict a gradual decrease in precipitation and an increase in variability, with a negative influence on water balance [41–43]. The decrease in effective infiltration into the karstified underground would obviously lead to a decrease in the groundwater levels, and one of the consequences would be an increased probability of frequent and intensive seawater intrusions.

Climate modelling for Croatian Adriatic region was conducted using five different regional climate models for the three 30-year periods during 2011-2100 and interpreted separately for northern, central, and southern parts of the Croatian coastal and insular area [44]. Results predict mean air temperature increase up to 3.5-5.5°C until the end of the century, with a swifter rise at the mainland coastal areas than on the islands. Changes in precipitation are characterized by high uncertainty, but their statistical significance increases going from present toward 2100. A drought during late spring and early summer is predicted (April-August), which will extend to September and October toward the end of the century. This trend is more significant in the southern Adriatic region. All models predicted that autumn and winter months will become slightly more humid than at present. Although weak, the prevailing trends are negative and consistent at all stations from the central to the southern Adriatic zone, thus in agreement with the drying trend observed across the Mediterranean according to IPCC [44]. If the climate data are inserted into water balance calculations, total infiltration tends to decrease significantly and by the end of the century, the water balance deficit could reach 30-47% of present values [45]. Such circumstances will probably lead to major deteriorating changes in

blatinas' hydrology and ecosystems, not to mention water supply issues. According to all climate models, extreme events such as droughts or flash floods will also become much more frequent.

6. Conclusions

Although morphology and size of the island of Mljet are not favourable for significant groundwater accumulation, its geological structure allows the formation of limited karst aquifers. Nevertheless, relatively low water demand and desalination created the possibility for local water supply. The groundwater is brackish at all extraction sites on the island and subjected to seawater intrusion in its natural state.

A combination of geological and geomorphological characteristics enables the appearance of groundwater at the surface in the form of brackish lakes (blatinas), the level of which roughly represents the water table of island karst aquifers. Blatinas are a unique natural phenomenon among Adriatic karst islands. According to presented hydrogeological conceptual model, it is possible to extract further groundwater quantities (most probably also brackish) in other parts of the island, but this should be corroborated by a multidisciplinary research program including geology, hydrogeology, hydrology, geophysics, and hydrogeochemistry.

The analysed data from diurnal monitoring of TDS at Sobranska blatina are indicative of the climatic influence to feed water composition. However, the monitoring period of two years is considered too short for an analysis of a complex karst island aquifer, additionally disturbed by seasonal anthropogenic activities. Taking into account the fact that the blatinas and karst aquifers in their vicinity represent a source of the majority of water supply on the island, it would be advisable to introduce a permanent TDS monitoring (e.g., by monitoring electrolytic conductivity using data loggers) and monthly chemical analyses, or at least two analyses annually, during hydrological minimum and maximum, at all feed water sources (blatinas and wells).

Prožurska blatina, which has the highest SP during both hydrological minimum and maximum, is not a part of the water supply system and is relatively inaccessible. Therefore, not enough data are available to derive the excess sulphate anion origin, other than seawater. Analysis of stable isotopes of sulphur from the sulphate could determine its origin as atmospheric contribution, mineral or rock contribution, marine and playa lake sources, volcanic sources, or biological contributions [46, 47].

One of the problems concerning Mljet island's water supply is an inadequate effluent management, which should be a topic of additional research. Sobra desalination plant, which is close to the coast, discharges effluent into the sea (Figure 7), but the plant in Blato discharges its effluent with an average TDS of 8,000 mg/l into the same karst polje and into Blatska blatina—its topographically lowest part. Such obviously undesirable practice has not resulted in visible negative consequences so far, which could be misleading since there is no monitoring. Effluent from RO treatment of brackish water can generally be discharged into surface water bodies if the salinity difference is less than 10% [48]. Since in

Blato the salinity difference significantly exceeds this standard, it is necessary to design a plan for treatment and sustainable effluent accommodation. If the standard is not maintained, the effluent can change the salinity of the recipient and the process can result in decreased dissolved oxygen concentrations in the water and negatively affect aquatic life [49].

This paper also tackled the question of climate changes. Climate change models predict an increase in average temperatures and precipitation variability and a decrease in effective aquifer recharge up to almost 50% by the end of this century. That suggests that the island groundwater system, which is currently operating near the maximum limit, will probably be useless if the predicted scenarios take place, especially during summer peak loads. Therefore, management plans have to be prepared for each possible scenario.

The NPKLM regional water supply system which connects Mljet to the mainland via submarine pipeline is currently being put into operation. The process will take years and presented water supply from the island's own resources will have to remain active. Even afterwards, these quantities should not be neglected and should stay operational. Water in NPKLM comes from a strong karst spring on the mainland, with minimal discharges of $3\,\mathrm{m}^3/\mathrm{s}$ and maximal above $10\,\mathrm{m}^3/\mathrm{s}$. Quantities used for water supply are approximately ten times lower than minimal discharges, so the supply can be considered secure. Still, this water has slightly increased sulphate anion concentrations as a result of the dissolution of gypsum and anhydrite rocks in its catchment area outside of the Croatian territory. Transboundary management of this large karst catchment area is still being established and is a topic of hydrogeological and geological investigations.

In the context of observed behaviour of the hydrogeological system of the island of Mljet and the predictions for both the narrower Adriatic and wider Mediterranean region, long-term sustainable water supply must be ensured taking into account the water demand, existing desalination practices, and connection of water supply system to the mainland, as well as the water availability in the context of climate change.

Data Availability

Data procured as described in "Materials and Methods" section which is not directly presented in the paper is public domain and can be procured from the corresponding author upon request.

Conflicts of Interest

The authors declare that there is no conflict of interest regarding the publication of this paper.

Acknowledgments

References

[1] J. Liu, C. Mei, H. Wang, W. Shao, and C. Xiang, "Mutual adaptability of renewable energy and water-supply systems in islands," *Energy Procedia*, vol. 105, pp. 799–804, 2017.

[2] C. Marín and G. Galván, *Towards 100% RES supply - renewable energy sources for island sustainable development*, ITER, San Isidro, Tenerife, 2001.

[3] A. Falkland, *Hydrology and Water Resources of Small Islands: A Practical Guide*, UNESCO, Paris, 1991.

[4] I. Ljubenkov, "Hydro climatic ranking of small Mediterranean islands," *Journal of Environmental Science and Water Resources*, vol. 2, no. 4, pp. 112–121, 2013.

[5] A. Corsini and E. Tortora, "The influence of water desalination systems on load levelling of gen-set in small off-grid islands," *Energy Procedia*, vol. 142, pp. 2230–2235, 2017.

[6] R. Clayton, *Desalination for Water Supply, Foundation for Water Research*, Marlow, U.K., 2015.

[7] J. Faričić, "What is the indentation index of Croatian coast?, in geografija.hr - Official portal of the Geography department, Faculty of Science, University of Zagreb (2004)," October 2018, http://www.geografija.hr/hrvatska/koliki-je-indeks-razvedenosti-obalne-crte-hrvatske/.

[8] T. Duplančić Leder, T. Ujević, and M. Čala, "Coastline lengths and areas of islands in the Croatian part of the Adriatic Sea determined from the topographic maps at the scale 1 : 25,000," *Geoadria*, vol. 9, pp. 5–32, 2004.

[9] S. Furlani, M. Pappalardo, L. Gomez-Puyol, and A. Chelli, "The rock coast of the Mediterranean and Black seas," in *Rock Coast Geomorphology: A Global Synthesis*, D. M. Kennedy, W. J. Stephenson, and L. A. Naylor, Eds., pp. 89–123, Geological Society Publishing House, Bath, 2014.

[10] J. Terzić, *Hydrogeology of Adriatic karst islands, Faculty of Mining, Geology and Petroleum Engineering, [PhD thesis]*, University of Zagreb, Zagreb, 2006.

[11] J. Terzić, F. Šumanovac, and R. Buljan, "An assessment of hydrogeological parameters on the karstic island of Dugi otok, Croatia," *Journal of Hydrology*, vol. 343, no. 1-2, pp. 29–42, 2007.

[12] J. Terzić, Z. Peh, and T. Marković, "Hydrochemical properties of transition zone between fresh groundwater and seawater in karst environment of the Adriatic islands, Croatia," *Environmental Earth Sciences*, vol. 59, no. 8, pp. 1629–1642, 2010.

[13] J. Terzić, "Hydrogeological relations on karst islands - example of the island of Vis," *Mining, Geology and Petroleum Engineering Bulletin*, vol. 16, pp. 47–58, 2004.

[14] J. Terzić, T. Marković, and Ž. Pekaš, "Influence of sea-water intrusion and agricultural production on the Blato aquifer,

island of Korčula, Croatia," *Environmental Geology*, vol. 54, no. 4, pp. 719–729, 2008.

[15] T. Šegota and A. Filipčić, *Climatology for Geographers*, Školska knjiga, Zagreb, 1996.

[16] D. Anić, V. Jovanović, and Z. Krulc, *Report on basic geological, geophysical and hydrological research for water on the islands of Lastovo and Mljet*, Croatian Geological Survey, Zagreb, 1953.

[17] A. Turalija, *Report on the results of drilling for the purpose of water supply on the Island of Mljet*, Geoistrage, Sarajevo, 1971.

[18] V. Goatti, *Hydrogeological research on the island of Mljet*, Croatian Geological Survey, Zagreb, 1996.

[19] B. Korolija, I. Borović, I. Grimani et al., *Basic geological map of the Socialist Federative Republic of Yugoslavia and the explanatory Notes, scale 1:100,000, Sheets Korčula, Lastovo and Palagruža*, Federal geological department, Belgrade, 1977.

[20] A. Husinec, B. Prtoljan, L. Fuček, and T. Korbar, *Basic geological map of the Republic of Croatia scale 1:50,000 sheet: the island of Mljet*, Croatian Geological Survey, Zagreb, 2016.

[21] N. Musladin, *Report on drilling the well B-2 on the Island of Mljet*, Blatsko polje, Libertas, Opatija, 2000.

[22] N. Musladin, *Report on drilling a exploration-exploitation well S-1 in Sobra, the Island of Mljet*, Libertas, Opatija, 2002.

[23] N. N. Kourgialas, G. P. Karatzas, Z. Dokou, and A. Kokorogiannis, "Groundwater footprint methodology as policy tool for balancing water needs (agriculture & tourism) in water scarce islands - the case of Crete, Greece," *Science of the Total Environment*, vol. 615, pp. 381–389, 2018.

[24] V. Kuk, E. Prelogović, and I. Dragičević, "Seismotectonically active zones in the Dinarides," *Geologia Croatica*, vol. 53, pp. 295–303, 2000.

[25] Č. Benac and M. Juračić, "Geomorphological indicators of sea level changes during upper Pleistocene (Würm) and Holocene in the Kvarner region (NE Adriatic Sea)," *Acta Geographica Croatica*, vol. 33, pp. 27–45, 1998.

[26] J. Masse and L. Montaggioni, "Growth history of shallow-water carbonates: control of accommodation on ecological and depositional processes," *International Journal of Earth Sciences*, vol. 90, no. 2, pp. 452–469, 2001.

[27] T. Šegota, "Seawater level and vertical seabottom movement of the Adriatic Sea from the Riss-Würm interglacial until today," *Geološki Vjesnik*, vol. 35, pp. 93–109, 1982.

[28] M. Surić, "Submarine karst of Croatia - evidence of former lower sea levels," *Acta Carsologica*, vol. 31, pp. 89–98, 2002.

[29] P. Fleury, M. Bakalowicz, and G. de Marsily, "Submarine springs and coastal karst aquifers: a review," *Journal of Hydrology*, vol. 339, no. 1-2, pp. 79–92, 2007.

[30] O. Bonacci, "Karst hydrogeology/hydrology of dinaric chain and isles," *Environmental Earth Sciences*, vol. 74, no. 1, pp. 37–55, 2015.

[31] W. B. White, "Karst hydrology: recent developments and open questions," *Engineering Geology*, vol. 65, no. 2-3, pp. 85–105, 2002.

[32] J. C. Davis, *Statistics and Data Analysis in Geology*, John Wiley & Sons, Kansas, US, 1986.

[33] S. M. Ahmed, M. Hussain, and W. Abderrahman, "Using multivariate factor analysis to assess surface/logged water quality and source of contamination at a large irrigation project at Al-Fadhli, Eastern Province, Saudi Arabia," *Bulletin of Engineering Geology and the Environment*, vol. 64, no. 3, pp. 315–323, 2005.

[34] V. Cloutier, R. Lefebvre, R. Therrien, and M. M. Savard, "Multivariate statistical analysis of geochemical data as indicative of the hydrogeochemical evolution of groundwater in a sedimentary rock aquifer system," *Journal of Hydrology*, vol. 353, no. 3-4, pp. 294–313, 2008.

[35] E. C. Galazoulas and C. P. Petalas, "Application of multivariate statistical procedures on major ions and trace elements in a multilayered coastal aquifer: the case of the south Rhodope coastal aquifer," *Environmental Earth Sciences*, vol. 72, no. 10, pp. 4191–4205, 2014.

[36] K. P. Singh, A. Malik, and S. Sinha, "Water quality assessment and apportionment of pollution sources of Gomti river (India) using multivariate statistical techniques – a case study," *Analytica Chimica Acta*, vol. 538, no. 1-2, pp. 355–374, 2005.

[37] S. Shrestha and F. Kazama, "Assessment of surface water quality using multivariate statistical techniques: a case study of the Fuji river basin, Japan," *Environmental Modelling & Software*, vol. 22, no. 4, pp. 464–475, 2007.

[38] Ministry of health of the Republic of Croatia, *Regulation on water for human consumption NN 125/2017 doc. 2848*, Official Gazette, 2017.

[39] C. A. J. Appelo and D. Postma, *Geochemistry, Groundwater and Pollution, Balkema*, Brookfield, Rotterdam, 1994.

[40] J. D. Hem, *Study and Interpretation of the Chenmical Characteristics of Natural Water*, USGS, Alexandria, VA, 1989.

[41] H. Aguilera and J. M. Murillo, "The effect of possible climate change on natural groundwater recharge based on a simple model: a study of four karstic aquifers in SE Spain," *Environmental Geology*, vol. 57, pp. 963–974, 2008.

[42] The physical science basis, *Climate Change*, S. Solomon, D. Qin, M. Manning, Z. Chen, M. Marquis, K. B. Averyt, M. Tignor, and H. L. Miller, Eds., vol. 2007, Cambridge, UK, 2007.

[43] I. Touhami, E. Chirino, J. M. Andreu, J. R. Sánchez, H. Moutahir, and J. Bellot, "Assessment of climate change impacts on soil water balance and aquifer recharge in a semi-arid region in south east Spain," *Journal of Hydrology*, vol. 527, pp. 619–629, 2015.

[44] Č. Branković, I. Güttler, and M. Gajić-Čapka, "Evaluating climate change at the Croatian Adriatic from observations and regional climate models' simulations," *Climate Dynamics*, vol. 41, no. 9-10, pp. 2353–2373, 2013.

[45] J. Rubinić and J. Terzić, *Water resources availability - test area Blatsko polje*, Croatian Geological Survey, Korčula Island (Croatia), 2011.

[46] M. Geyh, F. D'Amore, G. Darling, T. Paces, Z. Pang, and J. Šilar, *Groundwater: saturated and unsaturated zone*, IAEA-UNESCO Series, 2000.

[47] I. D. Clark and P. Fritz, *Environmental Isotopes in Hydrogeology*, CRC Press, Boca Raton, FL, 1997.

[48] M. Mickley, *Desalination and water purification research and development program treatment of concentrate*, USBR, Denver, CO, USA, 2009.

[49] L. F. Greenlee, D. F. Lawler, B. D. Freeman, B. Marrot, and P. Moulin, "Reverse osmosis desalination: water sources, technology, and today's challenges," *Water Research*, vol. 43, no. 9, pp. 2317–2348, 2009.

Research Article

Deep Electrical Resistivity Tomography for the Hydrogeological Setting of Muro Lucano Mounts Aquifer (Basilicata, Southern Italy)

E. Rizzo [1], V. Giampaolo,[1] L. Capozzoli,[1] and S. Grimaldi[2]

[1]*CNR-IMAA, Laboratorio Hydrogeosite, Tito-Marsico Nuovo, Italy*
[2]*Department of Science, University of Basilicata, Potenza, Italy*

Correspondence should be addressed to E. Rizzo; enzo.rizzo@imaa.cnr.it

The proposed work concerns the application of a deep geoelectrical survey to a carbonate aquifer in order to define the best location for exploitation well drilling for increasing water supply. However, an optimal characterization of a groundwater resource is the necessary condition to reach the indicated aim. Therefore, the geoelectrical investigation was guided from the previous geological and hydrogeological characterization. Moreover, geophysical methods are good tools to improve the groundwater model when detailed information is necessary, such as the localization of a pumping well. The work summarizes the hydrogeological knowledge at the West of the Basilicata Region (Muro Lucano, Italy). The investigated area is characterized by the presence of a karst aquifer which is made up of a carbonate ridge (Castelgrande, Muro Lucano) that tectonically dips southward and is widely covered by Pliocene deposits (sands and conglomerates), by the Irpinian unit and Sicilide unit formations, and by debris slope and landslide deposits. The assessment of the complex hydrogeological framework of the area was detailed by the use of a new multichannel deep geoelectrical technique (DERT). In details, the proposed technique was able to successfully locate a less resistive zone connected to a more fractured limestone and then it was suitable for the localization of a groundwater exploitation well.

1. Introduction

Hundreds of millions of people worldwide live in karst areas and are supplied by drinking water from karst aquifers. In particular, the karst aquifer map of Europe shows that 21.6% of the European land surface is characterized by the presence of (continuous or discontinuous) carbonate rocks; about 13.8% of the land surface is carbonate rock outcrop [1, 2]. Karst carbonate aquifers play an extremely important role in water supply, irrigation, and power generation due to the exceptional water quality and quantity. At the same time, they are a very vulnerable and dynamic system due to their peculiar features [3]:

(i) Heterogeneity: the properties of karst aquifers greatly vary in space

(ii) Anisotropy: the aquifer hydraulic properties depend on the orientation of geologic fabric elements (the hydraulic conductivity is typically high in the direction of large fractures and conduits, but may be low in other directions)

(iii) Duality of porosity and flow: there are two or even three types of porosity in karst aquifers (rock matrix, fracture, and conduit porosity), whereas groundwater flow in the matrix and small fissures is typically slow and laminar and flow in karst conduits (caves) is often fast and turbulent

(iv) Variability: at karst springs, discharge variations by factors of 10 to 100 within hours or days are common, and karst springs typically show also rapid variations of water quality

In particular, the geological structures and the local lithological variations play an important role in karst system, where various depositional and diagenetic processes and fracture distribution can produce a wide range of conduit size. These features make a karst aquifer very complex, so for these reasons, they require increased protection and application of innovative methodologies for their investigation.

For these reasons, in recent years, the use of geophysical investigations in karst regions has increased rapidly with the aim of (i) giving more detailed information on underground karst morphology characteristics (detecting and characterizing caves and fractures) and (ii) understanding karst hydrogeological functioning, as a support to hydrogeochemical information [4, 5]. These techniques have the advantage of greater spatial resolution, lower costs, simpler field procedures, and more rapid inversion and interpretation of data [6].

To date, the geophysical methods most used in a karst environment are geoelectrical, electromagnetic, gravimetric, and seismic [5, 7–9]. Seismic methods are the most suitable to delineate geological boundaries and the external geometry of the aquifer. Gravity can be used to identify large voids, such as potential sinkholes, as well as caves and major karst conduits [9–15]. Moreover, geoelectrical and electromagnetic methods, by determining lateral and vertical variations in subsurface electrical resistivity, are useful to identify geological and hydrogeological features, such as caves, fractures, and sinkholes, and are particularly sensitive to the presence of subsurface water [16–21].

In particular, the use of electrical resistivity tomography (ERT) for karst system exploration has considerably increased in the last 10 years [5, 8, 9, 20, 22–25]. The strength of such methods resides in their effectiveness to track changes in the electrical properties of the subsurface, reflecting petrophysical and hydrologic property variations such as porosity, hydraulic conductivity, fluid content, temperature, presence of clay, salinity, presence of contaminants, and biodegradation activity [26–33]. For these reasons, electrical resistivity surveys are the best known geophysical techniques in hydrogeological context for groundwater characterization and monitoring.

For porous media fully saturated by brine, Archie [34] proposed a simple correlation between bulk resistivity and pore resistivity depending on formation factor $F = \varphi^{-m}$, where φ is the porosity and m is the cementation exponent. The validity of Archie's equation was verified in many papers ([34, 35]; Wyllie, 1960; [6, 36–39]). However, many measurements showing a poor fit with Archie's equation have been reported, especially in the case of carbonate rocks characterized by primary, secondary (fractures and faults), and conduit porosity [40].

Fracture geometric characteristics such as fracture intensity, fracture network connectivity, and aperture distribution are crucial features controlling the hydraulic and geotechnical properties of rock formations. In particular, Kirkby et al. [41] and Roubinet et al. [42] explore the relationship between electrical resistivity and permeability in a fracture filled with an electrically conductive fluid by accurately modeling of fracture opening. They found that at small apertures, electrical conductivity and permeability increased moderately while, at the percolation threshold, defined in terms of the matrix to fracture resistivity ratio, for fracture networks surrounded by a low-porosity matrix, very small changes in aperture are associated with large changes in both the conductivity and permeability of the fracture. The position of this threshold depends on the rock and fluid resistivity and properties of the fracture. Therefore, small changes in the fracture network characteristics may be leading to large changes in both the rock resistivity and the permeability.

In order to increase resolution for deeper target, Deep Electrical Resistivity Tomography (DERT) approach (investigation depth > 200 m) can be used. It was described for the first time by Hallof [43], which was able to reach an investigation depth greater than 200 m, and consists in the use of physically separated tools between the injection system and the measured drop of a potential tool. Even if the Deep Electrical Resistivity Tomography (DERT) method is considered a geophysical approach for deep groundwater studies, it is not a common system for a deep hydrogeological target (>200 m). In fact, only few examples are reported in the literature [44–52].

Usually, in order to obtain the electrical resistivity distribution of a deep target, the magnetotelluric (MT) and control source audio magnetotelluric (CSAMT) are the most used electromagnetic methods, but due to their low resolution, their aim is usually connected with deeper geological target, such as tectonic faults, crustal studies, and geothermal and oil reservoir detection [53, 54].

In this paper, we focus our attention on the analysis of hydrogeological and electrical resistivity data, acquired by a new deep ERT (DERT) system, to have an image of Muro Lucano Mounts buried hydrogeological structures and to understand the deep water circulation system. The definition of the resistivity distribution allowed us to obtain important information on the hydrogeological characteristic of the deep aquifer.

2. Geological Setting

The carbonate aquifer of Muro Lucano is located in the NW of Potenza district (Basilicata region) and in the NE portion of the Marzano-Ogna carbonate massif in the central sector of Southern Apennines thrust-and-fold belt, between Basilicata and Campania regions (Figure 1). The investigated zone covers an area of about $40 \, km^2$, and some sectors are characterized by outcropped carbonate (Castelgrande-Muro Lucano ridge). The mean elevation is 870 m.a.s.l., and the morphological setting shows a typical tectonic valley extended in the NW-SE direction.

Southern Apennines are a NW-SE trending chain formed between the upper Oligocene and Quaternary [55] as a response to convergence between the African plate and the European and contemporary retreat towards the SE of the ionic subduction [56, 57]. Since the Middle Miocene, compressional deformation was responsible for the building up of a pile of rootless nappe. Mesozoic carbonates of the Western carbonate platform overthrust coeval pelagic sequences
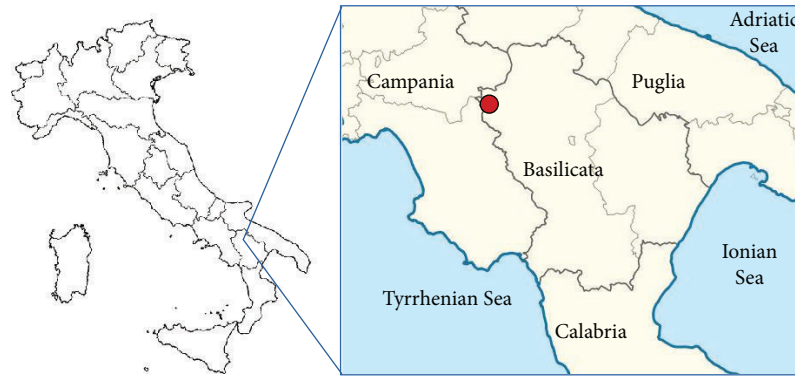
Figure 1: Localization of the investigation site.

of the Lagonegro basin, which in turn overlays tectonically deeply deformed Mio-Pliocene foredeep deposits [58]. Liguride-Sicilide units, from a basin domain located west of the Western carbonate platform, systematically overly both the carbonates and the Lagonegro units.

This stack of thrust sheets overthrusts with an overall E-vergence shelf limestones of the Apulia platform up to 7 km thick that underwent thick-skinned tectonics during Late Pliocene to Early Pleistocene times [59]. The detachment between the allochthon and the buried Apulian unit is marked by a mélange zone, generally several hundreds of meters thick and locally exceeding a kilometre in thickness [58].

In the nearest of the studied area, the complex thrust-and-fold system has been deeply explored by the commercial seismic reflection profile CROP 04 [60, 61] and two deep wells (San Gregorio Magno and San Fele). In particular, the Muro Lucano carbonate massif develops in the Meso-Cenozoic carbonate substratum of the Mt. Marzano-Maddalena Mounts unit (Apennines platform) overthrusted over Lagonegro unit terrain (Figure 2). The unit is formed by a powerful limestone dolomite succession of approximately 2000 m, aged between the Late Triassic and Early Eocene [62]. In the studied area, the carbonate succession is represented mainly by the Jurassic limestones and dolomitic limestones and by Cretaceous calcarenites, calcirudites, and carbonate breccias, which indicate that the sedimentation occurred at an escarpment that connected the Apennines platform with the Lagonegro basin [61]. Lagonegro II unit outcrops in the northeastern sector (Figure 2) constituted of middle Triassic to lower Cretaceous basin marine deposits with abundant shallow water-derived carbonate material (siliceous schists, galestrino flysch, and red flysch). Sicilide units (blue-gray clays) are localized in the W, and Irpinian units [63] are instead defined in the N and W and in the S between Monticello and Paratiello mountains (Figure 2).

In particular, Irpinian units are represented by calcarenites and limestones alternated to small layers of green and yellow clays and they were deposited from Burdigalian to Tortonian in a basin called the Irpinian basin, a wide Miocene Apennines chain foredeep. Finally, the syntectonic unit of the Muro Lucano basin (sand and polygenic conglomerates of lower Pliocene) covers the previous units by an unconformity. It is constituted mainly by sands and sandstone of medium to lower Pliocene. In the NE zone, the carbonate rocks generated debris slope deposits with huge thickness and extension.

The Monte Marzano-Ogna carbonate massif is bounded at south-west by high-angle N120°-trending left-lateral strike-slip faults and low-angle E-trending, N-dipping normal faults [64]. Some of these faults are active and reflect the present day extensional tectonic field responsible for the 1980 Irpinian earthquake and of other strong historical earthquakes, with epicentral intensity between IX and XI MCS, such as those of 990, 1561, 1694, and 1857 ([64] and references therein). Finally, the northern sector the carbonate massif is bounded by a low-angle thrust fault where the carbonate units overlay Lagonegro terrains.

In particular, the Muro Lucano carbonate massif shows a lens shape, which is extended 14 km in the E-W direction. According to Scandone et al. [60] and Scrocca et al. [61], the outcropping carbonate is constituted by undifferentiated Apennines platform terrains (chaotic complex) characterized by highly fractured and tectonized (cataclasites) limestones; it is partially buried by Muro Lucano basin units (sand-clay and conglomerates) and is bounded by two low-angle thrust faults. The structural survey of the main systems of fractures of the rock massif at the north of the Muro Lucano town highlighted the prevalence of high-angle N 30-50° and N 160-170° systems and subordinated the presence of other systems, among which is the N 90°. In several points, fractures are open to some tens of centimeters [65].

The eastern part of the carbonate structure is characterized by gravitational phenomena caused by neotectonic movements along active faults. Some of these, generally rockfalls, are associated to historical earthquakes (1561, 1857, and 1980) described above [66].
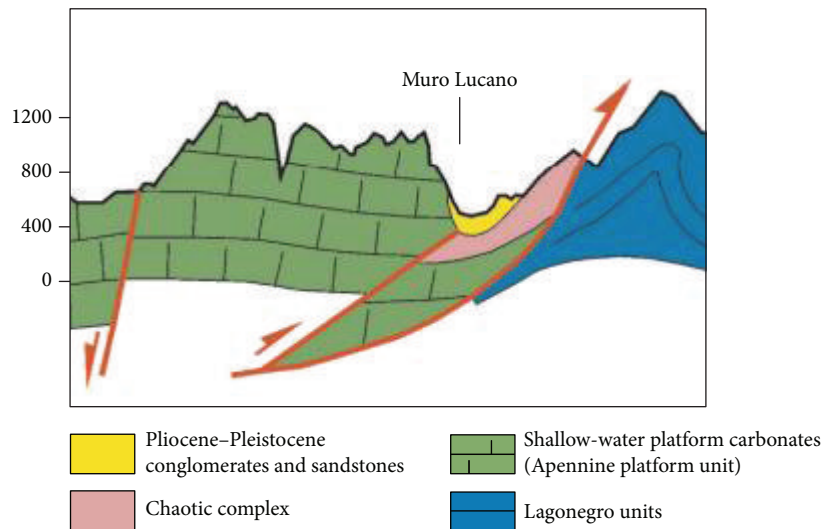
3. Methodology: Deep Electrical Resistivity Tomography (DERT)

The electrical resistivity tomography is largely applied in small-scale investigations to solve environmental and engineering problems. Recently, the improvements in the field technology and data processing allow us to apply this method
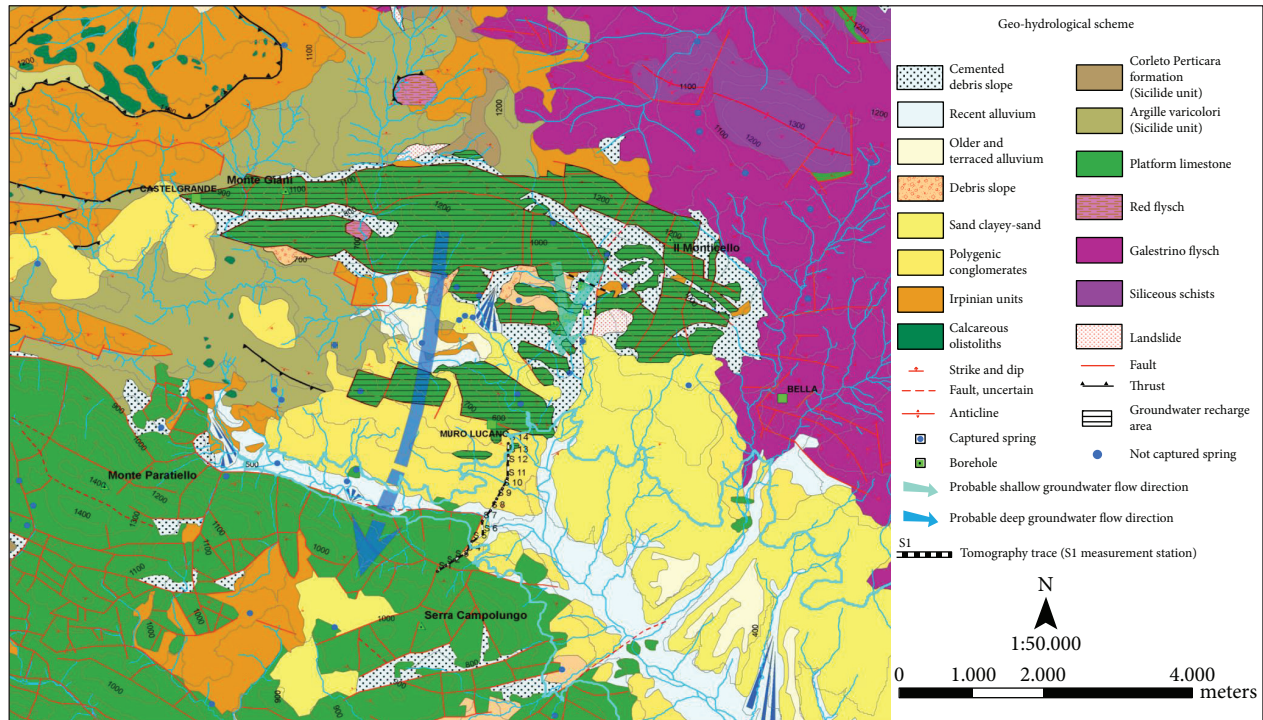
(a)

(b)

FIGURE 2: (a) Geological map with hydrogeological features. (b) Cross-section of the shallow geological structures along the Crop 04 deep seismic profile from San Gregorio Magno to San Fele. Modified by Scandone et al. [60].

in the large-scale investigations for geological structural studies [44, 45, 48–50]. In order to define the best location for deep drilling exploration well for having a low ratio between the economic effort and water pumping capacity, a Deep Electrical Resistivity Tomography was carried out in the investigated area (Figure 2).

It was used as a dipole-dipole array configuration, where the electric current (I) is sent into the ground via two contiguous electrodes x meters apart (200 m), and the potential drop (ΔV) is measured between two other electrodes x meters apart in line with the current electrodes (200 m).

The spacing between the nearest current and potential electrodes is an integer n times the basic distance x and the maximum number of measurements n depending from the signal-to-noise-ratio of the voltage recordings [67]. In this way, the electrode array geometry allows us to obtain a length of the deep electrical survey of 2600 m, with an exploration depth of about 350 m. The acquisition system (a prototype system built in the Hydrogeosite Laboratory of CNR-IMAA, Figure 3) consists of a transmitting station which injects the current (5-10 amperes) into the ground and a new multi-channel receiver device which records the generated voltage
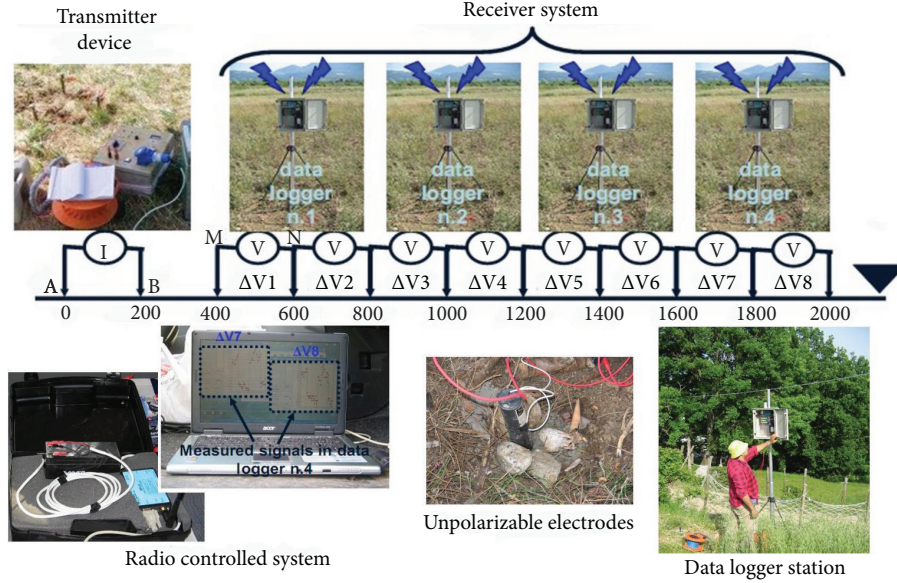
FIGURE 3: Geoelectrical prototype for Deep Electrical Resistivity Tomography, made by CNR-IMAA.

signals (mV). The receiving system is composed of 4 remote multichannel data loggers connected with a radio communication system to a personal computer. Therefore, at the same time, 8 voltage recordings from 5 to 20 min were acquired for each current injection related to different positions of the electrodes along the profile. Overall, we collected 56 voltage recordings.

The second step consisted in the extraction of the useful signal from voltage recordings to calculate the apparent resistivity values. In fact, in deep geoelectrical explorations, a crucial task is the extraction of useful signal from voltage recordings, taking into account that the signal-to-noise ratio depends on the distance between the current emitters and receivers. However, the quality of the signal also depends on the spacing between electrodes, worsening as the receiving dipole moves away from the energizing one. The distribution of electrical conductivity in the soil also affects the quality of the signal; in fact, in highly conductive areas, located between the transmitting and receiving dipoles, the electric potential is strongly masked to such an extent that the signal is completely erased from the background noise. Therefore, the success of the methodology is related to the duration of voltage recordings.

For the elaboration of acquired data, we used OriginPro software (OriginLab Corporation) where graphing and data analysis tools were used. The first step of the voltage data analysis was the spike removing, which consists to delete the spikes on the active graph window. The second step was the detrending analysis, which consisted in a polynomial or linear fit of the voltage data and a subsequently detrend approach, in order to remove the natural trend that enveloped the data. Successively, a FFT tool was performed to the detrending voltage data. The amplitude of the FFT results in the frequency of the acquired signal defines the amount of the drop of potential. A good signal-to-noise ratio, in the FFT spectrum of signal amplitudes, produces a peak right at the

energization frequency (which in our case was equal to 0.025 Hz). On the contrary, the spectrum of particularly noisy voltage signals presented a series of "spikes" that make the identification of the useful signal much more complex. At the end of the data analysis steps, the estimated voltage (ΔV), the injected current (I), and the position of each quadripole (geometric coefficient) permitted us to calculate the apparent resistivity (ρ_a) by the Hannenson formula:

$$\rho_a = [\pi a n(n+1)(n+2)]\left(\frac{\Delta V}{I}\right), \tag{1}$$

where a is the electrode distance (200 m in this investigation) and n is the pseudodepth level (max $n = 7$ in this investigation).

Resistivity measurements are associated with varying depths depending on the separation of the current and potential electrodes in the survey and can be interpreted in terms of a lithological and/or geohydrological model of the subsurface. Measured data are the apparent resistivity because the resistivity values measured are averages over the total current path length but are plotted at one depth point for each potential electrode pair (Figure 4). Two-dimensional images of the subsurface apparent resistivity variation are called pseudosections. Data plotted in cross-section is a simplistic representation of actual, complex current flow paths. Inversion software then helps to interpret geoelectrical data in terms of more accurate earth models. The inversion and optimization processes of the recorded values along the long longitudinal profile were executed by means of the ZondRes2D software (Zond geophysical software). It is a computer program for 2.5D interpretation of electrical resistivity tomography, and the finite-element method as the mathematical apparatus is used to solve a forward and inverse procedure. The first step was to prepare
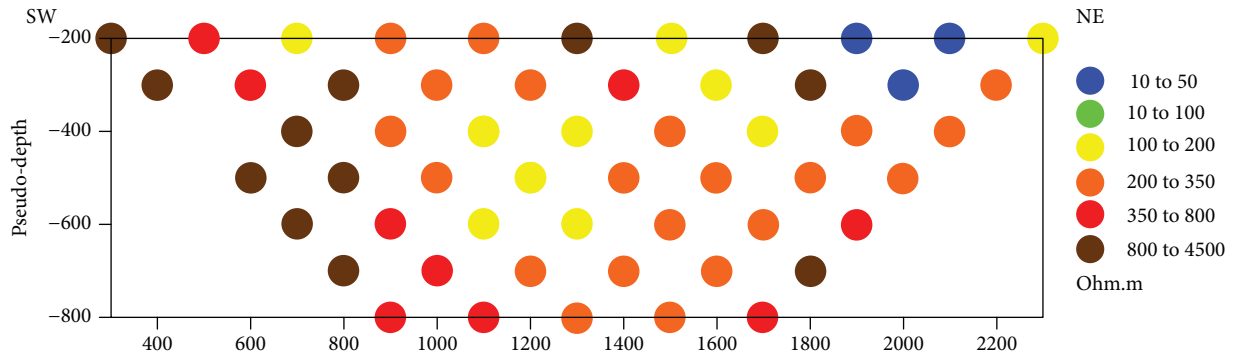
FIGURE 4: Distribution of the calculated apparent resistivity value.

the data for the inversion, such as poor data detection. The next step was to select the inversion type and parameters. In order to transform the apparent resistivity pseudosection into a model representing the distribution of calculated electrical resistivity in the subsurface, we used the smoothness constrained that is an inversion by a least-square method with the use of a smoothing operator. The inversion type was the Marquardt classic inversion algorithm consisted in a least-square method with regularization by a damping parameter [68]. In case of little quantity of section parameters, this algorithm allows receiving a contrast subsurface model. In order to follow the inversion algorithm, the data set was inverted by using a $100^* Y \, \mathrm{m}^2$ cell size, where Y is the vertical dimension which is a variable from 20 m and an increase factor of 1.10 for 13 levels. The starting homogeneous model was with an apparent resistivity of $100 \, \Omega$m, and the final RMS was 12.8%.

4. Results and Discussions

Figure 5 shows the resistivity distribution, where a resistivity range from $50 \, \Omega$m to more than $2000 \, \Omega$m is defined. In the resistivity image, it is possible to distinguish some main electrical layers. A shallow resistivity layer ($>800 \, \Omega$m) is recognizable from about 900 m and 2000 m of horizontal displacement from the origin up to the end of the profile. This electrolayer has a different thickness of around 100 m maximum. Under the shallow resistivity layer, it is possible to distinguish a relative conductive zone until 100 m.a.s.l. ($<200 \, \Omega$m). This electrolayer is located above a deep resistivity layer ($>800 \, \Omega$m) which is well highlighted along the whole tomography up to 100 m.a.s.l., and it is outcropped on the NE flank.

The not easy geological interpretation of the geophysical results reflects the complex geological setting of the investigated area characterized by the superimposition of different tectonic phases. Generally, the DERT image is characterized by relative resistive electrical values that can be associated to the carbonate formation (high resistivity). Moreover, a detailed qualitative analysis of the resistivity tomography highlights some hydrogeological features, just due to the strong correlation between the fluid in the fractures and the electrical resistivity. The relatively high resistive zone (shallow and deep) should be characterized

by a nonsaturated carbonate, while the medium electrolayer, characterized by relatively low resistive values ($<200 \, \Omega$m) should be associated to a saturated carbonate, due to a different fracturing degree. Lateral resistivity contrast is probably marked by tectonic contact.

A first geophysical and hydrogeological analysis suggested a high potential for exploiting the Muro Lucano carbonate aquifer. In particular, from a hydrogeological point of view, all the edges of the studied carbonates are boarded by faults and are plugged by Sicilide and Irpinian units characterized by low to medium hydraulic conductivity material. On the contrary, Muro Lucano and Monte Marzano carbonate massifs are characterized by a high permeability degree linked to an intense fracture network and karst features, such as sinkholes and caves, as testified by the presence, in the southern sector, of a karst system of active caves with a total length of more than 1500 m. Finally, the Muro Lucano unit terrain is characterized by medium to high permeability degree.

Moreover, it is possible to speculate two main groundwater flows: a very shallow one and a deeper one. The shallow water circulation is imposed in the Pliocene sands and conglomerates and is indicated by several springs and by the presence of several saturated shallow ground zones. A water capacity of about 20-30 l/s was estimated (data from the Water Protection Plan of Basilicata Region). On the contrary, the studied carbonate structure is lacking in basal springs and meteorological precipitations (with an average annual value of 907 mm recorded in the 2000-2004 period) do not produce a considerable increment of the discharge in the basal rivers (Forra di Muro river, etc.). Therefore, it is possible to consider the presence of a deep water circulation.

A lack of detailed knowledge on Muro Lucano buried aquifer characteristics, identification of areas with high recharge potential, dominant fracture and/or conduit porosity zones, and well-defined geological boundary conditions can hamper the ability to exploit the groundwater resources. However, taking into account the geophysical results and the most favorable topographic position, it was possible to localize the best site of an exploration well for water supply research.

In particular, the well was installed along the geoelectrical profile at 1100 m of horizontal displacement from the origin
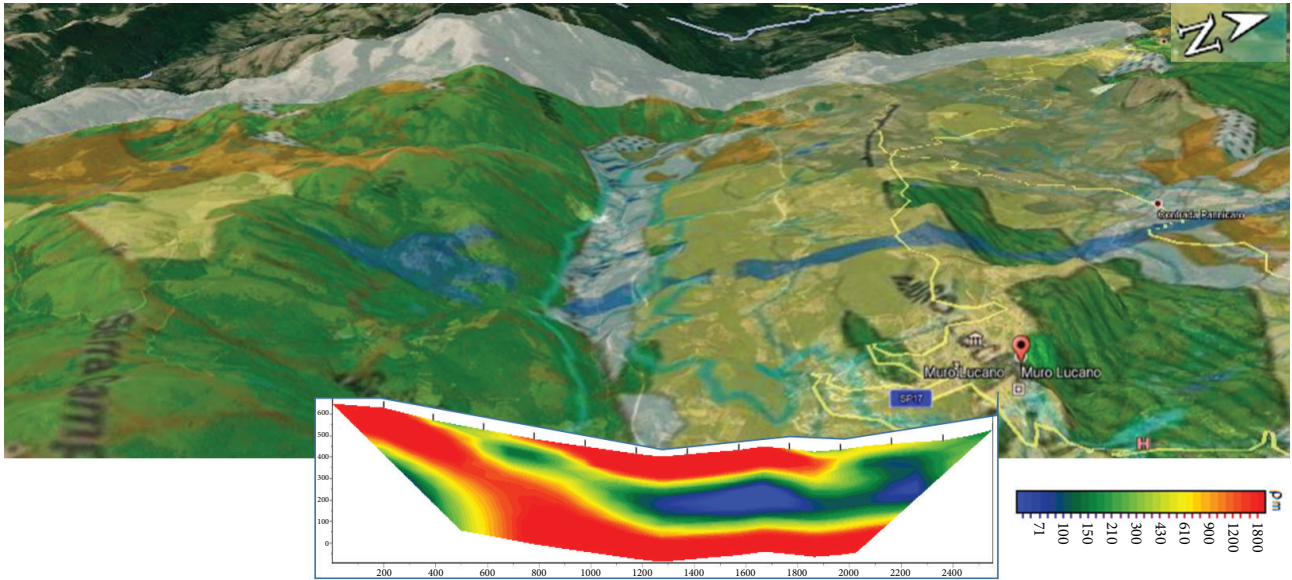
FIGURE 5: The hydrogeological map on a 3D vision (Google 3D) and the DERT image. The deep was carried out by CNR-IMAA prototype. The RMS is 12.8%.
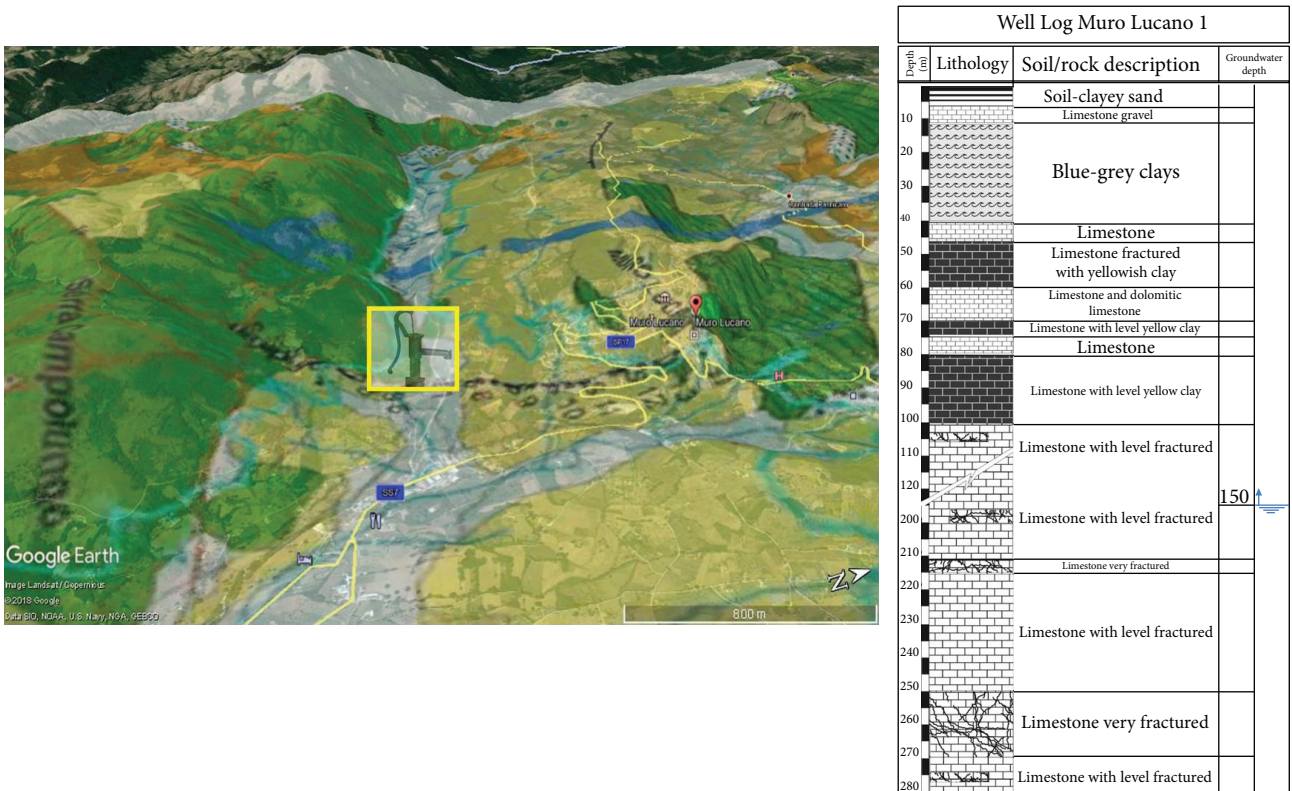

FIGURE 6: The hydrogeological map and the well log of the Muro Lucano 1 well.

up to the end of the profile, between the electrodes S7 and S8. The well, with a depth of 280 m from the surface, allowed us to reconstruct the lithological succession along it (well log in Figure 6). In particular, we found a very thick alluvial deposit layer (10 m), a shallow clay layer (30 m tick) of Sicilide unit, a 60 m thick layer of Miocene limestones and clays (Irpinian units), and a thick carbonate succession (from 100 m to 280 m) characterized by a different fracturing degree. Moreover, the water table was at 150 m from the surface, in correspondence of the more fractured carbonate layer. The
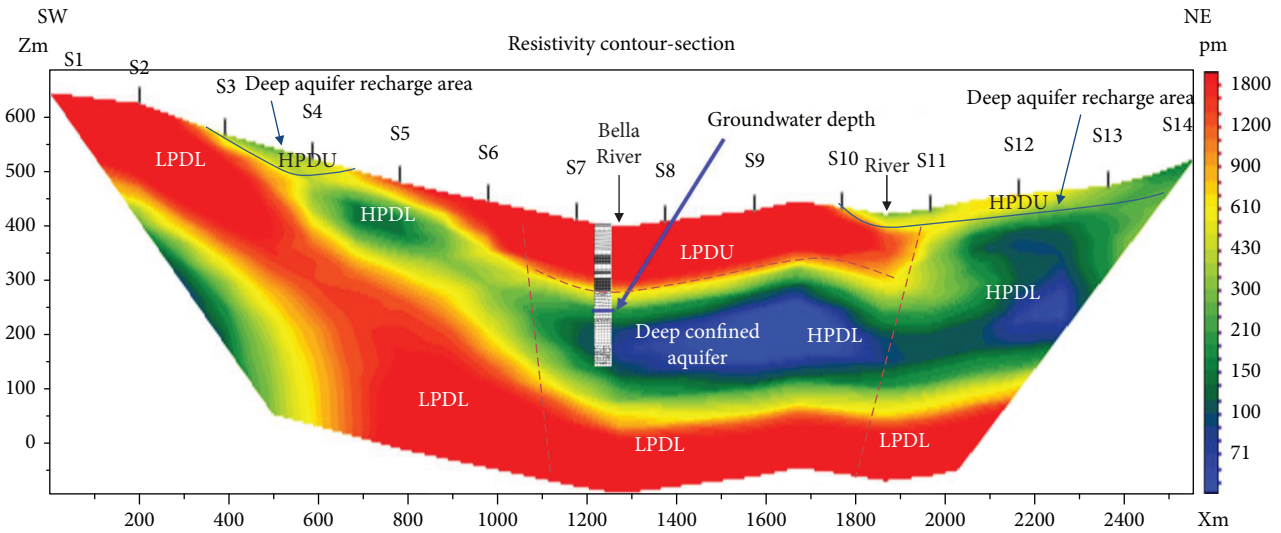
FIGURE 7: The well log applied on the DERT image. Red dotted lines are uncertain fault. HPDU = high permeability degree units; LPDU = low permeability degree units; HPDL = high permeability degree limestones; LPDU = low permeability degree limestones.

aquifer was in pressure, and after the drilling, the water table reached 120 m from the surface. This phenomenon proved the heterogeneity of the carbonate rock fracture state. Figure 7 shows a comparison between the deep electrical resistivity image and the well geological data. It is very interesting to notice that rocks characterized by a lower permeability degree (Sicilide unit clays and massive limestones) are generally associated to higher resistivity values. Moreover, carbonate rocks on the top and deep define an electrical resistivity range with high values (>800 Ωm).

In contrast, the carbonate rock with an important fractured state is highlighted in the DERT image with resistivity values < 200 Ωm. According to Kirkby et al. [41], this reflects a decrease in the contribution of the rock matrix resistivity to the passage of current. As fracturing increases, less current passes through the matrix, and therefore, the measured bulk resistivity is more strongly controlled by the fracture network and then by the water resistivity value.

Moreover, the deep groundwater level is localized in correspondence of a relatively deeper conductivity area. Therefore, it is possible to define that the NE shallow conductivity zone is represented by limestone formation with a high level of fractures; on the contrary, the southern limestones have relatively higher resistivity values due to low fracturing level.

Finally, DERT results allow us also to define the deep hydraulic aquifer recharge areas: there is a clear hydraulic connection between the shallower and the deep aquifers in both the N and SE where Pliocene sands and gravel represent a further recharge area of the deep aquifer. However, the deep aquifer is mainly fed by rainwater by outcropping carbonate at the N, with a groundwater flowing in the S-SW direction. In contrast, it seems that there is no hydraulic connection between the southern carbonate massif and the deep Muro Lucano aquifer. This deep water circulation is probably influenced by the local tectonic setting.

5. Conclusions

This work shows a useful case study for identifying deep aquifers in carbonate terrains and individuates the best place where to drill a well by using Deep Electrical Resistivity Tomography (DERT). In particular, the exploitation of the Muro Lucano deep aquifer was hampered by the complex geological and hydrogeological situation and by the lack of detailed data. Moreover, the geophysical survey provided more detailed information on buried geological features, aquifer characteristics, deep aquifer recharge zones, and probably conduit and fracture porosity zones along the DERT profile. In particular, the hydrogeological and geophysical analyses describe a high water yield and a not so deep hydrogeological structure which should be tapped to provide the W sector of the Basilicata region with a huge quantity of water. Moreover, DERT allows us to individuate low resistivity zones that are probably linked to higher permeability hydrogeological units. Finally, from geophysical data, it was shown that the studied hydrogeological structure has a deep and shallow water circulation system connected between them and probably influenced by the local tectonic setting. The future hydrogeological balance will help us to quantify in detail the groundwater resource potentiality for exploitation.

Finally, some general considerations have to be in account. The geological structure, aquifer properties, and groundwater heads are obtained from point measurements (wells and pumping tests) which are sparse, usually available at locations far apart, distances ranging from hundreds to thousands of meters. However, this kind of information in complex aquifers can lead to errors in the conceptual understanding of the aquifer when it is necessary to define the position of an exploitation well. Therefore, the definition of the best site, in terms of maximum efficiency, became a crucial point in the water exploitation. This work would like to show how the ability to make the best geophysical

investigation in order to reach the described aims is a crucial point for the geophysicist's community. Therefore, this kind of work highlights how the obtained results from a not-common deep electrical resistivity survey (DERT), properly integrated with the geological information, could give a strong information to define the best position of an exploitation well. Moreover, looking the amount of economic resources at stake, a DERT cost is only the 5% of the total amount for a single well.

Data Availability

The geoelectrical data used to support the findings of this study are available from one of the authors (Capozzoli Luigi), which is the chief of the Tomogea srl company (info@tomogea.it), that collected the data. The hydrogeological data are available from one of the authors Salvatore Grimaldi.

Conflicts of Interest

The authors declare that they have no conflicts of interest.

Acknowledgments

References

[1] M. Bakalowicz, "Karst groundwater: a challenge for new resources," *Hydrogeology Journal*, vol. 13, no. 1, pp. 148–160, 2005.

[2] Z. Chen, A. S. Auler, M. Bakalowicz et al., "The World Karst Aquifer Mapping project: concept, mapping procedure and map of Europe," *Hydrogeology Journal*, vol. 25, no. 3, pp. 771–785, 2017.

[3] A. Hartmann, N. Goldscheider, T. Wagener, J. Lange, and M. Weiler, "Karst water resources in a changing world: review of hydrological modeling approaches," *Reviews of Geophysics*, vol. 52, no. 3, pp. 218–242, 2014.

[4] T. Bechtel, F. Bosch, and M. Gurk, "Geophysical methods in karst hydrogeology," in *Methods in Karst Hydrogeology*, N. Goldscheider and D. Drew, Eds., pp. 171–199, Taylor and Francis/Balkema, London, U. K., 2007.

[5] K. Chalikakis, V. Plagnes, R. Guerin, R. Valois, and F. P. Bosch, "Contribution of geophysical methods to karst-system exploration: an overview," *Hydrogeology Journal*, vol. 19, no. 6, pp. 1169–1180, 2011.

[6] B. Berkowitz, "Characterizing flow and transport in fractured geological media: a review," *Advances in Water Resources*, vol. 25, no. 8-12, pp. 861–884, 2002.

[7] M. Beres, M. Luetscher, and R. Olivier, "Integration of ground-penetrating radar and microgravimetric methods to map shallow caves," *Journal of Applied Geophysics*, vol. 46, no. 4, pp. 249–262, 2001.

[8] L. Bermejo, A. I. Ortega, R. Guérin et al., "2D and 3D ERT imaging for identifying karst morphologies in the archaeological sites of Gran Dolina and Galería Complex (Sierra de Atapuerca, Burgos, Spain)," *Quaternary International*, vol. 433, pp. 393–401, 2016.

[9] F. J. Martínez-Moreno, J. Galindo-Zaldívar, A. Pedrera et al., "Detecting gypsum caves with microgravity and ERT under soil water content variations (Sorbas, SE Spain)," *Engineering Geology*, vol. 193, pp. 38–48, 2015.

[10] W. Brown, K. Stafford, M. Shaw-Faulkner, and A. Grubbs, "A comparative integrated geophysical study of Horseshoe Chimney Cave, Colorado Bend State Park, Texas," *International Journal of Speleology*, vol. 40, no. 1, pp. 9–16, 2011.

[11] C. M. Burberry, C. A.-L. Jackson, and S. R. Chandler, "Seismic reflection imaging of karst in the Persian Gulf: implications for the characterization of carbonate reservoirs," *AAPG Bulletin*, vol. 100, no. 10, pp. 1561–1584, 2016.

[12] E. Cardarelli, M. Cercato, A. Cerreto, and G. Di Filippo, "Electrical resistivity and seismic refraction tomography to detect buried cavities," *Geophysical Prospecting*, vol. 58, no. 4, pp. 685–695, 2010.

[13] V. Di Fiore, A. Angelino, S. Passaro, and A. Bonanno, "High resolution seismic reflection methods to detect near surface tuff-cavities: a case study in the neapolitan area, Italy," *Journal of Cave and Karst Studies*, vol. 75, no. 1, pp. 51–59, 2013.

[14] F. J. Martínez-Moreno, J. Galindo-Zaldívar, A. Pedrera et al., "Integrated geophysical methods for studying the karst system of Gruta de las Maravillas (Aracena, Southwest Spain)," *Journal of Applied Geophysics*, vol. 107, pp. 149–162, 2014.

[15] S. H. Wadas, U. Polom, and C. M. Krawczyk, "High-resolution shear-wave seismic reflection as a tool to image near-surface subrosion structures – a case study in bad Frankenhausen, Germany," *Solid Earth*, vol. 7, no. 5, pp. 1491–1508, 2016.

[16] E. Cardarelli, G. Di Filippo, and E. Tuccinardi, "Electrical resistivity tomography to detect buried cavities in Rome: a case study," *Near Surface Geophysics*, vol. 4, no. 15, 2006.

[17] V. Festa, A. Fiore, M. Parise, and A. Siniscalchi, "Sinkhole evolution in the Apulian karst of southern Italy; a case study, with some considerations on sinkhole hazards," *Journal of Cave and Karst Studies*, vol. 74, no. 2, pp. 137–147, 2012.

[18] V. Giampaolo, L. Capozzoli, S. Grimaldi, and E. Rizzo, "Sinkhole risk assessment by ERT: the case study of Sirino Lake (Basilicata, Italy)," *Geomorphology*, vol. 253, pp. 1–9, 2016.

[19] G. Kaufmann, "Geophysical mapping of solution and collapse sinkholes," *Journal of Applied Geophysics*, vol. 111, pp. 271–288, 2014.

[20] R. Martel, P. Castellazzi, E. Gloaguen, L. Trépanier, and J. Garfias, "ERT, GPR, InSAR, and tracer tests to characterize karst aquifer systems under urban areas: the case of Quebec City," *Geomorphology*, vol. 310, pp. 45–56, 2018.

[21] R. Valois, L. Bermejo, R. Guérin, S. Hinguant, R. Pigeaud, and J. Rodet, "Karstic morphologies identified with geophysics around Saulges caves (Mayenne, France)," *Archaeological Prospection*, vol. 17, no. 3, pp. 151–160, 2010.

[22] M. Gambetta, E. Armadillo, C. Carmisciano, L. Cocchi, and F. Caratori Tontini, "Determining geophysical properties of a near-surface cave through integrated microgravity vertical gradient and electrical resistivity tomography measurements," *Journal of Cave and Karst Studies*, vol. 73, no. 1, pp. 11–15, 2011.

[23] T. McCormack, Y. O'Connell, E. Daly, L. W. Gill, T. Henry, and M. Perriquet, "Characterisation of karst hydrogeology in Western Ireland using geophysical and hydraulic modelling

techniques," *Journal of Hydrology: Regional Studies*, vol. 10, pp. 1–17, 2017.

[24] A. Seren, A. E. Babacan, K. Gelisli, Z. Ogretmen, and R. Kandemir, "An investigation for potential extensions of the Karaca Cavern using geophysical methods," *Carbonates and Evaporites*, vol. 27, no. 3-4, pp. 321–329, 2012.

[25] J. Zhu, J. C. Currens, and J. S. Dinger, "Challenges of using electrical resistivity method to locate karst conduits—a field case in the Inner Bluegrass Region, Kentucky," *Journal of Applied Geophysics*, vol. 75, no. 3, pp. 523–530, 2011.

[26] E. A. Atekwana and E. A. Atekwana, "Geophysical signatures of microbial activity at hydrocarbon contaminated sites: a review," *Surveys in Geophysics*, vol. 31, no. 2, pp. 247–283, 2010.

[27] A. Binley and A. Kemna, "Electrical methods," in *Hydrogeophysics*, Y. Rubin and S. S. Hubbard, Eds., pp. 129–156, Springer, 2005.

[28] A. Binley, G. Cassiani, R. Middleton, and P. Winship, "Vadose zone flow model parameterisation using cross-borehole radar and resistivity imaging," *Journal of Hydrology*, vol. 267, no. 3-4, pp. 147–159, 2002.

[29] W. Daily, A. Ramirez, D. LaBrecque, and J. Nitao, "Electrical resistivity tomography of vadose water movement," *Water Resources Research*, vol. 28, no. 5, pp. 1429–1442, 1992.

[30] D. Dam and S. Christensen, "Including geophysical data in ground water model inverse calibration," *Groundwater*, vol. 41, no. 2, pp. 178–189, 2003.

[31] V. Giampaolo, E. Rizzo, S. Straface, and M. Votta, "Hydrogeophysics techniques for the characterization of a heterogeneous aquifer," *Bollettino di Geofisica Teorica ed Applicata*, vol. 52, no. 4, pp. 595–606, 2011.

[32] W. K. Kosinski and W. E. Kelly, "Geoelectric soundings for predicting aquifer properties," *Ground Water*, vol. 19, no. 2, pp. 163–171, 1981.

[33] L. Slater, M. D. Zaidman, A. M. Binley, and L. J. West, "Electrical imaging of saline tracer migration for the investigation of unsaturated zone transport mechanisms," *Hydrology and Earth System Sciences*, vol. 1, no. 2, pp. 291–302, 1997.

[34] G. E. Archie, "The electrical resistivity log as an aid in determining some reservoir characteristics," *Transactions of the AIME*, vol. 146, no. 1, pp. 54–62, 1942.

[35] G. E. Archie, "Classification of carbonate reservoir rocks and petro-physical considerations," *AAPG Bulletin*, vol. 36, no. 2, pp. 278–298, 1952.

[36] Y. Bernabè, M. Zamora, M. Li, A. Maineult, and Y. B. Tang, "Pore connectivity, permeability, and electrical formation factor: a new model and comparison to experimental data," *Journal of Geophysical Research*, vol. 116, no. B11, 2011.

[37] F. A. L. Dullien, "Porous media," in *Fluids Transport and Pore Structure*, Academic Press, 2nd edition, 1992.

[38] P. Glover, "What is the cementation exponent? A new interpretation," *The Leading Edge*, vol. 28, no. 1, pp. 82–85, 2009.

[39] B. Kozlov, M. H. Schneider, B. Montaron, M. Lagues, and P. Tabeling, "Archie's law in microsystems," *Transport in Porous Media*, vol. 95, no. 1, pp. 1–20, 2012.

[40] W. Z. Yue and G. Tao, "A new non-Archie model for pore structure: numerical experiments using digital rock models," *Geophysical Journal International*, vol. 195, no. 1, pp. 282–291, 2013.

[41] A. Kirkby, G. Heinson, and L. Krieger, "Relating permeability and electrical resistivity in fractures using random resistor network models," *Journal of Geophysical Research: Solid Earth*, vol. 121, no. 3, pp. 1546–1564, 2016.

[42] D. Roubinet, J. Irving, and P. Pezard, "Relating topological and electrical properties of fractured porous media: insights into the characterization of rock fracturing," *Minerals*, vol. 8, no. 1, p. 14, 2018.

[43] P. G. Hallof, *On the Interpretation of Resistivity and Induced Polarization Measurements, [Ph.D. Thesis]*, MIT, Cambridge, 1957.

[44] M. Balasco, P. Galli, A. Giocoli et al., "Deep geophysical electromagnetic section across the upper Aterno Valley: preliminary results after the April 6, 2009 L'Aquila earthquake," *Bollettino di Geofisica Teorica ed Applicata*, vol. 52, no. 3, pp. 443–455, 2011.

[45] A. Colella, V. Lapenna, and E. Rizzo, "High-resolution imaging of the High Agri Valley basin (Southern Italy) with electrical resistivity tomography," *Tectonophysics*, vol. 386, no. 1-2, pp. 29–40, 2004.

[46] A. Giocoli, C. Magrì, S. Piscitelli et al., "Electrical resistivity tomography investigations in the Ufita Valley (southern Italy)," *Annales de Geophysique*, vol. 51, pp. 213–223, 2008.

[47] S. Pucci, R. Civico, F. Villani et al., "Deep electrical resistivity tomography along the tectonically active Middle Aterno Valley (2009 L'Aquila earthquake area, Central Italy)," *Geophysical Journal International*, vol. 207, no. 2, pp. 967–982, 2016.

[48] E. Rizzo, A. Colella, V. Lapenna, and S. Piscitelli, "High-resolution images of the fault-controlled High Agri Valley basin (Southern Italy) with deep and shallow electrical resistivity tomographies," *Physics and Chemistry of the Earth*, vol. 29, no. 4-9, pp. 321–327, 2004.

[49] E. Rizzo and V. Giampaolo, "New deep electrical resistivity tomography in the High Agri Valley Basin (Basilicata, Southern Italy)," *Geomatics, Natural Hazards and Risk*, vol. 10, no. 1, pp. 197–218, 2019.

[50] H. Storz, W. Storz, and F. Jacobs, "Electrical resistivity tomography to investigate geological structures of the earth's upper crust," *Geophysical Prospecting*, vol. 48, no. 3, pp. 455–471, 2000.

[51] K. Suzuki, S. Toda, K. Kusunoki, Y. Fujimitsu, T. Mogi, and A. Jomori, "Case studies of electrical and electromagnetic methods applied to mapping active faults, beneath the thick quaternary," *Engineering Geology*, vol. 56, no. 1-2, pp. 29–45, 2000.

[52] G. Tamburriello, M. Balasco, E. Rizzo, P. Harabaglia, V. Lapenna, and A. Siniscalchi, "Deep electrical resistivity tomography and geothermal analysis of Bradano foredeep deposits in Venosa area (southern Italy): first results," *Annals of Geophysics*, vol. 51, no. 1, pp. 203–212, 2008.

[53] M. Balasco, A. Giocoli, S. Piscitelli et al., "Magnetotelluric investigation in the High Agri Valley (southern Apennine, Italy)," *Natural Hazards and Earth System Sciences*, vol. 15, no. 4, pp. 843–852, 2015.

[54] G. Romano, M. Balasco, A. Siniscalchi, E. Gueguen, Z. Petrillo, and S. Tripaldi, "Geological and geo-structural characterization of the Montemurro area (Southern Italy) inferred from audiomagnetotelluric survey," *Geomatics, Natural Hazards and Risk*, vol. 9, no. 1, pp. 1156–1171, 2018.

[55] E. Patacca and P. Scandone, "Geology of the Southern Apennines," *Bollettino della Società Geologica Italiana*, vol. 7, pp. 75–119, 2007.

[56] C. Doglioni, F. Mongelli, and P. Pieri, "The Puglia uplift (SE Italy): an anomaly in the foreland of the Apenninic subduction due to buckling of a thick continental lithosphere," *Tectonics*, vol. 13, no. 5, pp. 1309–1321, 1994.

[57] E. Gueguen, C. Doglioni, and M. Fernandez, "On the post-25 Ma geodynamic evolution of the Western Mediterranean," *Tectonophysics*, vol. 298, no. 1-3, pp. 259–269, 1998.

[58] P. Shiner, A. Beccacini, and S. Mazzoli, "Thin-skinned versus thick-skinned structural models for Apulian carbonate reservoirs: constraints from the Val d'Agri Fields, S Apennines, Italy," *Marine and Petroleum Geology*, vol. 21, no. 7, pp. 805–827, 2004.

[59] A. M. Noguera and G. Rea, "Deep structure of the Campanian - Lucanian Arc (Southern Apennine, Italy)," *Tectonophysics*, vol. 324, no. 4, pp. 239–265, 2000.

[60] P. Scandone, A. Mazzotti, G. L. Fradelizio et al., *Line CROP 04: Southern Apennines*, Mem. Descr. Carta Geol. d'It., LXII, 2003.

[61] D. Scrocca, S. Sciamanna, E. Di Luzio, M. Tozzi, C. Nicolai, and R. Gambini, "Structural setting along the CROP-04 deep seismic profile (Southern Apennines - Italy)," *Bollettino della Società geologica italiana*, vol. 7, pp. 283–296, 2007.

[62] T. Pescatore, P. Renda, M. Schiattarella, and M. Tramutoli, "Stratigraphic and structural relationships between Meso-Cenozoic Lagonegro basin and coeval carbonate platforms in southern Apennines, Italy," *Tectonophysics*, vol. 315, no. 1-4, pp. 269–286, 1999.

[63] F. Ortolani, E. Cocco, E. Cravero et al., "Le Unità Irpine nell'Area a nord di Monte Marzano, Appennino Meridionale," *Mem. Soc. Geol. It.*, vol. 13, pp. 607–654, 1974.

[64] A. Ascione, A. Cinque, L. Improta, and F. Villani, "Late Quaternary faulting within the Southern Apennines seismic belt: new data from Mt. Marzano area (Southern Italy)," *Quaternary International*, vol. 101-102, pp. 27–41, 2003.

[65] A. Marangella, G. Indelli, M. Mastrangelo, A. Miccoli, M. Parise, and S. M. Valdes, "La condotta forzata della diga sul Torrente S. Pietro (Muro Lucano, Basilicata)," *Memorie dell'Istituto Italiano di Speleologia*, vol. 2008, pp. 478–483, 2008.

[66] V. Del Gaudio and J. Wasowski, *Stima a Scala Regionale della Probabilità Temporale di Innesco Sismico di Frane in Irpinia*, GNGTS – Atti del 21° Convegno Nazionale / 04.19, 2002.

[67] V. Lapenna, M. Macchiato, D. Patella, C. Satriano, C. Serio, and V. Tramutoli, "Statistical analysis of non-stationary voltage recordings in geoelectrical prospecting," *Geophysical Prospecting*, vol. 42, no. 8, pp. 917–952, 1994.

[68] D. W. Marquardt, "An algorithm for least-squares estimation of nonlinear parameters," *Journal of the Society for Industrial and Applied Mathematics*, vol. 11, no. 2, pp. 431–441, 1963.